SYNTHESIS AND CHARACTERISATION OF HIERARCHICAL ZEOLITIC MATERIALS FOR HEAVY METALS ADSORPTION

A thesis submitted to the University of Manchester for the degree of *Doctor of Philosophy* in the Faculty of Engineering and Physical Sciences

2015

DAVID ALEJANDRO DE HARO DEL RIO

Supervised by: Dr Stuart M. Holmes

SCHOOL OF CHEMICAL ENGINEERING AND ANALYTICAL SCIENCE

The University of Manchester

Contents

Total word count: 42,151

List of Figures

List of Tables

Abstract

This thesis explains a method based on the homogenisation of zeta potential charges on carbon supports for the production of hierarchical structured zeolitic composites. The modification of carbons' surface chemistry allowed zeolite particles to be fixed to the support by electrostatic interactions. In order to achieve this, the size reduction of zeolite particles was carried out by two different methods: a) ball milling and b) a synthetic route to produce zeolite colloidal dispersions. Also, the seeding method, based on hydrothermal growth was compared.

The prepared materials in this work were designed to be used in the sorption of cations, and to allow vitrification and thereby reduce the final adsorbent volume. Results showed that a large pollutant amount can be trapped using a lower volume of material reducing costs and final waste disposal.

The zeolites used in this work were selected based on their low density framework and low Si/Al ratio. Synthetic zeolites A, Y and clinoptilolite were successfully produced. Natural clinoptilolite was also utilised in this work. Also, zeolite A was produced at nanometre scale following the clear solutions method. All materials were successfully incorporated onto supports to produce multimodal porosity materials. The hierarchical modification of natural clinoptilolite, following a straightforward and non-expensive methodology, is one the most significant contributions of this work.

Carbons are used as supports due to their high surface area, they can be obtained from low-cost sources such as agroindustrial wastes and carbons allow volume reduction if materials are vitrified at high temperatures. In this work, carbons were produced from corn cob and husk, sugar cane bagasse, cherry stones, date stones and hazelnut shells.

The prepared composite materials were tested in the removal of toxic ions from water solutions: cobalt, copper and caesium ions were effectively removed from aqueous media. Adsorption experiments showed that the distribution of supported zeolite particles improved their uptake efficiency and capacity. The kinetic studies revealed an enhanced rate constant for carbon-zeolites composites in comparison with pure zeolites. Diffusivity results suggested that mass transfer characteristics are modified by using hierarchical porous materials; results showed that particle size or support nature can modify diffusion resistances, reducing intraparticle diffusion and accelerating the overall kinetic processes. Adsorption equilibrium data was correlated using Langmuir and Freundlich models.

Declaration

No portion of the work referred to in this thesis has been submitted in support of an application for another degree or qualification of this or any other university or other institute of learning.

All the material, figures and data presented in this work are my own original work, except where specifically stated and acknowledged.

David Alejandro De Haro Del Rio

Manchester, 2015

Copyright Statment

Acknowledgements

First, I would like to thank my supervisor, Dr Stuart Holmes for all valuable guidance and advice. He greatly inspired me to work in this project and contributed in my formation as a researcher. His willingness to motivate me contributed tremendously to my project.

Besides, I wish to thank to the Mexican Council for Science and Technology (CONACyT) for funding my PhD. Also, to the Latin American Postgraduate Program of The University of Manchester and specially to her Director, Prof Dr Teresa Alonso. Also, I would to acknowledge to The University of Guanajuato for providing all the resources and guidance, specially to Dr Sergio Arias and Valeria Rangel.

I wish to thank all my friends in the School of CEAS that I had the chance to meet. These awesome people have greatly contributed to my personal development by sharing all kind of experiences. To mention all of them would be a very hard task.

Finally, an honorable mention goes to friends and colleagues in the Mill building for all valuable help: Liz Davenport, Paddy Hill, Patricia Turnbull, John Riley, Loris Doyle, Paul, Jim Fearrick, Gary Burns, Cath Davies, Shahla Kahn and many others. Without their help, I would have faced many difficulties while doing my PhD.

Dedication

To my mother, for her unconditional love and support.

To my beloved girlfriend Ariadna, who has always been there through the hard times.

Chapter 1

Introduction

The damage caused to the environment due to human activities is already well-known. It would be almost impossible to try to quantify the associated effects to human health or ecosystems but every day it is becoming more common to see these effects in the form of diseases and depletion of natural resources. Environmental pollution has been increasing as consequence of the massive production of goods and services, conferring on society responsibility to take major decisions related to environmental protection. It is commonly acknowledged that the water importance for most live organisms on earth is crucial. Water is a vital substance because it is present in all living entities and is responsible for carrying out almost every physiological process. Additionally, water use in daily life is paramount, people use it in everyday activities like sanitation, irrigate crops, cooking and many more.

Although around 70% of earth surface is covered by water and contamination is leading this resource to have poor quality making it a cause of a number of health problems. It is essential for humans to have clean and accessible water. Water pollution has diverse origins ranging from industrial to radioactive wastes passing through sewage, oil spillages and others. All of them with specific associated problems.

The heavy metals presence in water bodies is a direct consequence of industrialisation and natural resources exploitation without adequate legislation. A remarkable example of historical pollution for heavy metals is the mining industry in some latin

american countries during the Spanish occupation. For decades, silver and gold mines where exploited using mercury in the extractive processes without any environmental concern. Today, the mercury accumulation at the bottom of dams reaches several centimetres thickness. Recently, in August 2014, in the Sonora River (Mexico), due to leakage occurred in a mine, were spilled 40,000 m^3 of acidic solution of copper sulphate along with other dissolved metals such as chrome, nickel, lead and zinc. The polluted river can be seen in Figure 1.1. It is clear that industrial activities can represent extreme risks to public health if enforcement of legislation is not properly applied.

Figure 1.1: The Sonora River after the environmental accident where dissolved heavy metals were spilled[1]

Furthermore, there is a damage associated with heavy metals discharges, because some of those polluted streams are used to irrigate fields and eventually heavy metals are absorbed by some plants. Since heavy metals are hazardous materials [2] (most of them are bioaccumulative and carcinogenic) an important part of research around the globe is now focused on practical and sustainable solutions, many researchers are focused on designing and testing a variety of materials to uptake and confine heavy metals and thus, reduce the negative impacts on environment and human health. Note that some elements classified as heavy metals are vital for human metabolism, and

[1]CNN Mexico, August 2014, http://mexico.cnn.com/nacional/2014/08/29/519-pozos-en-el-rio-sonora-reabren-al-uso-agropecuario-tras-derrame-minero

not to ingest them can cause deficiencies. However, it is the long-term exposure and consumption of excessive dosage that causes related health problems.

Additionally, the radioactive species presence in waste streams represents a very serious environmental threat. Radionuclides are fission by-products of radioactive sources used as fuels to produce energy in nuclear plants. These radioactive wastes, are potentially harmful to environment and human health if leakages occur. Unfortunately, catastrophic accidents have occurred in nuclear plants. In 1986 in Chernobyl, Ukraine radioactive caesium , ^{134}Cs and ^{137}Cs, and iodine, ^{131}I, isotopes [3] were released to the environment. More recently in 2011 in Fukushima, Japan a massive earthquake and a consequent tsunami destroyed the nuclear reactor structure leading to the emission of radioactive iodine, caesium and radioactive gases to the atmosphere [4]. An image of the explosion can be seen in Figure 1.2.

Figure 1.2: Fukushima's nuclear plant explosion[2]

Different materials and methods to prevent and solve problems related to heavy metal disposal in water are now employed. Two of most used techniques are adsorption and ion exchange due to advantages such as high efficiency and easy methodology

[2]Imagen Contemporanea, November 2012, http://lineadeorigen.com/research/imagencontemporanea/2012/11-13-accidente-nuclear-de-fukushima

but these still have drawbacks like costs, selectivity and regeneration [5]. Both phenomena involve different mechanisms although it is common to group them in a general "sorption" concept.

Porous materials have been of particular interest in science due to their capacity to interact at atomic levels with other substances not only on the surface but also through the material's bulk [6]. This particular property has been responsible for the application of diverse porous materials in fields like adsorption, catalysis and ion exchange. Therefore, it becomes imperative to know the porous characteristics of these materials to understand the interactions with adsorbates and be able to tune specific porosity features to obtain enhanced performances in the the required applications.

Materials like zeolites are a good example of the application of porous media in environmental problems such as metal trapping. Natural and synthetic zeolites have been used in environmental protection applications. Zeolites are crystalline aluminosilicates with well-defined microporosity[3] and stronger acidity than amorphous aluminosilicates [7]. These materials have a negatively-charged framework usually balanced by exchangeable cations, which combined with their unique porosity, makes them suitable for applications such as ion exchange and catalysis. However, due to the narrow of their pores, zeolitic materials still have several disadvantages relating to diffusion [8], this reduces their efficiency and limits the applicability at large scale.

The use of materials with hierarchical structures, in porosity and particle size, have been shown to overcome some of diffusional drawbacks [9, 10]. As general definition, hierarchical structures are materials that have two or more porosity levels, regardless the pore uniformity in each level [11]. Many supports and templates have been used to produce these kind of materials but usually they are expensive and often they are removed by post-synthetic calcination which is wasteful and expensive [12, 13]. Thus, it is intended to use inexpensive materials as active phase supports and also that

[3]IUPAC defines three levels of porosity: Micro- (pores with diameters below 2 nm), meso- (pores with diameter larger than 2 nm and smaller than 50 nm) and macro- (pores with diameters above 50 nm)

can remain after synthesis, in this case carbons produced from agro-industrial wastes. Currently a large volume of solid wastes are produced by agro-industrial activities around the world, these residues are used mainly as fertilisers and to feed animals [14].

The main contribution of this work is to propose of an effective and straightforward methodology to produce hierarchical zeolitic composite materials based on the chemical modification of surface chemistry of supports to be applied in the removal of heavy metals from water. The supports are made of carbonised agroindustrial wastes possessing a suitable honeycomb-like microarchitecture. The method is intended to be suitable for the attachment of natural and synthetic zeolites onto a series of carbonaceous supports from different sources. It is believed that if zeolites are well dispersed onto the support, more effective/active area will be available for the adsorptive substances. i.e. the metallic cations. Materials will be tested for the adsorptive efficiency of the active zeolitic phase in the removal of copper, cobalt and caesium ions, in terms of uptake rates and sorption capacities.

The materials final disposal used in wastewater treatment in nuclear plants requires volume reduction as these materials are buried underground. The fact of that ions removal is related only to zeolite particles, make the materials suitable for encapsulation by vitrification method at high temperature levels. Hence, final volume can be reduced, depending on the type of composite, up to 60% of initial volume with enhanced sorption capacity.

1.1 Aims and Objectives

The main objectives of this work are summarised:

1. To synthesise hierarchical zeolite composites following a method based on the deposition of reduced size particles (seeds) on the supports and subsequent crystal growth under hydrothermal treatment. The supports are produced from waste materials and their conditioning is carried out by simple thermal methods. The seeds production of different zeolite types is carried out by different methods such as ball milling and the

nanozeolites synthesis following the clear-solution method.

2. To produce synthetic members of the heulandite (HEU) family by a hydrothermal method and its incorporation into hierarchical structures by seeding method.

3. To synthesise hierarchical zeolitic composites following a proposed methodology based on the chemical modification of the support surface allowing the zeolite particles fixation by electrostatic interactions. Carbon supports are produced by thermal treatment and consequent chemical surface conditioning.

4. To evaluate the proposed method extrapolation to different types of carbon and zeolites such as clinoptilolite, which it has not been widely explored in their hierarchical forms. In this work, the use of supports coming from a non-cost residue and make them a cheap and effective option for the removal of metals.

5. To comprehensively characterise structural, chemical and morphological features of the prepared materials using the adequate techniques.

6. To evaluate and compare the sorption performances of cobalt (Co^{2+}), copper (Cu^{2+}) and caesium ions (Cs^{+}) of prepared materials, varying parameters such as initial pH, by kinetic and diffusive models; and to be able to predict, under described conditions, future operational variables and relate them with materials characteristics.

1.2 Thesis Outline

The thesis is divided in three parts: a) literature review, b) experimental part (including methodology, results and discussion) and c) conclusions and further work. The first part is divided into four chapters comprising the methods description for heavy metasl and radionuclides removal, the main characteristics and zeolites and porous media applications, the methods description for the hierarchical zeolitic materials preparation and the sorptive phenomena in zeolitic materials.

The second part has five chapters: The characterisation techniques used in this work are described, the carbons preparation and zeolites synthesis, the synthesis of hierarchical zeolites by seeding method and their cobalt ions adsorption. Also, the

composites preparation by the chemical surface modification of supports and their copper ions sorption. Finally, the evaluation of their adsorptive properties in the removal of caesium ions and the influence of several variables. Results, discussion and conclusions are included in each chapter.

The final part corresponds to general conclusions and further work.

Part I

Literature Review

Chapter 2

Removal of Heavy Metals from Aqueous Media

Industrial activities are mainly responsible for the release of heavy metals to the environment. Unlike organic pollutants, heavy metals are non-biodegradable, moreover, they accumulate in the organisms forming part of the food chain. By definition, heavy metals are chemical elements that exceed 5 g cm^{-3} in density and have atomic weights in the range 63.5 to 200.6 [15]. These properties are the cause of the major problem, that metals sediment and form thick layers of toxic matter at rivers and lakes bottom. Many metals can be classified as heavy metals, however, those that represent a real threat to humans and other living organisms due to their toxicity are arsenic, cobalt, cadmium, chromium, copper, nickel, lead, mercury and zinc. Cobalt is an element that is present in many sites such as surface water, sediments and even in the air. Cobalt sources are natural and also many industries such as alloys manufacture, mining, battery production, turbine fabrication and others industries use cobalt as a raw material in their processes [16]. Although cobalt is an essential element for humans since is a major constituent of the vitamin B12; depending on the compound's type, time of exposure and physicochemical state it could be very harmful causing cardiomyopathy, polycythaemia, respiratory and reproductive problems among others [17]. Copper is a also a essential element in the human metabolism and it plays a key role in the repro-

ductive system; nevertheless, copper exposure and ingestion in acute doses can cause poisoning such as gastric and intestinal stresses, haemolytic anemia, neurological abnormalities and corneal opacity [18]. Copper sources in waste water bodies have their origin in several industrial activities such as mining activities, the pigment industry, foundry activities and electroplating.

2.1 Methods to Remove Heavy Metals from Water

2.1.1 Precipitation

Is the most used method to remove heavy metals from waste streams due to its simplicity and low-cost. In principle, pH values are adjusted to be high, above 9, the metal is coordinated with the excess of OH^- ions and it precipitates. Research has been carried out to precipitate ions using sulphides at acidic pH levels [19]. The solid phase is then removed by filtration or sedimentation. Usually cheap and accessible materials such as lime and limestone have been utilised as precipitating agents. Hydroxide precipitation by calcium and sodium hydroxide has been used to remove copper and chromium ions [20]. Calcium oxide has been utilised to remove copper, zinc, chromium and lead ions in the pH range 7-11 [21]. Also, copper and zinc precipitation has been investigated by the use of hydrogen sulphide at pH 3 [19]. The main drawbacks are obvious: a considerable amount of chemical reagents are used, then a large amount of toxic sludge is generated and usually involves extra disposal or regenerative treatment [22].

2.1.2 Coagulation/Flocculation

This method has been used to replace precipitation or when the sedimentation process is very slow due to the formation of very small particles. Coagulation and flocculation are generally two connected phenomena and it is common to use them together. These combined processes are based first, for coagulation, on the modification of pH until suspended particles reach zero net charge, and then subsequent use of flocculation

agents to favour the particle agglomerates attachment and eventually achieve sedimentation [23]. Figure 2.1 represents a generic coagulation process for the heavy metals removal.

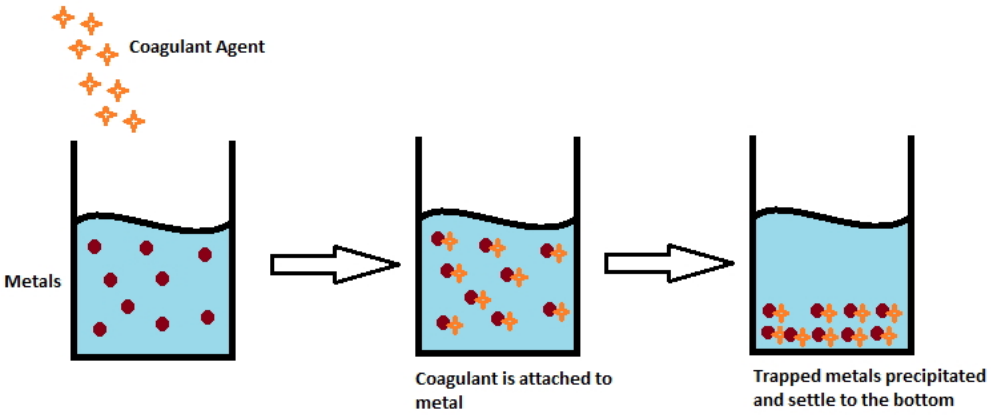

Figure 2.1: Main stages in a typical coagulation process

Cobalt and copper ions have been removed by the use of coagulation-flocculation technique using montmorillonite composites as flocculating agents [24]. Similarly to precipitation, the main limitation of these methods is the production of excessive volume of final solids.

2.1.3 Membranes

Since many metals have high value mainly in electrochemical and electric industries, their recovery has become another important field where membranes have been applied. The membranes use is based on the rejection of larger molecules and the flow through the pores of smaller particles. There are different filtration types depending upon the membrane's pore size, such as ultrafiltration and nanofiltration [18]. Various factors need to be considered when using these techniques such as pH, concentration, ionic strength and membrane parameters (pore size, mechanical properties and functional groups) [25].

2.1.3.1 Ultrafiltration

Ultrafiltration membranes have pore dimensions of 5-20 nm. It has been shown that under certain conditions, surface groups modification on membranes leads to enhanced capabilities to retain heavy metals as a consequence of chemical interactions between them [25]. Ultrafiltation is a method that works at "transmembrane pressure" [25] i.e. the pressure required to pass water through the membrane pores. Cu^{2+}, initial concentration 50 mg l^{-1}, has been filtered using polyethersulfone membrane achieving efficiencies of 94-100 % [26] Also, a ceramic membrane was investigated to remove Cu^{2+}, initial concentration 160 mg l^{-1} , and near to 100 % of removal [27]. Moreover, membranes have proven to be effective dealing with very low concentrations, for example, a Cu^{2+} solution containing 1 ppm was successfully treated [28]. Cobalt ions have been removed by the use of enhanced-membranes with micellar surfactants, up to 95 % of rejection was achieved [29]. Polyamide membranes also have been used to remove Co^{2+} ions with 95 % of performance [30].

2.1.3.2 Nanofiltration

Nanofiltration is known as the intermediate processes between ultrafiltration and reverse osmosis. It is considered to be less expensive in energy-consumption terms and to have some improved characteristics such as being easy to operate and having enhanced efficiency [31]. Solute rejection or retention is governed for several factors: surface interactions, solute present in membrane and solute-pore size restrictions. The selective filtration of cobalt ions also has been achieved using nanofiltration [32]. Nanoflitration was evaluated for the cobalt retention in simulated nuclear wastes. Several factors such as pH, feed concentration and ion competition were investigated and removal levels ranged from 5 % to 97 % [33].

2.1.3.3 Reverse Osmosis

Reverse osmosis is a different type of separation process where membranes are involved. An osmotic process occurs when a solute is transferred from a low-concentration area to other more concentrated through a membrane. Reverse osmosis is then the inverse process, where high pressure is exerted, higher than osmotic pressure, to achieve solute transfer to a low concentration from another with higher concentration [25]. The fact that these type of membranes do not allow the solvent transit and only the solute, makes them semi-permeable. Cu^{2+} cations were removed using a semi-permeable polyamide membrane, initial concentration 200 mg l^{-1}, and the rejection rate near 98 % [34]. Non-metallic ceramic membranes with montmorillonite also have been studied for Co^{2+} retention, 25 mg l^{-1} initial concentration and nearly 100 % of recovery. In Figure 2.2 the separation range is presented.

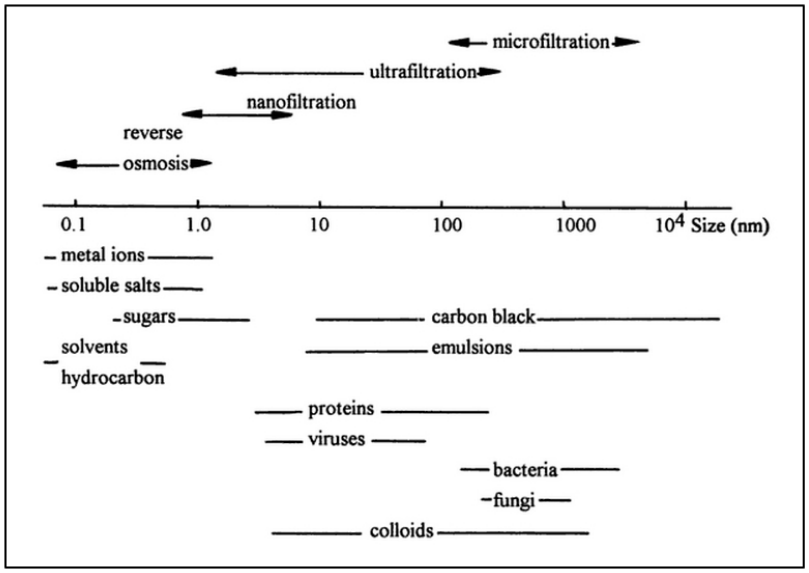

Figure 2.2: Size range of the application of membranes' technology [35]

As main drawbacks, membrane fouling can cause flux problems and back pressure. Also, the membrane degradation has impact on the operational costs [22]. The major drawback of reverse osmosis is the high cost generated by pump pressure. Recently, it has been used to recover valuable metals from effluents from electronic industries and similar. Reverse osmosis also has been shown to be non-selective for some monovalent

ions and radionuclides [25].

2.1.4 Electrochemical Methods

Electrochemical methods are based on the use of electric current in order to achieve the separation. In this section two methodologies are briefly described: Electrodeposition and electrodyalisis (use of membranes).

2.1.4.1 Electrodeposition

Electrodeposition is a method that applies direct current over two electrodes in order to oxidise or reduce heavy metals. When current is applied, ionic species are transferred to the cathode or anode depending on their electric charges [36]. Generally, ionic species of heavy metals are cations, thus, they are reduced at the cathode. The metals recovery with high purity can be achieved. The typical reaction occurring in the cathode is:

$$M^{n+}(aq) + ne^{-} \rightarrow M(s) \tag{2.1}$$

2.1.4.2 Membrane electrolysis (Electrodialysis)

This is a methodology that makes use of a ion-exchange membrane to retain ions that flow through it by the application of an electric field [37]. It has been used to separate specific ions from water taking advantage of the movement caused by the current but different to electrodeposition, cations do not reach the cathode surface, instead they are contained by a membrane. This is generally used to separate a metal when is combined in binary or tertiary solutions. The method is based on electrochemical interactions between these species and an electrical field produced in an electrodialysis cell. In order to achieve the separation, sometimes a complexing agent is added to modify the charge [38]. Figure 2.3 shows the typical configuration of an electrodialysis cell.

Cobalt cations have been removed from water using the electrodyalisis method from binary solutions containing nickel with the use of Ethylenediaminetetraacetic

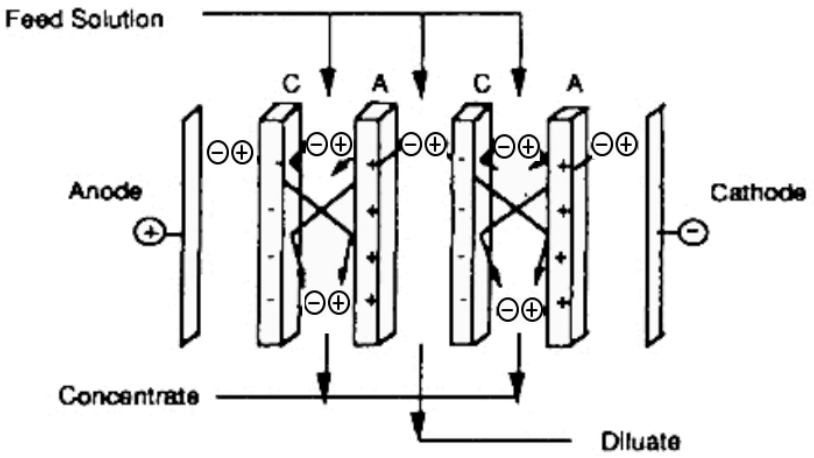

Figure 2.3: Schematic representation of a typical electrodyalisis cell [39]

acid (EDTA) as complexing agent [40]. In general, the major limitation of all electrochemical methods is the high energy consumption for both separation and electrode regeneration. Also a large amount of toxic solids is usually generated.

2.1.5 Adsorption and Ion Exchange

Adsorption is broadly defined as the accumulation of matter on a surface by physical or chemical interactions. Sorption is a concept that involves several processes and mechanisms where substances are attached to the adsorbent surface. In the heavy metals removal from solution, different processes can occur with different theoretical background which are subject to different conditions. The main mechanisms are a combination of ion exchange, adsorption and/or precipitation depending on the media conditions such as pH and ionic strength, it is a hard task to differentiate when exclusively one mechanism is actually happening. Adsorption is currently the most promising technology in the removal of toxic metals from water because is easy to implement and costs are relative cheap. In order to reduce costs, a new generation of low-cost adsorbents have been investigated in recent years. A brief description of current adsorbents used in heavy metal adsorption is given here. Notice that in this section zeolites are classified as adsorbents and ion exchangers without distinction.

2.1.5.1 Adsorbents

2.1.5.1.1 Activated Carbons Activated carbons are popular adsorbents and are defined as "a highly porous material (generally microporous) produced from a carbon-rich precursor by some form of chemical or physical activation" [41]. Main sources are wood, anthracite and bituminous coal. Carbons usually posses high BET surface area, up to 3000 $cm^2\ g^{-1}$. The activation concept is related to the generation of *active* sites, i.e. functional groups that are provided by chemical or physical means. Typically, an activation method involves two steps: first, the raw material is *carbonised* under non-oxidising atmosphere at high temperatures, and second, a catalytic activation is carried out using different chemical compounds such as zinc chloride, phosphoric acid, sulphuric acid and potassium hydroxide [42]. Two main types carbons can be considered: non-ordered porous carbons and ordered porous carbons. The most representative of the non-ordered ones are the carbon blacks and the ordered are represented by carbon nanotubes, mesoporous carbons and fullerenes [41]. However, the application of these materials has gained more importance in gas storage and other applications where a profit can be obtained. On the other hand, in the adsorption of heavy metals from solution, the preparation of these kind of materials is prohibitive due to their costs. In order to overcome this, low-cost active carbons have been prepared from more than two decades by many research groups. The main consideration for a carbon or any adsorbent to be considered low-cost is a small amount of processing and its abundance (it can be a by-product from industry [43]). The materials selection mainly depends on the availability. Some examples are: bagasse, bones, lignite, coffee grounds, pulp-mill wastes, wasted tires, rubber, coir pith (coconout fibre), nut shells, fruit pits, peat, rice hulls, sawdust corn cob, sunflower seeds, sugar-beet sludge, newspaper and many others [42]. The activation process is similar. If temperature and concentration are varied, different porous properties can be obtained.

Cobalt has been removed from water using different precursors of low-cost activated carbons such as apricot stones (30.07 $mg\ g^{-1}$) [44], hazelnut shells (13.88 $mg\ g^{-1}$) [45],

almond shells [46], almond green hull (45.5 mg g^{-1}) [47], bagasse pith [48] (153 mg g^{-1}) among others. Also copper has received enormous attention, Cu^{2+} ions adsorption has been reported on carbons prepared from apricot stones (24.08 mg g^{-1}) [44], almond shells, olive and peach stones under CO_2 atmosphere (7.1 - 9.2 mg g^{-1}) [49], eucalyptus bark (28.3 mg g^{-1}) [50]. The adsorption on these materials have been modelled mainly using Langmuir and Freundlich models.

These materials have been probed to be an alternative to expensive adsorbents such as ion exchange resins in developing countries. However, activation processes are expensive due to high levels of energy required for the activation, and sometimes the use of non-environmental chemical reagents limit their use.

2.1.5.1.2 Zeolites Natural materials have been used as adsorbents due to being inexpensive and abundant. Natural zeolites represent promising materials in environmental remediation or prevention since they have good removal capacity, non-toxicity, efficiency, high mechanical stability, and they are cheap [51]. Natural zeolites have been identified in many regions of the world. Deposits with promising applications have been discovered in Mexico, Iran, Turkey, United Kingdom, Greece, Italy and Jordan [52]. Among natural zeolites, clinoptilolite is the most abundant and it has been tested in the removal of many heavy metals. Also, modified clinoptilolite has been investigated in the soprtion of Cu^{2+}, Mn^{2+} and Zn^{2+} ions [25]. The ions that are inherently present within zeotype material can be exchanged due to being weakly linked by electrostatic interactions. Therefore, external cations in solution can take the place of the original cations under specific conditions. External factors that influence the ion exchange process are: the nature of cations, temperature, pH, initial concentration of cations in solution and anionic species present in solution [53, 54]. It is important to point out that modelling adsorption process differs from ionic exchange because this always has stoichiometric relationships; although, often it is a hard task to demonstrate which phenomenon is occurring either adsorption or ion exchange, and the modelling of ion exchange has been carried out as the modelling of adsorption [55].

2.1.5.1.3 Other Low-cost Adsorbents In practice, although their regeneration is expensive, synthetic resins are preferred over natural materials. They have been shown to be more efficient and have higher capacities than other market competitors, although as expected synthetic resins are far more expensive materials. The most common synthetic resins have very acidic sulphonic sites and also, weak acidic resins having carboxilic groups as exchangeable sites. [25]. Nevertheless, many other low-cost materials or even wastes have been explored as adsorbents of heavy metals. A brief description including biological wastes, agroindustrial by-products and natural clays and zeolites are reviewed. In addition, their applications in the removal of cobalt and copper is reviewed. It is necessary to say that local problems should be addressed by local solutions.

Natural products such as clays and other ceramic materials; industrial by-products such as fly ash and iron wastes from foundries and agroindustrial residues also have been evaluated as low-cost adsorbents [22]. The removal of copper has been reported with natural zeolite (25.4 mg g^{-1}) [56] and natural clay kaolinite (0.919 mg g^{-1}) [57]. Both following similar methodologies, in this the improvement can be related to crystalline and porous features of zeolite over clay. Main limitations using zeolites and clays is the scale-up process, they can work at laboratory level but in industrial practice they still have some major drawback. The fine zeolitic powders cause blockage and are eluted within the output flow.

Plant wastes have been used as adsorbent with and without chemical treatment. Chemical modification has shown to enhance the adsorption capacity for heavy metal ions. Different plant wastes such as rice husk, corn cob and leaf, grape stalks, orange peel, shells (nut, pecan, hazelnut and more) [58]. Some investigations show the simplicity of use with little processing, giving good selectivity and efficiency. Usually, the chemical modifying agents are bases, acids and some oxidising agents. Bases such as NaOH, $Ca(OH)_2$, Na_2CO_3; mineral acids such as HCl, HNO_3, H_2SO_4; organic acid such as citric and tartaric; and H_2O_2 as oxidising compounds have been used to modify plant residues [58]. Growing plants have shown to have less adsorption capacity, nev-

ertheless, the removal mechanism is not straightforward. Living organisms have many different ways to uptake the metals thus characterisation of the biochemical process is no always well defined. Also, another limitation is that intrinsic features such as chemical and biological oxygen demand can threaten aquatic life in a real practical application [58].

Chitosan has been widely used as low-cost adsorbent. Chitosan is "a linear copolymer of d-glucosamine and N-acetyl-d-glucosamine produced by the deacetylation of chitin[1]" [59]. Chitosan has been obtained from residues of fishery, mainly from shrimps, lobster and shells [52]. Usually chemical modification is needed, and since it is a non-porous material, capacity can be limited due to its low surface area.

Cobalt has been removed from water using different substances with/without modification: lemon peel (22 mg g^{-1}) [60], Coir pith (12.82 mg g^{-1}) [61], marine bacterium (4.38 mg g^{-1}). In addition, copper (12.3 mg g^{-1}) by carrot residues, soy bean hull (154.9 mg g^{-1}) [62] acid-treated clay (83.3 mg g^{-1}) [63], banana and orange peel (4.75 mg g^{-1}) [64] and peanut husk (8.5 mg g^{-1}) [65].

2.2 Summary

It is clear that there is no an uniform methodology to asses the adsorption capacity of materials in terms of concentrations and how isotherms have to be constructed. The main reasons why adsorption performance can not be compared between different adsorbents are the lack of uniformity in experimental conditions due to different variables depending on the research group. Also, the occurrence of different mechanisms that occur varies in each material. Commonly it will then be a compromise between the cost of the adsorbents and performance, maybe spending time and resources in the preparation of materials could be compensated by the low or non-cost of natural materials.

[1]Chitin is a polymer derivative of glucose, it is present in the exoskeletons of marine crustaceans, insects and other species

The ideal adsorbent features are: a reproducible and regular material, with enhanced and controllable adsorption capacity, high adsorption uptake, mechanical and chemical stability, consistent in size and textural properties and compatible with scale-up process. Low cost, chemical and mechanical stability, efficient, and it allows fast transfer rates.

Currently, the development of new environmental technologies for the removal of heavy metals is focused on reduction materials and operative conditions. A simple implementation is imperative. The concentration reduction has to be achieved by one of several joint methods. It is clear that there is not an unique methodology which is totally effective. All methods find their suitability depending upon the required performance and effectiveness.

In the next chapter, a complete description of the main characteristics of zeolites is presented. This includes historical review; theoretical background about structure, porous and chemical properties; methods for their production and some relevant materials.

Chapter 3

Porous Media and Zeolites

3.1 Introduction

Porous materials are of particular interest due to their ability to interact with matter at an atomic level, not only at the outer surface but also the inner space, providing increased active surfaces. Porosity is a concept related to the texture of a particular material and it is associated with the number of voids in a solid matrix. A more formal definition states that porosity is "the fraction of total pore volume over the total or apparent volume" [66]. Porous solids can be classified based on the availability of their pores to an external fluid [5], basically there are two main categories: those pores with an access pathway to the outer surface of the particle called *open pores* and those ones which are isolated, known as *closed pores*. Furthermore, Rouquerol [66] classifies the pores as closed, interconnected, blind and through. These different types of pores can be observed in Figure 3.1.

Although the closed pores contribute to material's properties, such as density or mechanical strength, these pores are inaccessible, thus, they are practically useless in many applications based on the porous features such as adsorption or catalysis [67]. In addition, a different pore classification is based on their shape: cylinder, conical, slit and ink bottle as shown in Figure 3.2. Different characteristics can be present in these shapes in porous materials. Usually, these shapes can be identified by gas physisorption

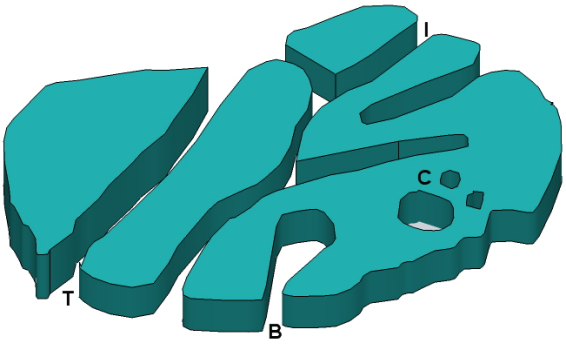

Figure 3.1: Types of pores: (C) closed, (I) interconnected, (B) blind and (T) through, adapted from [66]

analyses and/or electron microscope [68].

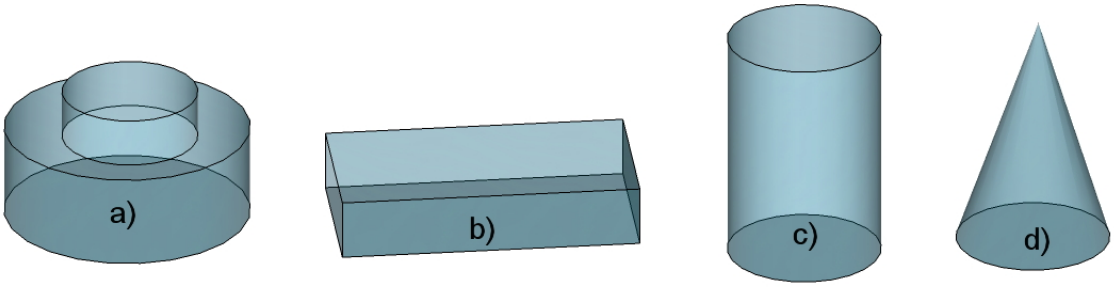

Figure 3.2: Classification of pores based on their shape. a) ink bottle, b) slit, c) cylindrical and d) conical, adapted from [68]

Additionally, the International Union of Pure and Applied Chemistry (IUPAC) categorises the pores according to their width [69]:

- Micropores: Pores with widths lesser than 2 nm.
- Mesopores: Pores of widths 2 nm but less than 50 nm.
- Macropores: Pores with widths larger than 50 nm.

Zeolites possess unique characteristics such as increased surface area compared to conventional minerals, crystalline features, ion-exchange capabilities and an interconnected-porous system with very consistent size and shape [70]. These characteristics have made zeolites useful in a wide spectrum of applications.

3.2 Zeolites

3.2.1 Background

In 1756 the mineralogist Axel F. Cronstedt discovered and gave name to the first zeolite. He coined the term zeolite (from Greek, *zeo* "to boil" and *lithos* "stone") when he observed that this kind of *rock* was able to retain water within its structure, and when it was heated, the water evaporated [71]. Originally, this mineral was believed to be stilbite, but a more recent study has demonstrated that actually it was a mixture of mineral phases in which the predominant one was stellerite, with less of 10 % of stilbite [72]. However, for more than two centuries, zeolites had few practical applications and they were only considered as geological curiosities [73].

Over a long period more types of zeolites were found in nature, but only in small quantities and the attempts to purify them just led to crystallinity loss and other damage to final products. Nevertheless, some later contributions led to the first industrial applications of zeolites. In the mid-nineteenth century, a pair of articles referring to the ion exchange properties of zeolites were published. In 1850 Wey and Thompson [74] explained that some types of soil were capable of retain various compounds from aqueous media, and at the same time they could release others. Later, in 1858 H. Eichorn [75] demonstrated the cationic exchange properties of certain natural zeolites and these began to be applied in the treatment of hard water and the detergents industry.

In 1932, J.W. McBain [76] established the *molecular sieve* concept after he analysed the previous work made by O. Weigel and E. Steinhof [75]. In that article, they found a relationship between the pore size of zeolites and the type of molecules that were trapped in their interior. McBain grouped these concepts and explained that molecules having smaller dimensions could *travel* through the zeolites inner pores, while larger molecules were rejected simply because they did not fit.

At that, researchers were interested in the preparation of synthetic zeolites in laboratories in order to expand the application horizon. Initially, it seemed imperative to achieve high pressure and temperature conditions, to emulate how natural zeolites

from volcanic rocks were originally formed, this was impractical in energy costs terms. Geological studies led to the discovery of more natural zeolites in sedimentary rocks at upper layers of the earth, i.e. formed at milder pressure and temperature levels [77].

Nevertheless, the very first synthesis of a well-identified zeolite in laboratory was achieved by Richard M. Barrer in the 1940s [78]. For the synthesis, Barrer applied hydrothermal techniques and some well-developed methodologies used in organic chemistry. Previously, in 1938 he published a work where established that certain natural zeolites types were capable of trapping some molecules but not others in their structure. The molecular sieving properties in zeolites, as McBain had established previously, were recognized and confirmed [79]. In 1948, Barrer succeeded in producing chabazite and mordenite zeolites under relatively high temperature conditions ($\sim$270 °C) [80]. These contributions led to him being recognised as the father of zeolite chemistry.

R. Milton, who in 1949 was studying the adsorptive capacities of different materials, successfully discovered and synthesized zeolite X and A at milder temperature conditions ($\sim$100 °C) [70], then, the commercial explosion of zeolites began and even today these species are two of the most popular and remarkable zeolites used in industrial applications such as adsorption. By the mid-1950s R. Milton and D. W. Breck prepared zeolite Y, the synthetic counterpart of faujasite [81], a material that has been widely used in catalysis applications.

Although the use of hydrothermal techniques for minerals synthesis were reported before Barrer's contributions, it was not possible to identify them properly due to the lack of available and accurate characterisation techniques and also, the technical difficulties replicating those experimental protocols [55]. The development of X-Ray Diffraction (XRD) acted a key role in the progress of zeolite science. In a recent work published by Baur and Fischer [82] it is said that the first to determine the crystal structure of a particular zeolite type using X-ray diffraction, was the Dutch chemist F. M. Jaeger in 1929. However, other textbooks recognise Pauling as the pioneer in utilising XRD techniques for the zeolite phase identification in 1930 [75]. Both contributions helped to determine the exceptional structure of zeolitic materials.

Over the next two decades, petrochemical and detergent companies made developments and found different applications for zeolites. For example, Mobil Oil began to use the X type in reactions with hydrocarbons and by the end of the 60s, materials with high silica ratios were synthesized [83]. In a similar way, Henkel (a detergent company), solved an environmental issue when zeolites were used to substitute phosphates by mid-70 [77].

In 1967 the International Zeolite Association (IZA) was established. IZA has developed a structure code for the proper zeotype materials identification, that is applied to particular structure types but does not indicate any aspect of chemical composition. Thus, for example zeolite types A, X and Y, and ZSM-5 are *officially* known as LTA, FAU, and MFI (for Linde Type A, Faujasite, and Mobil Five) respectively [84, 85]

During the 1980s, two new families of molecular sieves were discovered by researchers from Union Carbide: aluminophosphates (ALPOs) in 1982 and silicoaluminophosphates (SAPOs) two years later. Both ALPOs and SAPOs were found to share some features and applications with traditional zeolites but with the main characteristic that they have phosphorous in their framework providing them with different structures [86, 87]. Later studies have demonstrated their improved thermal stability in catalytic applications [88].

Porous molecular sieves with larger dimensions than micropores had been synthesised previously, but it was not until the 1990's when the mesoporous materials started to have a significant importance in both catalysis and adsorption fields due to their capacity to host larger molecules in their inner surface area and extended pore volume [89]. The advances in mesoporous materials have led to the theory that it is possible to develop mesopores in any inorganic oxide. For example: titanium, zirconium and other oxides have been synthesized in their *meso* form [70].

In time, natural and synthetic zeotype materials have become one of the most significant materials in contemporary technology and theoretically more discoveries of new compositions and structures and consequently more applications are expected. Nowadays the molecular sieves production and application in industrial processes, in

which zeolites play the most important role, is a multimillion pound industry. In 2008 about 1.8 and 3 million tons of synthetic and natural types, respectively, were consumed. The price of these functional solids ranges from £1.00 to £12.00 per kg depending upon the class of substance and applications [77].

3.2.2 Definition

Zeolites belong to the minerals family and more specifically they are classified as aluminosilicates with a well-defined crystalline structure. Their main constituents include aluminium, silicon and oxygen. These elements are arranged in tetrahedral structures of SiO_4 and AlO_4 which in turn form the different types of three-dimensional zeolitic frameworks depending on their arrangement [90]. Central atom, Al or Si, is bonded by covalent ions to four oxygen atoms, as can be seen in Figure 3.3. The central atom is also known as T atom and the formula TO_4 is often used to define it along with the oxygen atoms.

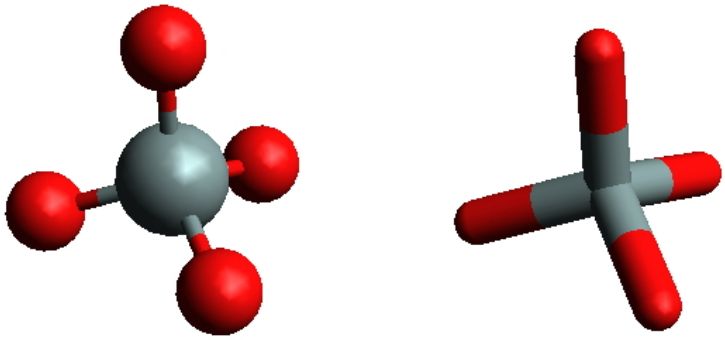

Figure 3.3: Basic tetrahedron where central atom represents the T atom and oxygen is represented by red spheres; a stick model is also represented

Zeolitic tetrahedra have a characteristic negative charge in their structure, which is generated when Al^{3+} replaces Si^{4+} in the lattice. For this reason, ions that include potassium, calcium, sodium, magnesium and water molecules are present in zeolites to balance the negative charges [53]. This characteristic provides zeolites the ion-exchange properties due to these "balancing species" being loosely bonded to the framework mainly by electrostatic interactions. In contrast to other amorphous aluminosilicates,

zeolites have a particular periodic structure and a well-defined porosity typically defined in the microporosity range.

Zeolites have the general formula [91]:

$$M_{x/n}(AlO_2)x(SiO_2)_y \tag{3.1}$$

Where n represents the cation valence M, x and y are the total number of tetrahedra that are in each unit cell and y/x is the atomic ratio between Si and Al, it can take values from 1 to infinity.

The term *molecular sieve* is a more general concept that includes porous materials whose pore diameter ranges from 0.3 to 2.0 nm, including both amorphous and crystalline phases [55]. Thus, zeolites along with carbons, oxides and others sub-groups fit within the definition of molecular sieves. R. Szostak explain the differences between each group saying that zeolites are aluminosilicates, in which only Al or Si atoms occupy the centre of the tetrahedron, while molecular sieves could have different chemical compositions [92]. Furthermore, the presence of aluminium, or only silicon in the case of silicalite, is required within the zeolites unit cell. Additionally, the anionic framework in zeolites makes it different to the variable charge in molecular sieve framework. Also, the term *zeotypes* is used to denote related materials which are beyond the typical zeolites definition, i.e. materials with elements other than Si and Al replacing the T atom and/or having porosities larger than the micro- level, e.g. the substitution of gallium, germanium and other species have been reported [93, 94].

3.2.3 Structure

3.2.3.1 From Basic Building Units to Frameworks

Many of the properties that make zeolites attractive are controlled by their structure. The zeolite framework construction begins with the simple tetrahedral structure known as primary building unit (PBU). PBUs are linked by the oxygen atoms positioned at the corners in the individual tetrahedra, since the T atom is in the centre of the PBU,

each oxygen atom acts as a bridge between two T atoms. The formula TO_4 is accepted to describe the PBU [95], The union of two T atoms is shown in Figure 3.4.

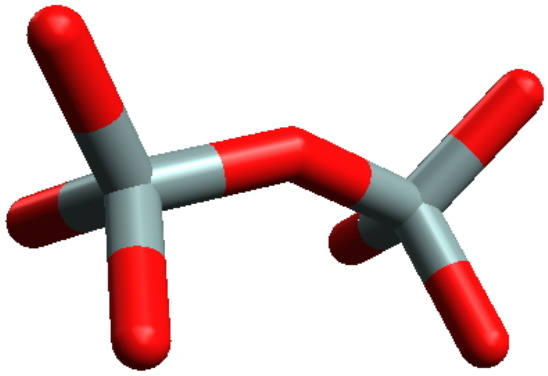

Figure 3.4: Two Primary Building Units (PBUs) linked by one oxygen atom

The framework type describes how the T atoms are interconnected and distributed through the three-dimensional network. Each zeolite has a particular framework type, which also defines attributes such as topology and pore dimensions [96]. The framework provides the identity to each zeolite irrespective of chemical composition. However, there exists a restriction when the TO_4 tetrahedra are linked with each other. According to the Lowenstein's rule [96], there cannot be any Al-O-Al links, i.e. two AlO_4 tetrahedra neighbours, this is attributed to the negative charge present in each PBU, which generates unfavourable interactions when zeolites are formed. For this reason the minimum Si/Al value in any zeolite framework is always 1.

The linkage of several PBUs leads to the formation of more complex structures named secondary building units (SBUs) [97]. The most simple types of SBUs are known as rings, and they are classified depending on the number of T atoms. For example, if a ring is composed of four T atoms, then the ring is a 4-ring and so on. Pores in zeolites that are surrounded by a number of rings can be classified as small (8-rings), medium (10-rings), large and extra large (12 and 14-rings respectively) [6]. When ring delineates an orientated face of the three dimensional framework, then the term *window* is applied. It is possible to find frameworks in zeolites that range from 4 to up to 20 rings [6, 96]. In Figure 3.5 are represented 4-ring and 12-ring windows.

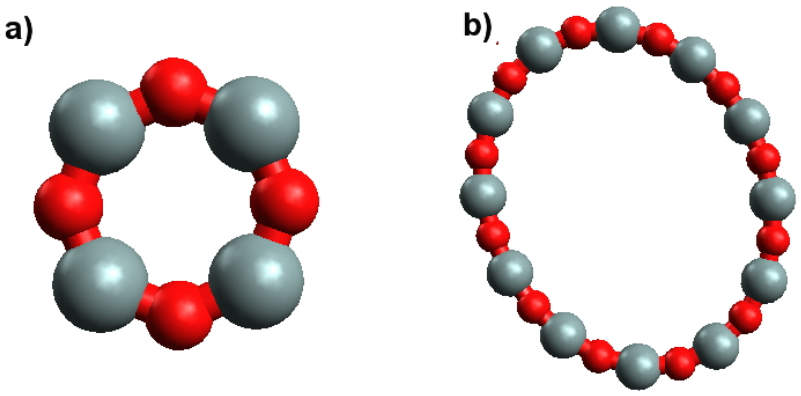

Figure 3.5: a) 4-ring and b) 12-ring windows, considered to be small and medium-size windows respectively

When these rings are assembled, a more complex cage structure of SBUs is formed. Meier originally presented eight different types of cages [97], but with the characterisation techniques development the identification of more cages has been possible. These cavities are categorised in terms of their type and number of rings [6]. For instance, a $[4^6 6^2]$ cage has 8 windows in total: 6 are formed by the 4-rings and 2 by the 6-rings. Several examples of rings can be observed in Figure 3.6 and under each figure the correspondent classification according to their number and rings type.

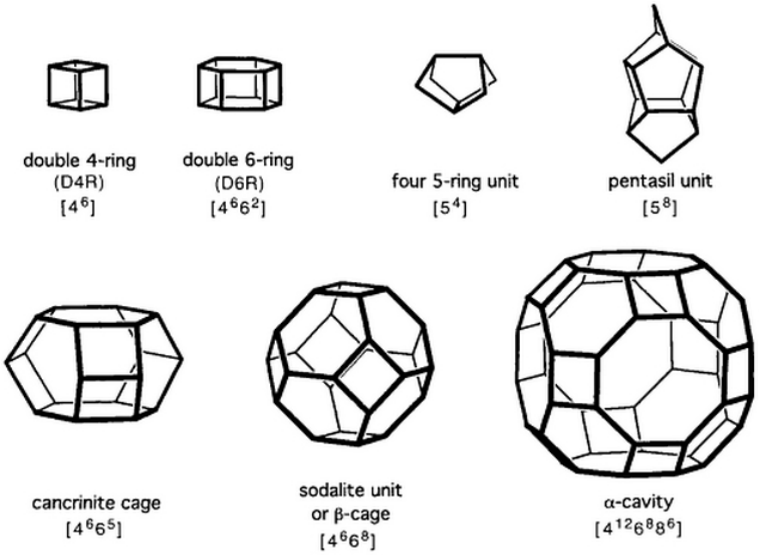

Figure 3.6: Several types or cages for the formation of zeolites frameworks [98]

As can be seen in the graphical representation of cages, the presence of the oxygen atoms, as connecting atoms between T atoms, are omitted for a better understanding

of the overall structure.

In addition, some zeolitic structures are identified using Greek lettering. For example, the α-cage or $[4^{12}6^8 8^6]$ and β-cage (sodalite cage) or $[4^6 6^8]$. The latter is famed because it is present in the framework of the widely used zeolites A, X and Y [53]. In fact, zeolites X and Y share same framework, FAU, but they have different chemical composition. Finally, the cages and rings connections produce the formation of channels and pores in one, two or the three dimensions [97]. The channels intersection leads to the creation of the whole zeolite framework. Figure 3.7 shows the LTA framework arrangement having the α-cavity as the inner void.

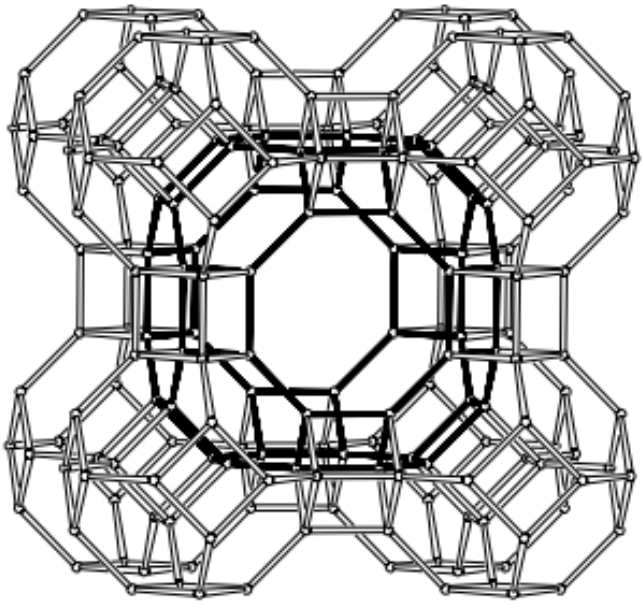

Figure 3.7: The intersection of cages leads to the formation of the framework of zeolite A or LTA. The inner void is known as α cavity [85]

Thus, the well-defined porosity features in zeolites has its origin in the enormous possibilities of periodic arrangements that these channels can create.

3.2.3.2 Nomenclature

The Structure Commission of the International Zeolite Association (SC-IZA) is the organisation responsible for assigning the codes for the proper nomenclature of the zeolite frameworks. The codes are also accepted by IUPAC. The nomenclature code is

based on three Roman capital letters and only defines the T atom network topology, independent of the chemical composition or symmetry [85]. For example, LTA, MOR or FAU. If there exists an interrupted framework, i.e. one that periodicity breaks at some point, a hyphen is written before the code, for example -CLO, -LIT or -PAR. The letters used are often determined by reasons such as: the place where the material was found or discovered, a researcher name, the name of a company or if the material presents some specific property [84] and so on. To July 2014, the SC-IZA had assigned codes to 218 zeotype frameworks [99].

3.2.4 Chemistry

3.2.4.1 Si/Al ratio

It is common to find a molecular sieves classification based on their chemical composition. Often, this composition is related to the amount of Al atoms per Si present in the framework, the so-called Si/Al ratio. Having in mind that the minimum ratio is Si/Al equal to 1 according to the Lowensteins rule. Low Si/Al ratios are those materials that have Si/Al in the range of 1 - 1.5, intermediate ratios in range 2-5 and high ratios equals to 10-100 [77]. Very rare materials have ratios above 100, moreover are considered as pure silica zeotypes.

Zeolites with low Si/Al ratios, i.e. high aluminium content, are hydrophilic and have well-defined polar features [6]. Also, these kinds of materials exhibit an increased cationic exchange capacity because of the presence of considerable aluminium quantity and as consequence easy-to-exchange cations attached to their anionic framework as shown in Figure 3.8. Potentially, each Al atom in the framework represents an exchangeable site, as the presence of Al leads to unbalanced charges in the zeolite structure [92]. Higher Si/Al ratio zeolites show hydrophobic behaviour and less polarity than low-ratio materials. Nevertheless, silica-rich zeolites having lower cation exchange capabilities, have enhanced chemical and thermal stability [6].

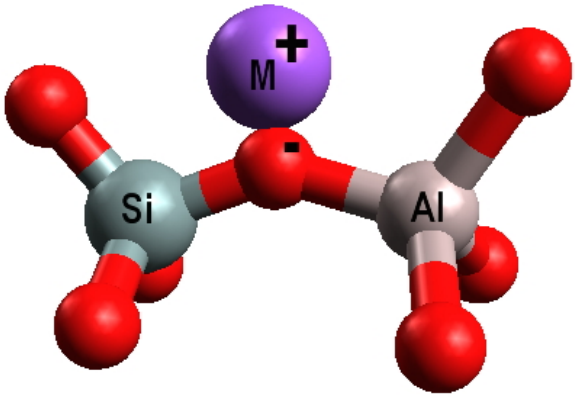

Figure 3.8: Ion exchange in zeolitic materials. Negative charge is associated to the aluminium presence and M represents a cation [91]

3.2.4.2 Cationic Exchange Capacity (CEC)

The cationic exchange capacity (CEC) is defined as the total amount of exchangeable cationic species within the zeolitic framework [100]. This plays a paramount role when choosing a particular material to use it in ion exchange processes. CEC is related directly to the Si/Al ratio [100] and it can be determined simply by the chemical composition of the zeolite or formula. Apart from the original framework cations, the secondary source of cationic exchange capacity is associated to the structural faults in zeolitic materials and it has been demonstrated to have a strong influence, specially for those species with high silica ratios [101]. The relatively high CEC values of zeolites A, Y and X are 7, 6.4 and 5 meq/g respectively [53]

The extra-framework species is the consequence of having an electronically unbalanced framework. Although the chemical composition of the synthetic zeolites is related to the experimental pathway, the adsorptive and ion exchange capacities are influenced by the presence of these attached species, which often are inorganic ions such as Na^{+}, Ca^{2+}, Li^{+}, Ba^{2+}, Cs^{+} and K^{+} but also organic species and protons [55, 102, 103]. The position and amount of these ions can also affect the performance of zeolites, these extra-framework cations have been studied in order to correlate the amount and distribution with the performance in particular processes such as adsorption and ion

exchange [103].

3.2.4.3 Acidity

Reactivity in zeolites is based on their active acid sites which are provided by the negative charge as a consequence of aluminium atoms present in the framework. Theoretically the higher aluminium amount, low Si/Al ratio, the increased chemical activity. Although reactivity can be also regulated by the porous (structural properties) cha rønsted and Lewis acidity definitions have been useful to understand the chemical activity of zeolites [104] mainly in reactions occurring in the petrochemical industry. In order to understand the chemical reaction mechanisms using zeolites, the Brønsted acid sites are provided by the H^+ groups contained in the surface, which act as protons donors. Moreover, and according to Lewis acid definition, to accept a pair of electrons [105].

In Figure 3.9 the most common method for the activation of zeolites can be seen.

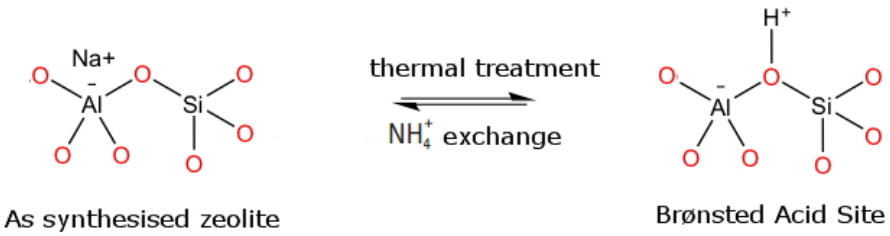

Figure 3.9: Generation of Brønsted acid sites in zeolites [106]

This method is based on providing to zeolite surface with active acidic sites by the substitution of original cations with NH_4^+ ions by ion exchange method and a consequent thermal treatment to generate the protonated zeolite form H^+ [106]. Typically, zeolites have an amphoteric character depending on the substances with which they interact. The main methods to characterise acidity in zeolites are Temperature Programmed Desorption (TPD) and methodologies involving spectroscopic techniques as Nuclear Magnetic Resonance (NMR), Infrarred (IR) and X-Ray Photoelectron Spectroscopy (XPS) [107].

3.3 Synthesis of Zeolites

Natural zeolites original formation has inspired scientists to develop synthetic approaches. The processes by which zeolites were formed have been replicated and modified in order to obtain the same or different materials, sometimes, with totally different properties as a final product. Usually, the zeolitic materials formation in nature is carried out under hydrothermal conditions regardless of their origin [108]. The aim of earliest synthetic routes was to reproduce closely the conditions in which natural zeolites were produced.

3.3.1 The Hydrothermal Method

The hydrothermal concept is defined as "heterogeneous reactions to dissolve and recrystallise materials that are relatively insoluble under ordinary conditions" [70]. Hydrothermal methodologies, as the name suggests, usually are carried out using water under relatively high pressure levels (1-100 MPa), generally autogenous, and at high temperature (100-1000 °C) [70]. Although a more recent definition states that hydrothermal procedures are carried out above ambient temperature and 1 bar [109]. In this method the pressure increases as a consequence of temperature, the pressure at the interior of the reactor is rarely known but the value that is taken as reference corresponds to the vapour pressure at that temperature. Sometimes when a different solvent is replacing water the method is generically called solvothermal. Some authors have gone further, calling the process according to the solvent used, for instance; glycothermal and ammonothermal [110].

A hydrothermal environment requires the presence of alkaline media in the form of basic solutions [111]. The fundamental species needed for the formation of zeolites in laboratory are: a source of silica (SiO_2), a source of alumina (Al_2O_3), an alkaline media and a solvent. All are put together to react under high temperature conditions to achieve the crystallisation after an ageing[1] period. Cundy [112] summarises a typical

[1] Ageing is not a compulsory step in the synthesis process

process for the zeolitic materials production following the hydrothermal method:

1. Amorphous sources of silica and alumina are dissolved and conditioned together in highly alkaline solutions in which are present cations, for example, NaOH or KOH. The sources selection is vital since the formation process involves the dissolution and remineralisation of silica and alumina species.

2. Heat is applied to previously formed mixture which often takes place inside of a sealed autoclave[2]. The purpose of this is the generation of pressure to accelerate the formation of products.

3. A period called induction time then occurs. The amorphous gel reaches the reaction temperature. In this time period, precursors remain amorphous and no crystallographic phases are detected. Induction time finishes when the very first crystals start to be formed.

4. After the induction time, gradually almost all the material is converted into crystals, this stage is the known as the crystallisation period.

5. Final stage occurs after crystallisation, the recovery is done by filtration, washing and drying. If templates were used, calcination process at high temperature is carried out to remove them.

All scientific and technological developments in the zeolite field have been achieved thanks to the manipulation and exploration of several key factors. In general, the main factors to consider in zeolite and zeolite-like synthesis are composition, reaction variables (such as time and temperature) and reaction kinetics (mechanisms). These concepts are described.

[2]An autoclave consist of a inner non-reactive Teflon-lined, the outer part is a stainless steel jacket able to support high pressure conditions

3.3.1.1 Composition

In order to obtain the desired Si/Al ratios, reaction mixtures are formed by the corresponding amounts of SiO_2 and Al_2O_3 precursors. There are a wide range of possibilities and typical sources include precipitated silica powders, silicates, colloidal silica sols, gels, and clay minerals for SiO_2. Also aluminium alkoxides, aluminium salts, aluminates, aluminium hydroxides (including clays) for Al_2O_3 [111, 113]. Agroindustrial wastes with a high silica content, have been used as an alternative silica source [114]. Most of the time the component that allows the formation of Al-O-Si linkages is the hydroxide ion OH^-, but also F^- has been used as mineralising agent in production of other molecular sieves that include species substitution such as Fe and Ga in the T atom position. Regardless of the specific product, the alkaline media, generally in aqueous solution form, acts as a mineraliser agent.

The direct consequence of having OH^- ions in the reactive mixture is a high pH, which dissolves SiO_2 and Al_2O_3 precursors, is leading to the creation of new chemical bonds between T atoms and oxygen. The OH^- ions concentration has a strong influence on crystal growth rate which is improved at higher pH levels [55].

The solvent is also responsible for reagents mobility. The greater mobility, the more interactions between them. This is governed by how soluble are the sources which in turn is governed by the supplied energy to the system.

3.3.1.2 Temperature

Temperature is a variable that controls the solubility of reacting species. The viscosity decreases as temperature increases and promotes mobility of dissolved species as stated previously. The temperature level in synthesis has a direct effect in nucleation and crystallization rate and also establishes the final framework structure [70].

Zeolites with industrial applications such as X, Y and A type crystallise at low temperature levels ($\sim$100 °C) meanwhile other, such as ZSM-5; crystallize at ca. 180 °C; mordenite and analcime are formed at temperatures above of 360 °C [92].

3.3.1.3 Ageing and Crystallisation

There are two key stages in the zeolite formation process: ageing and crystallisation. Ageing is the period before the crystallization stage and is related to final product yields. The ageing process occurs when the precursor gel is mixed for some time at ambient conditions before induction and crystallisation, ageing has a big impact on the crystal size and yields of the final product. Depending on the nature of reactants or conditions, reaction times can take from hours to months [115].

The crystallisation period has a crucial importance in the synthesis. A reaction mixture under the same temperature and initial composition can lead to different zeolite framework if the length of this period is modified [94]. This effect is explained by Ostwald's rule of successive transformations [84]. This rule states that the zeolites formation involves the transformation of crystallographic phases from one less stable phase, called metastable, to another one more thermodynamically stable. Zeolites are solid metastable phases. For example, zeolites type A and X are metastable phases of zeolite P, i.e. if the heating period of precursors gels of A and X is extended, the final product will be zeolite P. Breck [53] states that artificial zeolites with no natural counterpart could not exist in *true equilibrium conditions* because they are in this metastable state.

Crystallisation fields are ternary diagrams that describe the zones where a specific zeolite is formed [84]. Crystallisation diagrams have been adapted from equilibrium diagrams used in geological science. The composition triangle has "axes" of three main components generally Al_2O_3, SiO_2, Na_2O or H_2O. Certain types of zeolites are formed inside the surface limits where thermodynamically and chemically possible. An example is presented in Figure 3.10

The use of these diagrams has to be used with caution, although they can provide some information about possible combinations in the original composition, zeolites do not represent an equilibrium state. Moreover, other variables involved in the synthesis are not shown in the graphic. In time, zeolites synthesis using microwaves have been

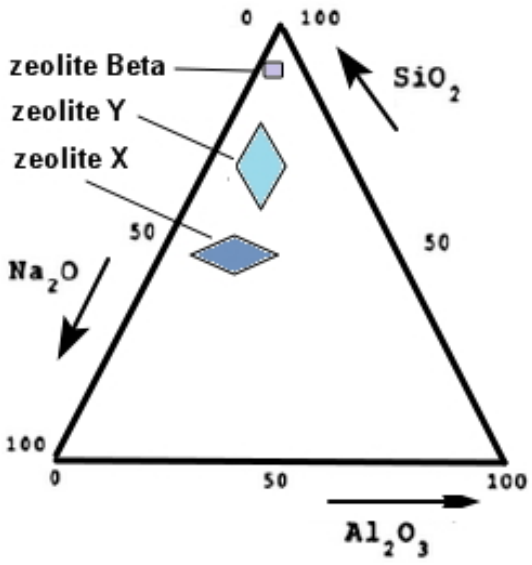

Figure 3.10: Crystallisation fields for several zeolites represented in a characteristic ternary diagram [84]

developed due to the low energy consumption and shorter production times, it has been reported that the synthesis of zeolite type A can be achieved in 1 minute [116]. The main drawback using microwaves as a heating source is the lack of homogeneity in the energy transfer, causing structural inconsistencies in final products.

3.3.1.4 Nucleation

Commonly, the reaction mixture is known as reaction gel and is formed by the suspended alumina and silica precursors in the solvent. The formation of the zeolite phase, starting from the amorphous gel, begins when individual particles are chemically produced under hydrothermal conditions; each of these particles is a single crystal nucleus (the simplest unit of a crystalline phase), thus, this process is known as nucleation. It is proposed that nucleation takes place in the induction time.

In the nucleation process two consecutive stages can be distinguished: primary and second nucleation. The primary nucleation stage can be divided in a) homogeneous and b) heterogeneous, depending on where nuclei are in the same reactive initial solution or if is provided by external means (external nuclei). The secondary nucleation is promoted by already formed crystals in the primary nucleation stage [117].

3.3.1.5 Crystal Growth

After the nucleation stage, the formed nuclei start to grow nurturing from the remaining Si- and Al- components in reactive gel, and at same time they, Si and Al precursors, continue dissolving until depletion of reactants and consequent crystals enlargement, this second main step is called crystal growth [118].

The crystal growth stage can be defined as "a series of processes by which an atom or a molecule is added to the surface of crystals causing an increase in size" [119]. The overall crystal growth process can be summarised in four stages: 1) atoms are transported in the solution bulk, 2) atoms reach the crystal surface and are attached, 3) atoms move on surface and finally, 4) atoms are attached to the edges [119]

Recent investigations based on tracking the synthesis reactions *in situ* with the aid of more sophisticated XRD and electron microscopes, mainly in the field of the clear solutions as model mixtures, has allowed a better understanding of where nucleation finishes and crystal growth begins. However, this thin line where exactly the two phenomena are divided is not completely clear.

In certain zeolites syntheses, such as in zeolite Y, "seeds" have been used. Seeds is the name given to already formed crystals, which in the presence of a "nutrient" solution will promote crystal growth. Also, seeds enhance crystallisation rates of final particles and simultaneously help to direct towards the desired crystalline final product. Actually, the synthesis of zeolite Y without seeds favours the crystal growth of different species leading to a less pure phase and longer crystallisation time periods [114].

3.3.1.6 Structure Directing Agents and Templates

Barrer and Denny contributions [120] about incorporating organic cations with higher charge density replacing smaller ones used in previous experiments, was significant in the developing of new synthetic routes. The practical importance of this modification has had an impact in the thermochemical stability of zeolites, also, organic cations have allowed the creation of novel framework structures with original features, such as higher

Si/Al ratios [70]. Further, it is known that these organic cations can be found occluded in zeolites pores and the shape of the cation could define the shape and size of inner space [6]. For this reason, the term template was employed to refer to these substances; however, as there is not always an exact geometric correspondence between zeolite and cation, and since this effect is not a rule in the host-guest interactions, the concept of structure directing agent (SDA) is used more commonly [108, 115]. A major drawback in using organic templates is that in order to remove them from the framework, high temperatures are required. This imply high costs and also toxic compounds are often generated and released to atmosphere [121].

3.4 Industrially Important Zeolites

3.4.1 Type Y FAU

Zeolite X and Y types have the same zeolite framework FAU. The main difference between the X and Y types is their Si/Al ratios; X type is in the range of ∼1.1 to 1.8 meanwhile in the Y type ranges from ∼1.8 to ∞. [83, 96]. FAU framework has a void volume of 0.47 cm^3 cm^{-3}, i.e. almost the half of its volume is empty when dehydrated; constituting the biggest void in zeolites [53].

Framework density (FD) is a parameter related to the pore volume and does not specify the pores size. This is utilised to differentiate between the zeolytic open-frameworks and other more dense aluminosilicates. FAU has a FD of 17.2 T-atoms/1000 $Å^3$ [70]. To understand how the frameworks are constructed in this material, the idea of assemblage of cages can be used. To build the FAU framework, β-cages (sodalite cages) are linked by double 6-rings [53]. When assembled, the greater three-dimensional void is known as the *supercage* as can be observed in Figure 3.11.

Zeolite Y is one of the most used molecular sieves in the petrochemical industry, specifically in the hydrocarbon conversion. Zeolite Y has an improved thermal stability, because its Si/Al ratio can vary enormously, making it more appropriate for high-

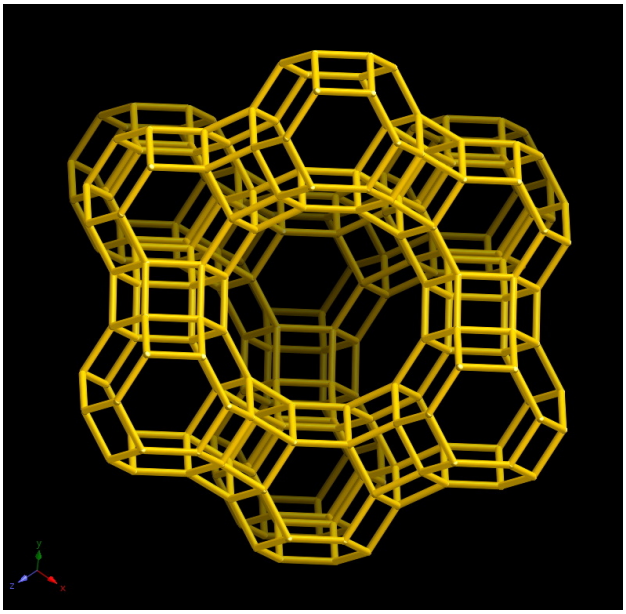

Figure 3.11: Faujasite (FAU) framework [85]

temperature reactions such as petrochemical fuel production [96].

3.4.2 Type A LTA

This framework type is constructed joining the sodalite cages as in FAU framework but instead of using double 6-rings, this structure has double 4-rings [70]. Also, it can be visualised as a cubic array of eight tetrahedra, as shown in Figure 3.12. The void that is made when assembled is called an α-cage.

Generally, sodium is the cation present in the LTA framework. It can allow the flow to the interior to atomic or molecular species as small as 4 Å(zeolite 4A). This number can be changed depending upon the synthesis path. For example, if potassium (K) is present in the framework the pore window is reduced to 3 Å, and if is calcium (Ca) then the window is expanded to 5 Å(zeolite 3A and 5A respectively) [96]. LTA framework has a ratio Si/Al $\sim$1 and framework density of 12.9 T-atoms/1000 Å^3. As the Si/Al ratio is even lower than in FAU, the content of Al is higher. Thus, the amount of exchangeable and loosely bonded cations is higher.

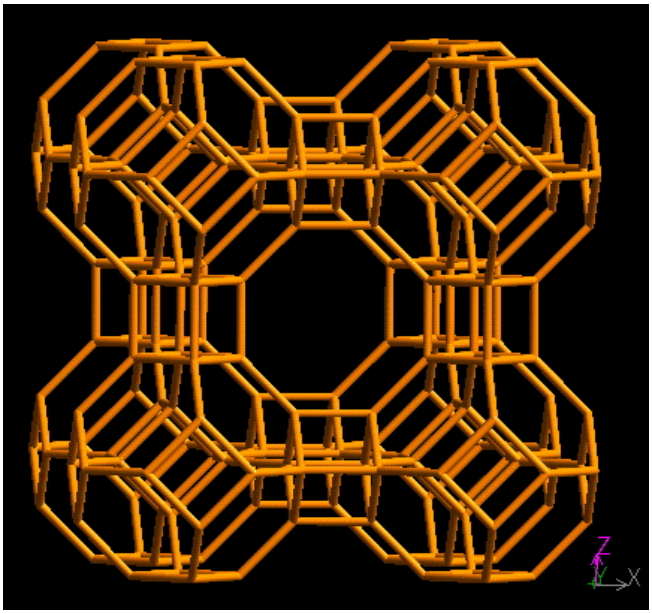

Figure 3.12: Linde Type A (LTA) framework [85]

3.5 Nanozeolites

Recently, researchers have shown an increased interest on the size reduction of diverse materials. The global trend to the "miniaturisation" is well known and finds its origin in the develop of microchips in computer science [122]. In zeolites, the size reduction to the *nano* level has its motivation in the formation of materials with a superior active surface area. A zeolite with more exposed surface area, can provide more intimate contact for chemical species to be adsorbed or exchanged with more specific and selective characteristics allowing a larger number of molecules [123]. For example, it has been shown that LTA nanocrystals gained about 500 % in specific BET area compared to micro sized *traditionally* prepared. Also, the smaller the crystals, the shorter the path to the outer matter to reach the active sites inside porous structures. Thus, diffusion paths are been reduced as exemplified in the sketch shown in Figure 3.13.

Nanozeolites are defined as zeolites in the 0.1-1000 nm range, however, the main importance is considered to those having under 200 nm in the particle size distribution [123–125]. For particles under 200 nm it is complicated to achieve high yields and also difficult to manipulate in the corresponding applications.

Nanozeolites have found application in purification/separation technologies, micro-

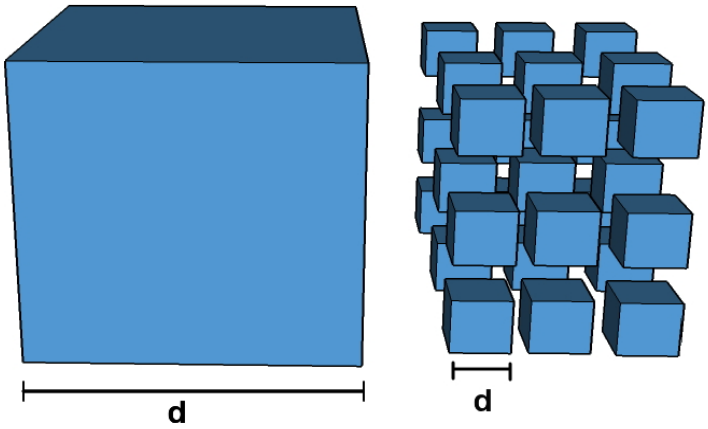

Figure 3.13: Reduced diffusion lengths in nanozeolites compared to a classical micro-sized crystal

electronics, chemical sensing, catalysis and others [123] and are currently contributing to the pollution control by trapping toxic substances within their porosities [124].

3.5.1 Synthesis of Nanozeolites

The synthetic methodologies generally are based on the use of supersaturating agents that favour the nucleation instead of crystal growth. Most of the synthetic protocols involve the formation of the so-called *clear solutions* [123] before the crystallisation process. In order to achieve this, organic structure direction agents such as tetramethylammonium (TMA), tetraethylammonium (TPA), and tetrabutylammonium (TBA) in their hydroxide forms are used to provide as well the high alkaline media required to dissolve completely the silica and alumina precursors (instead of common alkaline hydroxides such as NaOH and KOH) reducing also the temperature levels needed for crystallisation. Additionally, these lower temperature levels also favour the crystal size reduction since is directly proportional to the temperature level [125]. Zeolitic frameworks that have been prepared in their *nano* form are LTA, FAU, MFI, MOR, BEA, ZSM-5 among others.

The main limitations of these syntheses are low yields, longer time periods and the high cost of organic templates. The very high-concentration solutions containing the SDA, needed to achieve supersaturation conditions, make these the more expensive part

of the process. Although new methodologies that recylcle SDA's have been reported, long periods of time are still needed. SDA's use, necessarily will lead to post-synthetic removal of the template confined in the porous structure, generally achieved by the thermal treatment (up to 600 °C). Furthermore, chemical reactions are not that efficient since it has been reported that the maximum yields are usually under 10 % [125], which makes the recovery processes (usually ultracentrifuge) costly due to high-energy demand.

One of the main challenges in the application of nanozeolites is their use in solid state rather than in dispersed colloidal suspensions to take advantage of all described properties. A possible solution can be the use of these materials in hybrid materials in order to optimise their use and reduce their cost, i.e. in form of thin films or coatings.

3.6 Natural Zeolites

Natural zeolites have been used even before the systematic understanding of their properties, since ancient times natural zeolites were used in agricultural applications and construction industry. In agriculture, the presence of zeolites with sedimentary origin has shown good results as soils conditioners: zeolites naturally present in soils allowed a more efficient way to water the crops and act as exchanger between some soil nutrients [126]. Also, ancient Greek and Romans used zeolites as a binder in their constructions [51].

Historically, synthetic materials have been preferred over natural materials in terms of efficiency in profitable applications i.e. catalysis. However, in applications such as pollution control, natural zeolites are a real alternative because of their low cost, efficiency and accessibility [127]. The main disadvantage of natural materials is the lack of purity and consistency. Nevertheless, sometimes these defects have no real effect on applications or they can be negligible, for instance in the treatment of contaminated water streams. However, an extensive characterisation is always required. Some of the main applications of natural zeolites are soil conditioners, animal feed additives,

Table 3.1: Main natural zeolites and their principal cations and cationic exchange capacity (CEC) [51]

Zeolite type	Crystallographic Formula	Chemistry	
		Cations	CEC (meq g^{-1})
Analcime	$Na[AlSi_2O_6]H_2O$	Na	3.6 - 5.3
Chabazite	$(Ca_{0.5}$,Na, K$)_4[Al_4Si_4O_{24}]_{12}H_2O$	Ca, Na	2.5 - 4.7
Clinoptilolite	(MeI, $Me0_{0.5})_6[Al_6Si_{30}O_{72}]$ $20H_2O$	Na, K, Ca	2.0 - 2.6
Erionite	$K_2(NaCa_{0.5})_8[Al_{10}Si_{26}O_{72}]$ $30H_2O$	K, Na, Ca	2.7 - 3.4
Faujasite	$(Na,Ca_{0.5},Mg_{0.5},K)_x$[AlxSi$_{12}$-x$O_{24}$]$16H_2O$	Ca, Na, Mg	3.0 - 3.4
Ferrierite	$(K,Na,Mg_{0.5},Ca_{0.5})_6[Al_6Si_{30}O_{72}]$ $18H_2O$	Mg, K, Na	2.1 - 2.3
Heulandite	$(MeII_{0.5}$, MeI$)_9$ $[Al_9Si_{27}O_{72}]$ $24H_2O$	Ca, K, Na	2.6 - 3.6
Laumontite	Ca_4 $[Al_8Si_{16}O_{48}]$ $18H_2O$	Ca	3.8 - 4.3
Mordenite	$(Na_4$, Ca, $K_2)_4$ $[Al_8Si_{40}O_{96}]$ $28H_2O$	Na, Ca, K	2.0 - 2.4
Phillipsite	(K, Na, $Ca_{0.5}$, $Ba_{0.5})_x$ [AlxSi$_{16}$xO_{32}] $12H_2O$	K, Na, Ca	2.9 - 5.6

municipal and industrial wastewater treatment and the removal of radionuclides and more recently as human food supplement [128].

Natural zeolites with relevance in environmental applications have a volcanic origin. Despite there being more than 60 natural zeolites types that have been found in more than fifty countries only clinoptilolite, analcime, phillipsite, chabazite, mordenite, erionite, laumontite and ferrierite form the majority of their distribution [129]. In Table 3.1 the main natural zeolites and their cations are summarised as well their cation exchange capacity (CEC) based on the correspondent crystallographic formula.

3.6.1 Clinoptilolite

Zeolite deposits are usually near to volcanic areas. The most abundant natural zeolite is clinoptilolite. Clinoptilolite belongs to the framework family heulandite (HEU) and it is characterised for having Si/Al $>$ 4 ratio whereas heulandite family is characterised to have Si/Al = 3-5 ratios [130]. Characteristic particle size distribution ranges the order of micrometers. In Figure 3.14 the 3-D model of heulandite framework is shown.

However, there is an agreement that natural zeolites are structurally asymmetric when compared to synthetic materials. This behaviour is not completely understood yet, but it could be a direct consequence related to different levels of preference for

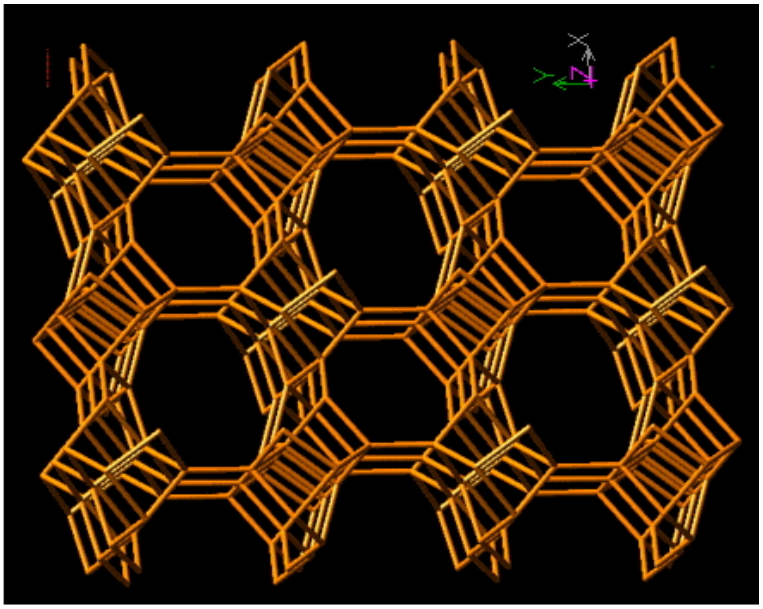

Figure 3.14: Heulandite (HEU) framework [99]

aluminium in certain framework sites where is substituting silicon tetrahedra. The aluminium amount is non-stoichiometric which ends in an "occupational disorder" [128].

To date there has been an agreement that clinoptilolite has a very narrow zone where it crystallises as a pure phase and it is hard to know completely how natural materials have been formed over thousands of years and the original conditions. Several studies have revealed that it is possible to produce heulandite members in laboratory but generally at conditions that demand high temperature (>170 ° C) and longer crystallisation time periods (> 60 h).

3.7 Summary

In this chapter the porous materials importance in different technological fields was reviewed as well the main classification of different porous systems. A comprehensive description of zeolites as part of functional porous materials was carried out. An historical review of zeolites was presented including the initial discoveries, the development of main characterisation techniques and an applications overview along their current

market. Also a theoretical background, covering characteristics that make zeolites attractive materials such as chemistry features and structural configuration, was described. The hydrothermal method involved in the synthetic routes for the preparation of zeolites was explained.

In the chapter was also mentioned that zeolites find in the diffusional limitations its major drawback. Hence, in the next chapter, hierarchical porous systems that have shown to overcome diffusional restrictions, are described. Besides, the description of different methods for the production of hierarchical porous materials is presented.

Chapter 4

Hierarchical Porous Structures

4.1 Introduction

Hierarchical systems are present in many aspects of daily life, from the simplest cell to the most complex organs and systems that constitute the human body. For example leaves on trees, butterfly wings and even fluvial systems. Generally, a hierarchical system is formed by different levels of a particular type of characteristics with the aim to accomplish altogether the same function [131]. These characteristics allow natural systems to perform different tasks simultaneously optimising the use of energy, mass transport and storage as a clear sign of evolution and adaptability.

In materials science, hierarchically structured materials are growing in importance. The observation and mimicking of diverse natural systems have led to the development of synthetic hierarchical structures in many technological fields such as catalysis and separation processes. These materials have shown to have a significant improved characteristics compared to conventional non-hierarchical organised materials [132]. Hierarchical bodies have been explored over the past decades with remarkable results. For example in bioengineering, materials have been used in the tissue regeneration and replacement [133]. In catalysis, chemical reaction performances have been improved with the use of hierarchical catalysts, in part because the reagents have a more intimate contact, leading to a more efficient reactions [134]. In separation processes such

as filtration and adsorption, the matter to be removed finds wider and more accessible *pathways* to reach adsorption sites in porous materials interior.

The main reason why these materials are been used successful in a range of applications is because they have overcame diffusion limitations, specially in microporous materials such as zeolites, increasing the adsorption and reaction rates [135]. Currently, there is a large variety of synthetic hierarchical materials that have been prepared, in this chapter the main preparation methods of zeolitic hierarchical structures is reviewed. Also, the main applications of these prepared materials are summarised.

4.2 Definition

Hierarchical porous materials are defined as materials containing two or more porosity levels in its structure [131]. Notice that hierarchical materials are also those that contain different particle size ranges within the same body. Egeblad *et al.* [136] classifies the hierarchical zeolitic materials within three categories: a) hierarchical zeolite crystals, b) zeolites with nanosized crystals and c) supported zeolites. A graphical description can be seen in Figure 4.1.

The desirable configuration of a hierarchical porous structure is having the best features of three porosity levels -micro, -meso and -macro, i.e. an enhanced activity, increased internal and external surface area, high exchange capacity, an improved mass transport through the materials interior and also, a highly crystalline structure and therefore higher stability [8].

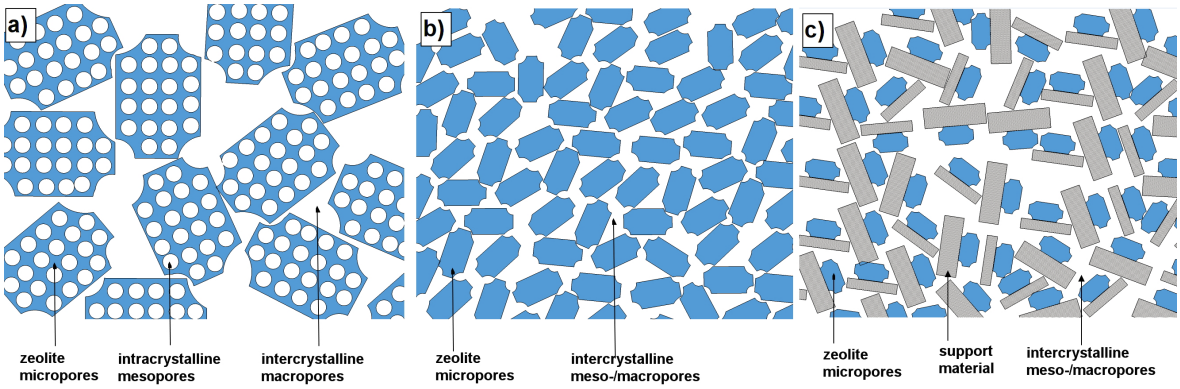

Figure 4.1: Three different zeolite hierarchical configurations. a) Hierarchical zeolite crystals, b) nanosized zeolite crystals and c) supported zeolites crystals, adapted from [137]

4.3 Methods for the Preparation of Hierarchical Porous Zeolites

In general, two main objectives can be pursued when synthesising hierarchical porous materials: i) to provide an extra level of porosity to zeolites and/or ii) to enhance diffusion rates through wider channels to reach active or exchangeable sites [138]. Three main methods are distinguished for the hierarchically structured zeolites synthesis: a) Demetalation, b) use of templates and c) zeolitisation of already-formed solids. These methods have led to different configurations of micro-meso, micro-macro and even micro-meso-macro porosity materials have been reported [139].

4.3.1 Demetalation

Most of the zeolites with mesoporous characteristics currently used in industry are prepared by post-synthetic methods. The demetalation involves the metallic atoms extraction from the framework in order to produce larger pores (meso or macro). Two of the most used demetalation techniques are steaming and leaching [140].

The steaming process is an hydrothermal procedure that requires high temperatures, usually up to 500 °C, these temperatures are needed to break the Si-O-Al bonds within the zeolite framework. This method is non-selective and it removes part of the

framework having crystallinity loss as a direct consequence.

Leaching techniques generally uses a substance, with specific characteristics such as acidity or alkalinity, suitable for the specific extraction of metals from the framework [141]. For example, acid solutions have selectivity for aluminium atoms (dealumination) and alkaline solutions are used to leach silicon atoms (desilication). Leaching has allowed the larger pores creation due to there being no formation of amorphous *chunks* that block the pore system, as is the case of steaming. Materials prepared by leaching have shown to have enhanced diffusion properties in catalytic applications, associating this with more open pores. However, using these procedures, crystallinity and mechanical properties are usually affected because the original structure is partially destroyed [140]. Leaching is classified in desilication and dealumination methods.

4.3.1.1 Desilication

The first approaches to break Si-O-Si bonds and remove silicon from the zeolitic framework were made using alkaline solutions in the '1960s [142], although the mechanism was not completely clear, set the precedent for the use alkaline substances to achieve desilication. A main disadvantage using this methodology is the solid dissolution, where a large amount of the solid is dissolved. Depending on the type of structure, aluminium content plays a key role in the desilication process.

4.3.1.2 Dealumination

Dealumination is the most common method to produce mesoporous zeolites with industrial applications. Dealumination is the process that removes aluminium atoms from the Si-O-Al bonds within aluminosilicates framework. It was first used to increase the acidic properties of low Si/Al ratios zeolites and a parallel effect was noticed: increasing acid concentration, mesopores were created [143]. Hydrochloric, nitric and sulphuric acids have been utilised as leaching agents along with organic acids such as tartaric, oxalic and acetic [144].

The well-known destructive nature of acid solutions led to the use of chemical

chelating agents such as ammonium hexafluorosilicate $(NH_4)_2SiF_6$ and silicon tetrachloride $SiCl_4$ and others [145]. These substances substitute the displaced aluminium with silicon atoms. Dealuminated β, MOR and ZSM-5 have been prepared in their mesopores forms [144]. Nevertheless, these substitutions reduce the micropore volume due to its silicon filling the empty spaces left by aluminium reducing the mesoporous character of materials.

4.3.2 Templating Methods

In this section, the term *template* is related to materials used to produce an extra porosity level, unlike the previously described structure directing agents (SDA's) which are needed to produce certain zeolite structures types.

Templating methods are mainly divided into two, depending upon the type involved, are distinguished soft and hard templates, the latter also called solid templates [146]. The methodologies based on the use soft templates, are often simpler than hard templates, where in general multi-step procedures are required [147, 148]. Templates that have been explored include materials such as polymers, gels, resins, plant parts and other biological matter such as bacteria [149], however, in solid templates porous carbons have been used widely and have become one of the more used templates due to their mechanical stability and their relatively ease to be removed after the synthesis, if required, with simple thermal treatments. The templates selection is of great importance and special attention should be paid to several factors such as stability (chemical and thermal), degree of interactions with zeolite precursors, morphology and cost [137].

4.3.2.1 Soft Templates

Soft templates are large molecules that can be cationic surfactants [143]. The strategy is based on the formation of micellar aggregate solutions [146], i.e. molecules with surfactant properties that self-assemble in different shapes and dimensions depending on their miscibility properties. This also is known as *dual template* approach and

has its principle in the size of molecules that control the crystal growth in the zeolite precursor but do not form part of the final framework [138]. In the crystallisation of zeolitic materials, templates interact directly with the silica species due to their hydrophilic behaviour. Examples of soft templates include surfactants, ionic liquids and block copylmers [148]. A general method is shown in Figure 4.2.

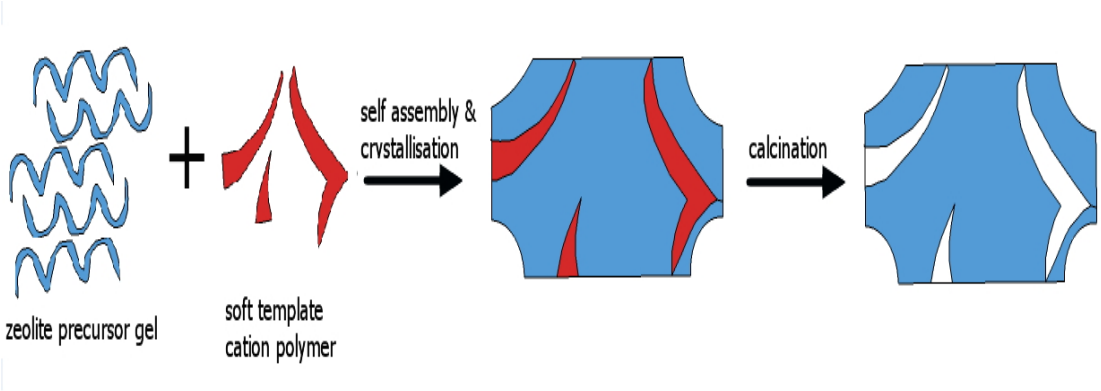

Figure 4.2: Mesopores are formed by the use of cationic polymers as soft templates, adapted from [137]

One of the first successfully attempts using soft templates was the hierarchical zeolite β preparation with intracrystaline mesopores using high-molecular-weight poly-electrocations [150], this work also led to the preparation of industrially important zeolites such as MFI and FAU memebers in their hierarchical forms. Zeolite type FAU has been prepared using carbon aerogel[1] as a template [151]. The production of the aerogels is usually expensive compared to other templating methods.

4.3.2.2 Hard Templates

The use of solids as hard templates can be divided into two: a) sacrificial solids, materials that are removed after synthesis, and b) non-sacrificial solids, materials that actually remain after synthesis. In the latter case, composites are formed , i.e. two different materials in one body.

[1]An aerogel is a very low density material in which the liquid particles of the precursor gel have been replaced by a gas.

4.3.2.2.1 Sacrificial Solids In hard templating, solid materials with specific size, from 2 to 50 nm for mesopores and larger than 50 nm for macropores, are utilised as *hard* templates. Generally, the template removal generates an extra porosity level with a geometrical correspondence [136].

A common method using solid templates is the so-called confined space. In this procedure the zeolite crystallisation is carried out within a meso- or macro- porous system provided by a non-reactive matrix [152]. In early studies made by Jacobsen *et al.* [152], carbon matrix (black carbon) was used to prepare different zeolite types such as β, LTA, ZSM-5, MCM-41 and X with mesoporous characteristics.

One of the main disadvantages using solid matrices is the cave-like mesopores formation which are closed to external phases [153] and being inaccessible for large molecules. Carbon nanotubes have been used to overcome these drawbacks [154]. Nanotubes favour the mass transfer due to their large and open channels, however, the production cost of the nanotubes is a major limitation for its use. A cheaper alternative to carbon nanotubes, but with similar properties, are carbon fibres. The hierarchical silicalite-1 crystals synthesis have been reported using hollow fibres as templates [155]. Other carbon sources such as carbohydrates have been employed, for example, sucrose has been the precursor of the mesoporous carbon source [156].

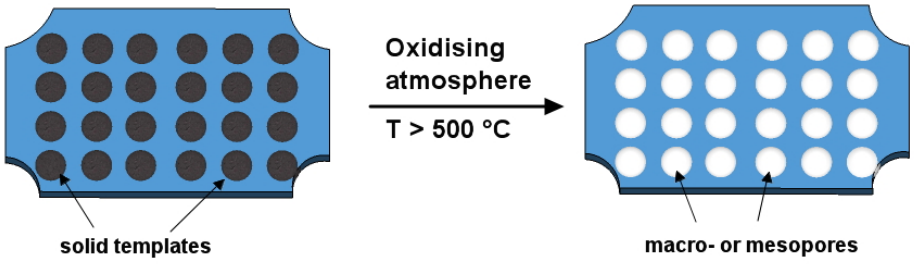

Figure 4.3: Hard templating with carbon. A general approach adapted from [157]

4.3.2.2.2 Non-Sacrificial Solids - Composites Templates that remain after synthesis support zeolite crystals forming composites. In these materials, the additional porous strucure is based on the support characteristics. Different materials have

been employed as zeolite particles supports such as metals, polymers, ceramic clays and carbons [158–161]. In particular, carbon has been explored as it is low cost and has both chemical and thermal stability in a non-oxidising environment [162]. Nevertheless, hydrophobic characteristics on the carbon surface do not favour the interactions between zeolite particles or precursor gels and carbons [162]. In order to overcome these problems, several methods have been proposed: the deposition of zeolite *seeds* on carbon prior to zeolite growing process [163], the use of binder with hydrophilic features such as SiO_2, Al_2O_3, ZrO_2 and TiO_2 [164].

The disadvantage of using seeds is that is not always possible to control the zeolite amount and/or zeolite-layer thickness. Also, certain supports do not resist hydrothermal conditions leading to partial or complete scaffolds collapse. The use of binder, generally in the fabrication of membranes, causes structural defects originating from thermal stresses [165].

4.3.3 Zeolitisation of Solids

The process of converting an already-formed material into zeolite is called zeolitsiation [166]. Materials subject to this process are rich in zeolite precursors, i.e. SiO_2 and Al_2O_3. The major advances in the preparation of these materials are mainly using two methods: vapour phase transport (VPT) and steam assisted conversion (SAC) [157]. Both procedures are based on the contribution of Xu *et al.* [167] in which a different hydrothermal method based on the crystallisation of a dry zeolite precursor by the enrichment by vapour was described. The main difference between VPT and SAC is that the first uses water and structure direct agents (SDAs) for the enrichment of the dry gel meanwhile in SAC, only water is vaporised as SDAs are already contained in the dry gel [157]. Zeolitised materials using these methods include silica monoliths, silica nanoparticles, gels, meso- and macroporous solids.

Alternative methods for the zeolitisation are the support impregnation in the *protozeolite* phase solution and the subsequent crystal growth under hydrothermal condi-

tions. Impregnating is a one-step method and it is based on the formation of nanocrystals on the meso- or macro- porous structure, crystallisation of microporous zeolite phase ocurrs on the walls' support after the support is soaked in zeolite precursor phase. One of the earliest contributions was made by Kolestra *et al.* [168], in which hierarchical oxides were prepared using metalalkyl quatrernaty salts as direct agents. α-alumina has been used as porous support to MFI and β types [164]. Nevertheless, harsh conditions such as high temperature and high alkalinity, can lead to the scaffold collapse.

Diatomite is a pure-silica material formed after the death of unicellular diatoms, it is found in the bottom of sea or lakes [166]. The three dimensional macroporous and chemical characteristics have allowed them to be used as a zeolite supports through diverse methodologies. Diatomite zeolitisation has been also achieved using vapour phase transport after being seeded with nanoparticles [169]. Anderson *et al.* [166] reported the seeding process coupled with ultrasonication to prepare hierarchical structured silicalite-1 over diatoms. The main advantage of using seeds followed by secondary hydrothermal growth is based on the fact that nucleation and crystal growth are no longer coupled processes.

4.4 Hierarchical Porous Materials in Environmental Applications

The work conducted by Jin-Song *et al.* [135] reviews different hierarchical structured materials: Iron, titanium and aluminium oxides with different shapes have been evaluated for the adsorption of chromium and arsenic. The remarkable adsorptive properties of ZnO nano-micro sized materials for Cu^{2+} ions compared to comercial ZnO powders have been reported [170]. Mesoporous hollow-sphere shaped molybdenum oxides have been used to adsorb Cr^{2+} ions from water [171]. Carbonised hierarchical maritime algae such as *E. prolifera* has been used as a low-cost adsorbent for CO_2 [172] that

could be regenerated at low cost, this material showed micro-meso pores configuration. Meso-macro $CaCO_3$ solids has been prepared and several heavy metals have been adsorbed efficiently; the sorption of Cu^{2+} has been reported [173]. In a recent paper published by Zhang and Tsapatsis *et al.* [174] the hydrocarbons adsorption was reported on a hierarchical MFI form. In the adsorption of toxic and carcinogenic nitrosamines from tobacco smokes, MCM-22 zeoptype have been functionalised by organic functional groups leading to a hierachical porous structure [175]. Macro-meso porosity of aluminum phosphonates prepared using organic acids were reported for the Cu^{2+} and proteins removal [176].

4.5 Summary

Besides some of the described methods leading to materials with low mechanical strength and crystallinity loss, in general, most methods are not cheap. In some cases the use of expensive templates makes the production processes of hierarchical materials costly, this being a major restriction for the mass scale production. It is clear that the function to be performed by the material is the main factor that will adjust the budget. A real challenge is to balance the cost of materials preparation with the effectiviness in their specific application.

Different to first zeolitc discoveries, where the applications were a consequence of those new discoveries, current applications are now dictating how materials should be tuned. The major impact of these materials is in catalysis where hierarchical materials seems to be playing a more predominant role. This can be due to the high-profile industries backing research and moreover the petrochemical industry for the production of gasolines. Thus, the pollutants removal from different media using hierarchical materials has not achieved the same degree of development. However, the use of cheap sources for templates such as residues or natural sources, cheap and straightforward methodologies have a good prospectives in this field. In this context the use of non-expensive, accessible and local resources is presented as a very good option with the

aim of contributing to sustainable solutions.

In the next chapter, the adsorption phenomenon is studied. Also, the role that zeolites play as adsorbent and ion exchanger is described along with the different factors involved in the sorptive process. The kinetic and diffusive characteristics are also included.

Chapter 5

Sorptive Phenomena in Zeolites

5.1 Adsorption

Most industrial processes include the purification of substances and regularly, this means molecular mixtures separation. The phenomenon that zeolites uses in separation is based on adsorption. The adsorption features in zeolitic materials are based on their ion exchange characteristics, porous geometry and structure [95].

5.1.1 Background

There have been outstanding contributions that transformed the adsorption theory. In 1918 Langmuir [177] published a remarkable paper in which he compiles previous ideas about how molecules were attached to liquid and solid surfaces, and he unified them in the concept of mono-molecular layer, the so-called *monolayer*. Langmuir explained that a layer of one-molecule thickness is generally implicated in adsorption of gases on both solid and liquids [177]. In late 1930s Brunauer, Emmet and Teller (BET) [178] established the theoretical background for solids characterisation by the use of gases, they also proposed the BET equation to describe the adsorption equilibrium by an isotherm curve. They analysed the adsorption of several gases near to their boiling point and observed different behaviour to those previously presented by Langmuir, they proposed the formation of multiple stacked-layers of molecules. This phenomenon is known as

multilayer adsorption and the main assumptions were that forces that produce initial condensation are similar to those ones responsible for the formation of this less-ordered thermodynamically multilayer adsorption [179]. Currently, the BET equation is still used as the standard method to asses the surface area of solids, although recent publications have suggested that this method lacks a rigorous theoretical background and therefore it has to be used under conditions keeping in mind certain precautions, i.e. the case of zeolites where it could only be utilised in the qualitative analysis of their pores [180, 181]. In 1960, Dubinin [182] identified the differences between the adsorption in small and narrow pores, and open surfaces. Further, Dubinin described the importance of dispersive forces in gases adsorption on "extreme structural types of carbonaceous adsorbents" .

5.1.2 Definition

Adsorption is defined as"the enrichment of material or increase in the density of the fluid in the vicinity of an interface" [180]. The adsorption concept was coined by Kayser in 1881 [183] referring to the adhesion of air molecules onto charcoal. Adsorption is usually understood as the accumulation of any substance, *adsorbate*, on a solid surface due to an energy excess on the *adsorbent*. When the inverse process occurs, is called *desorption*. Generally the concept *sorption* is helpful to include different mechanisms or contributions by which molecules are attached to a surface. The adsorption process is exemplified in Figure 5.1.

5.1.3 Classification

Depending on the force of interactions between the adsorbent and the accumulated substances three types of adsorption are distinguished: chemisorption, physical sorption (physisorption) and ion exchange [5]. Each sorption type is the direct consequence of different forces involved. Chemisorption is attributed to those ones implicated in the formation of chemical bonds, whereas physical sorption has its origin in a weaker

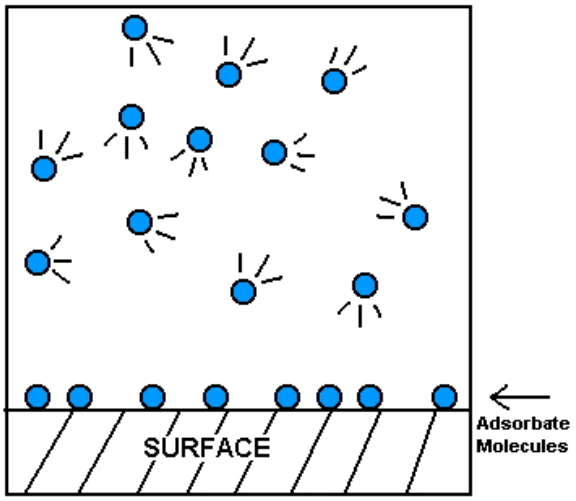

Figure 5.1: Adsorption process, the adsorbent surface and adsorbate particles

form of interactions known as van der Waals forces [181]. It is evident that in physisorption it is easier for the adsorbate to be desorbed. Also, chemisorption occurs in the monolayer form, since molecules are adsorbed only to the solid surface. At high pressure, multilayer physisorption takes place. If a molecule was chemically adsorbed it is transformed, but if a molecule is physically adsorbed, it will not change and after desorption it will return to its original state in the fluid phase [180]. Additionally, the chemisorption energy is similar to the energy in a chemical reaction in contrast to physisorption where it can be compared to the molecules condensation energy to be adsorbed. In addition, adsorption can also be controlled by ion exchange as the main mechanism. It involves the interaction between opposite charged ions [5].

5.1.4 Ion Exchange as an Adsorption Mechanism

5.1.4.1 Background

The first evidence of the use of ion exchange dates back to ancient Greece when Aristotle used sand to reduce the amount of salt in seawater [184]. In 1850, the first systematic description of the ion exchange process, that coincided with the first practical discoveries of zeolite technology, was made by Wey and Thompson [74]. They explained that some types of soil were capable of retaining various compounds from aqueous media

and at the same time they could release others. In 1917 ion exchange was systematically applied for the first time when Frolin and Bell [185] separated ammonium ions from urine samples using zeolites. Ion exchange in a column for anion analysis was carried out in 1927 by Bahrdt [186]. Adams and Holmes [5] in 1935, synthesised organic resins with higher capacity and stability than all previous known materials by that time. Boyd [185] in 1943 adsorbed trace amounts of lanthanides isotopes using ion exchange. This discovery directly contributed to the Manhattan project where the understanding of lanthanides properties was crucial in nuclear weapons yields, but their very similar properties made them difficult to isolate them. After the end of World War II, much information regarding ion exchange technologies was made public and led to the development of polymeric resins. Also, the discovery of the chemical element Promethium was made thanks to the use of ion-exchange chromatography in 1948 [185]. One of the most profitable fields where ion exchange takes place is in the detergent industry. In fact, the actual development in zeolites is in part thanks to the investigations that began when they were used to substitute toxic phosphates to remove calcium and magnesium ions from *hard* water [74].

5.1.4.2 Definition

In ion exchange, solid materials are capable of retaining (adsorbing) charged species from solutions due to they posses an excess of charge which is neutralised by inversely-charged ions called *counter ions* [5]. Different to other sorptive mechanisms, where no species are released to solution, ion exchange is a stoichiometric phenomenon [101], i.e. the amount of adsorbed and released ions is equivalent. The driving force for the mass transfer in ion exchange is the difference of concentrations in two phases and also, selectivity, i.e. the preference of the solid for one ion over another [101]. The ion exchange capacity is defined as "the quantity of ions exchangeable by a solid exchanger depending on its chemical and structural features" [187]. Ion exchange is a reversible process and electroneutrality is always maintained [188]. For an anionic solid exchanger it can be represented as follows:

$$\mathbf{M^-A^+ + B^+ \rightleftharpoons M^-B^+ + A^+}$$

where M^- is known as fixed ion, and A^+ and B^+ are the counterions.

This is an adaptation of the law of mass action [189]. When in a liquid/solid system the exchangeable ion in the solid has a different valence number the ion in solution then is called *heterovalent* and when they having same valence is known as *homovalent*. For example, zeolites often have only monovalent ions (Na^+, K^+, Li^+ among others) and they are usually applied to remove divalent ions. This system is called heterovalent and an example of homovalent exchange is presented in Figure 5.2.

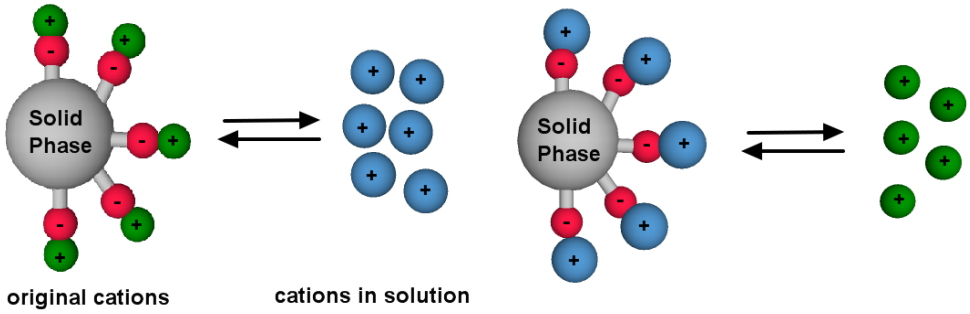

Figure 5.2: Ion exchange process; Initial adsorbed ions on solid surface are displaced for ions in solution

5.2 Factors Influencing Sorptive Processes

In the sorption processes of metallic species involving the use of zeolites, many factors have to be considered in order to have a better understanding about the materials and interactions. In this section the effect of the main variables when conducting sorption experiments such as pH, initial concentration, temperature, particle size and dosage are summarised.

5.2.1 pH

Heavy metals sorption using zeolites is dependant on pH. In many industrial effluents pH values are different but tend to be acidic. In the study of heavy metals adsorption,

it is fundamental for the ions to be as *free* species, i.e. they are not coordinated due to the increase of OH^- concentration. If pH value is over the figure where metallic species start to precipitate, the use of adsorbent is useless since precipitation is the main phenomenon taking place. At lower pH values however, a reduced uptake occurs. This is due to the competition with H^+ with metals to occupy negative sites in zeolites framework. Furthermore, specially in zeolites with low Si/Al ratios, low pH level can not only damage the structure but also can dissolve it [143]. It is crucial to know the metallic species behaviour as a function of pH in order to neglect precipitation effects as the removal mechanism. In Figure 5.3 is shown a graph of the cobalt speciation as a function of pH. Co^{2+} remains as ionic specie at values below pH 8 [48, 190]. Although a complete control of the pH during the sorptive process would be ideal, in practice it involves the use of complicated control systems and an initial pH value is usually adjusted.

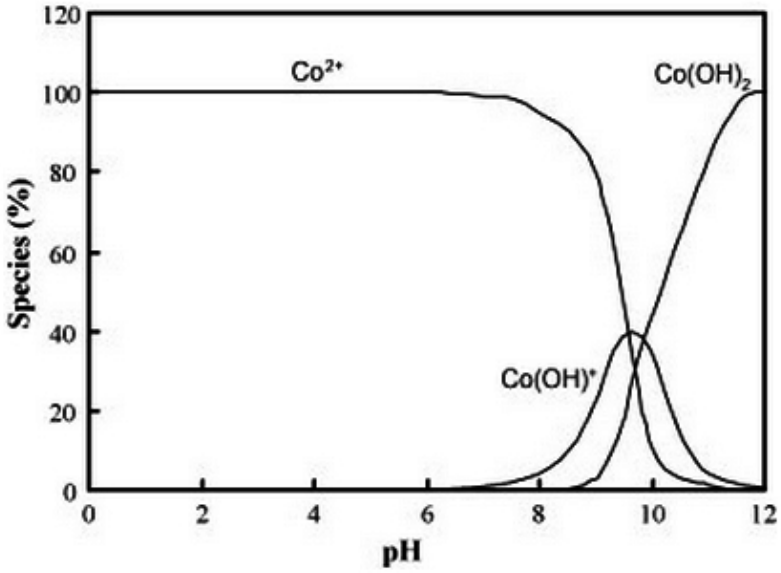

Figure 5.3: Speciation digram of cobalt as a function of pH [48]

5.2.2 Initial Concentration

Since adsorption is governed by the electrostatic or non-electrostatic interactions between solid and dissolved metal, initial concentration often acts as driving force in the

sorptive processes. These forces are strong enough to surpass the mass transfer resistive forces from solution to the surface of the adsorbent [191]. Generally, adsorption capacity is directly dependent on the initial concentration until the saturation of the adsorbent sites is reached. However, studies have been shown that in certain types of zeolite lower concentration levels are removed more efficiently than the higher initial concentration values [56].

5.2.3 Temperature

The effect of the temperature on the adsorbent performance is relevant since temperature governs the equilibrium state. Furthermore, temperature affects the interactions between adsorbent and adsorbate because of the energy levels modification required for the process. Generally these interactions can the displace the equilibrium in two different ways. For example, the adsorption capacity of copper cations has been favoured by the increase of the temperature level, from 20 to 50 °C [192]. On other hand, calcium ions adsorption equilibrium is favoured with a temperature reduction [193] from 60 to 20 °C.

The expression that relates equilibrium constant, temperature and enthalpy is given by Van't Hoff equation [194]:

$$\frac{d \ln K}{dt} = \frac{\Delta H}{RT^2} \tag{5.1}$$

Where K is the chemical equilibrium constant, T is absolute temperature and ΔH is the enthalpy change of the system.

5.2.4 Particle Size

A reduction in the particle size of a material usually leads to an increase of external surface area, i.e. the higher possibility for the adsorbate to find a site to be adsorbed. The adsorption capacity usually increases with a particle size reduction [195]. This can be explained by an improved accessibility to active sites inside the porous adsorbent.

For example, a reduction in the distribution of actual particle size of natural zeolite has been shown to increase the zinc uptake assuming also a reduction in the intraparticle diffusion resistance [196].

5.2.5 Dosage

Although an increased amount of mass can provide more available adsorptive sites, there is not a direct relationship between the amount of adsorbent and the sorption capacity [197]. An excessive adsorbent mass generates solid aggregation [198]. Generally, adsorption systems are assumed to be at infinite dilution, i.e. the effect of adsorbent volume is negligible. Thus, having an excessive solid/solution ratio can cause that infinite dilution assumption to be not longer valid. The optimal ratio would be a function of two choices: a) knowing the solid capacity or b) representing real and representative industrial effluent conditions.

5.3 Applications of Zeolites

5.3.1 Adsorption and Ion Exchange

Zeolites and molecular sieves find application in the production of widely used gases such as oxygen, nitrogen and hydrogen by the pressure swing adsorption method (PSA) [199]. Also in gas purification, the uptake of NO_2 from air [200] for example. In addition, molecular sieves are used to dry and purify trace-level contaminated gas streams [95]. The MCM-22 [201] and MCM-41 [202] zeotypes have been used to adsorb organic dyes from waste effluents and zeolite Na-A has been used as a refrigerant gas dryer [203].

In environmental sciences, some toxic ions have been removed from industrial and public waste water based on this phenomenon. Due to their relatively high efficiency as adsorbent, zeolites have been demonstrated to be very effective in heavy metal removal. Natural materials such as clinoptilolite, chabazite and mordenite have been

utilised to remove chromium, iron, lead, caesium, cadmium, copper, zinc, ammonia among others [204–207]. Additionally, some synthetic zeolites that have been used in similar way are P, A, X and Y. They have been used to remove and immobilise ammonium and cadmium, iron, lead, zinc, and radioactive nuclides such as caesium and strontium [208–211]. Also, it has been possible in some cases to change the surface charge from negative to positive by modification with organic compounds allowing zeolitic materials to carry out anionic exchange processes.

In the detergents industry, zeolites act as a water softener, i.e. uptaking calcium and magnesium ions from water and releasing sodium ions. Particularly clinoptilolite, zeolite A and X types are the most used [94]. Recently the discovery of zeolite MAP, with enhanced adsorbing and tunable porosity, showed superior performance as detergent zeolite [212].

Zeolite particle size ranges from 1 μm to 4 μm commonly. This exemplifies one advantage of synthetic zeolites since the precise engineering of their properties such as crystal size, composition and polarity is now possible in contrast to their natural counterparts.

Ion exchange and adsorption are considered within the sorption concept, leading to an easy and practical approach for the potential applications. Based on the contributions of Helfferich [213] both adsorption and ion exchange are two phenomena that are shown to be governed by diffusion, thus both can be analysed using the same proposed thermodynamic, kinetic and diffusive models [5, 214].

5.3.2 Catalysis

The presence of framework cations gives attractive catalytic characteristics. Acidity is related to active sites that are defined by cationic places. The kinetic characteristics in catalysis are controlled by physical interactions between molecules and the catalyst. The active sites in aluminosilcate zeolites are a combination of hydroxyl groups (that links Si and Al atoms) and oxo bridges [215]. The former behave as Brønsted acids

and the latter as Lewis bases giving zeolite unique bifunctional characteristics. Figure 5.4 describes the acid and basic sites in zeolites. By definition, a Brønsted acid gives a proton and a Lewis acid can provide an electron pair [216].

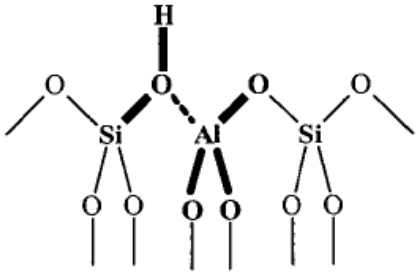

Figure 5.4: Acid and basic active sites in aluminosilcate zeolites [215]

The process known as fluid catalytic cracking (FCC) is one of the most used in the petrochemical industry. As its name suggests, the requirement of a catalyst is crucial. For this, zeolites are in charge of the selectivity and chemical activity in the whole process. For example, in Figure 5.5 a hydrocarbon reaction with a Brønsted acid in the zeolite framework is shown.

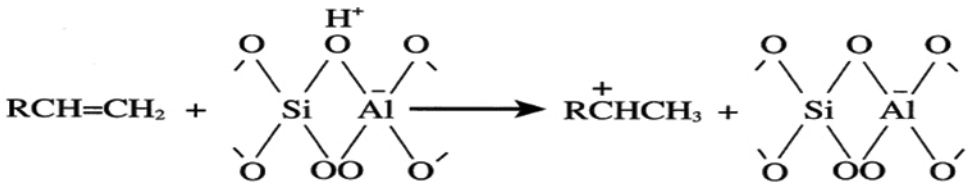

Figure 5.5: Reaction of olefin and acid site in zeolites [215]

FAU and MFI are two of the zeolitic frameworks most used because of their thermal and thermochemical stability [91]. The use of FAU in the FCC process has caused a revolution in the industry having multimillion dollar profits after its implementation. Motor fuel is being produced using zeolite Y as a catalyst because it represents bigger yields compared to previous catalysts, in fact, there are estimates that relates zeolite Y to around a trillion dollar profits since its implementation [217]. Currently, the environmental use of zeolitic catalysis is growing because more restrictions on the quality and amount of certain species, such as sulphur and lead in fuels, are increasing [218].

5.3.3 Emerging Applications

Different scientific scenarios have been explored over recent years and new applications along with new ways to use zeolites is increasing in importance. In biology for example, zeolitic materials have been used for the regeneration of solutions utilised in dialysis and also, in the construction of cellulosic membranes [75,219]. ITQ-6 and BEA frameworks were used to immobilise and stabilise certain enzymes and proteins types respectively [220,221]. In medicine clinoptilolite has been demonstrated to be useful in carcinogenic tumour treatment [222]. X type has been used to confine contrast agents within nuclear medicine applications [223]. In electronics, molecular sieves such as ALPOs have been used in light emission applications, a composite with this zeolitic material and an organic dye was synthesized to include it in the making of a laser [10]. Where molecular sieves could have a great potential is in the storage of fuels. Recent contributions using zeolites (MAZ, Y, X and A among other with low framework density) to store methane and hydrogen have been published [66, 224–226]

5.4 Sorption Kinetics in Liquid/Solid Systems

Kinetic models are important components in the adsorption/desorption phenomena characterisation. Since adsorption is a time-based process, the rate of change gives important information about how chemical properties are changing with time. For example, the minimal residence time to achieve an equilibrium state. In contrast to the thermodynamic models, when only final states are described, kinetic information such as rates of changes and the possible mechanism are crucial parameters in the design, regeneration and scale-up of adsorptive processes and materials [227]. Several kinetic models have been proposed and applied for the analysis of the adsorption in solid-liquid systems.

5.4.1 Lagergren's Pseudo First Order Equation

In 1898 Lagergren proposed the Pseudo First Order (PFO) equation for the adsorption of organic acids on charcoal [228]:

$$\frac{dq}{dt} = k_1(q_e - q) \tag{5.2}$$

q and q_e (g mg^{-1}) represent the adsorption uptakes at different time and at equilibrium respectively, k_1 (min^{-1}) is the Pseudo First Order kinetic rate constant. Equation 5.2 is integrated within limits $t = 0$ to $t = t$ and $q = 0$ to $q = q_e$ [229].

$$\ln \frac{q_e}{q_e - q} = k_1 t \tag{5.3}$$

It can be rearranged in the linear form:

$$\ln(q_e - q_t) = \ln q_e - k_1 t \tag{5.4}$$

The rate constant for this equation could be physically interpreted as "the proportionality between adsorption rate and the distance of the system from the equilibrium" [230].

A considerable literature amount has been published referencing Lagergren's equation. The concept of *pseudo* comes from two main differences with a *true* first order system. First, the fact that this model is based adsorption capacity and not concentration as in the case of a first order system, and second, the number of available sites are not represented by the term $k_1(q_e - q)$ [231].

5.4.2 Pseudo Second Order Equation

In 1984 Blanchard presented an new equation based on the assumption that concentration does not change significantly during the first stage of the adsorptive process and the influence of more than one type of adsorptive sites was noticed then "the kinetic order is two with respect to the number of available sites for the exchange" [127].

The original work reported the removal of ammonium and metallic ions from drinking water using natural zeolites. In 1999 Y.S Ho and G. McKay [232] reviewed the Pseudo Second Order equation, analysing kinetic data of previously published works that had been reported as first order systems. Their findings revealed that Pseudo Second order model described more accurately their results than the Pseudo First order equation, they also stated that Pseudo First order is a restricted model for just a segment of the reaction range.

$$\frac{dq}{dt} = k_2(q_e - q)^2 \tag{5.5}$$

k_2 (g g^{-1} min^{-1}), is the correspondent rate constant and its integrated and linear form:

$$\frac{t}{q} = \frac{1}{k_2 q_e^2} + \frac{1}{q_e}t \tag{5.6}$$

q_e and k_2 are obtained from the slope and interception of the plot t/q against t.

The main assumptions of Pseudo Second Order equation are that adsorption is dependent on the adsorptive solid capacity in the form of available fraction of active sites and can involve chemisorption, contrasting with first order model where the reaction kinetics is dependent only on the solution's concentration [233].

Recent theoretical studies have suggested that Pseudo Second order is more accurate when the adsorptive initial concentration is low, but when concentration is higher data better fits Pseudo First Order equation [227]. Nevertheless, there is not a proper homogenisation of concepts regarding what is *high* or *low* sorbate concentration and sometimes this can be ambiguous since a large number and types of sorbent-sorbate systems, with arbitrary concentration values, have been reported. Also, some controversy has raised about the use of Pseudo Second Order model where, according to Zhang [234], there is an "inflated statistical correlation" when this model is used. However, more than 100 systems have been applied and reported agreement with Pseudo Second Order equation and there is a large volume of published studies referring to

Ho's [232] original publication (more than 4000) which correlate experimental data with Pseudo Second Order equation.

5.5 Diffusivity in Solid/Liquid Systems

The early studies by G.E. Boyd [235] have brought a better understanding of the diffusive processes in ion exchangers. Boyd based his research on the previous theories of Nernst, in which he had defined the concept of "liquid diffusion layer" that makes reference to a theoretical film surrounding the solid exchanger where mass transfer is driven by diffusion only [213]. This layer is also called boundary film diffusion.

The overall sorptive process can be divided into four main stages: a) mass transfer from the solution bulk to the external surface of the ion exchanger particles, b) external mass transfer through film diffusion, c) internal diffusion from the surface to the inner pores of the material and d) the adsorption of the ions onto the active sites at the interior of the pores [236]. In general, the first stage effect is neglected in stirred systems and the last step is usually very fast and it has no significant influence on the overall process. Thus, the ion exchange kinetic behaviour is controlled by boundary diffusion (film diffusion) or intraparticle diffusion (pore diffusion) or a combination of both [237]. Usually, the slower process will determine the ion exchange rate. Several models have been used to describe the diffusivity characteristics and to obtain the diffusivity coefficients.

5.5.1 Weber-Morris Model

W. J. Weber and J. C. Morris in 1963 proposed a model that describes the uptake as function of square-root of concentration [238] which is based on the Boyd's contributions:

$$q_t = k_{id} t^{1/2} \tag{5.7}$$

Where k_{id} is the intraparticle diffusion rate. The main assumption of this model is that intraparticle diffusion controls the process, the rate is dependant on pore characteristics and electrokinetic interactions between ions and exchanger. Also, if the the plot q_t v $t^{1/2}$ is linear and passes through the origin, it is assumed that intraparticle diffusion is the rate controlling-step in the process. In addition the slope of this line corresponds to rate of intraparticle diffusion k_{id}.

5.6 Equilibrium Models for Sorption from Solution

The modelling of the adsorption equilibrium isotherms plays a fundamental role in the adsorption processes design and the prediction of adsorbents uptake capacities. In contrast to kinetic analysis, adsorption isotherms are required to obtain thermodynamic parameters needed for the quantitative analysis of the fluid-solid systems. These parameters offer information related to adsorption capacity, possible adsorption mechanism and describe the surface features such as the attraction to the sorbate [239]. The definition of a graphical isotherm applied for the analysis of a liquid/solid system is "a curve describing the phenomenon governing the retention or mobility of a substance from aqueous media to a solid phase at constant temperature" [240]. The equilibrium state is achieved when adsorption and desorption rates are equal and sorbent concentration remains constant. An isotherm that describes the adsorption from solution is constructed plotting q which is the difference of initial (C_i) and equilibrium concentrations (C) normalised by the volume (V) and adsorbent mass used (m), against the final concentration at equilibrium (C). Different initial concentration values are needed [1].

$$q = \frac{C_i - C}{V} m \tag{5.8}$$

An adosprtion isotherms classification was proposed by Giles *et al.* in 1974 [241]. Four types are distinguished: C, L, H ans S types and in Figure 5.6 can be seen.

C type is characterised by having the q/C ratio constant all over the range of

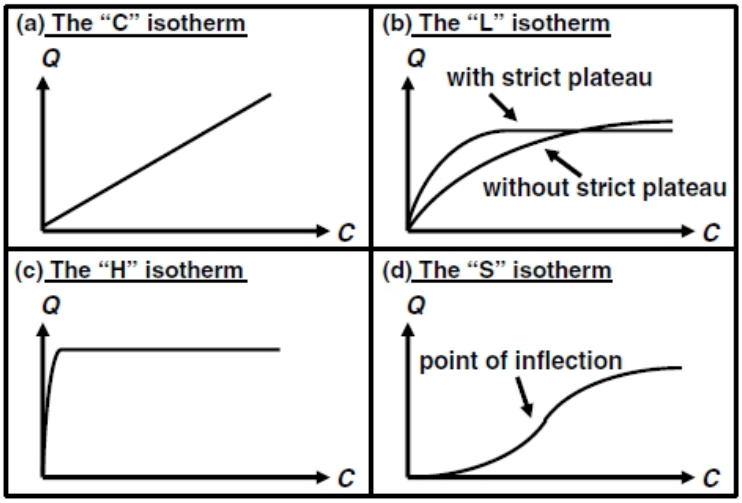

Figure 5.6: Four types of isotherms to describe adsorption from solutions

initial concentrations. L type exhibits two types of concave curves: one is asymptotic and suggests a saturation of adsorbent capacity. The second type does not show a proper plateau suggesting solid can allow still more solute molecules. Some authors may suggest an increase of the concentration in order to asses maximum capacity. In isotherm type H a sharp increase is observed, this can be a consequence of the high degree of affinity between sorbate and sorbent. The S type shows a sigmoid shape, this is characteristic for solutes that adsorbs deficiently at low concentration levels, but as concentration increases adsorption capacity also increases, this is because adsorbed molecules *help* other to be attached to surface, this is known as "cooperative adsorption" [1].

In order to model the adsorption from solutions the use of concave isotherms has been widely used. Two of the most used models in the analysis when removing heavy metals from aqueous systems are based on the isotherms proposed by Langmuir and Freundlich respectively.

5.6.1 Langmuir Isotherm

The theoretical aspects of Langmuir equation are based on the energetic uniformity of all adsorptive sites on the adsorbent's surface. Also, the formation of single layer

of adsorbed molecules, the so-called monolayer, is assumed [214]. Each interaction solid-solute are considered to be independent of each other.

$$q = \frac{Q_m b_L C_e}{1 + b_L C_e} \tag{5.9}$$

Where Q_m is the maximum adsorption capacity (monolayer), b_L is the Langmuir constant and it is used to describe the affinity between sorbent and sorbate. In order to calculate these parameters, a linearisation is commonly proposed:

$$\frac{1}{q_e} = \frac{1}{b_L C_e} + \frac{1}{Q_m} \tag{5.10}$$

5.6.2 Freundlich Isotherm

Freundlich isotherm is an empirical equation that describes and predicts the adsorption onto heterogeneous surfaces [214]:

$$q_e = K_F C_e^{b_F} \tag{5.11}$$

Where K_F it is assumed to describe the adsorption capacity; b_F defines the adsorption intensity and is also known as the "heterogeneity factor" [1]. Also, these parameters can be obtained from a linear form and plotting:

$$\log q_e = \log K_F + b_F \log C_e \tag{5.12}$$

The most used method to obtain equations' parameters has been the linearisation, i.e. the process in which the equation is transformed into a linear form. Nevertheless, recent publications have objected linearisation methods, saying that when linearise these kind of equations the transformation into linear of originally non-linear equations lead to deviation of the error distribution and threat the statistical fundamental of the least square method [242] [243]. Additionally, the different final linear forms from same original equation can lead to different degree of fitting [243]. Thus, there is

an agreement in the inappropriate of the linear methods to correlate experimental data. The use of non-linear methods based on iterative mathematical methods is then suggested [244]. The non-linear regression methods generally involve the use of error functions in order to "minimise the error between the experimental and predicted data" [242], one of the most used functions is the correlation coefficient R^2.

5.7 Summary

Several studies have agreed that processes where ion-exchange is clearly identified as the main mechanism cannot be modelled using the widely-used adsorption models, such as Freundlich and Langmuir, since ion exchange it is a competitive process of at least two ionic species, thus, it is not purely an accumulative process and ion-exchange deviates from the ideal adsorption process where only species are attached to solid surface [245, 246]. Also in zeolites, not being energetically homogeneous surfaces, the use of simplified models is very restrictive, and often incorrect. Nevertheless, since thermodynamic models consider initial and final states only, models can complement the kinetic results providing significant information about the adsorption capacity, the type of interactions between sorbate and adsorbent (in terms of energy) and adsorptive sites homogeneity.

Since the appearance of hierarchical materials to overcome diffusive limitations in microporous zeolites, the methods to quantify how the effectiveness of materials have improved. These methods are based on the identification of rate-controlling steps and the calculation of diffusion rates and diffusive coefficients.

In the next part of this thesis the methodology and results are presented. The immediate next chapter describes the characterisation techniques to analyse the prepared materials in further chapters.

Part II

Methodology and Results

Chapter 6

Characterisation Techniques

6.1 Introduction

A wide range of analytical techniques are currently available to analyse zeolites characteristics. The main purpose is to establish relationships between their different properties and applications. It should be emphasised that not all the techniques are suitable for all zeolites. It is important to identify what specific characteristic is intended to study in order to choose the most appropriate techniques. Several techniques are considered to play a crucial role in identifying zeolites' preoperties. Thus, the major scientific fundamentals of X-Ray Diffraction (XRD), N_2 physisorption (BET), Scanning Electron Microscopy (SEM), Transmission Electron Microscopy (TEM), Zeta Potential and Dynamic Light Scattering (DLS) techniques are described. For the heavy metals quantification, involved in adsorption applications, Inductively Coupled Plasma Optical Emission Spectroscopy (ICP-OES) was used and it is also described in this chapter.

6.2 X-Ray Diffraction (XRD)

X-Ray Diffraction (XRD) is one of the most important techniques to characterise crystalline solids. This methodology identifies the structure through the crystallographic phases of analysed material. Also it can be used to estimate the crystallinity degree

and/or the purity of a phase [247]. XRD data can also provide information about chemical composition [92]. The development of this technique has allowed understanding of the structural configuration of zeolites. Nevertheless, some controversy has risen about the first use of XRD in the identification of zeolite phases. Pauling, recognized to be the pioneer, when in 1930 he identified sodalite-like compounds [248]. More recently, literature has emerged establishing that Pauling's contribution was not entirely complete. Baur *et al.* [82] give the credit to Jaeger, who in 1929 was investigating the composition of blue pigments, solved for the first time the sodalite structure.

6.2.1 Definition

X-Rays are a form of radiation that exist in the range of 10-10^{-3} nm of the electromagnetic spectrum [247]. This scale is similar to the inter-atomic spacing. When these beams interact with solid materials at a determined angle, they are dispersed in many directions by the atoms present on their way. Part of this radiation is reflected by the surface with same angle of incidence but different intensity. This phenomenon is called diffraction [248]. Diffracted light Intensity is detected and measured with respect to the angle of incidence. The graph of intensity as a function of the angle is named diffraction pattern or *diffractorgram*.

6.2.1.1 Bragg's Law

XRD analyses are based on Bragg's Law which explains that if monochromatic radiation[1] λ hits two parallel planes A and B in a material separated by distance d at specific angle θ, the reflected, i.e. diffracted waves, will produce a constructive interference only if their "path difference is equal to an integer number, n, of wavelengths [249] and in order to have a maximum intensity this condition has to be satisfied. This requirement is known as Bragg's condition. If this condition is not fulfilled, waves could have a destructive interference and both waves are cancelled, with no intensity at all. The

[1]Monochromatic makes reference to radiation within same wavelength.

Bragg's law is defined as:

$$n\lambda = 2d\sin\theta \tag{6.1}$$

The path difference is understood as the additional distance that X-Rays travel in the bottom layer B as it is seen in Figure 6.1 this is represented by the segment SQ+QT

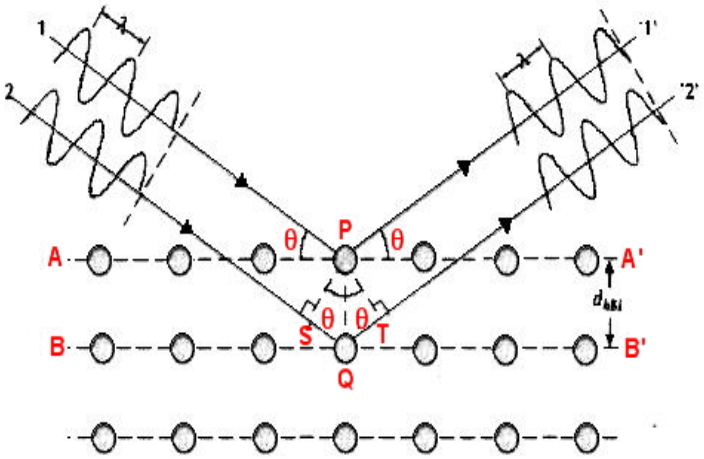

Figure 6.1: The phenomenon of X-ray Diffraction. [250]

6.2.2 The Diffraction Pattern

The main structural information that can be obtained from the diffraction pattern is the peak position, diffraction intensity of peaks, peaks width and the background signal [98]. Figure 6.2 exemplifies this. Peak position is a consequence of the unit cell geometry, 2θ values are function of the d-spacing of their respective reflections. Relative intensity is defined by the atomic positions in the cells and peak width depends on crystallite size [98]. The relationship between the peak width and crystallite size is given by Scherrer equation [251]:

$$\Gamma = \frac{K\lambda}{L\cos\theta} \tag{6.2}$$

Where Γ is the full width at half maximum (FWHM), L is the average crystallite size, K is the Scherrer constant, λ is the wavelength of X rays and θ is the position angle of the selected peak.

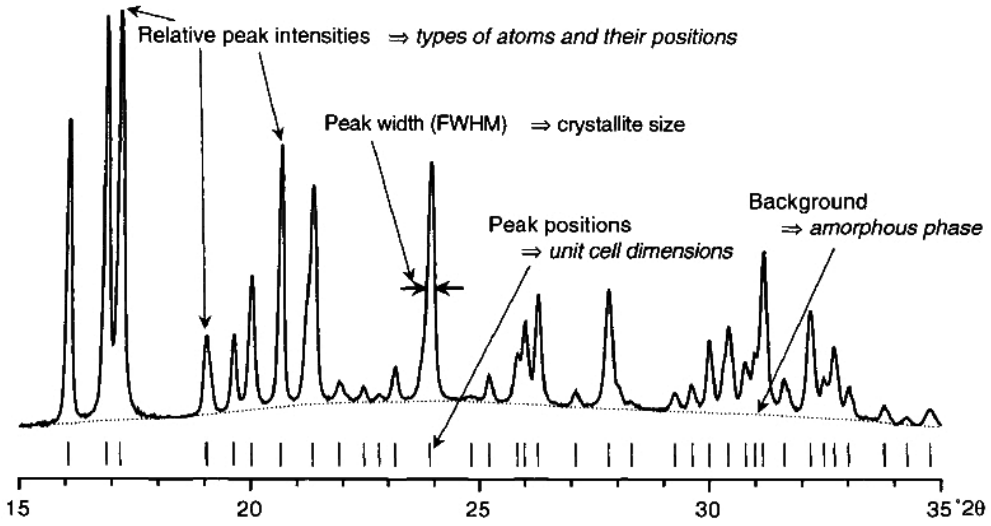

Figure 6.2: Different aspects of pattern diffraction that provide information about analysed material [98]

6.2.3 Diffractometer

The diffractometer is the device in which the XRD analyses are carried out. Figure 6.3 shows the schematic configuration of a generic diffractometer. Three main sections are distinguishable: the source S, sample holder H and the detector D. The sample is placed in the centre of the device, the X-ray source is fixed and lined parallel to the sample. The detector is "attached " on the 2θ angle. In order to satisfy the experimental condition given by "the angle between the plane of the sample and angle incident equals to that of direction of diffracted beam" [247]. 2θ axis spins twice the times than ω-axis when measurement is carried out.

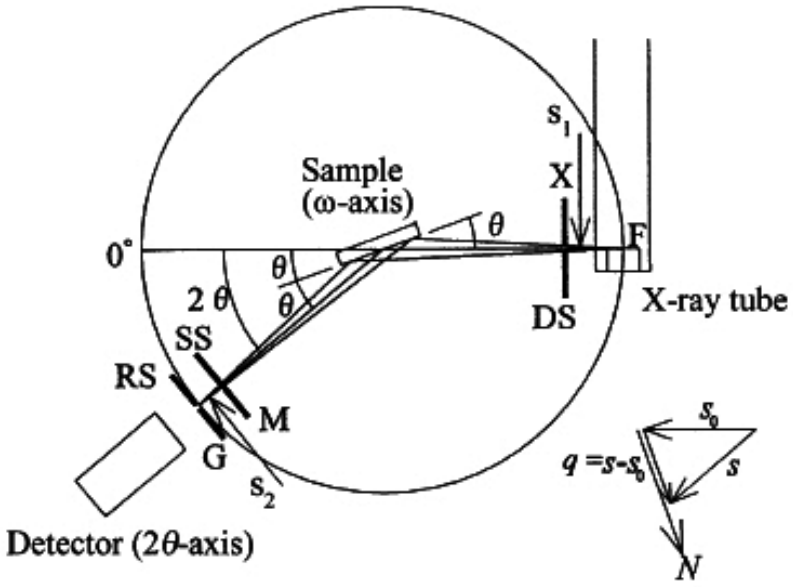

Figure 6.3: Schematic representation of a X-Ray Diffractometer [247]

6.3 Electron Microscopy

In general, a microscope is any device that allows details detection that it is impossible for the human eye. The main difference between a traditional (optical) and modern electron microscopes is related to their resolution. The concept of limit of resolution is defined as the minimal distances by which two structures can be separated and still appear as two distinct objects [252].

In 1931, E. Ruska and M. Knoll developed the first electron microscope. Its operation was based on the classic optical microscopy, but instead of visible light as source, it uses electron beams [216]. Electron microscopy techniques have found diverse applications in zeolite science. In time, different electron microscopes types have been employed for real-space imaging and structural analyses (by electron diffraction techniques) [253]. The earliest use of electron microscopy in the zeolites' field dates back to 1958, when Menter *et.al.* [254] presented a sodium-faujasite crystal micrograph. After, in 1972 a complete study about the porous structure of zeolite L by electron microscopy was published by Frety [255]. However, the first high-resolution image of a zeolitic material is attributed to Sanders in 1979 [256]. In this chapter Scanning

Electron Microscopy and Transmission Electron Microscopy are described.

6.3.1 Transmission Electron Microscopy (TEM)

The typical operation involves the use of accelerated electrons which are a consequence of the application of high voltages, usually in the range of 100 - 1000 kV. In order to condense and focus the electron beam, magnets and metallic slits are utilised. When the beam hits the sample they interact, some radiation is absorbed by the sample and some other portion is deflected crossing a system of magnetic lenses that focuses and amplifies the signals, forming two-dimensional images. A simplified TEM diagram is shown in Figure 6.4. TEM techniques have allowed zeolite scientists to obtain information about structure related to connections, defects and nature.

TEM is a very expensive technique due to the high-energy levels needed for its operation. A report in late '90s stated the operative costs for commercial TEM were about £1.23 for each electron volt [257]. Resolution limit in TEM can reach 0.2 nm.

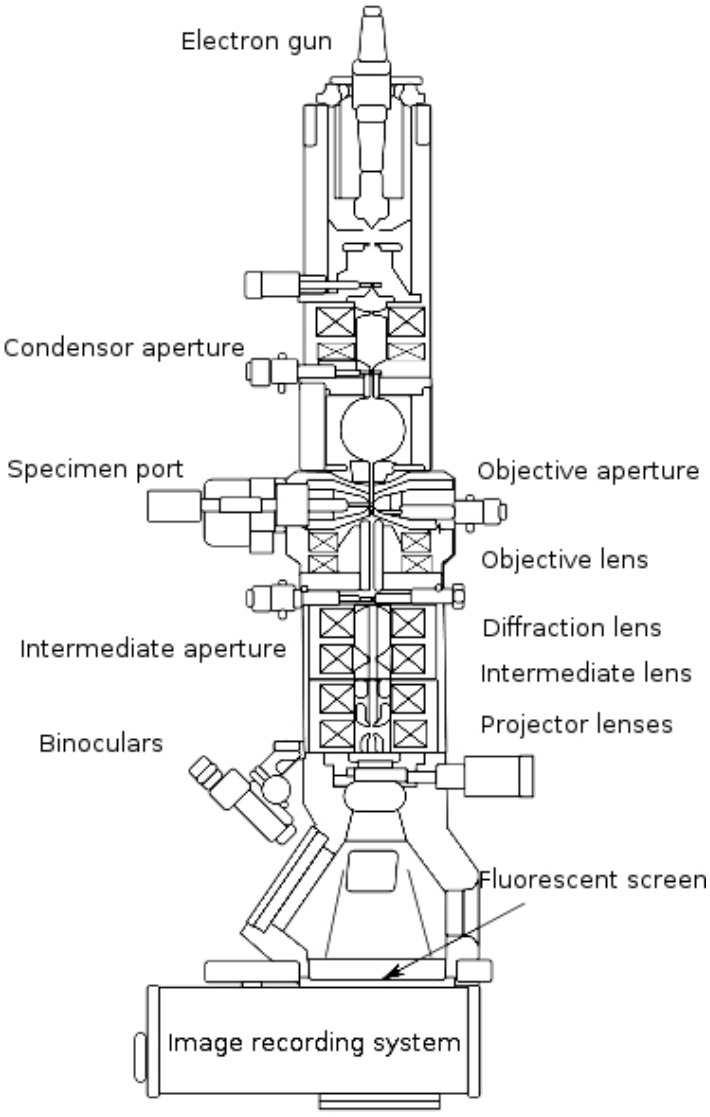

Figure 6.4: Schematic diagram of a Transmission Electron Microscope [216]

6.3.2 Scanning Electron Microscopy (SEM)

In zeolite science, SEM is a tool that is commonly used to analyse zeolites' morphology. If compared to TEM techniques, SEM has less resolution. However, SEM has good enough resolution for analysing *classical* zeolites (up to 0.1 μm) and provides three-dimensional images. The operating principle of a scanning electron microscope is similar to TEM, the main differences lay in how electron beams are used to hit the sample and how reflected particles are converted into images. SEM operation is based on a high-energy beam of electrons ranging from 5-50 kV that *impact* a solid bulk, i.e. the sample. The beam runs through a lenses system where its condensed (focused); according to the principles of electronic microscopy, the smaller the beam the better resolution because the energy is concentrated in a smaller surface. Also, a coil arrangement magnetically deflect the incident beam, responsible for scanning the electrons on the specimen, line by line and point by point [258]. In this case, the electrons that are not absorbed by the sample, are *bounced* in different directions and with different characteristics such as such as backscattered electrons and X-rays, Auger electrons, secondary electrons among others [252] as it can be seen in Figure 6.5. The image of the sample is usually generated by secondary and backscattered electrons meanwhile X-rays are used for elemental identification.

These *bounced* particles, produce different type of signals due to their different nature and properties like density and chemical identity [259]. Finally, signals are collected, amplified and transformed into visual images on a cathode ray tube, similar to the previous-generation of televisions. The requirement for samples being analysed under electron microscopes, is they can conduct electricity, zeolites are non-conductive materials, thus these kind of materials are usually coated with thin films of conductive metals such as gold. Figure 6.6 shows principal constituents of SE microscope.

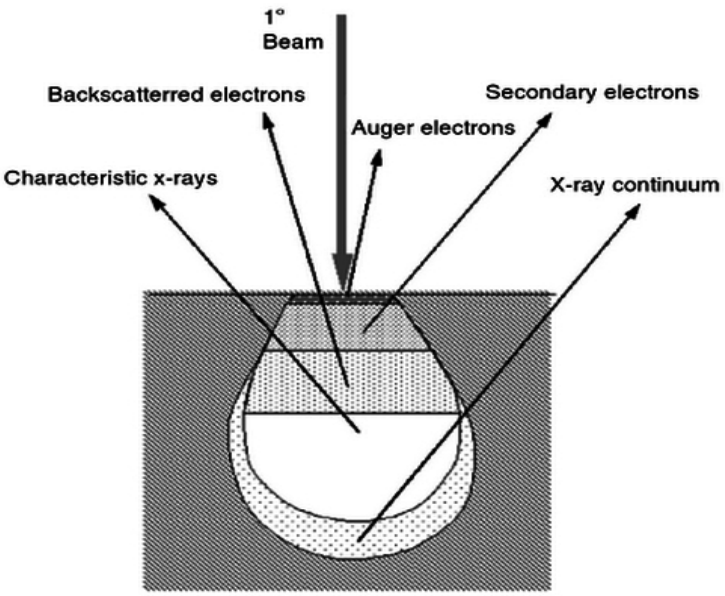

Figure 6.5: Different kind of bounced particles after hitting the sample in SEM [252]

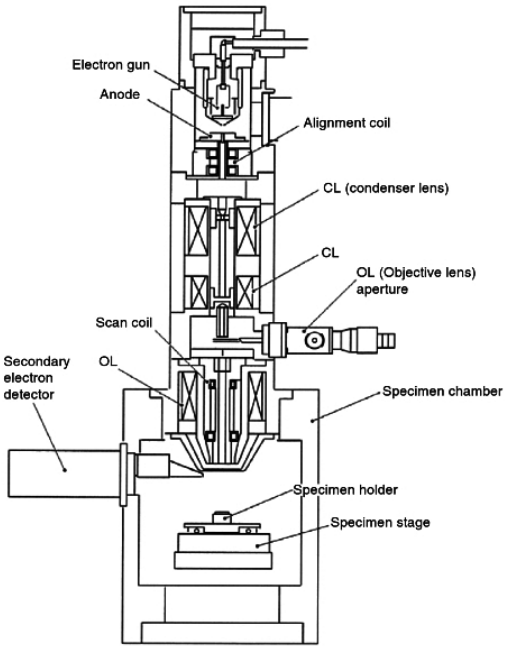

Figure 6.6: Diagram of main constituents of the Scanning Electron Microscope [252]

6.4 Dynamic Light Scattering (DLS)

Particle size is a key materials characteristic. It has influence on a variety of properties such as: reactivity, suspension stability, texture, appearance and viscosity. However, in real systems, where many particles are non-spherical it is extremely rare to find the exact size in each particle in a bulk. To overcome this, the particle size distribution (PSD) is the accepted approach. It is said that all materials have a PSD, and depending on how narrow it is, one can find *monodisperse* and *polydisperse* distributions [260]. Generally PSD are presented plotting the % frequency against particle sizes.

6.4.1 Definition

Dynamic Light Scattering (DLS) is an analytical technique that measures the average particle size and particle size distribution of dispersed particles in suspensions [260]. This technique is based on the measurement of the motion of particles as a consequence of the random collisions in a fluid using lasers. This motion is known as Brownian movement. In a suspension, Brownian motion of dispersed particles defines the "rate of change" of emitted light intensity. These changes are transformed into diffusional coefficients or a distribution of diffusional coefficients and these are converted into particle size or particle size distributions using the Stokes-Einstein equation [260].

$$d = \frac{K_B T}{3\pi\eta D} \tag{6.3}$$

where, D is diffusional coefficient, K_B is the Boltzmann constant, T is absolute temperature, η is viscosity and d is the hydrodynamic particle diameter.

Similar to X-ray diffraction and electronic microscopy, DLS is based on the effect of impacting matter with electromagnetic radiation, in this case this radiation takes the form of a laser.

The laser impacts the suspension and the electric field generates a continuous polarization of atoms in the molecules, causing that molecules act as a secondary source

light. Figure 6.7 shows a schematic representation of DLS equipment. A laser beam is focused at the sample using a lens (L) and pinholes (P). The sample is usually placed in a cubic cell located at 90° with respect to the source. A beam stop (BS) is located behind the sample holder, to collect the light.

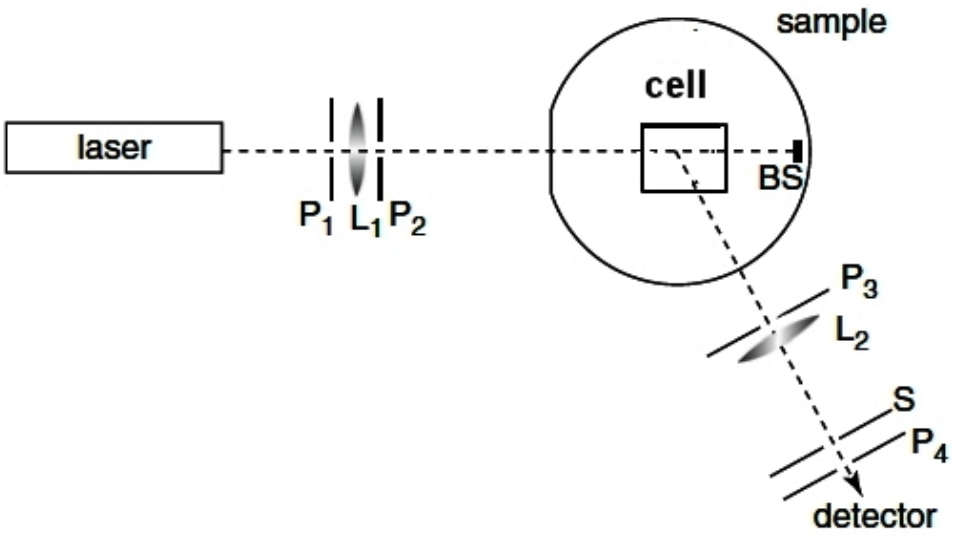

Figure 6.7: Diagram of main constituents of the Dynamic Light Scattering equipment [260]

This technique finds its main limitations in the variations of particle size. Really small particles move faster but they are not particularly good to scatter light, usually particles below 0.005 μm are different to measure. On the other hand, for larger particles (> 0.5 μm), it is possible that sedimentation occurs. Also high viscosity levels lead to a reduction in the movement of particles limiting the technique applicability [260].

6.5 Zeta (ζ) Potential

In order to quantitatively analyse materials' charges on surfaces, zeta potential measurements has been widely applied. It provides information about the intensity and charge (+ or -) of electric potential present in surfaces. The zeta potential measurements are based on the *electrophoretic mobility*. This mobility is a cause of the application of an electric field to charged and suspended particles. When an electrically

charged particle is suspended in a conductive solution it will attract opposite charges. If an electric field is applied particles will move to the opposite-charge electrode. The theoretical separation distance between oppositely charged species is known as *shear plane*.

6.5.1 Definition

The zeta potential is defined as "the electric potential in volts from the plane of shear to the solutions' bulk" [261]. Often, this plane is also called the *double layer*. Electrophoretic mobility (EM) is related to the ζ potential by Henry's equation [262]:

$$EM = \frac{v}{(dV/dx)} \tag{6.4}$$

Where v is the particle velocity, dV is voltage potential and dx is the distance between electrodes.

The velocity of the moving particles and consequently the zeta potential distribution is usually assessed using "interferometric" techniques. Particularly laser techniques are also used since same instrument (Malvern Zetasizer in this case) to measure the particle size distribution. The equation that usually relates the velocity with zeta potential was proposed by Helmholtz and Smoluchowski [261]:

$$\zeta = \frac{4\pi\mu}{D} EM \tag{6.5}$$

Where ζ zeta potential, μ viscosity of water and D is the dielectric constant for the medium.

Typically, zeta potential values are an average of the distribution of zeta potential. The zeta potential values fall in the range from -100 mV to 100 mV. This values can also determine how stable a colloid can be. Suspended particles out of the $\pm$ 25 mV range are considered to be more stable. On the contrary, particles with a zeta potential distribution within this gap tend to agglomerate. Zeta potential values are influenced

by the pH of the media. In fact, when zeta potential is equal to 0, it is said that material is at its isoelectric point.

6.6 BET Method

The method most widely used to asses surface area and porous characteristics of materials with technological importance is the Brunauer-Emmet and Teller (BET) using N_2 at 77 K. In fact, it has been recognised as an standardised method. BET theory was first proposed in 1934 while working on ammonia catalysts. It is an extension of the theory proposed by Langmuir in 1916. BET theory originally defined and described the point B in a isotherm type II. According to them, point B is an inflection point where the surface is completely covered by a *monolayer* of adsorbed molecules. After this point more molecules are adsorbed on top the previous ones forming the so-called *multilayer* [180]. Point B can be seen in Figure 6.8.

Sing [180] pointed out limitations of this method saying that it is an "empirical procedure" and it is not dependent on the BET theoretical model. Additionally, the methodology has been criticised because of a lack in the theoretical background. Thus, cautions have to be considered when using it. For example, the suitability of the technique for the material being analysed.

6.6.1 Definition

The monolayer capacity is obtained from the BET plot, and consequently if the cross-sectional area of the adsorbed molecules is known, specific surface area can be calculated. In order to obtain the plot, a linear form of BET equation is used:

$$\frac{p/p_0}{n(1-p/p_0)} = \frac{1}{n_m C} + \frac{C-1}{(n_m C)(p/p_0)} \tag{6.6}$$

"where n is the number of adsorbed molecules, n_m the number of adsorbed molecules in the monolayer, p is the pressure of the system, p_0 is the vapour pressure of adsorbate

and C is a constant related to the enthalpy and heat of vaporization" [263] but its real physical interpretation is still unknown [180]. $(p/p_0)/(n(1-p/p_0))$ is plotted against p/p_0 (relative pressure), the slope $(C-1)/n_mC$ and interception in $1/n_mC$ are calculated and n_m is obtained. This value leads to the surface area, (also known as BET surface area, S_{BET}) of the solid material if size and cross-sectional area of a single adsorbed molecule is known.

6.6.2 The Adsorption Isotherm

Adsorptive processes are always influenced by temperature, pressure and the interactions nature of adsorbate with adsorbent E. If temperature T is fixed, the relationship between the amount of sorbed matter W and the pressure P (or concentration for liquids) is called adsorption isotherm [264]:

$$W = f(P, E)_t \tag{6.7}$$

In the volumetric approach, the isotherm is usually plotted by adding known amounts of adsorbate at certain intervals increasing the system's pressure. Certain amount of total gas is adsorbed on the solid [181]. After equilibrium is reached, pressure is reduced in order to have a desorption branch. The isotherm analysis are important because often it can be possible to obtain valuable information by visual inspection. For example, they give an idea of the pore size distribution. There are six types of adsorption isotherms recognised by IUPAC [181, 263], all are shown in Figure 6.8.

Type I. Is the characteristic isotherm of microporous materials such as zeolitic materials and activated carbon. It exhibits concavity to the pressure or concentration axis

Type II. Is related to the presence of macropores. Shows an inflection point (B) indicating the monolayer section, after this point the formation of multilayer is indicated.

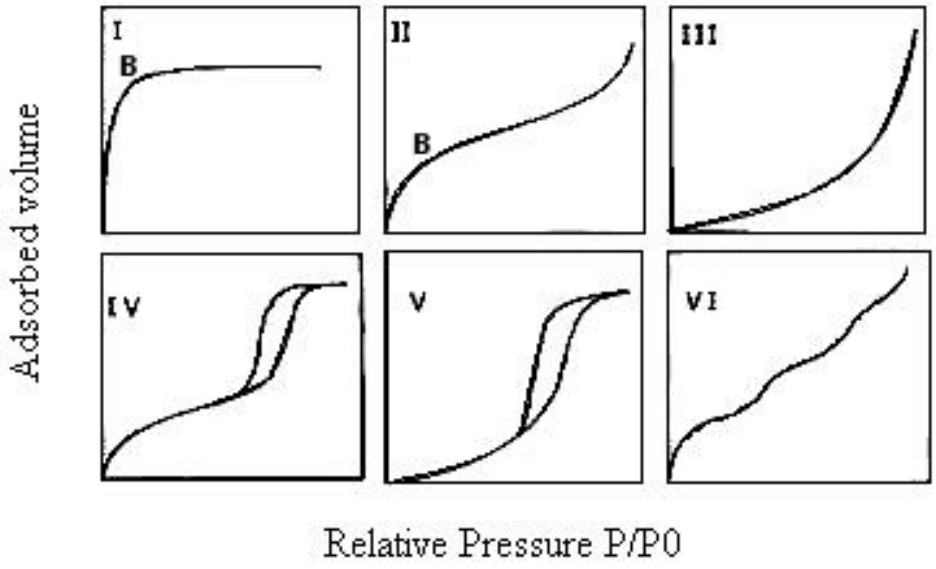

Figure 6.8: The six types of adsorption isotherms [181]

Type III. Is convex to the pressure axis. This type is characteristic of materials with low adsorption capacities.

Type IV. The major feature about this type is the hysteresis loop related directly to the presence of mesopores in the material. Also, the silhouette of hysterisis loops are related to the shape of the pores

Type V. This type of isotherm is similar to Type III in the adsorption branch, but the hysteresis loop formed by the desorption branch indicate the presence of mesopores.

Type VI. It is related to non-porous materials. It is not a very common isotherm

In Figure 6.9. the instrumental configuration of the porosity analyser is shown.

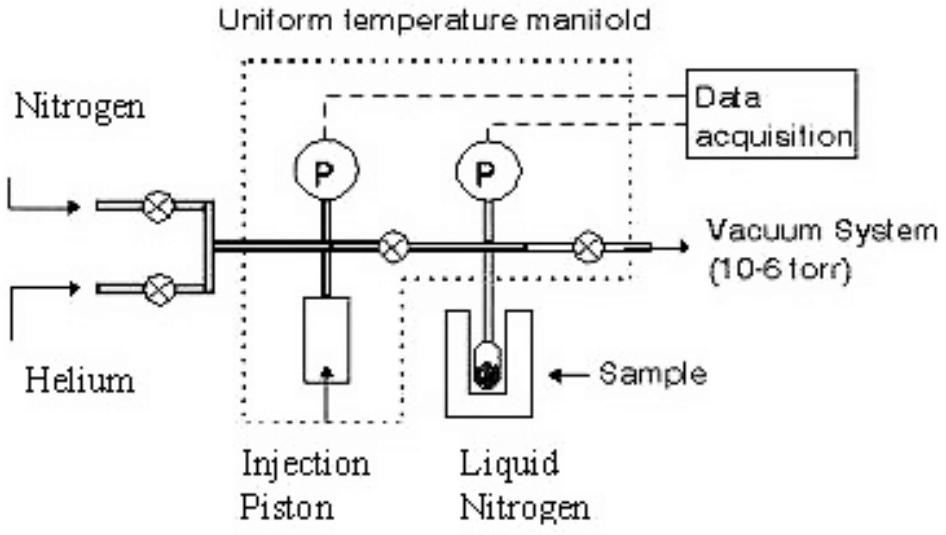

Figure 6.9: Diagram of surface analysis equipment [265]

6.7 Thermogravimetric Analyses

Thermal methods are useful in a variety of fields in materials science. Thermal analyses are carried out to evaluate the thermal stability of samples, to determine the amount of moisture or volatile compounds in samples and to quantify the percentage of any phase present in a composite. Also, thermogravimetric analysis gives useful information about the different compositions forming a composite if one of the substances present can be evaporated at certain temperature levels during the experiment. The species amount adsorbed in their micropores can influence the behaviour in applications such as adsorption and ion exchange.

Three different regions are considered when analysing zeolites under the action of temperature. These regions are not completely fixed, and they change depending on the type of material or composition: a) The first section ranges from ambient temperature to 220 °C, in which the desorption of interstitial water molecules contained within the zeolite pores occurs; b) the second region ranges from 620 °C to 1200 °C, where zeolite, depending on the type of framework, collapses; and c) the third one, that occurs at temperatures higher than 1200 °C where recrystallisation or phase changes

take place [266].

6.7.1 Definition

Thermal analysis is defined as "the monitoring of a change in property of a sample which is related to an imposed temperature alteration" [267]. If the property subject to analysis is the mass, the thermal technnique is known as thermogravimetry. In a typical run, the sample is collocated in a crucible[2]in a furnace under a controlled atmosphere and a temperature program is defined. Atmospheres during the TGA experiments can be either inert or oxidising and programs can be isothermal, linear incremental or programmed steps combining these two. After the temperature starts to increase, the mass of the sample decreases. Sometimes, if chemical reactions occur for instance, there is a mass increase. Transducers convert these changes into electric signals and after they are recorded and plotted. [267]. The results are known as *thermograms* which is a graph of the weight percentage against temperature or time. Also, the first derivative is used to detect exactly where largest changes occur. In Figure 6.10 a typical TG instrument scheme is shown.

[2]Crucibles are made of materials with low thermal deformation coefficient such as platinum or stabilised alumina

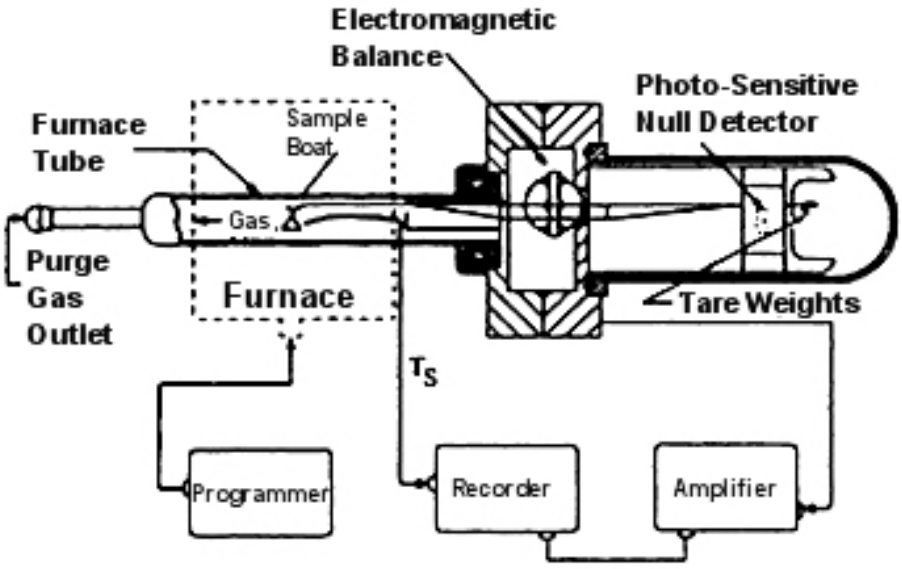

Figure 6.10: Simple scheme of Thermogravimetric Equipment [268]

6.8 Inductively Coupled Plasma – Optical Emission Spectroscopy (ICP-OES)

Inductively Coupled Plasma (ICP) is an analytical method widely used to quantify amounts of dissolved metals. In general, measured samples are contained in liquid phase and often a digestive or dissolution method is required. ICP is a very versatile technique that has been used in many fields such as metallurgy, geochemistry, food industry, environmental, biological and nuclear sciences [269]. The technique is similar to other spectroscopic methods and is based on the measurement of electromagnetic radiation which is adsorbed or emitted from specific atoms or sample of interest. ICP can provide researchers qualitative information through the specific wavelengths of the emitted or absorbed light whereas the quantitative data can be obtained from the intensity of this particular type of radiation [269]. The extension Optical Emission Spectroscopy is related to the detectors system that is based on. As the name points out, optical detectors of emitted light are used, in contrast to ICP-MS where mass

spectroscopy is used and is in direct relation with the amount of measured ions.

6.8.1 Definition

When an atom is excited with the incidence of electromagnetic radiation it undergoes a series of energy transitions. Excitation means that one electron is displaced from a low energy level to another one with more energy it will produce an excited atom. Eventually, this excited electron will be drop back to the original state but this process is companied with the emission of light (photon). If energy is high enough to *separate* one electron from the atom, ionization is taking place. Photons have a particular wavelength for each element [269]. If appropriate detectors are utilised, it will be possible to identify elements present in samples and if intensity or amount of radiation is measured concentration can be assessed. In Figure 6.11 are exemplified the differences between excited and ground states and different energy levels in a atom.

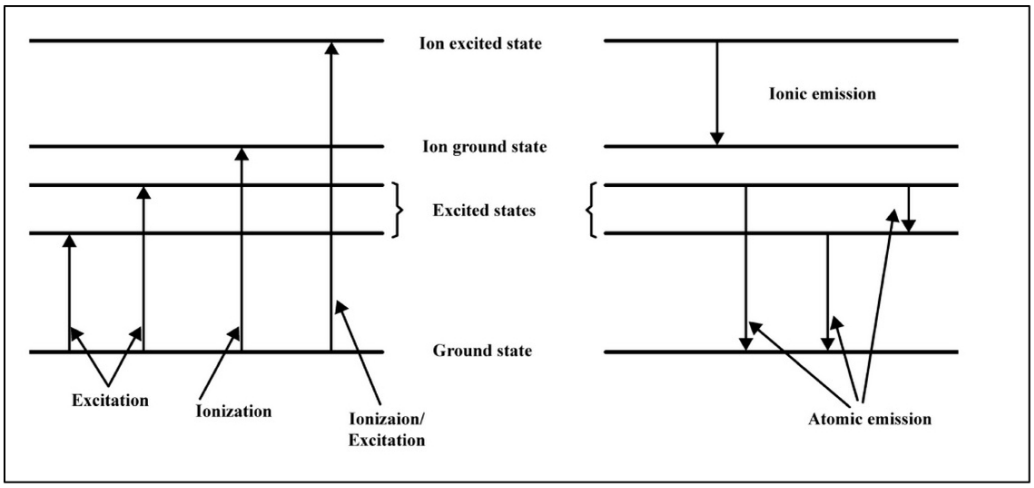

Figure 6.11: Simple represtanation of electrons in different energy levels; ground and excited states [269]

First, high-energy electrons are produced by the ionization of an inert gas, generally argon. At the top of the torch there is a coil system where argon is decomposed into ionic species with the aid of radiofrequency generator (RF). This usually works in the range of 0.5-2 kW and 27 to 40 MHz to accelerate electrons. This method is known as inductive coupling and it causes a consequential decomposition of the gas into plasma.

The sample is first carried to a chamber and then to the torch through a nebuliser, with the aid of peristaltic pumps, in the form of aerosol. Temperature levels produced are usually in the range of 6,000 K to 10,000 K that breaks chemical bonds in sample. Then, radiation which has different wavelengths is split with a monochromator in order to identify the element present by optical emission systems. Finally, the pumping system also removes waste samples after analysis [269]. In Figure 6.12 a schematic diagram of a generic ICP-OES is shown.

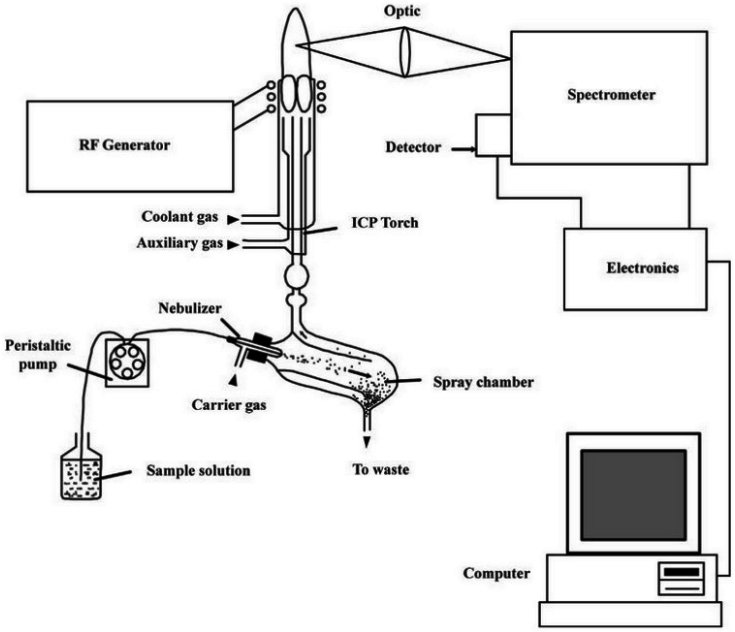

Figure 6.12: Diagram of main constituents of an Inductively Coupled Plasma - Optical Emission Spectroscopy equipment [269]

Major advantages about the use of ICP methods is the detection limits, speed and low spectral interferences. Typical instruments have detection limits up to some parts per billion (ppb) to 0.1 parts per million (ppm) [270].

6.9 Summary

In this chapter the characterisation techniques involved in this thesis were described. The theoretical background of each technique and how the operational principle is related to the analysis of the materials was reviewed. Also, a description of typical devices

and limitations were presented. All revised techniques aim to analyse the structure, texture, morphology, surface chemistry, particle size distribution and thermal analyses of materials used in this work. All this in order to obtain a better understanding about the materials properties and be able to make a correlation with their behaviour in the adsorption performance.

In the next chapter, experimental methodology is presented including characterisation results. The preparation of range of synthetic zeolites and the conditioning of carbonaceous supports prepared using different sources is described. Results and discussion to the particular methodology is included along with a conclusions section end of the each forthcoming chapter.

Chapter 7

Preparation of Zeolites and Carbon Supports

7.1 Introduction

In this chapter, the methodology for the preparation of synthetic zeolites type A (LTA), type Y (FAU), nanosized type A (NZA) and clinoptilolite (HEU) is described. Natural clinoptilolite characteristics are also summarised. The methods for the carbonisation and conditioning of raw materials in order to produce the scaffolding systems are explained. Additionally, the results regarding prepared materials are presented and discussed.

7.2 Methodology

7.2.1 Zeolite Type A - LTA

Zeolite type A (LTA) was prepared following the composition [271]:

$$3Na_2O{:}0.85SiO_2{:}Al_2O_3{:}180H_2O \tag{7.1}$$

First, 0.52 g of NaOH (99 % Fisher) was dissolved in 35 g of H_2O. Then 2.20

g of sodium aluminate ($NaAlO_2$ technical grade, BDH), as alumina precursor, were added until homogeneous (1 h) and finally, 1.38 g of sodium silicate (Na_2SiO_3 technical grade, BDH) was added and aged for 24 h under vigorous stirring. The reactive mixture was transferred to a Teflon-lined stainless-steel autoclave and put in the oven varying crystallisation time (3, 6 and 24 h) at 100°C. The product was recovered by filtration and washed until pH < 9 and solids were finally dried overnight at 70°C in order to obtain the final powder.

7.2.2 Nanozeolite LTA

7.2.2.1 Reduction Size using Ball Milling

The ball mill was used for the preparation of reduced-sized LTA. 20 ml of dried zeolite A, prepared following previously described methodology, were ground with 20 ml of ZrO beads and 40 ml of H_2O in a in a 6 cm-radius mill for 24 h at ∼150 rpm. Then the material was recovered using a metallic sieve to separate from the zirconia beads. Final material was dried overnight at 70°C.

7.2.2.2 Nanozeolite A (NZA) using Organic Templates

Originally this methodology was chosen as an alternative to the ball milling having in mind that the particles' sizes possibly are not completely homogeneous and the impacts can cause crystallinity loss. Thus, nanosized zeolite A (NZA) was prepared by using the so-called "clear solutions" method. For NZA the composition used was [124]:

$$0.3\,Na_2O{:}11.25\,SiO_2{:}\ 1.8Al_2O_3{:}13.4\,(TMA)_2O{:}\ 200\,H_2O$$

Two solutions were prepared: Solution A was made using 1.50 g aluminium isopropoxide ($C_9H_{21}O_3Al$, 98 %, Sigma-Aldrich), 19.54 g TMA-OH (25 wt. % in H_2O, Sigma-Aldrich), 0.04 g NaOH (99 %, Fisher) and 4.85 g H_2O until all solids were dissolved and formed a clear solution. For solution B, 3.38 g of colloidal silica LUDOX HS-40 (40 wt. % in H_2O, Sigma-Aldrich) and 3.38 g H_2O (pH ∼10) were used. Then,

solution B was slowly added to A under vigorous stirring; closed polypropylene jars were used as ageing containers. The mixture was left under agitation at room temperature for 24 h, after this, the reactant mixture was heated in the oven at 100 °C for 24 h. After crystallisation, a centrifuge was used to separate two phases, 11,000 rpm for 30 min, and particles were recovered and washed with deionised water to remove remaining OH^- ions in solution. After this, the material was dried and calcined at 600 °C under an oxidising atmosphere for 3 h to remove the remaining organic template. Finally, zeolite particles were redispersed in deionised water.

7.2.3 Zeolite Type Y - FAU

The synthesis of zeolite Y (FAU) involved the use of a seeding gel that reduces the crystallisation time [271]

7.2.3.0.1 Seeding gel The initial composition of seeding gel was :

$$10.97\,Na_2O{:}Al_2O_3{:}10\,SiO_2{:}180\,H_2O$$

Initially 6.88 g of NaOH were dissolved in 20 g of deionised water and 1.88 g of $NaAlO_2$ were added to a 100 ml plastic beaker. The mixture was stirred until solids was completely dissolved. After this, 13.13 g of colloidal silica (LUDOX HS-40, Sigma) were added to previous mixture and stirred for 30 min. The ageing was carried out at ambient temperature for 1 day under static conditions.

7.2.3.0.2 Feedstock gel For the feedstock gel, the original composition was:

$$4.3\,Na_2O{:}Al_2O_3{:}10\,SiO_2{:}180\,H_2O$$

In a 100 ml beaker, 2.08 g of NaOH were dissolved in 20 g of deionised water. Then, 1.78 g of $NaAlO_2$ were added. The mixture was stirred until solids were completely dissolved. Later, 13.12 g of colloidal silica (LUDOX 40-HS, Sigma) were added to

previous mixture under vigorous stirring until gel became homogeneous with a milky appearance. The FAU synthesis was made mixing the seeding and feedstock gels in a proportion of 10 % wt. seed gel and 90 % wt. feedstock gel. The total weight of the feedstock gel was 36.30 g of which 4.04 g of seed gel were added under stirring for 30 min. The whole content was finally transferred into an autoclave vessel and heated at 100°C varying the crystallisation time 18, 24 and 28 h.

7.2.4 Clinoptilolite - HEU

7.2.4.1 Natural Clinoptilolite

Natural clinoptilolite is originally from Turkey and no pretreatment or conditioning method has been applied. The chemical composition[1] is SiO_2 71.0 %, Al_2O_3 11.8 %, TiO_2 0.10% ,Fe_2O_3 1.7 %, Na_2O 0.4%, K_2O 2.4 %, CaO 3.4 %, MgO 0.10 %. Raw zeolite was only sieved to using metallic sieve #100 (0.149 mm) to remove larger particles of quartz. This material was also used as seeding agent in the subsequent protocols for the preparation of synthetic samples of clinopltilolite.

7.2.4.2 Synthetic Clinoptilolite

Two different experimental procedures to prepare synthetic clinoptilolite were carried out. The preparation methods were adapted from [130, 272, 273] and they were called Protocol 1 and Protocol 2 respectively.

7.2.4.2.1 Protocol 1 To produce the reactive gel were mixed: 16.27 g of H_2O, 1.24 g of NaOH (99 %, Fisher), and 3.57 g of $NaAlO_2$ (technical, Riedel de Haen) until solutions became transparent (1 h). Then 28.95 g of colloidal silica (Ludox HS-40, Sigma-Aldrich) were added and stirred for 1 h. After this, 20 % and 28 % wt. of natural clinoptilolite were added respectively and stirred for 10 min. All content was

[1]Holistic Valley. (December 2014). Clinoptilolite [Technical Data]. Retrieved from `http://www.holisticvalley.co.uk/wp-content/uploads/2012/11/Tech-Clinoptilolite-0-300um.pdf`

transferred then to a Teflon-lined stainless-steel autoclave and put in the oven for 2, 4 and 6 days at 140 °C under static conditions.

7.2.4.2.2 Protocol 2 For this protocol the effect of two silica sources, Ludox HS-40 and LS-30[2], is compared. The synthesis started dissolving 0.78 of aluminium hydroxide, $Al(OH)_3$ (Sigma-Aldrich) 0.59 g of 6M NaOH (99 %, Fisher) also are added 2.8 g of 6M KOH (analytical, BDH) and stirred for 30 min. Then, 7.5 g of colloidal silica Ludox HS-40 (or 10 g of LS-30) were added under stirring for 1 h. Finally, commercial clinoptilolite was used as seeding agent (5 % and 10 % of total mass) and it was added to the reactive gel and transferred to an autoclave at 180°C for 60 h for crystallisation.

For both Protocols 1 and 2, final materials were recovered by filtration and washed with deionised water to remove the excess of hydroxide ions, pH level was reduced to ∼9 and materials were then dried overnight at 70°C.

7.2.5 Carbonisation Process

7.2.5.1 Thermal Treatment

First, six materials were chosen as carbon precursors: corn husk, corn cob, sugar cane bagasse, cherry stones, date stones and hazelnut shells. Raw materials were cut, washed with deionised water and dried at 70°C for 12 h. Carbonisation was carried out in a tubular furnace under nitrogen atmosphere heating to 200°C at 5°C min^{-1}, held for 2 hours followed by ramping at 5°C min^{-1} to 600°C, again held for 2 hours prior to a final ramp of 5°C min^{-1} to 900°C the temperature was held for two hours after which the sample was allowed to cool to room temperature as shown in Figure 7.1. The process was carried out in a tubular furnace under nitrogen gas to create an inert atmosphere. After carbonisation, materials were crushed and sieved in order to obtain an homogeneous powder. Carbonised materials prepared using corn husk, corn cob, sugar cane bagasse, cherry stones, date stones and hazelunt shells were called CH, CC,

[2]The main difference between two silica precursors is the stabiliser counter ion sodium amount, SiO_2/Na_2O (wt.) for LS is 280 and for HS is 95

SCB, CS, DS and HN respectively.

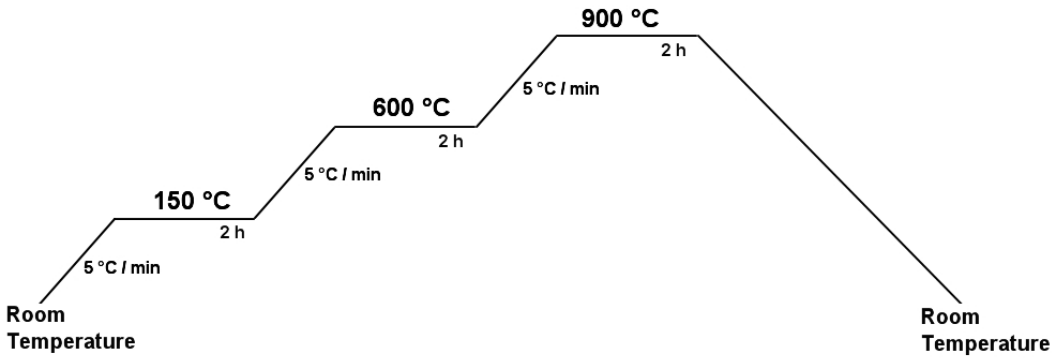

Figure 7.1: Thermal treatment carried out under nitrogen atmosphere

Further results, in Section 8.3.1.3 in (p.150) show carbon materials being used as zeolite supports. Preliminary results showed that materials being less dense as corn husk, corn cob and sugar cane bagasse did not support certain hydrothermal conditions leading to the structural damage and eventual collapse. For this reason, more dense materials were chosen to carry out subsequent methodologies. In the next section a method for the chemical surface modification of hazelnut shell, cherry and date stones is described.

7.2.5.2 Chemical Modification of Supports

After the carbonisation, CS, DS and HN materials were treated using polydiallyldimethylammonium chloride (PDDA , 20,000 MW, Sigma) solution (1 % and 2 % wt. in 0.1 M NaCl, pH 9.5) to provide positive electrical potential on carbons surface, this was done under ultrasonic mixing for 1 h (1 g of carbon in 20 ml solution). Finally, the PDDA excess was removed with deionised water and all carbon particles were dried overnight at 70°C. The selection of PDDA as adhesive material is based on its proven extended use, cost and easy to manipulate.

7.2.6 Characterisation Techniques

In order to identify the presence of zeolite phases were analysed by X-Ray Diffraction (XRD) using a Rigaku powder diffractometer. Particle size distribution and Zeta potential was assessed by Malvern Zetasizer 1000HS. In order to study microtopography of composites and to observe how zeolite particles were distributed on supports, Transmission and Scanning Electron Microscopy (TEM and SEM) was conducted using FEI Technai and FEI Quanta 200 respectively. To determine the final zeolite/carbon ratio Thermogravimetric analyses using a QA5000 (TA Instruments) were conducted under an O_2 atmosphere.

7.3 Results and Discussion

7.3.1 Zeolite Type A - LTA

In order to confirm the success in the preparation of the LTA phase, commercial samples (BDH, molecular sieve type 3A) were used to compare the prepared materials described in section 7.2.1. The results, in Figure 7.2, indicated that the XRD pattern of the different synthesized zeolites type A agreed with the reference pattern and there is evident the characteristic peaks on 7.1°, 10.1° and 23.9° [274]. It is noted that intensity increased as the crystallisation time increased.

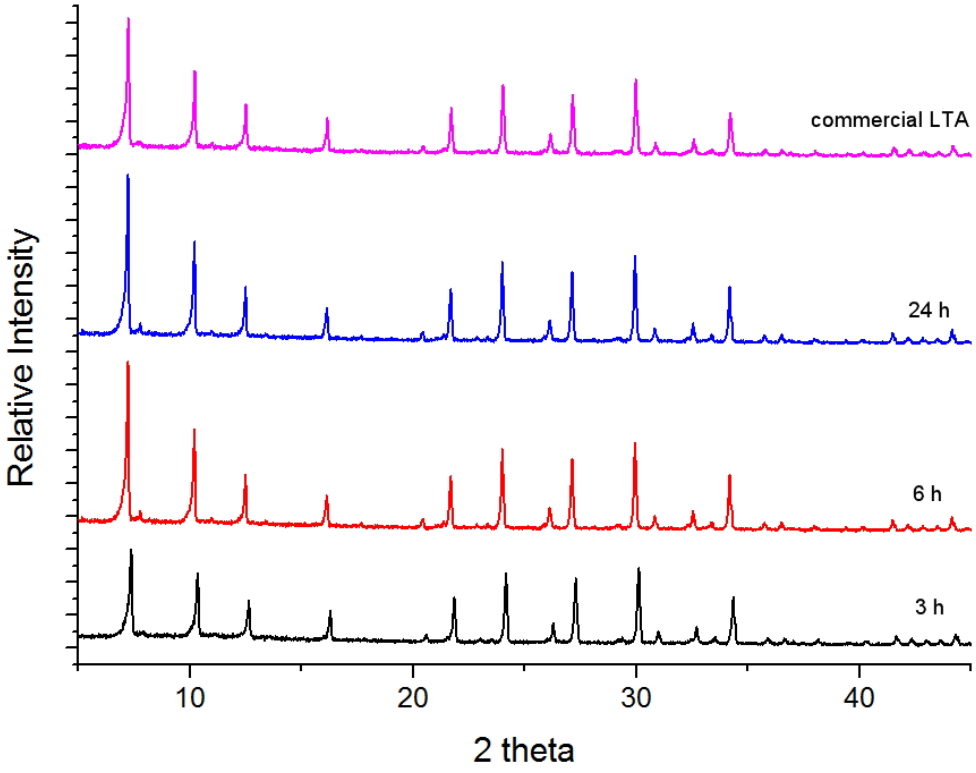

Figure 7.2: XRD patterns: zeolite LTA standard, 3 h, 6h and 24 h respectively

The morphological analysis performed by scanning electron microscopy shows in Figures 7.3 a), b) and c) zeolite type A prepared at 3, 6 and 24 h respectively. The image a) shows a poor crystallization compared with b) and c), observing a larger amount of amorphous material or transition phases which are related to the less intense peaks in the XRD patterns in Figure 7.2.

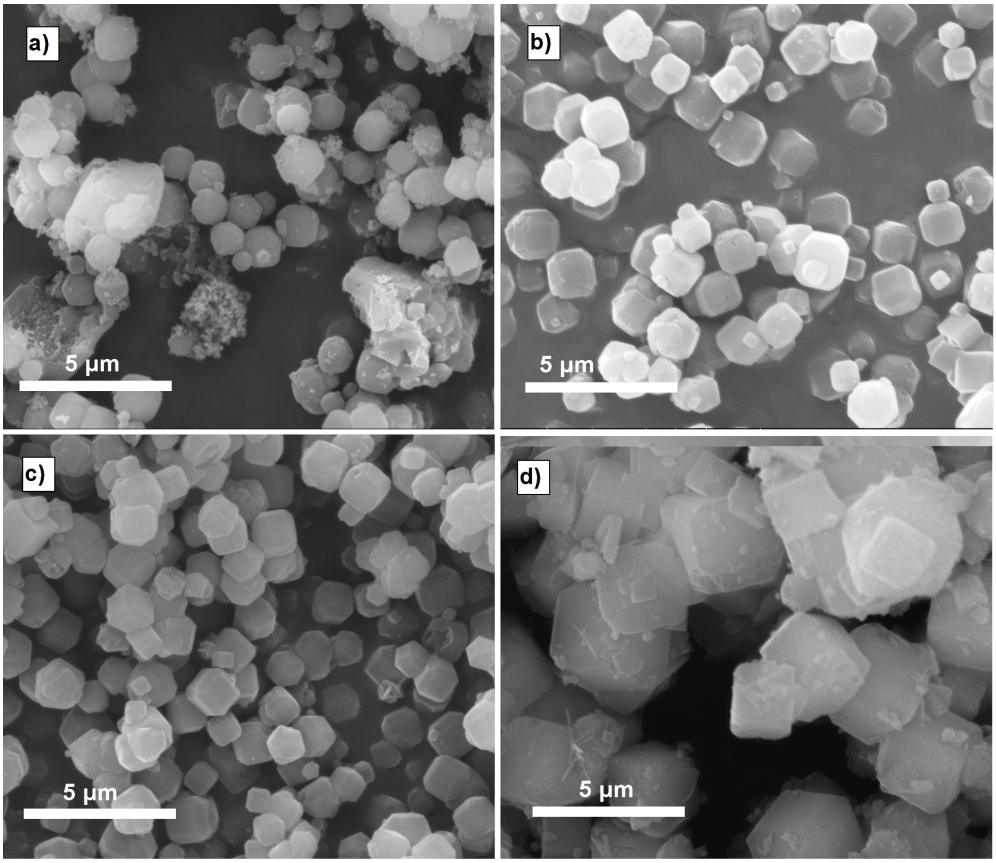

Figure 7.3: SEM pictures of synthesized and standard zeolite A. All micrographs show zeolite A images varying the crystallization times: a) 3 h, b) 6 h, c) 24 h and d) commercial sample

After 6 h of crystallisation, particles are more homogeneous and the morphology of zeolite A can be observed with well defined chamfered-edged cubes with crystal particle size around 2 μm. For the case of the sample prepared after 24 h. a more uniform particle size is observed, showing a reduced amount of amorphous material coinciding with higher peaks in the XRD pattern shown in 7.2. A high percentage of crystallisation after 6 h was achieved. Thus, for practicality and economical reasons, all consequent synthesis involving LTA procedures were carried out for 6 h for this particular zeolite type.

7.3.2 Nanozeolite A - NZA

7.3.2.1 Ball Milled

Figure 7.4 a) shows SEM image for ball-milled zeolite A and the particle size distribution obtained by DLS technique. In the figure can be seen reduced-sized particles along with deformed cubic-shaped crystals, this is associated with the impacts of the milling particles. Particle size plot shown in 7.4 b) exhibits a narrow distribution having 60 nm as the average size. In Figure 7.4 are observed larger particles than in particle size distribution. In this case, DLS results are representing small particles suspended in the supernatant after the ball milling. In further experiments, these supernatant dispersions were used as seeding agents to ensure the reduced particle size distribution.

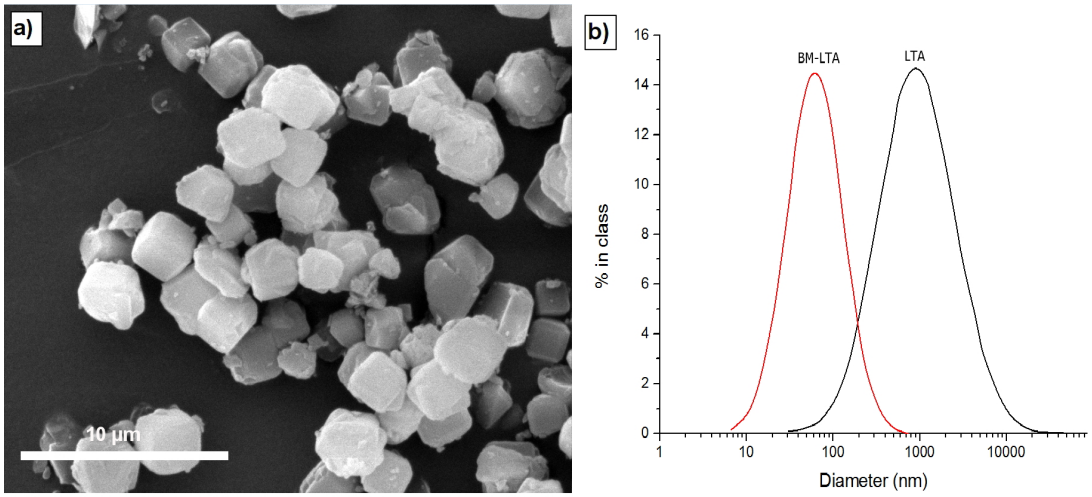

Figure 7.4: a) SEM of Ball-milled Zeolite A and b) DLS of Zeolite A before (LTA) and after ball milling process (BMZA)

7.3.2.2 Clear Solutions

The XRD pattern of NZA is shown in Figure 7.5 where sharp diffraction peaks can be observed, denoting high crystallinity and matching perfectly with LTA framework [274]. The pattern for NZA, after TMA-OH removal (organic template removal), was obtained observing that crystalline structure was not influenced by the calcination process.

Figure 7.6 a) shows the TEM image of NZA in which it is possible to observe the

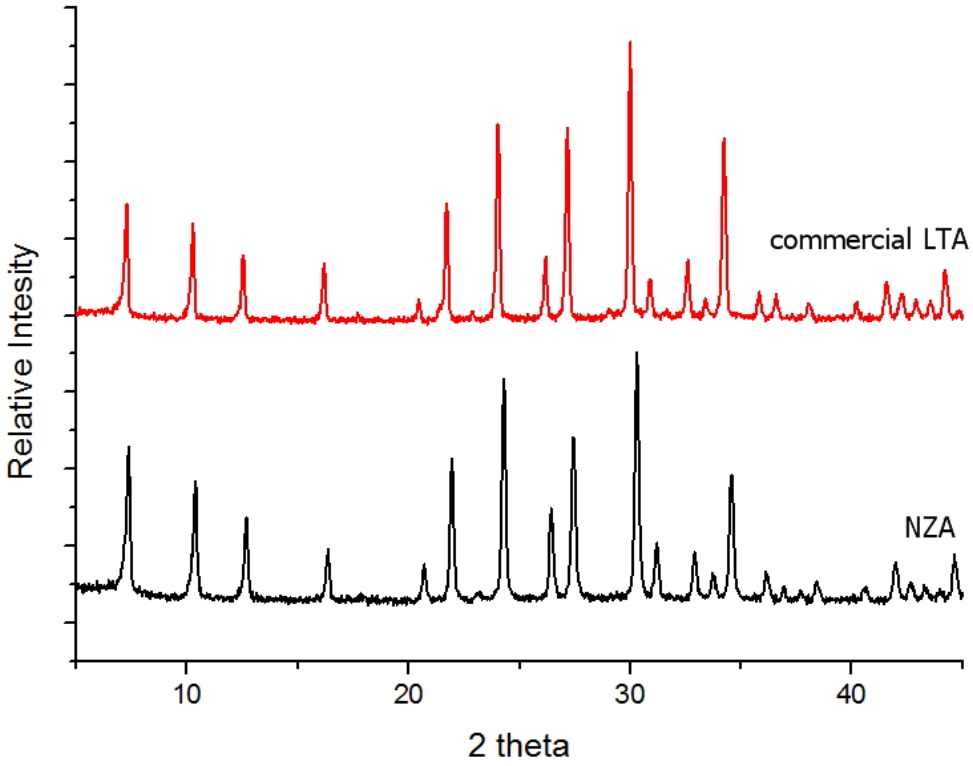

Figure 7.5: X-Ray patterns of nanozeolite A (NZA) after calcination prepared using organic templates and commercial sample

typical LTA cubic shape. Also, the largest particles are less than 200 nm, agreeing with the particle size distribution assessed by DLS. According to these results the average particle size is 114 nm with a narrow size distribution as is shown in 7.6 b).

In order to obtain the temperature level at which organic template TMA-OH will be removed after synthesis. TGA program was carried out and results can be seen in Figure 7.7.

The complete template removal was achieved at 600°C. In fact, after 500°C no changes in weight were noticed as Figure 7.7 a) shows. The derivative line in the plots indicates where the larger changes are taking place. After 200°C most of adsorbed water has been removed and from 200 to 500°C, in Figure 7.7 a), can be observed the correspondent wider peaks for the organic template. In Figure 7.7 b) peaks are not observed above 200°C.

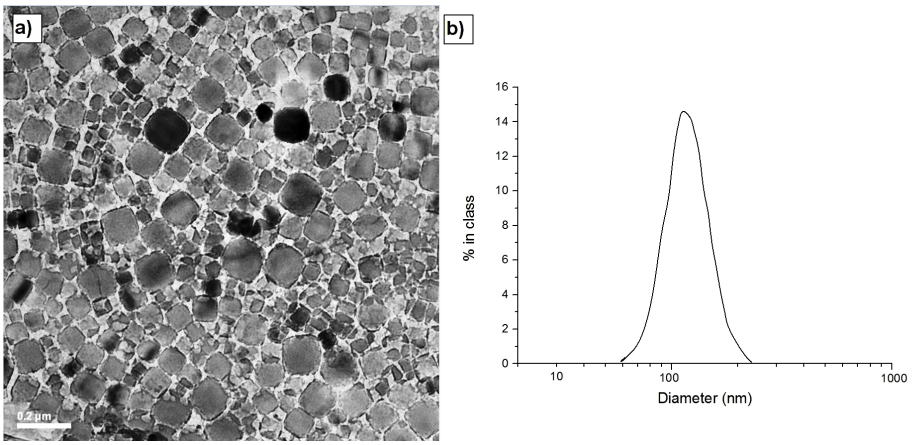

Figure 7.6: a) TEM of nanozeolite A NZA) and b) Particle size distribution by DLS

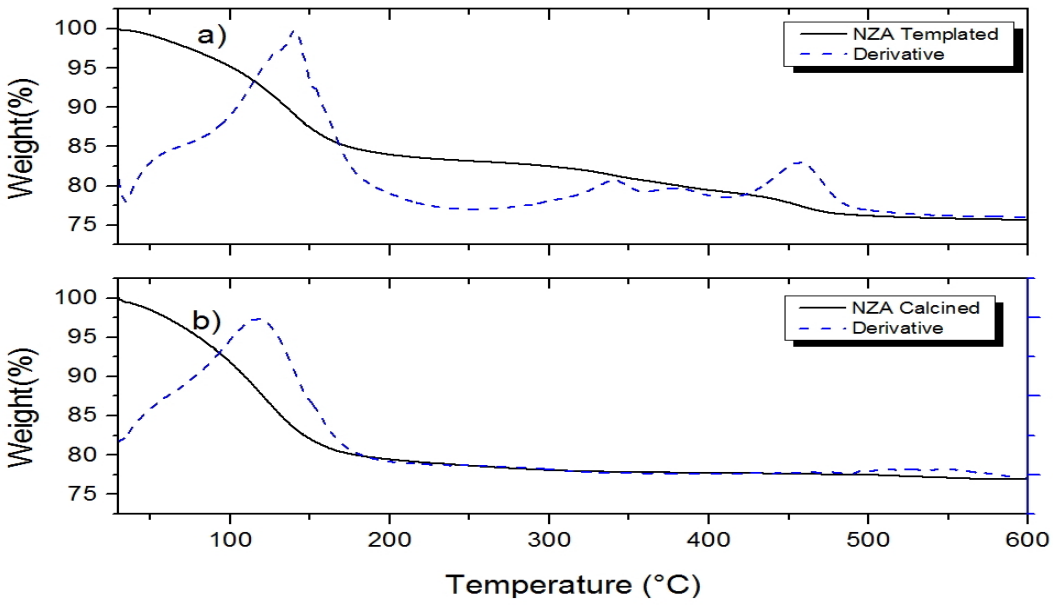

Figure 7.7: TGA of nanozeolite A (NZA) before, a), and after calcination b).

7.3.3 Zeolite Type Y - FAU

The XRD patterns of the final samples indicated the formation of zeolite Y for all the crystallisation times. In Figure 7.8 the pattern of zeolite type Y is provided for commercial zeolite Y (Sigma-Aldrich sodium Y zeolite powder). Intense peaks on 6.1°, 10.1° and 15.6° confirm the FAU framework of the prepared material. It was found that the three synthesised materials have similar relative diffraction intensities.

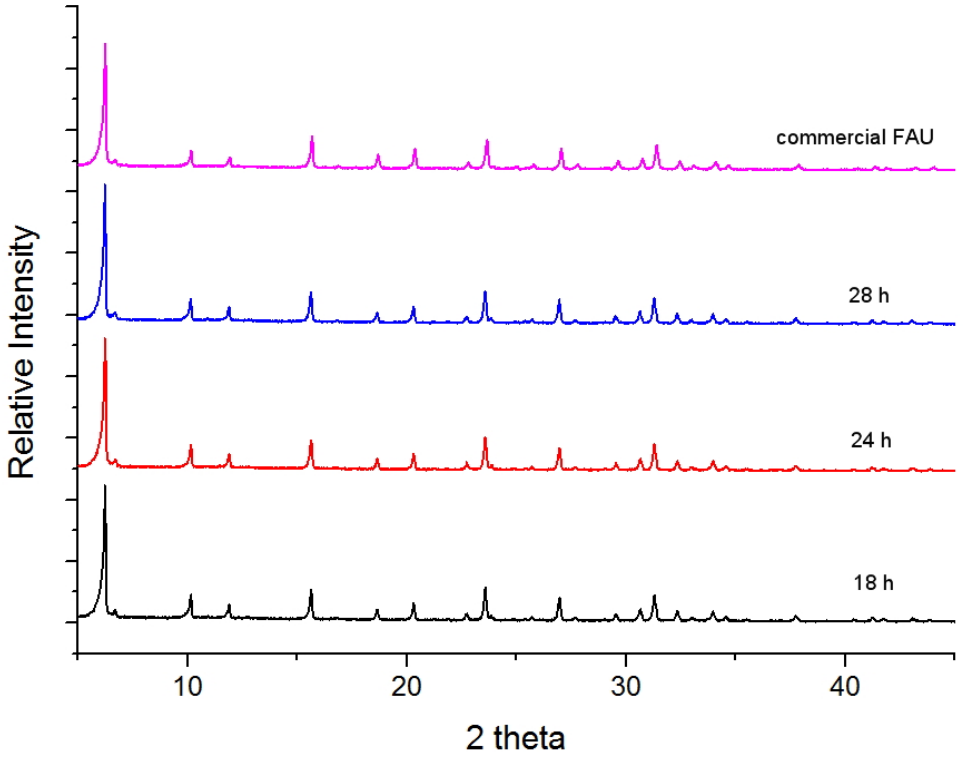

Figure 7.8: XRD patterns of zeolite standard FAU, and prepared at 18, 24 and 28 h respectively

Figure 7.9 shows the SEM images of zeolite Y after different crystallisation times. It can be shown the characteristic shape of FAU but the most of the material does not have a well-defined morphology and the larger particles are around 2 μm. Something similar occurs with Figure 7.9 b) and c).

Additionally, the images suggest that crystals fuse simultaneously to form agglomerate particles. But in the case of Figure 7.9 c) the particle size distribution is improved showing more uniformity. Something to notice, particularly in Figure 7.9 c), is an hexagonal morphology and a kind of stacking layers which could be related to the

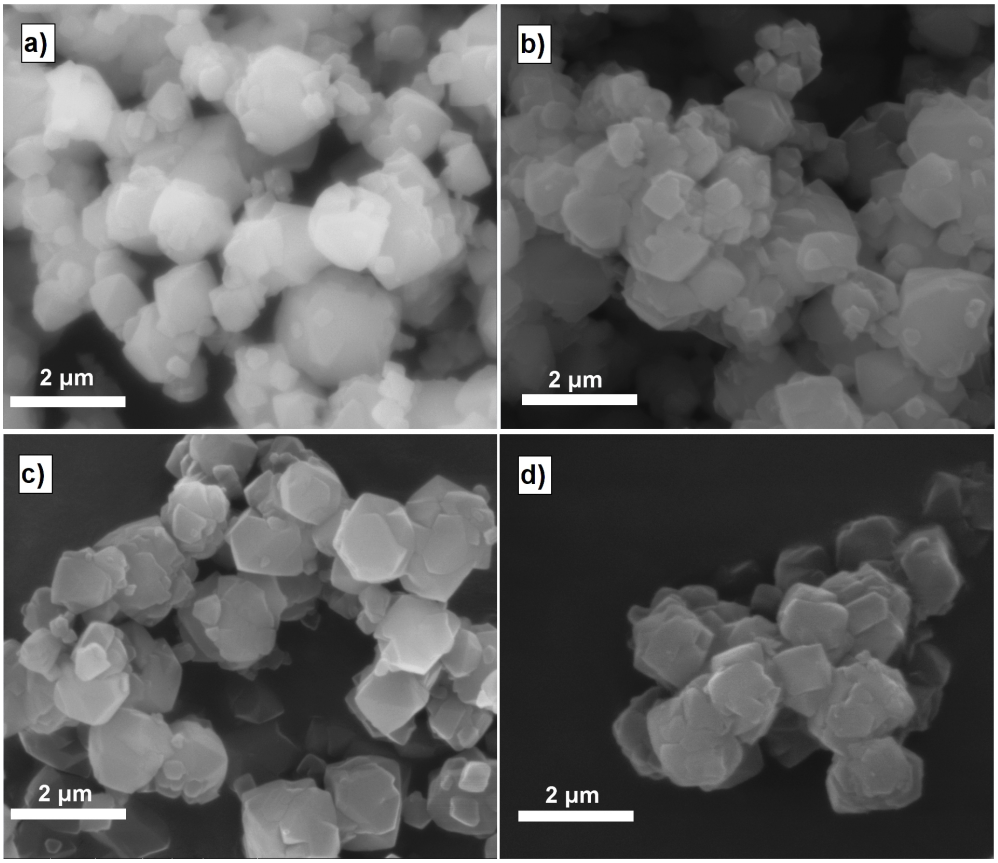

Figure 7.9: SEM pictures of synthesized and standard zeolite Y. All micrographs show different zeolite Y samples where crystallisation time is varied: a) 18 h, b) 24 h, c) 28 h and d) commercial sample

hexagonal faujasite phase. In this case, the standard materials have similar particle size to prepared samples.

7.3.4 Synthetic Clinoptilolite

7.3.4.1 Protocol 1

For the crystallographic description of materials following the two described protocols, XRD patterns were compared to a simulated one which can be seen below the diffractograms as a bar histogram. As can be seen in Figure 7.10, the HEU phase is present in material regardless the % wt. of seeds in the material or crystallisation time.

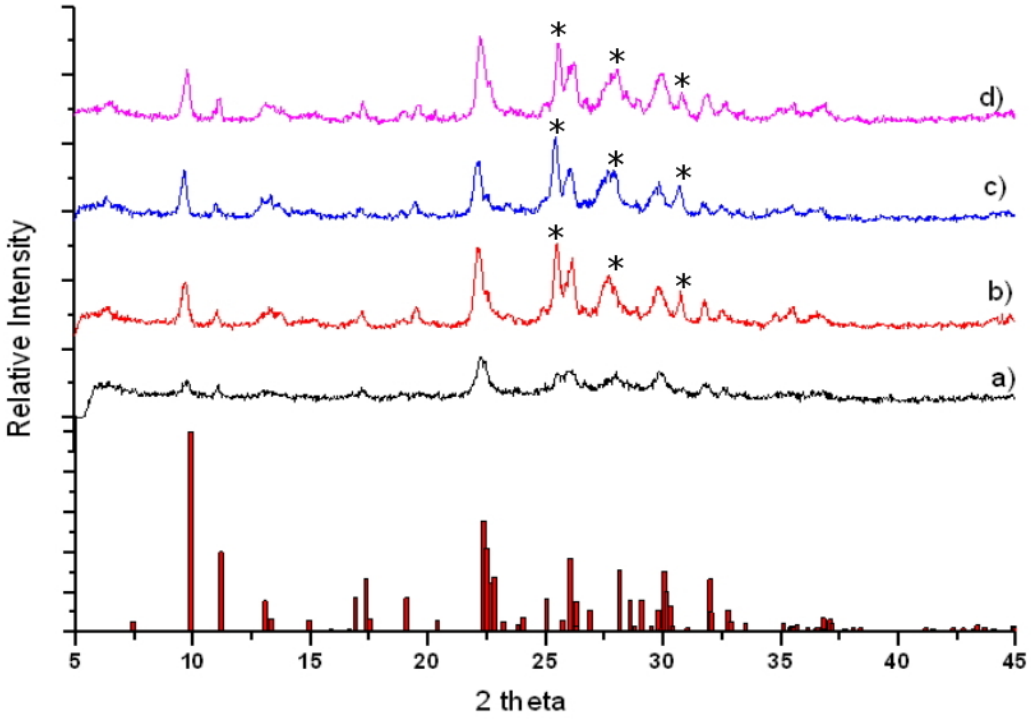

Figure 7.10: X-Ray patterns of different clinoptilolite samples following P1. a) 2 days, b) 4 days and c) 6 days using 20 % seeds and d) 4 days using 28 % seeds. * marks indicate Mordenite phase

Figure 7.10 shows a crystallographic study over time using 20 % wt. of seeds. After 48 h, HEU phase is forming as showing by Figure 7.10 a). The sample has more defined peaks after 96 h as shown in Figure 7.10 b), relating this to a higher phase purity. After 144 h, a peak reduction for HEU phase can be observed in Figure 7.10 c). Peaks at 25.6°, 27.6° and 30.8°. This suggests the presence of impurities in the form of a mordenite (MOR) phase [274] increased. This is an example that a transition is taking place. Additionally, in Figure 7.10 d), 28 % wt. of seeds were used. The XRD

pattern shows similar intensity peaks when using 20 % wt. seeds. However, the larger solid seeds amounts make reactive gels thicker, and their manipulation becomes less simple. Also, MOR phase was detected.

SEM results show that large agglomerates of synthetic clinoptilolite are formed. According to the SEM in Figure 7.11, these particles do not look to have a uniform morphology. Thus it is not possible to establish, from these results, a minimum particle size or the particular shape of the material. The use of the DLS technique is restrictive for materials with these characteristics due to settling.

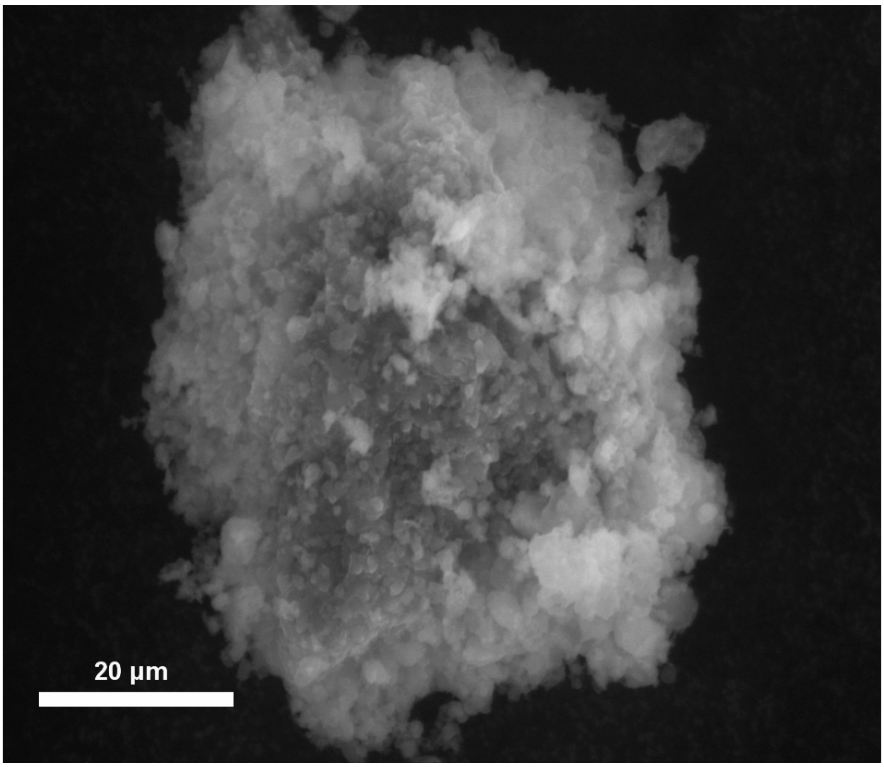

Figure 7.11: SEM of clinoptilolite particles prepared following Protocol (P1)

7.3.4.2 Protocol 2

Figure 7.12 shows the XRD patterns of prepared samples using 5 % and 10 % wt. of seeds using LUDOX HS-40. All the main HEU phase peaks are present which confirms the success using this experimental procedure. Also, when using 5 % wt. seeds, MOR at 25.6°and 27.6°and also some phillipsite (PHI) impurities appeared at 30.96°as indicated.

On the other hand, when LUDOX LS-30 was used as silica precursor, it was possible to significantly reduce extra peaks associated with MOR impurities that can be seen in Figure 7.12 c), achieving a good agreement with theoretical structure. However, analcime (ANA) phase is suggested to be present in material since a peak appeared at 18.28°. Finally it can be deduced that these peaks diffracted with more intensity when LUDOX LS-30 was used suggesting an improved HEU phase crystallinity.

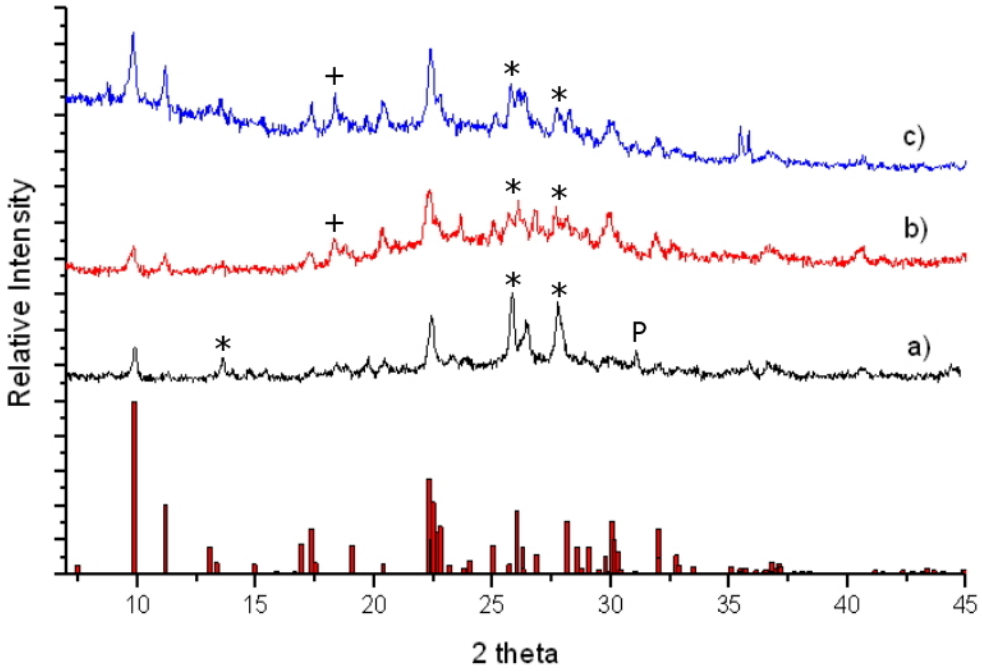

Figure 7.12: X-Ray patterns of clinoptilolite following Protocol 2. a) Using 5% seeds and HS-40, b) Using 10% seeds and HS-40 and c) Using 10% seeds and LS-30. * marks indicate MOR, P = PHI and + = ANA

SEM images of the material prepared using Protocol 2 (using HS-40) are shown in Figure 7.13 a) and b). The material looks more uniform than following Protocol 1. For the materials following Protocol 2 using LS-30, as silica precursor, is it possible to observe in Figures 7.13 c) and d) that the previous MOR impurities (needle-shaped particles) were reduced, and now it is possible to distinguish in some spots the hexahedron prism characteristic of the HEU phase, these results have a good correlation with previous X-ray patterns in Figure 7.12.

Table 7.1 summarises and compares the experimental data when Protocols 1 and 2

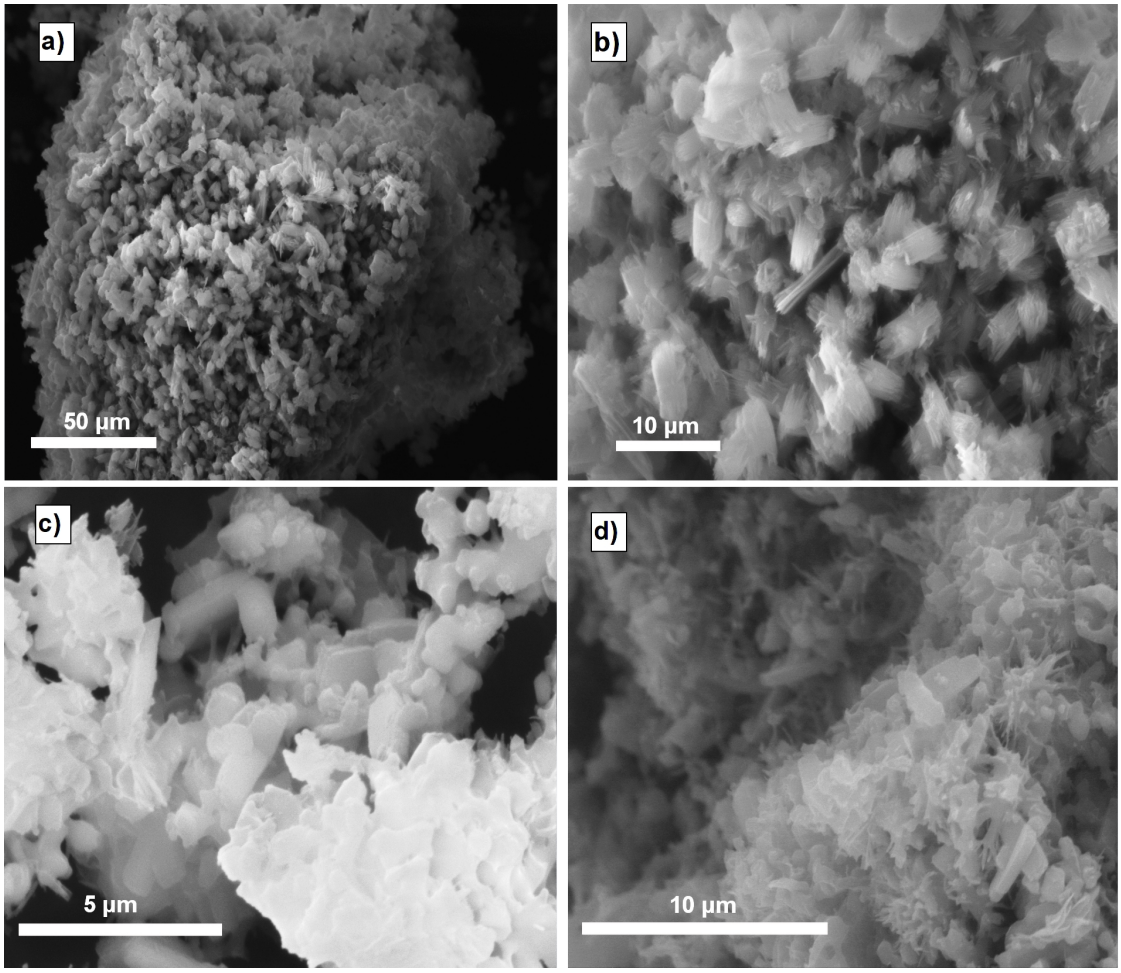

Figure 7.13: SEM of clinoptilolite sample prepared following Protocol 2 (P2)

were followed. Also, the chemical composition of the materials is presented.

Table 7.1: Characteristics of HEU-members materials prepared following P1 and P2.

Protocol	Average Si/Al	T (°C)	t(h)	Phases
Commercial seeds	4.60	...	...	HEU
P1 (20% seeds)	4.90	140	48-96	HEU-MOR
P2 (HS-40, 5% seeds)	4.5	180	60	HEU-MOR-PHI
P2 (HS-40, 10% seeds)	4.06	180	60	HEU-MOR
P2 (LS-30, 10% seeds)	4.79	180	60	HEU-ANA

According to these results, it can be deduced that following Protocol 2, represents a more efficient method to prepare HEU than Protocol 1. Also, samples prepared according to Protocol 2 varying the SiO_2 precursor showed different final characteristics.

7.3.5 Natural Clinoptilolite

The X-ray diffractogram of natural clinoptilolite (HEU) is shown in Figure 7.14. In this diffractogram can be clearly observed the peaks for HEU at 9.86°, 11.17° and 22.34° [274].

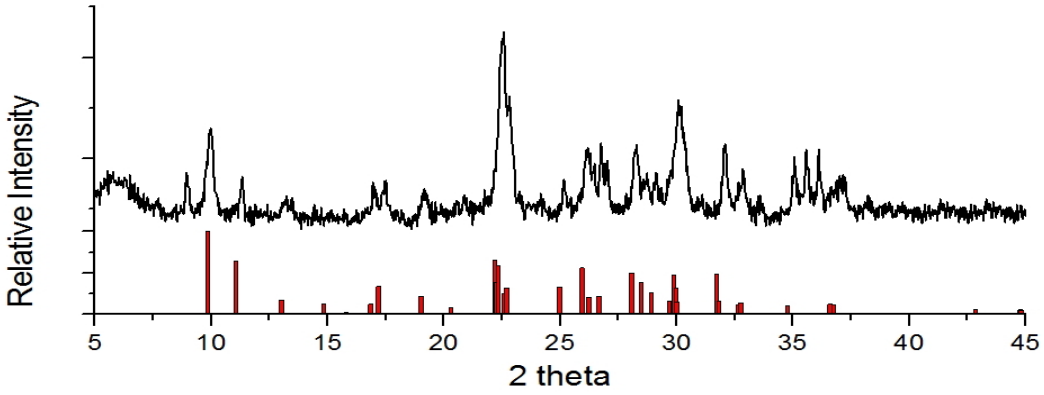

Figure 7.14: X-Ray pattern of natural clinoptilolite. The red histogram below represents the theoretical pattern for HEU framework type [274]

In Figure 7.15 a) the SEM image of natural HEU is presented, the image shows characteristic flake-shaped particles with a width size of ∼400 nm. DLS results are in agreement with average particle size for this zeolite, 388 nm, as is shown in Figure 7.15 b).

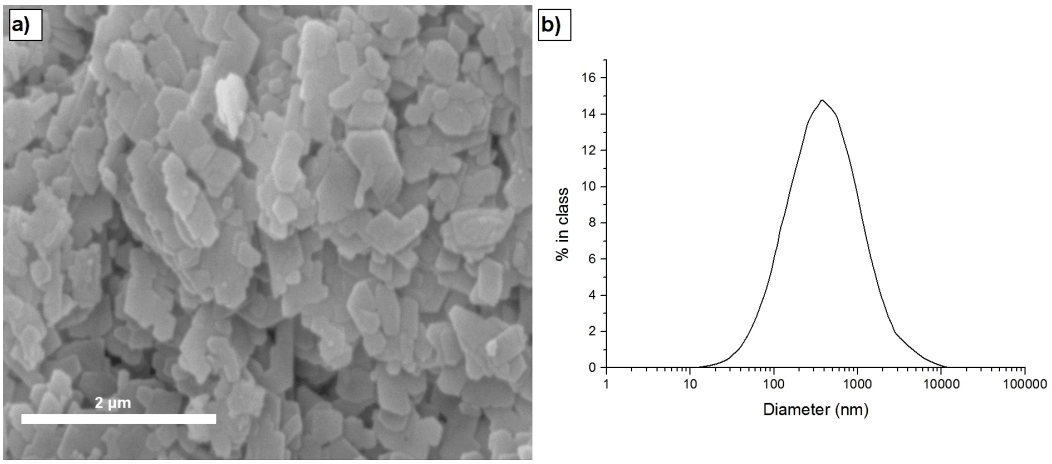

Figure 7.15: a) SEM of natural clinoptilolite and b) Particle Size Distribution of same material

DLS measurements were carried out in deionised water suspensions at 25 °C. Every

DLS analysis takes ten measurements and the average is presented, also all experiments were conducted at least two times to ensure reproducibility.

7.3.6 Carbons Produced by Thermal Treatment

Figure 7.16 shows the different surface area values for the carbons. These plots are showing Type IV isotherms, which are associated with the presence of mesopores in the material. Also the hysteresis loops in all isotherms have similar a shape, all of them are considered to be type H4, thus, narrow pores slit-shaped is suggested. Also, in all carbon plots the presence of micropores can be observed due to plots show Type I isotherm behaviour at low relative pressure values.

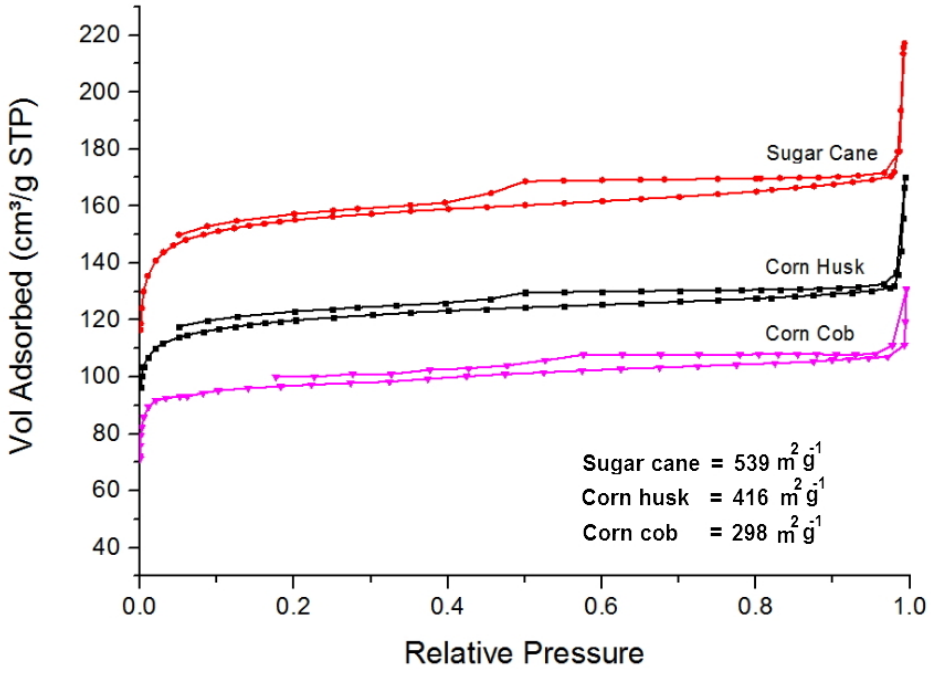

Figure 7.16: Nitrogen adsorption-desorption plots prepared by just thermal method

Additionally, at high relative pressure, > 0.98, it can be observed that all plots exhibit typical Type II behaviour, i.e. macropores and open surfaces are present in the system [181].

Figure 7.17 shows three different carbons produced from corn husk (CH), corn cob (CC) and sugar cane bagasse (SCB). Three materials show wide openings. CH and

SCB show open-transverse channels across the bulk due to their fibrous nature while CC have the openings all over the material.

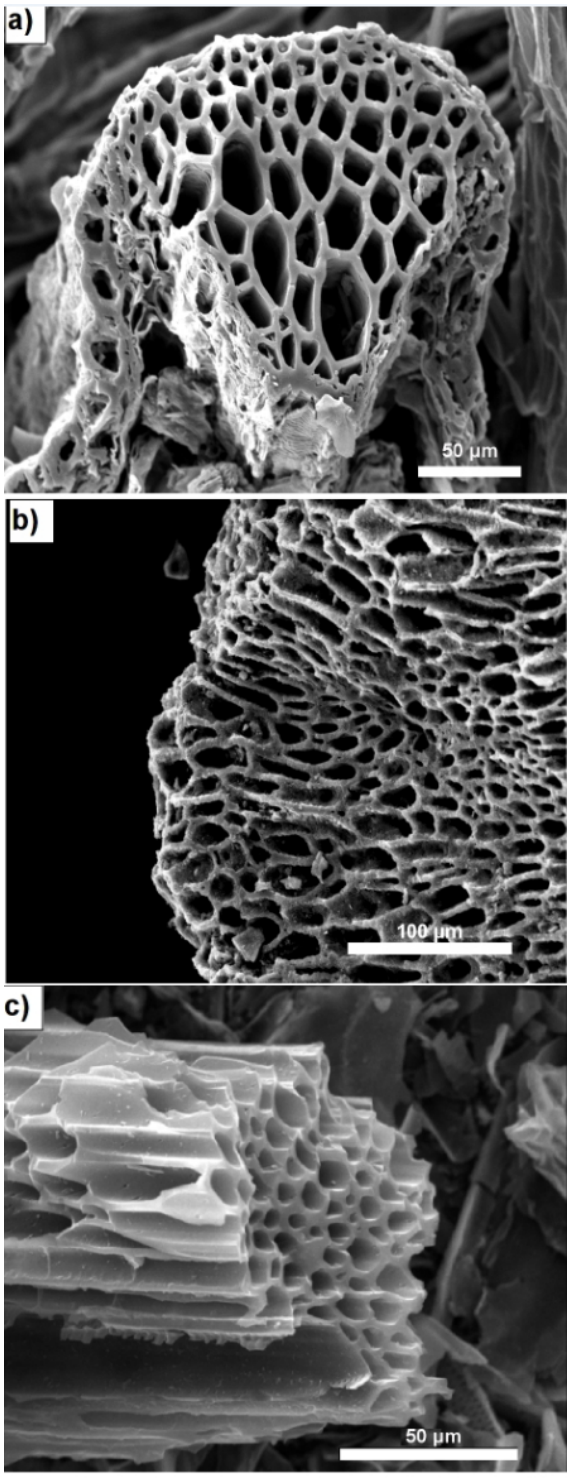

Figure 7.17: SEM images of three carbons prepared by thermal method. a) Corn husk (CH), b) corn cob (CC) and c) sugar cane bagasse (SCB)

7.3.7 Surface-Modified Carbons

In Figure 7.18 three images corresponding to carbonaceous hazelnut shell (HN), cherry stone (CS) and date stone (DS) are presented. All carbons exhibit a honeycomb-like morphology. This result confirms that thermal treatment used for these materials was successful creating voids of enough size and adequate shape so zeolites can be supported. These materials also exhibit more rigid walls than carbons prepared from corn by-products and bagasse.

The modification of the chemical surface was evaluated by zeta potential measurements. In Figure 7.19 a) the plot of the electrical potential as a function of pH is shown. Prior to surface modification by PDDA, for three carbonised materials, HN, DS and CS, it was possible to detect the isoelectric point: pH ∼4.2 and ∼3 for HN and DS respectively. CS shows only negatively-charged surface over the measured pH range. This results suggest the presence of different functional groups on the surface. Also, the zeta potential of zeolites is compared in Figure 7.19 a), HEU and NZA exhibit an increase of negative charge as pH increased; HEU finds its maximum negative charge at pH ∼10 and NZA after pH 8, -40 mV. It was not possible to read below pH 3 for NZA because this material was dissolved by the acid used to adjust pH value.

The difference using 1 or 2 % PDDA solution has not a significant effect but when using 2 % carbons showed a slightly *more* positive electrical potential as seen in Figure 7.19 b). After treatment, these supports show that charge on surface had been reversed successfully. Zeta potential values for treated carbons range from ∼55 mV to ∼27 mV.

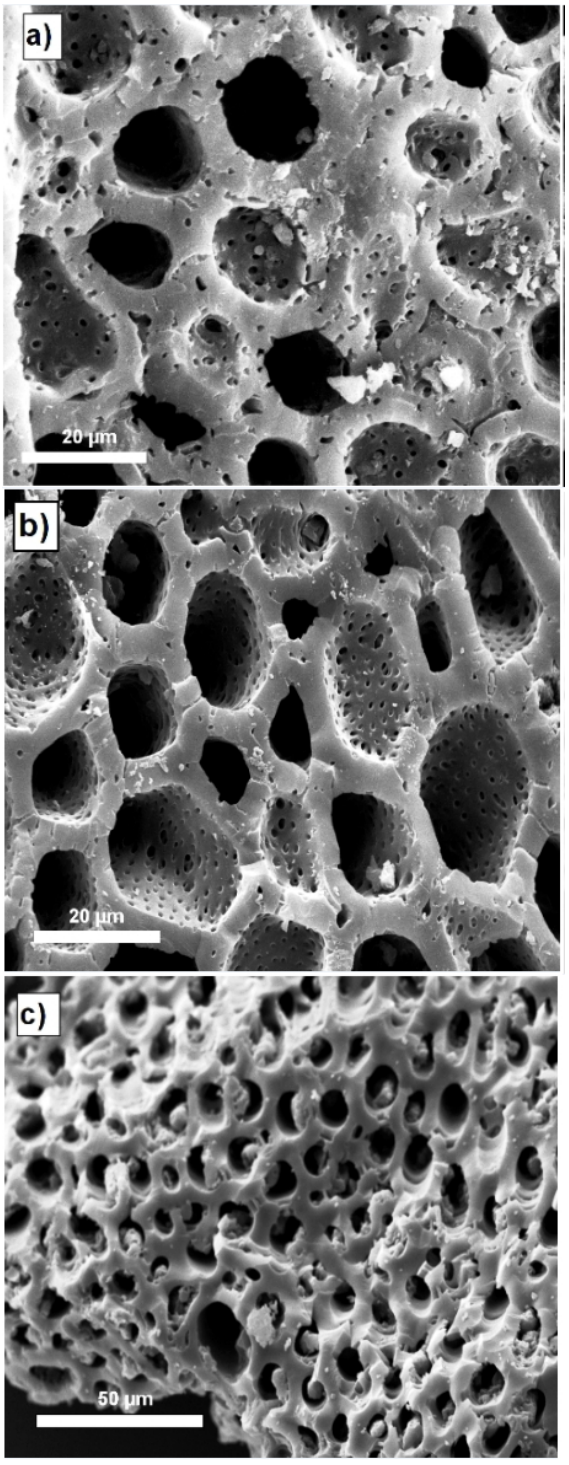

Figure 7.18: SEM of PDDA-treated carbons. a) Hazelnut shell (HN), b) cherry stone (CS) and c) date stone (DS)

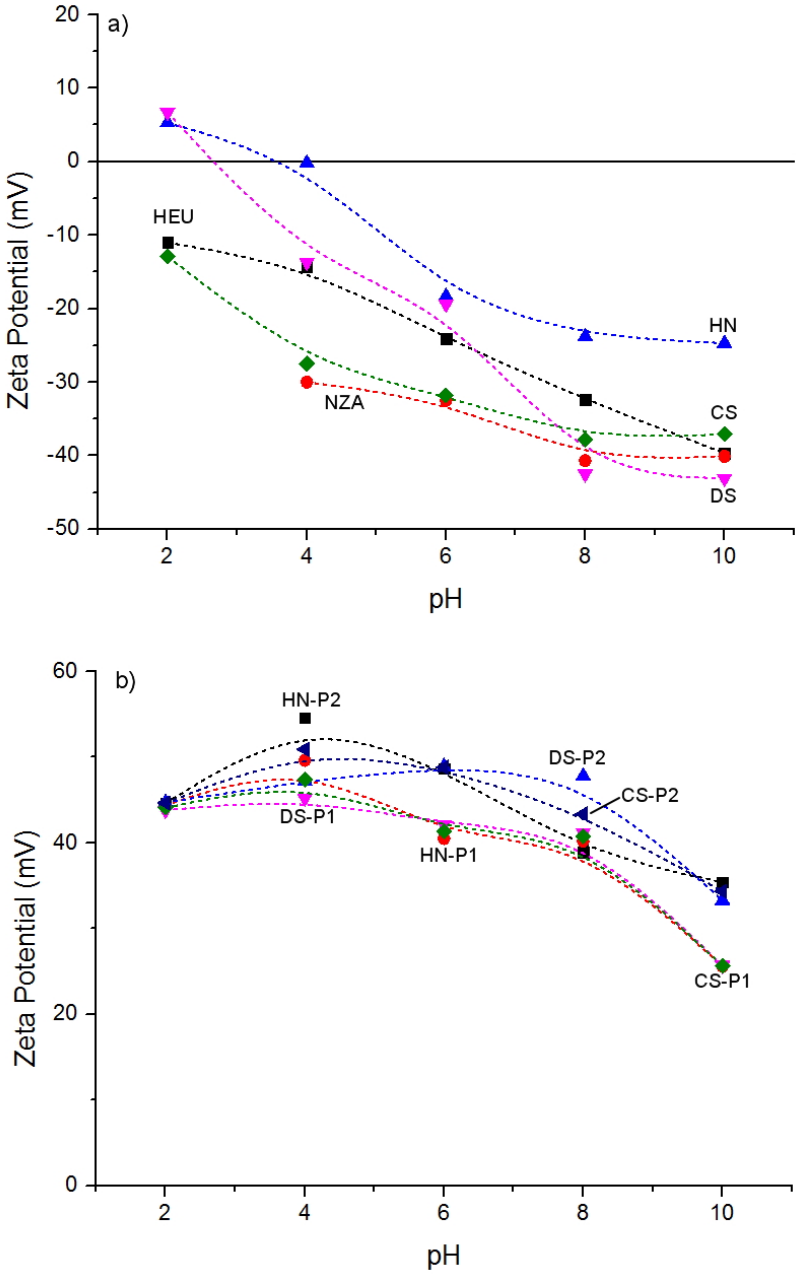

Figure 7.19: Zeta Potential graphs showing the surface distribution of charges in function of pH a) zeolites HEU, NZA, carbons with no treatment, HN, DS and CS; and b) hazelnut shell using 1% and 2% PDDA (HN-P1 and HN-P2), date stone using 1% and 2% PDDA (DS-P1 and DS-P2) and cherry stone using 1% and 2% PDDA (DS-P1 and DS-P2) carbons after surface modification

7.4 Conclusions

In this chapter, a range of zeolites with relatively low density framework values, such as microsized LTA, nanosized LTA, FAU and HEU were successfully prepared. For zeolite LTA, it was found that at reduced time periods, 3 h, high crystallisation levels were achieved.

A simple and cheap ball milling process showed a very small particle size distribution (60 nm) when analysed supernatant dispersion. On the other hand, preparing synthetic seeds led to small and consistent zeolite particles of $\sim$ 100 nm.

The HEU members synthesis was carried out successfully. In all experimental protocols it was possible to prepare HEU phases. However, samples came accompanied with a reduced amount of impurities in the form of MOR, ANA or PHI phases as XRD analyses revealed.

Carbonaceous templates, using agroindustrial by-products, were prepared following a thermal route. Corn cob, corn husk and sugar cane bagasse were selected as precursors of macro and mesoporosity as can be observed in nitrogen adsorption/desorption results. All these materials presented values higher than 290 $m^2 g^{-1}$.

Also hazelnut shell, cherry and date stone (materials with wood-like characteristics, believed to have more mechanical strength) were chosen to be chemically modified. It can be observed in SEM micrographs that the all materials could be suitable, according to their topology and geometry, to incorporate microporous materials such as zeolites and to produce a novel material with hierarchical porosity features in order to be utilised as ion exchanger in environmental applications. Finally, zeta potential results evidenced that chemical surface on carbons was modified from having a range of negative-to-positive zeta potential values as pH function to only have positive electrical potential values. This will contribute to the attachment of zeolites to the surface.

Chapter 8

The Synthesis and Characterisation of Zeolitic Hierarchical Composites and their Cobalt Co^{2+} Sorption Applications

8.1 Introduction

This chapter describes two methodologies to produce hierarchical composite materials using zeolites type A (LTA), Y (FAU) and synthetic clinoptilolite (HEU). The first method is based on the use of ball milled particles, i.e. seeds, that will allow the formation and anchorage of microsized particles to the carbonaceous support surface under hydrothermal conditions. The second method is based on the immersion of the supports within nanozeolite solution (clear solutions) before the formation and growing of nanozeolite particles by hydrothermal method. XRD, SEM and TGA were the characterisation techniques used to analyse the products. Also, the application of the prepared composites in the removal of cobalt ions (Co^{2+}) was studied. Soprtion kinetics and diffusion characteristics were also analysed by the Pseudo First Order and Pseudo Second Order and Weber-Morris models respectively.

8.2 Methodology

8.2.1 Seeding Method

For the preparation of zeolite/carbon composites using ground seeds for zeolites A, Y and synthetic clinoptilolite the same initial conditioning process was followed: 1 g of carbon (from corn husk and cob) were seeded using with 100 μL of ground zeolite seeds suspension and 5 ml of deionised water as dispersing media. Ultrasonication for 6 h at constant temperature was carried out. The recovery of seeded carbons was done by filtration and dried overnight at 70 °C. After this a precursor zeolite gel, as *nutrient* media, was prepared according to the methodology for the zeolite types as previously described.

8.2.1.1 LTA - Composites

The procedure and the composition of the synthesis gel of LTA were previously described in Section 7.2.1 (p. 116). Prior to the gel being transferred to the autoclave, the previously seeded carbons were added to the gel (4 g of SiO_2 per g of carbon) and stirred for 30 min. Then all content was transferred to a Teflon-lined stainless steel autoclave and heated in the oven for 6 h at 100 °C. Final composites were recovered by filtration and dried overnight at 70°C.

8.2.1.2 FAU- Composites

Similar to LTA composites, FAU gel was also prepared following the method described in Section7.2.3 (p.118). Mass ratio 4 g SiO_2 :1 g C was also used. After 18 h at 100°C under hydrothermal conditions products were recovered, washed with deionised water, filtered and dried overnight at 70°C.

8.2.1.3 HEU - Composites

Carbons seeded with commercial clinoptilolite were mixed with a HEU reactive gel prepared following Protocol 2, described in Section 7.2.4.2.2 (p. 120). Seeding ratio

for carbons is the same as zeolites A and Y, i.e. 10:1 (1 g of carbon in 100 μL of seeds suspension). Also, 5 ml of deionised water were added and dispersed under sonication for 6 h at room temperature. Afterwards, all content was transferred to a Teflon-lined autoclave and heated in the oven for 4 days at 140 °C under static conditions. Finally, material was recovered by filtration and washed with deionised water, samples were dried overnight at 70 °C.

8.2.2 Supports Immersion Method (Non-seeding Method)

This method was developed from the attempt to produce synthetic LTA seeds. It was believed that nano-crystals could produce a better carbon coverage; preserving the voids and openings in the carbons, the reactive mixture prepared in section 7.2.2 (p. 117) was used as the zeolitic gel. In this case the main interest is on crystals that actually can be crystallised on carbon surface, once the proper anchorage sites have been conditioned by ultrasonic dispersion. It was believed that sonication produces better and improved distribution of zeolite gel on carbon surface.

8.2.2.1 NZA - Composites

The method for the preparation of clear solution that will lead to colloidal dispersion of nanozeolite A was decribed in section 7.2.2 (p. 117. Carbonaceous materials (without seeding) were then added to the reactive solution (0.1 g in 10 g of clear solution) and immersed in the ultrasonic bath for 6 h for a complete impregnation. Then, zeolite composite crystallisation was carried out hydrothermally at 100°C for 24 h. The final material was recovered as by filtration and washed with deionised water in order to remove the OH^- excess.

8.2.3 Characterisation Techniques

The presence of zeolite phases was assessed by X-ray Diffraction (XRD). The morphology of composites and zeolite coating were observed using Scanning Electron Mi-

croscopy (SEM). Finally, Thermogravimetric analysis (TGA) was carried out to quantify the zeolite/carbon ratio in composite.

8.2.4 Cobalt Adsorption Experiments

Kinetic experiments were carried out using 50 mg of material in 10 ml of 500 mg $l^{-1}$of Co^{2+} solution. Bottles were mixed in a rocker for certain period of time (10, 30, 120 and 240 min) and the final concentration was assessed by ICP-OES (Varian MX). Co^{2+} uptake was calculated using:

$$q_t = (C_0 - C_t)\frac{V}{m}, \tag{8.1}$$

where q_t (mg g^{-1}) is the ion uptake, C_0 and C_t represent initial and after t concentrations (mg l^{-1}) respectively, V is volume (l) and m is the solid mass (g). In order to quantify the sorption performance of the zeolite present in the composite, the equation:

$$q_{composite} = q_z x_z + q_c x_c \tag{8.2}$$

was used. Where q_z and q_c are the experimental uptake values for zeolite and carbon respectively and x_c and x_z are the weight fractions for carbon and zeolite in composite respectively being obtained by TGA analysis. Then, the theoretical uptake of zeolite present in the composite, q_z^* can be calculated from:

$$q_{z^*} = \frac{q_{composite} - q_c x_c}{x_z} \tag{8.3}$$

All analytical results from ICP device presented in this work are an average of at least two measurements. The ICP-OES device was calibrated all time with three standard concentrations at least, and the correlation factor for the calibration curve always was R>0.999 to ensure quality and reproducibility of the data.

8.3 Results and Discussion

8.3.1 Characterisation of Composites Prepared by Seeding Method

8.3.1.1 LTA composites

The results obtained from XRD analysis are presented in Figure 8.1. Results confirm that LTA phase is present with LTA/CC and LTA/CH materials showing the characteristic diffraction peaks for the LTA framework.

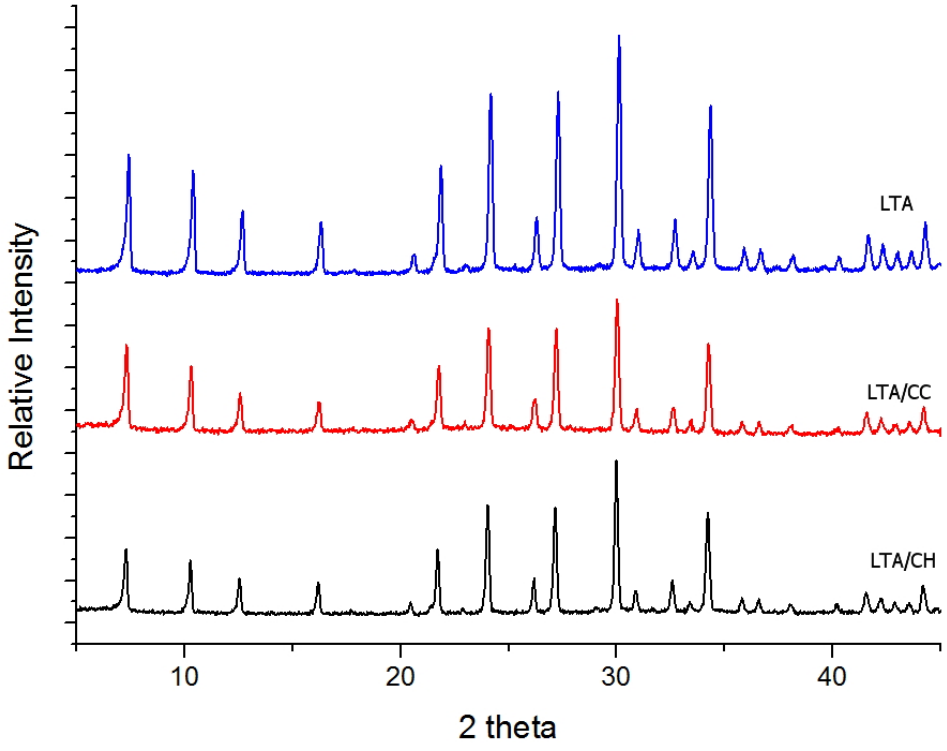

Figure 8.1: Diffraction patterns of commercial LTA; LTA/CC and LTA/CH composites

Figures 8.2 a) and b) show the morphology of LTA/CC and LTA/CH exhibiting a complete zeolite coating. Also, is possible to observe in the SEM images, the initial carbon openings remained visible in the structure after the hydrothermal process.

Something similar happened to corn cob supports. A comparison of these two structures reveals that in corn cob all carbon scaffolds also remained visible after the crystallisation process as is shown in Figure 8.2 c) and d).

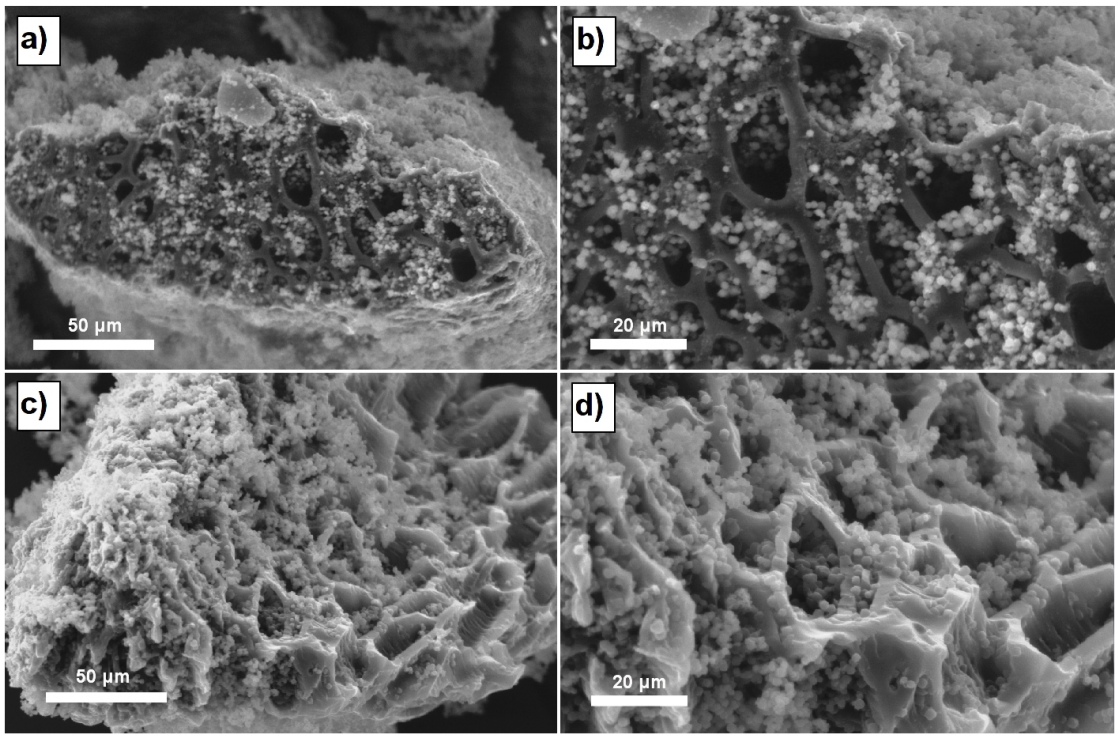

Figure 8.2: Scanning Elctron Micrograpahs: a) and b) LTA on corn husk support, c) and d) corn cob

Thermogravimetric results quantified the amount of zeolite on the composite materials. Graphs in Figure 8.3 show TGA analysis for LTA/CH and LTA/CC composites. These results showed a similar amount of zeolite in each composite material after the carbon gasification. LTA/CH and LTA/CC values were 70.6 %, and 70.2 % respectively. All final compositions are summarised in Table 8.2 in page 170.

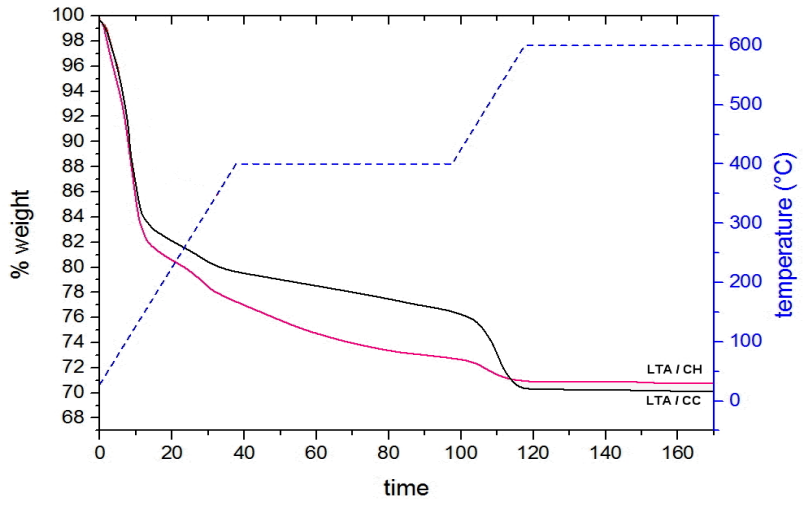

Figure 8.3: Thermogravimetric Analysis of Zeolite A on: Corn husk and Corn cob

8.3.1.2 FAU Composites

The XRD patterns of supported zeolite Y on carbonaceous corn cob (CC) and husk (CH) were obtained and are presented in Figure 8.4. These results show the XRD patterns agreement of prepared materials with the main FAU peaks of the standard material as can be observed. The reduction of peak intensity can be related to the reduced amount of zeolite in the composite. Additionally, in the diffraction patterns it was possible to observe the amorphous fraction of the composite being this related to carbon phase in the sample.

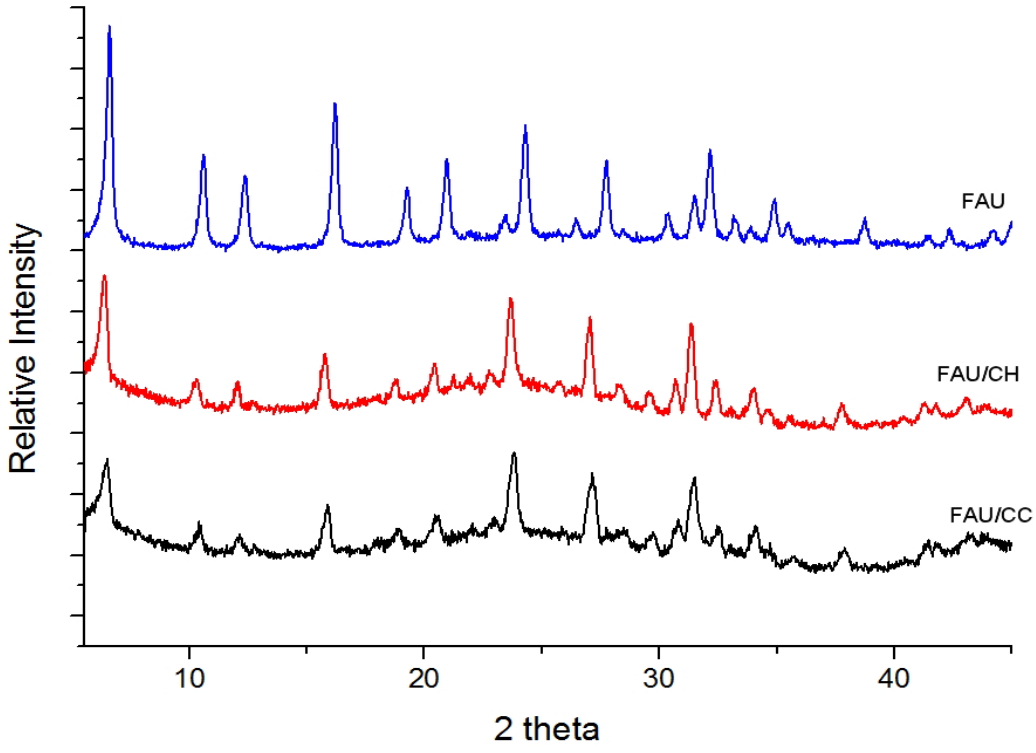

Figure 8.4: X-Ray patterns of commercial FAU, FAU/CH and FAU/CC

In Figure 8.5 zeolite Y particles are supported on carbons produced by corn husk and cob. It is clear from SEM images that zeolite is not entirely covering the carbon. TGA results for FAU composites in Figure 8.6 showed that final zeolite weight was 37.5 % and 35 % for FAU/CC and FAU/CH respectively.

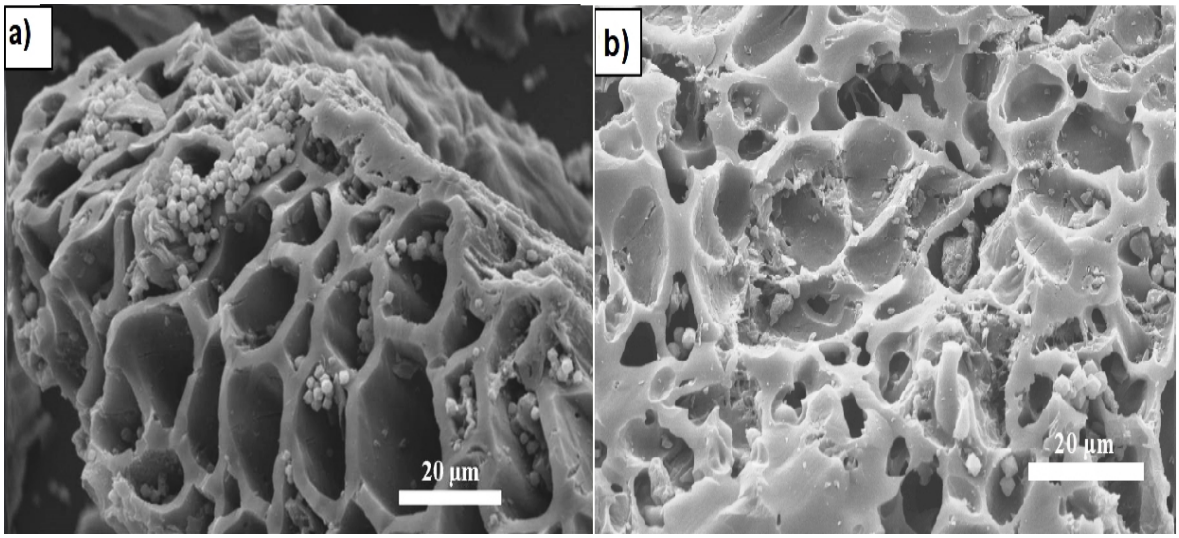

Figure 8.5: SEM images of zeolite Y/Carbon composites. a) FAU/CH and b) FAU/CC

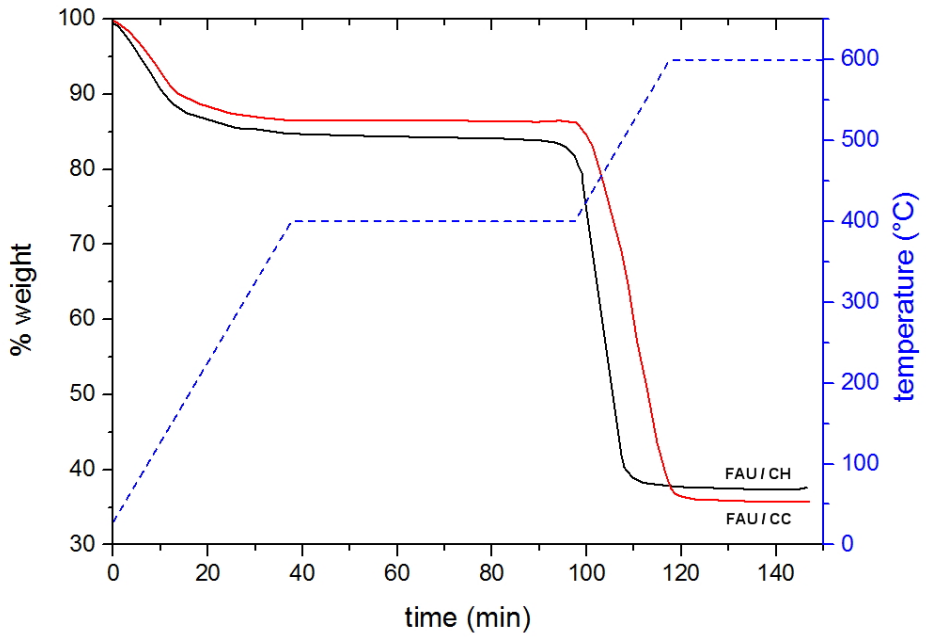

Figure 8.6: Thermogravimetric Analysis of FAU/CH and FAU/CC

8.3.1.3 HEU Composites

In Figure 8.7 the corresponding X-ray patterns of synthetic clinoptilolite on carbon husk (CH) and carbon cob (CC) are presented. The analysis revealed that HEU phase is present in the composite. However, as discussed in section 7.3.4.2, zeolitic material shows some impurities in the form of ANA phase as peak at 30.5°suggests.

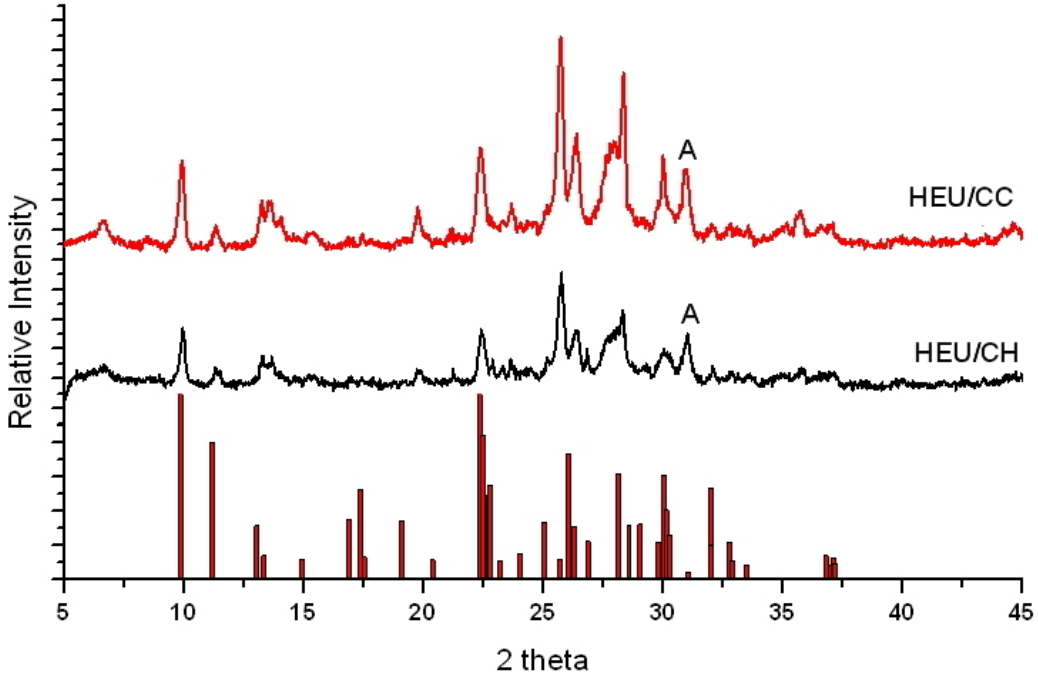

Figure 8.7: X Ray patterns of clinoptilolite on carbon supports following P1: a) HEU/CH and b) HEU/CC. A indicates ANA phase

In Figure 8.8 it is possible to observe the morphology of HEU composites over CH and CC respectively. Particularly in Figure 8.8 a), synthetic clinoptilolite is well-distributed on the support and also in the interior. The zeolite seems to be attached to the carbon surface but also carbon openings appear in final material as was intended.

In contrast to previous composites, carbon is no exposed in HEU materials. Nevertheless, there is visual evidence that carbon remained in the composite after synthesis. Also, TGA results revealed a large percentage of carbon in the composite as Figure 8.9 shows suggesting that either zeolite particles are completely filling the carbon voids or some carbonaceous structures collapsed due to the conditions of synthesis for the formation of HEU following Protocol 2 (180 °C for 4 days and high alkalinity). Never-

theless, as results indicated carbon remained in the material.

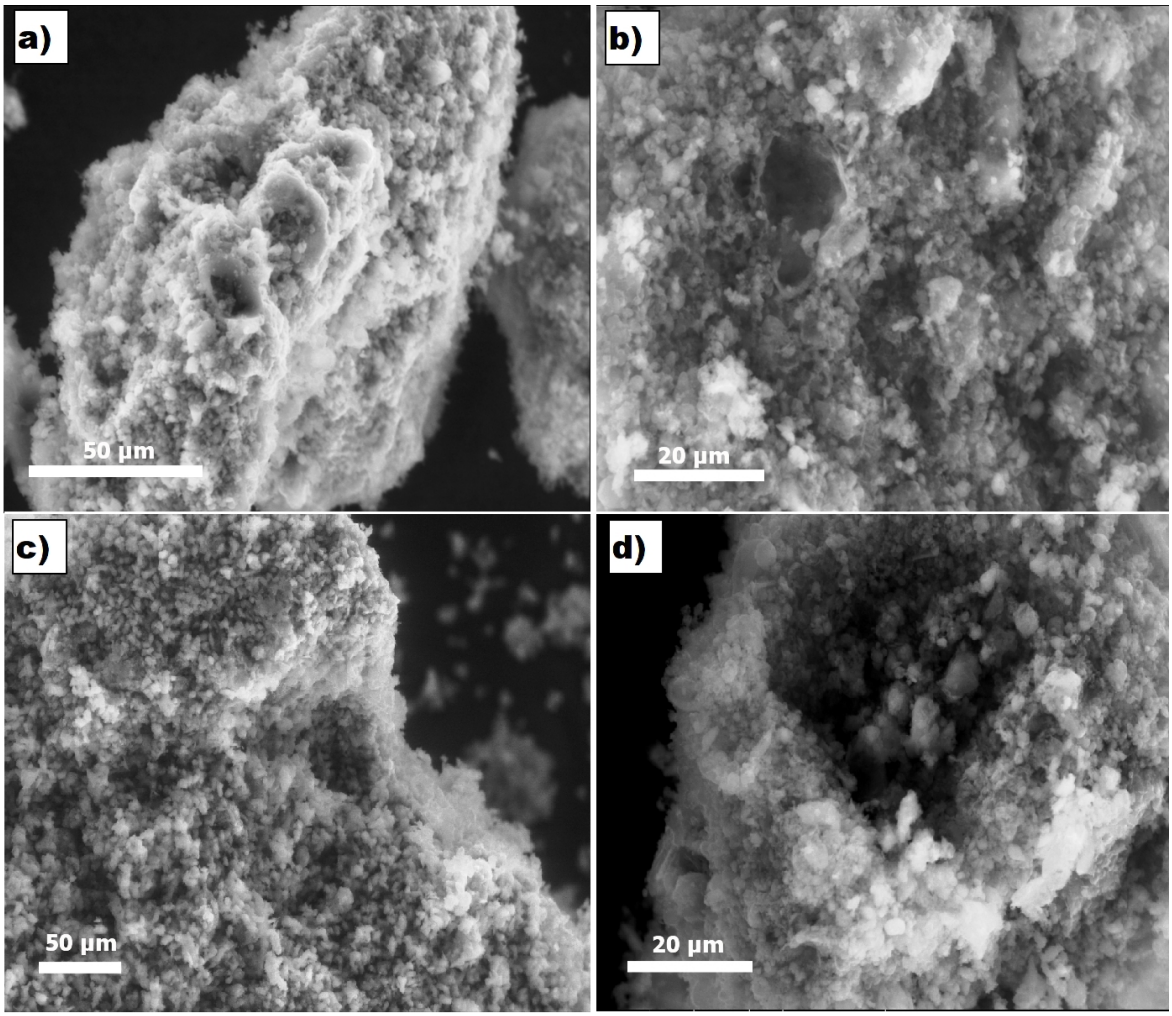

Figure 8.8: SEM images of: a) and b) HEU-CH; c) and d) HEU-CC

Something similar happened to corn cob composites. Images in Figure 8.8 c) and d) show that zeolite material is completely surrounded by the zeolite at crystallisation time. TGA results, shown in Figure 8.9, indicate that nearly 50.0 % of material is zeolite. 49.0 % for HEU/CH and 53.9 % for HEU/CC.

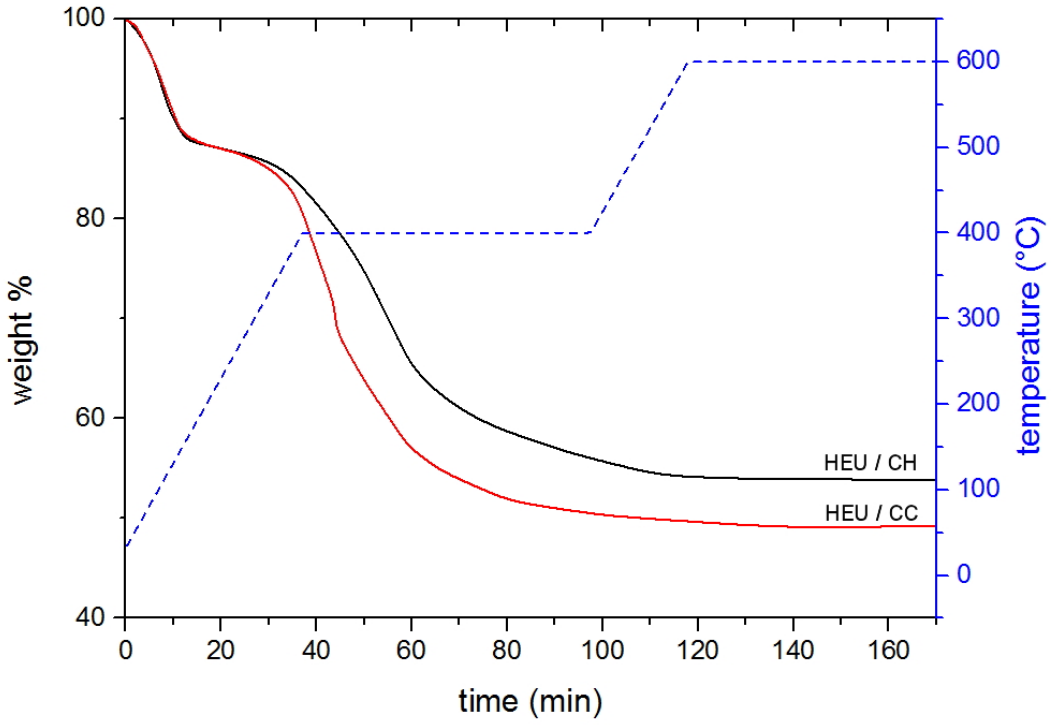

Figure 8.9: Thermogravimetric analysis of HEU composites

8.3.2 Characterisation of Composites Prepared by Immersion Method

8.3.2.1 NZA Composites

Figure 8.10 shows that LTA phase in NZA/CC and NZA/CH is the zeolitic material in both composites since the XRD pattern matched the standard material. Also, a large amorphous hump can be seen, this is because the carbon occupies a larger weight percentage than previous samples as TGA results revealed.

These results show that it was possible to grow nanosized LTA on carbons when present in the reactive clear solutions as seen in Figure 8.11. For CH material, NZA looks to be attached forming a well-spread and uniform layer of zeolite on the outer surface of the "tubes". Also, it was possible to deposit a homogeneous layer of nanozeolite on surface as Figure 8.11 b) shows.

These results are significant because smaller crystals do not tend to block or clog the carbon openings, as small particles adopted carbon geometry as can be seen in

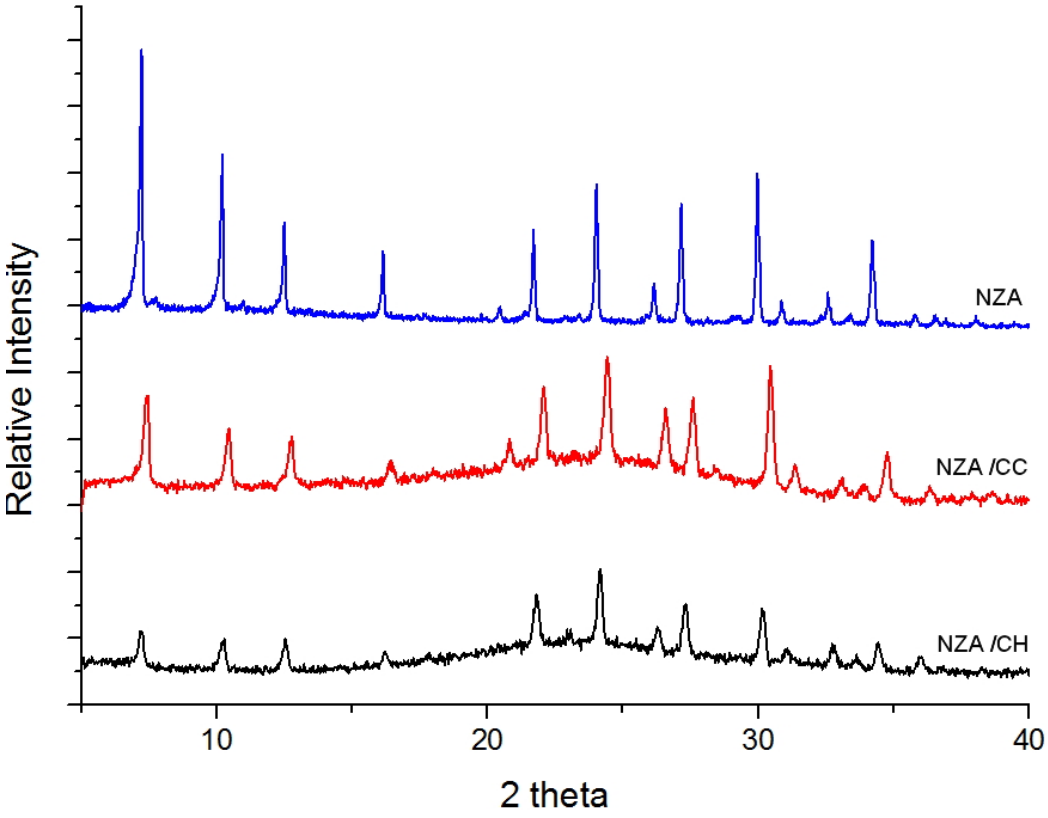

Figure 8.10: XRD patterns of non-seeded NZA composites

Figure 8.11 c) and d). Also, the crystallisation stage for this method seems not to have an effect on the carbon structure preserving the scaffold structure.

As previously discussed, NZA composites by the impregnation method, contains less NZA amount in composite. TGA results can confirm this. Figure 8.12 shows that the amount of zeolite in NZA/CH composite was 15.9 % wt and 11.5 % for NZA/CC .

In Table 8.2 the zeolite composition in all prepared composites in this section is summarised. A relationship can be seen when a specific type of zeolite is used, the differences in the zeolite amount in composite using CC or CH differ from 2.5 % to 13.5 %. From these results it can be said that there is not a direct relationship between the different type of carbon and the amount of zeolite coverage.

8.3.3 Removal of Cobalt(II) using Zeolites

In this section, kinetic studies in the sorption of cobalt ions using zeolites and composites are shown. The carbon effect on the cobalt uptake is considered. Additionally,

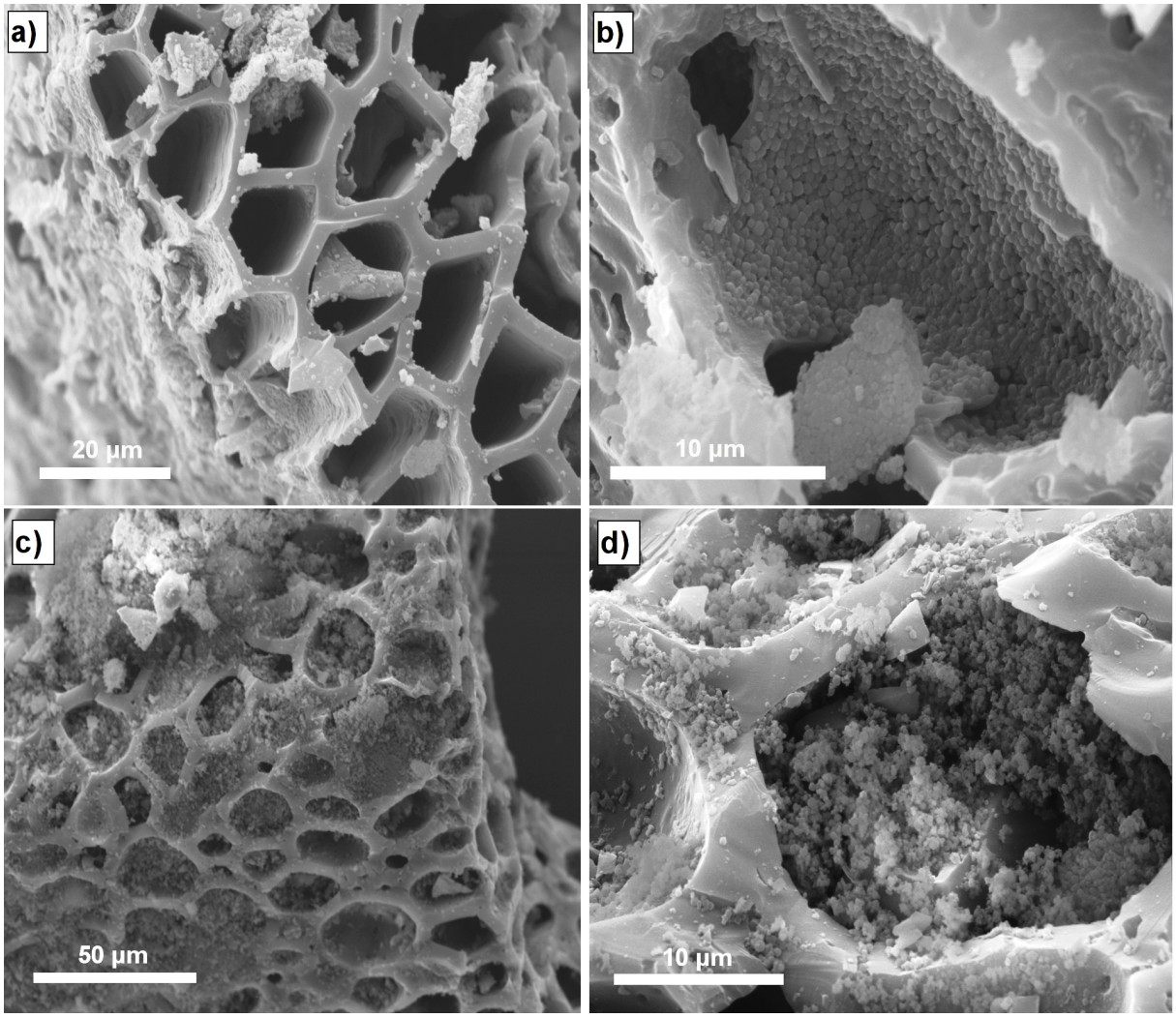

Figure 8.11: SEM images of non-seeded NZA composites. NZA/CH a) and b) and NZA/CC c) and d)

experimental data are analysed by Pseudo First Order (PFO) and Pseudo Second Order (PSO) models. The Weber-Morris model is used to describe the intraparticle diffusive characteristics of the metallic ions inside the composites' pores. Finally, adsorption equilibrium was modelled using Langmuir and Freundlich models.

8.3.3.1 Co^{2+} Sorption using Pure Zeolites

The cobalt uptake by the zeolites type A (LTA), Y (FAU), natural clinoptilolite (HEU(n)), synthetic clinoptilolite (HEU(s)) and nanozeolite A (NZA) as a function of time is shown in Figure 8.13.

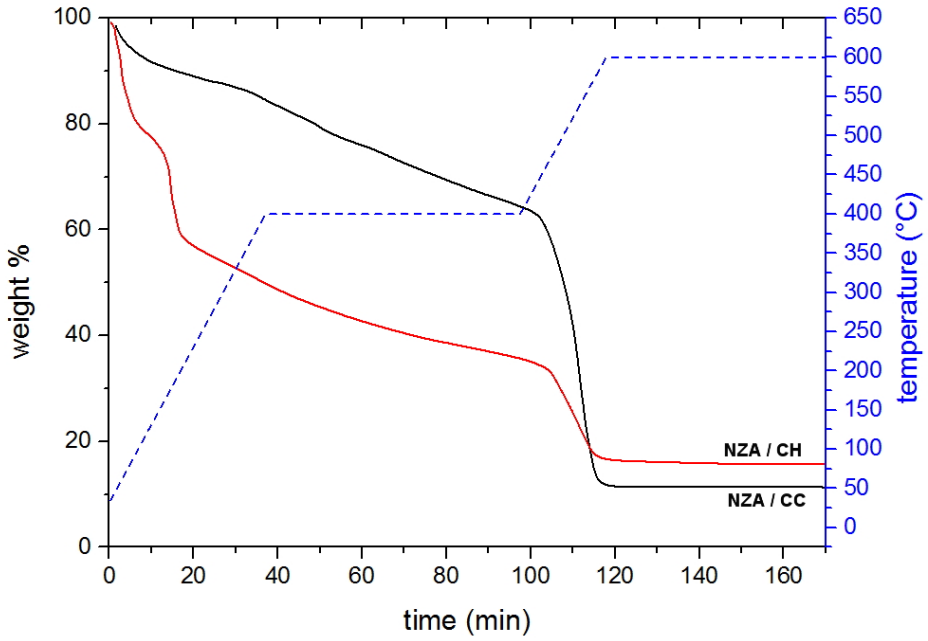

Figure 8.12: Thermogravimetric Analysis of no-seeded LTA-Corn husk composite

These results show that pure NZA has the highest capacity to remove Co^{2+} under the described conditions, 89.7 mg g^{-1}; followed by LTA, 61.2 mg g^{-1}; FAU, 36.7 mg g^{-1}; HEU(s), 26.5 mg g^{-1}; and HEU(n), 15.7 mg g^{-1}. However, NZA, was the slowest material reaching equilibrium state, after 120 min, whereas for LTA and FAU equilibrium was achieved after 60 min, and for both HEU(s) and HEU(n) the equilibrium stage was reached after 10 min. These differences can be related to different particle size, diffusion resistances, porous characteristics and exchangeable ions in zeolites.

8.3.3.1.1 Pseudo First and Second Order Models Results of kinetic data analysis by the Pseudo First Order model for the pure zeolites, showed that NZA and LTA zeolites have a better agreement with the model, $R^2 > 0.95$, than FAU, HEU(synthetic) and HEU(natural), $R^2 < 0.89$. k_1 rate values are similar for all materials as can be seen in Table 8.1 in page 159. Pseudo Second Order equation showed a better representation of the process for all pure zeolites showing a more accurate prediction of equilibrium uptake values, $R^2 > 0.98$. Figures 8.14 and 8.15 shows kinetic and Weber-Morris model respectively. The lines in this plot are a guide for the eye and do not represent any adjustment or model.

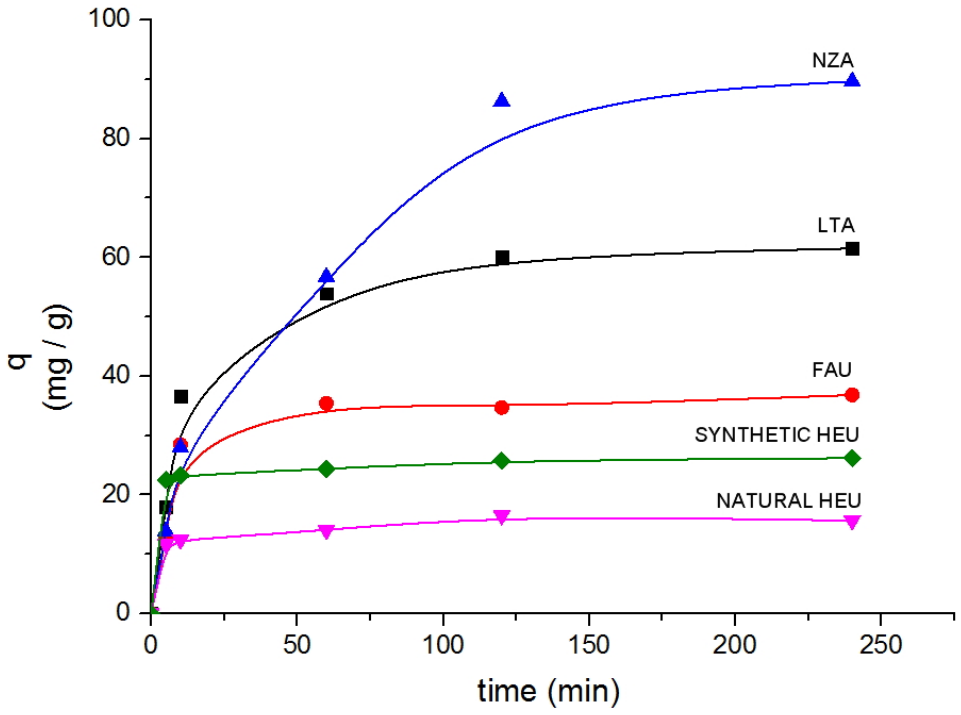

Figure 8.13: Cobalt removal by LTA, FAU, HEU(s), HEU(n) and NZA. Zeolite dose 50 mg, solution volume 10 ml, initial concentration 500 mg/L

Based on these results, sorption kinetic behaviour seems to be more dependent on solid active sites for all zeolites under described conditions as the Pseudo Second Order theory proposes in difference of Pseudo First equation where initial solution concentration is the main driving force for the adsorption.

8.3.3.1.2 Weber-Morris Model According to results shown in Figure 8.15, for both HEU(n) and HEU(s) film diffusion is not taking place or was not observed under these conditions. Dotted lines represent the intraparticle stage for each zeolite. Also, as the straight line is crossing close to the origin, can be said that intraparticle diffusion is rate-limiting for natural and synthetic clinoptilolite. In contrast, for LTA and FAU materials, it is observable that there is a contribution of the film diffusion resistance in the sorptive process, since different linear sections in the curves can be identified. Intercept values of the dotted lines are related to the thickness of empirical diffusive film surrounding the particle. Hence, the higher the value the thicker the film. LTA and FAU showed a similar behaviour, this can be attributed to similar particle size and

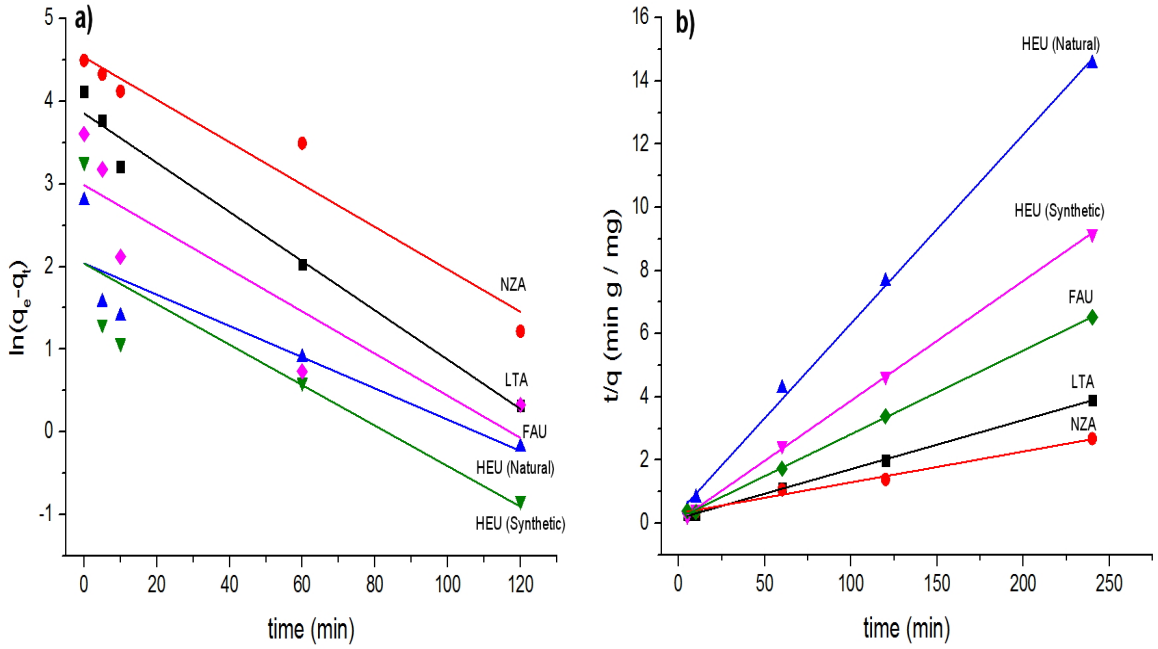

Figure 8.14: Pseudo First and Second Order Equations for LTA/ CH and LTA / CC

chemical composition. Finally, NZA shows a larger intraparticle diffusion segment, however correlation is not as high as the other zeolites have other more mechanisms could be intervening in the rate of adsorption. However, inner diffusion seems to be the biggest resistance. The intrapraticle diffusion coefficients and intercept values for all zeolites are summarised in Table 8.1.

8.3.4 Removal of Cobalt(II) using Composite Materials by Seeding Method.

8.3.4.1 Co^2 Sorption using LTA Composites

Figure 8.16 shows the results obtained from ion exchange experiments using LTA/CH and LTA/CC.

The uptake of cobalt ions by carbonaceous CH and CC can be observed at the bottom of the graph having 5.1 mg g^{-1} and 4.8 mg g^{-1} for CC and CH respectively inferring that both carbons have similar surface properties. From these results, it can be seen that the kinetic behaviour of both composites is similar. LTA/CH removed 52.6

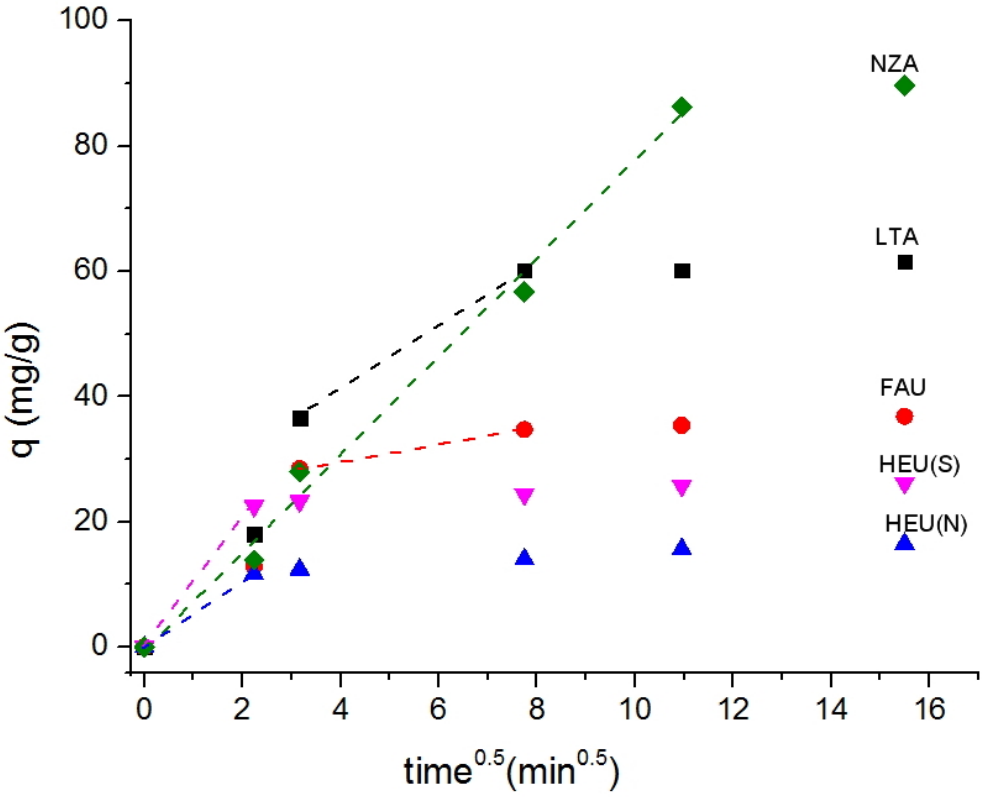

Figure 8.15: Weber-Morris plot for zeolites LTA, FAU, HEUs, HEUn and NZA. Dotted lines represent intraparticle diffusion stage

mg g^{-1} meanwhile LTA/CC 45.5 mg g^{-1}. This can be related directly with the amount of the zeolite on the material. Noticeably the zeolite contained on the composites showed an increased uptake capacity 129.2 mg g^{-1} for LTA*/CH and 156.6 mg g^{-1} for LTA*/CC after the balance made by Equation 8.3, where the contribution of zeolite and carbon in composite is considered in the ions uptake. This result suggests that the porous characteristics of the rearranged zeolite particles, in prepared composites, can improve the sorption capacity.

8.3.4.1.1 Pseudo First and Second Order Models It was found for LTA composites that Pseudo-Second Order better describes the process, $R^2 > 0.999$, agreeing with previous results of pure zeolites. The Weber-Morris model has shown that rate-controlling mechanisms are combinations of different diffusive contributions, film and intraparticle diffusion, similarly to pure LTA. Figures 8.17 and 8.18 show PFO and PSO and Weber-Morris models respectively.

Table 8.1: Kinetic parameters of pure zeolites in the sorption of cobalt ions

	LTA	FAU	HEU (Natural)	HEU (Synthetic)	NZA
$q_{e,exp}$ (mg g^{-1})	61.52	36.80	16.49	26.19	89.68
Pseudo First Order					
$q_{e,calc}$ / (mg g^{-1})	47.16	19.80	7.68	7.66	93.01
k_1/(min^{-1})	0.0298	0.0255	0.0189	0.0245	0.0257
R^2	0.9795	0.8159	0.803	0.187	0.9535
Pseudo Second Order					
$q_{e,calc}$ (mg g^{-1})	64.51	37.73	16.72	26.31	102.04
k_2 / (g mg^{-1} min^{-1})	0.0015	0.0041	0.0105	0.0170	0.0003
R^2	0.9995	0.9994	0.9983	0.9997	0.9898
Weber-Morris					
k_{id} (mg g^{-1} $min^{-0.5}$)	5.124	1.363	5.219	10.067	7.775
C	20.43	24.16	0	0	0.50
R^2	1	1	1	1	0.9899

The adsorption rate constant values of PSO model (k_2) for both composites LTA/CH 0.0017 g mg^{-1} min^{-1} and LTA/CC 0.0090 g mg^{-1} min^{-1}, are higher than for only LTA, 0.0015 g mg^{-1} min^{-1} allowing faster sorption kinetics. This implication of this result is that it can be influenced by the distribution and new arrangement of zeolite particles onto carbon supports as previous results indicated.

8.3.4.1.2 Weber-Morris In Figure 8.18 the Weber-Morris model for LTA composites is shown. Three linear segments are clearly observed. For LTA/CC the process reached equilibrium state before LTA/CH. According to the model, intraparticle diffusion is not exclusively controlling the process, film diffusion occurs at the beginning agreeing with pure LTA results. In this case, the values of intraparticle coefficients showed to be smaller than just LTA, confirming that significant contribution of external diffusion in composites. Also, carbon from corn cob (CC) are shown to improve the diffusive features since the intraparticle diffusion stage was reduced and equilibrium was reached earlier than when LTA used over CH.

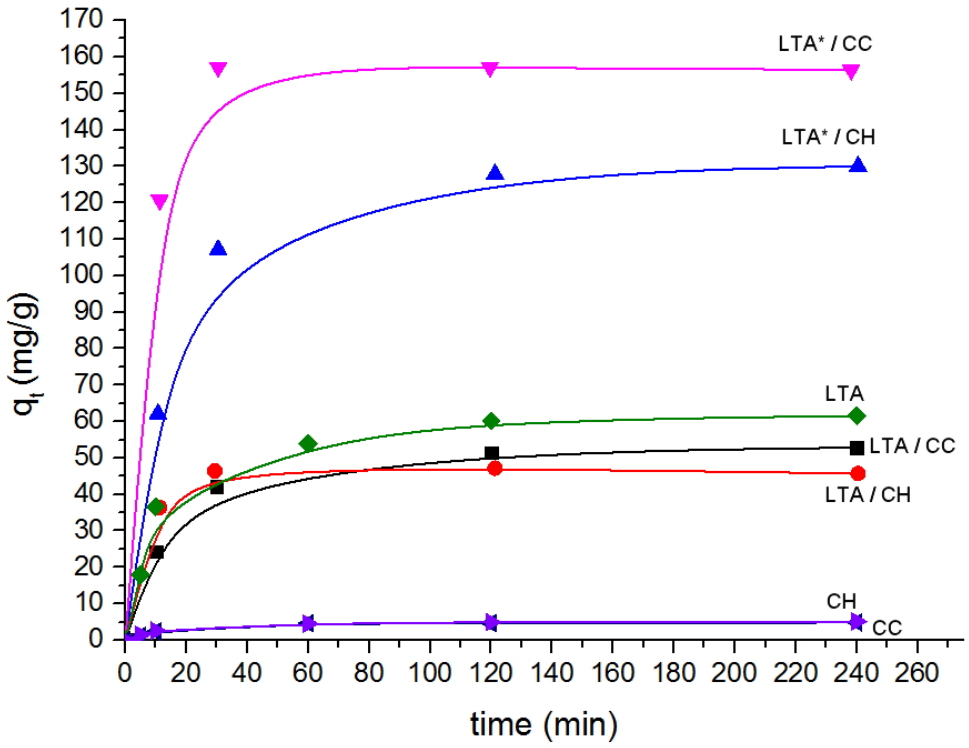

Figure 8.16: Cobalt removal by LTA/CC and LTA/CH as a time function. LTA* corresponds to cobalt uptake for zeolite on composite and CH and CC to carbons uptake. Sorbent dose 50 mg, solution volume 10 ml, initial concentration 500 mg/L

8.3.4.2 Co^2 Sorption using FAU Composites

The kinetic curves of FAU composites used in the sorption of cobalt can be seen in Figure 8.19. The amount of zeolite on both composites is similar, this being the main reason why the uptake in FAU/CC and FAU/CH is almost the same; 25.0 mg g^{-1} and 24.8 mg g^{-1} respectively. From these results, it can be seen that composites reached equilibrium after 120 min. Kinetic curves of composites differ from pure FAU, in which equilibrium was achieved faster. In the estimation of uptake based on individual contributions of carbon and zeolite, using Equation 8.3, results show similar uptake at the equilibrium stage, 62.4 mg g^{-1} and 61.6 mg g^{-1} for FAU*/CH and FAU*/CC respectively. Similar to LTA composites, the different shape of the curves suggest that different diffusive mechanisms may be controlling the overall adsorption rate. Additionally, the support does not have a significant effect for this particular system as LTA composites results showed.

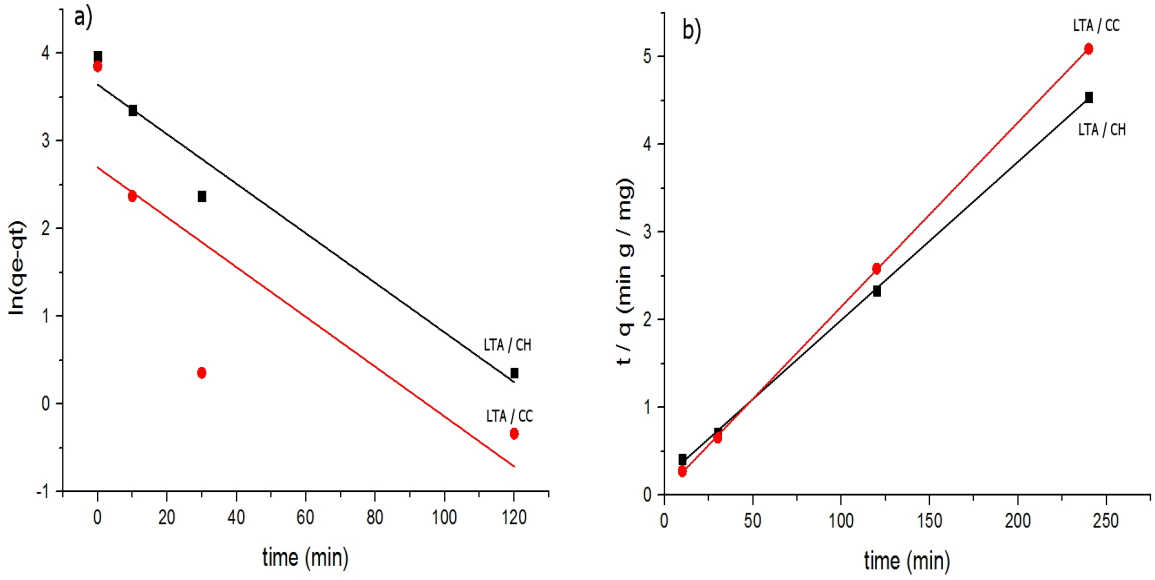

Figure 8.17: First and Second Order Equations for LTA/ CH and LTA / CC

8.3.4.2.1 Pseudo First and Second Order Models As expected, experimental data for FAU composites are better represented by PSO, $R^2 > 0.98$, than PFO $R^2 < 0.88$. Weber-Morris model showed that the process is also mainly controlled by intraparticle diffusion. In Figures 8.20 and 8.21 kinetic models and intraparticle model results are shown.

PFO coefficient k_1 values for FAU/CH, 0.0418 min^{-1}, and FAU/CC, 0.0275 min^{-1}, are higher than for pure FAU, 0.0255 min^{-1}, representing an enhanced rate uptake as linear model shows in Figure 8.20. However, PSO k_2 values for composites, 0.0021 g mg^{-1} min^{-1} and 0.0013 g mg^{-1} min^{-1} are under the rate for pure FAU, 0.0041 g mg^{-1} min^{-1}. These results may be a consequence of the larger exposed carbon surface as previous SEM results revealed.

8.3.4.2.2 Weber-Morris According to Weber-Morris model for FAU composites in Figure 8.21, soprtion of cobalt ions by FAU/CH and FAU/CC is largely controlled by intraporous diffusion, similarly to pure FAU as expected. Also, intraparticle coefficients k_{id} for FAU composites are higher than for pure FAU showing for these composites intraparticle diffusivity properties are enhanced. Coefficients and intercept values can

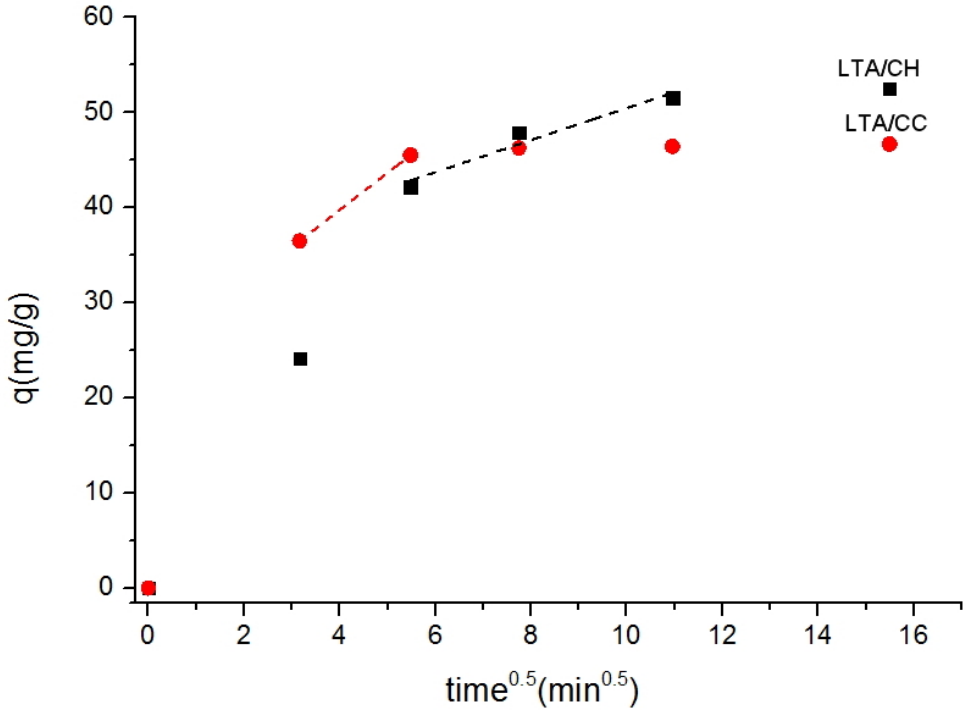

Figure 8.18: Weber-Morris plots for LTA composites. Dotted lines represent the intra-particle diffusion stage

be seen in Table 8.2. Supports did not show any reduction of diffusive restrictions. Both composites followed almost the same behaviour when this model was applied suggesting that the morphology and nature of two supports are very similar.

8.3.4.3 Co^{2+} Sorption using HEU Composites

Figure 8.22 compares the sorptive uptake using HEU composites as a function of time. From the graph, it can be seen that cobalt uptake from solution was 18.2 mg g^{-1} and 17.7 mg g^{-1} for HEU/CC and HEU/CH respectively. The concentration remained constant after 60 min.

The sorption capacity of the synthetic clinoptilolite after the balance, considering the contribution to carbon and zeolite in the adsorption, in Equation 8.2 is 69.2 mg g^{-1} for HEU*/CH and 80.0 mg g^{-1} for HEU*/ CC. These results are significant because the pure clinoptilolite removed 26.3 mg g^{-1} and carbonaceous materials values were close to 5 mg g^{-1} as shown before. In Figure 8.23, the experimental data with two kinetic models are compared.

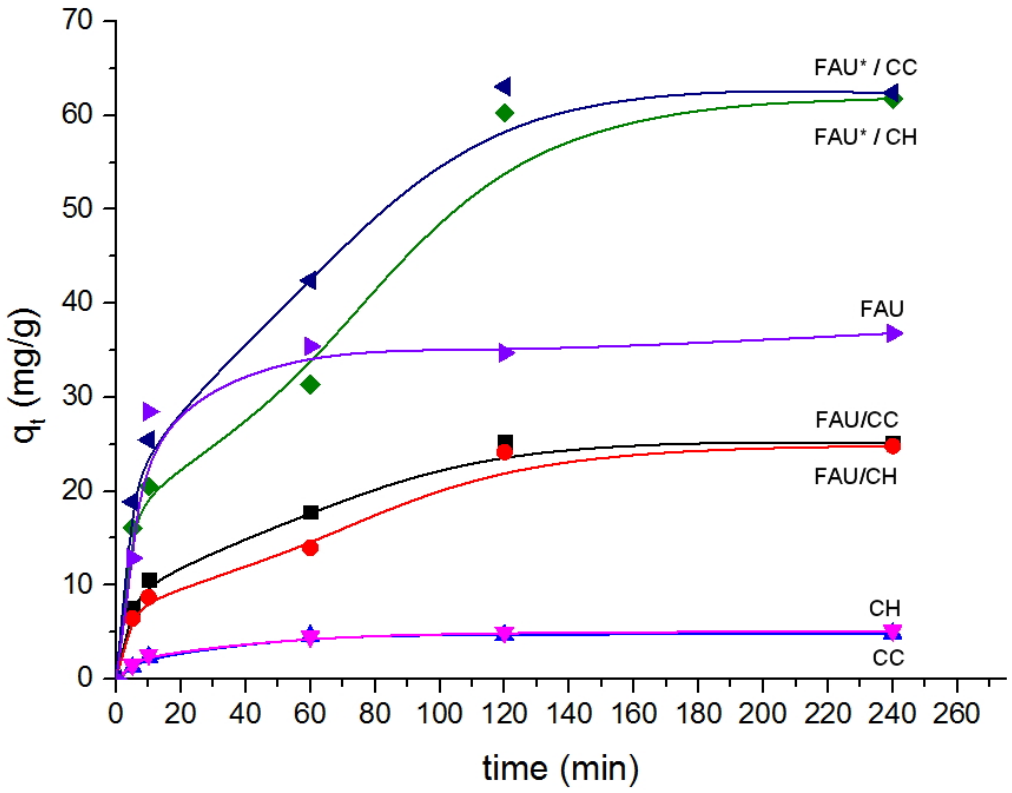

Figure 8.19: Removal of Co^{2+} over time. a) FAU/CC, b) FAU/CH, c) is the uptake associated to FAU on CH and d) is the uptake associated to FAU on CC

8.3.4.3.1 Pseudo First and Second Order Models Similar to previous results, HEU composites also showed a better overall agreement with PSO equation, $R^2 > 0.99$ when compared to PFO model, $R^2 < 0.89$. Figures 8.23 and 8.24 show kinetic and intraparticle Weber-Morris models.

For the PFO model shown in Figure 8.23 it is possible to observe multi-linear behaviour before and after 60 min. These kind of shapes are related to the presence of multiple diffusive resistances as previously described. Kinetic rate values k_1 are higher for both HEU composites 0.0271 min^{-1} and 0.0278 min^{-1} than for HEU 0.024 min^{-1} implying that the use of prepared materials has an improved performance under these specific conditions.

8.3.4.3.2 Weber-Morris Weber-Morris model for HEU composites are shown in Figure 8.24 and is comparing HEU/CH and HEU/CH.

Results indicate that film diffusion is not taking place since straight line is crossing

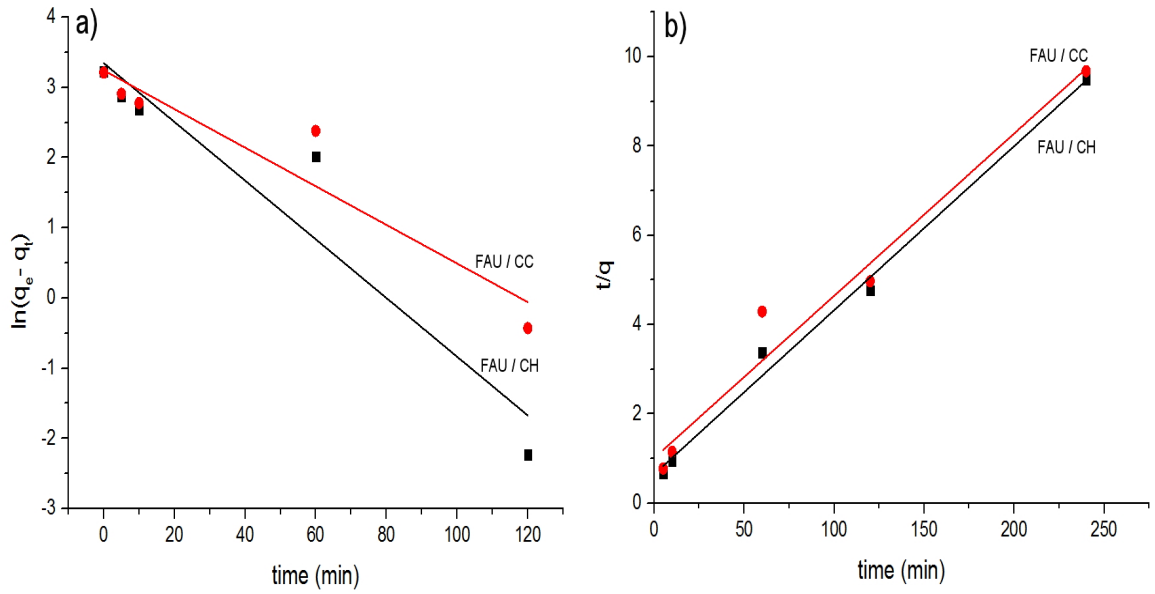

Figure 8.20: First and Second Order Equations for FAU synthetised over CC and CH

near the origin. Intraparticle diffusion governs all the process for both composites in agreement to pure HEU(s) in which the sorption is also controlled mainly for inner diffusion. In Table 8.2 all kinetic parameters for all composites are summarised. Similarly to Weber Morris model results in FAU composites, the supports did not play a significant role in the diffusive characteristics as both composites showed a very similar behaviour as can be seen.

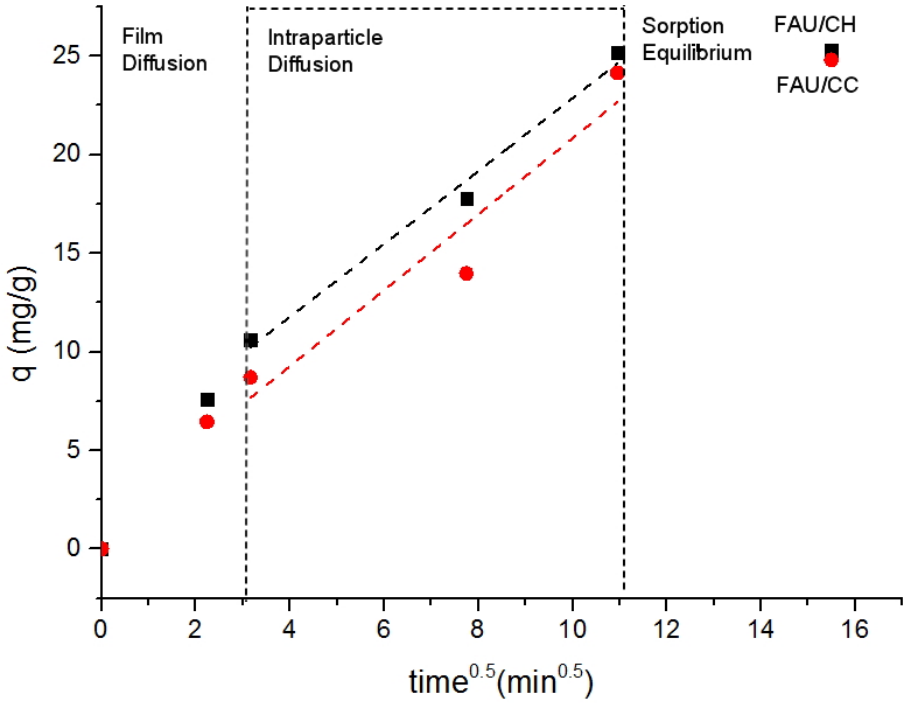

Figure 8.21: Weber-Morris plots for FAU composites. Dotted lines represent the intra-particle diffusion stage

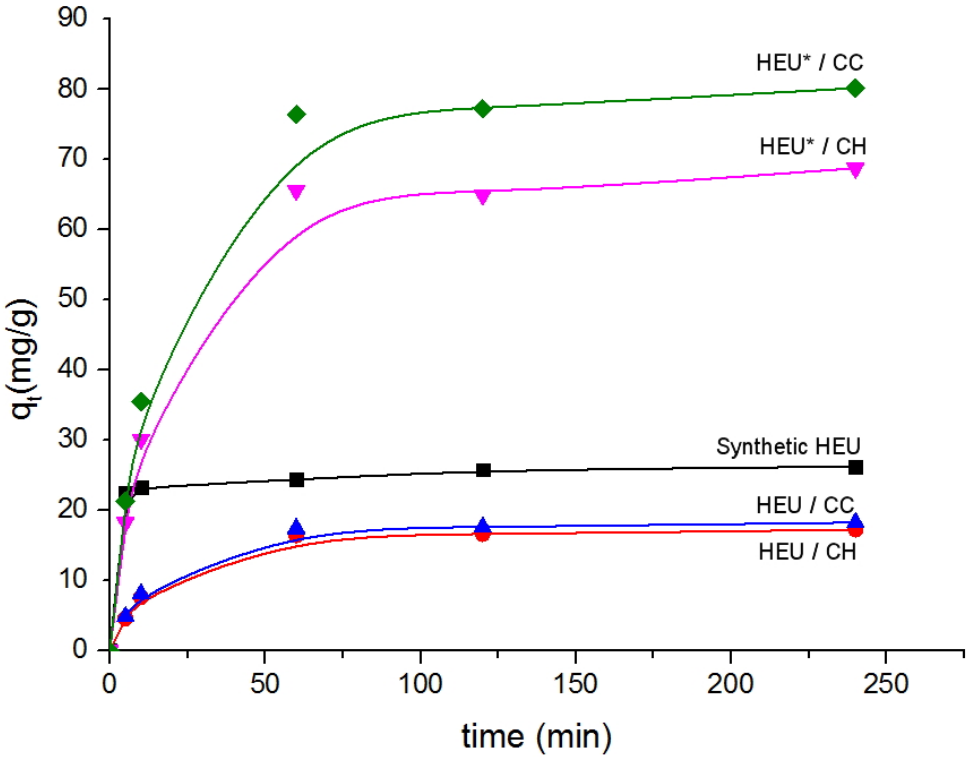

Figure 8.22: Removal of cobalt ions as time function using HEU composites. Sorbent dose 50 mg, solution volume 10 ml, initial concentration 500 mg l^{-1}

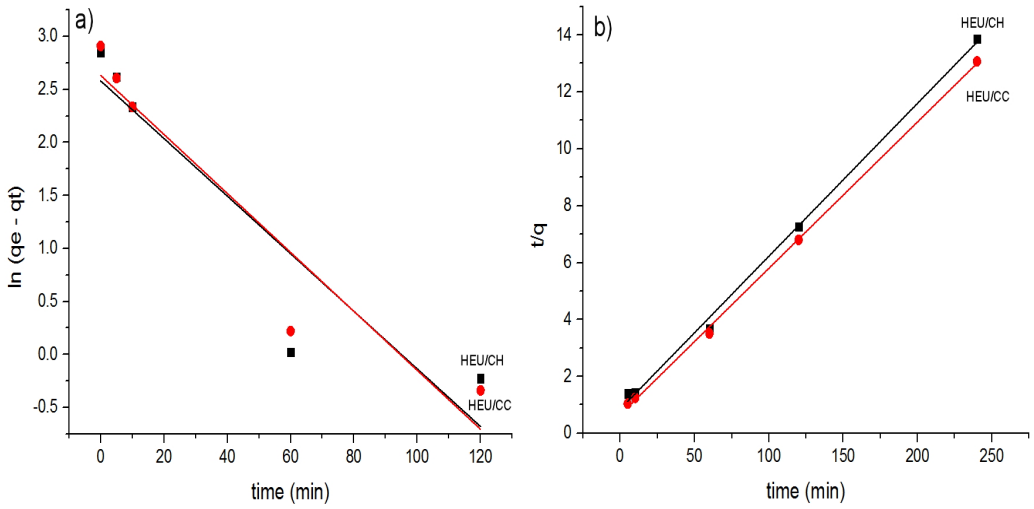

Figure 8.23: First and Second Order Equations for HEU onto CC and CH

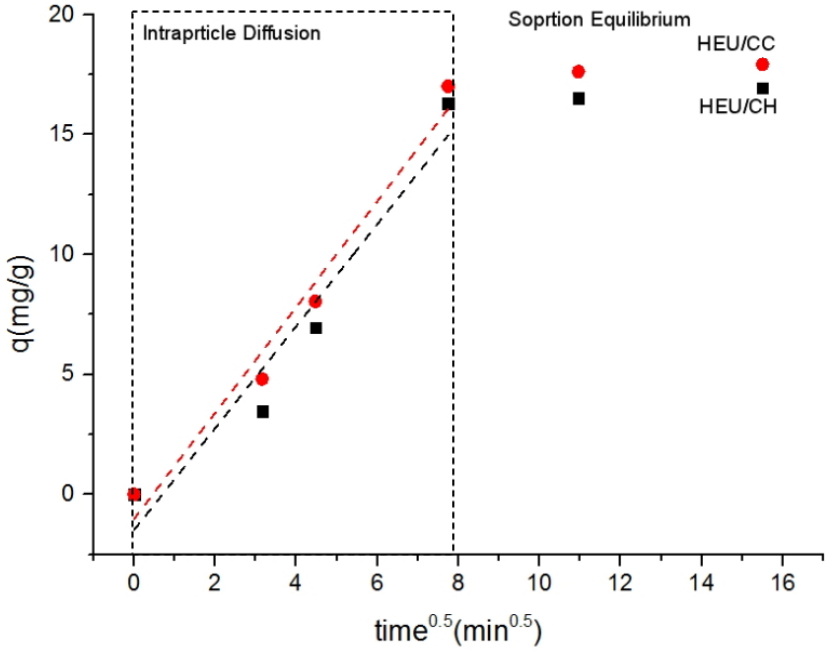

Figure 8.24: Weber-Morris plots for HEU composites. Dotted lines represent the intraparticle diffusion

8.3.5 Removal of Cobalt (II) using Prepared Materials by Impregnation Method

8.3.5.1 NZA Composites

Figure 8.25 compares experimental data on Co^{2+} uptake using NZA, NZA/CH and NZA/CC; the equilibrium was reached after 2 h. According to these results all materials showed a remarkable capacity to uptake cobalt ions from solution, even in composites where the amount of zeolite is significantly reduced when compared to previously prepared composites. Uptake values at equilibrium are 87.3 mg g^{-1}, 55.4 mg g^{-1} and 38.6 mg g^{-1} for NZA, NZA/CH and NZA/CC respectively.

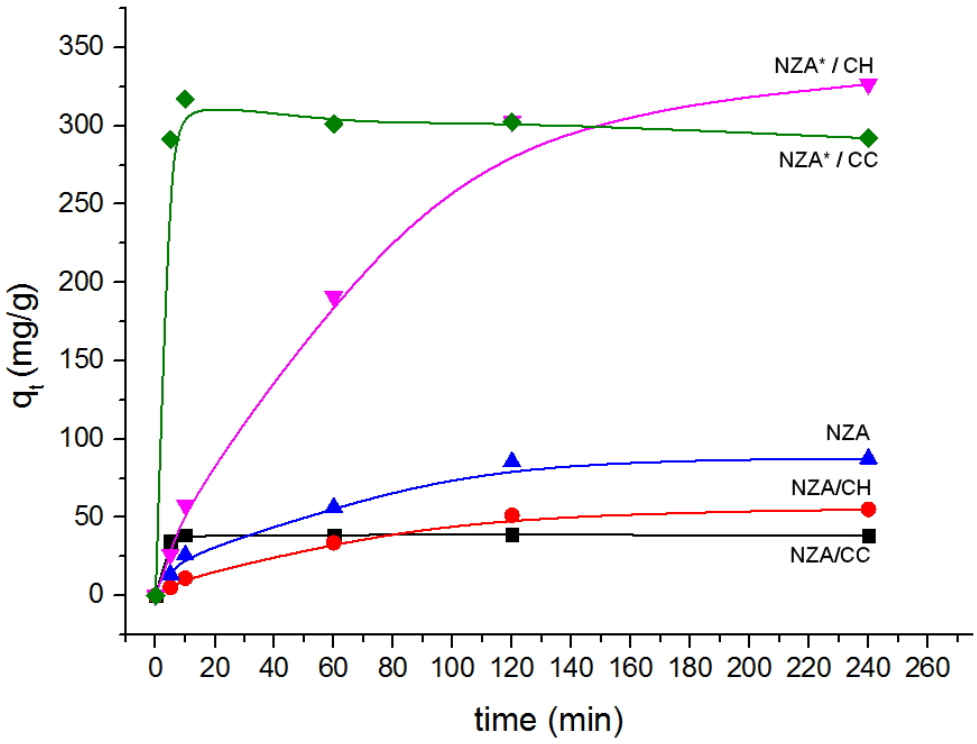

Figure 8.25: Removal of Co^{2+} over time using NZA, NZA/CH and NZA/CC. NZA* represents the theoretical adsorption of zeolite particles supported on CH and CC accordingly

For NZA* supported on both materials, CC and CH, a increased uptake capacity was observed, 292.4 mg g^{-1} and 325.3 mg g^{-1} respectively. However, NZA*/CC showed a decrease in the uptake. These results are possibly related to the presence of its organic template TMA-OH and causing cobalt desorption after the almost in-

stantaneous removal as plot shows. Moreover, it is believed that the distinct origin of carbonaceous supports has an effect (and not the zeolite amount) on the adsorption behaviour for these particular systems, where TMA-OH was not removed after synthesis, producing two kinetic graphs with different behaviour. TMA-OH molecules were not removed after synthesis due to the supporting materials will carbonise in an oxidising atmosphere.

8.3.5.1.1 Pseudo First and Second Order Models Kinetic results for NZA composites agreed with previous results showing a higher coefficient correlation, $R^2 > 0.99$ for PSO, while for PFO is $R^2 < 0.95$. In this case both materials showed differences in the shape of the trend lines as can be seen in Figure 8.26.

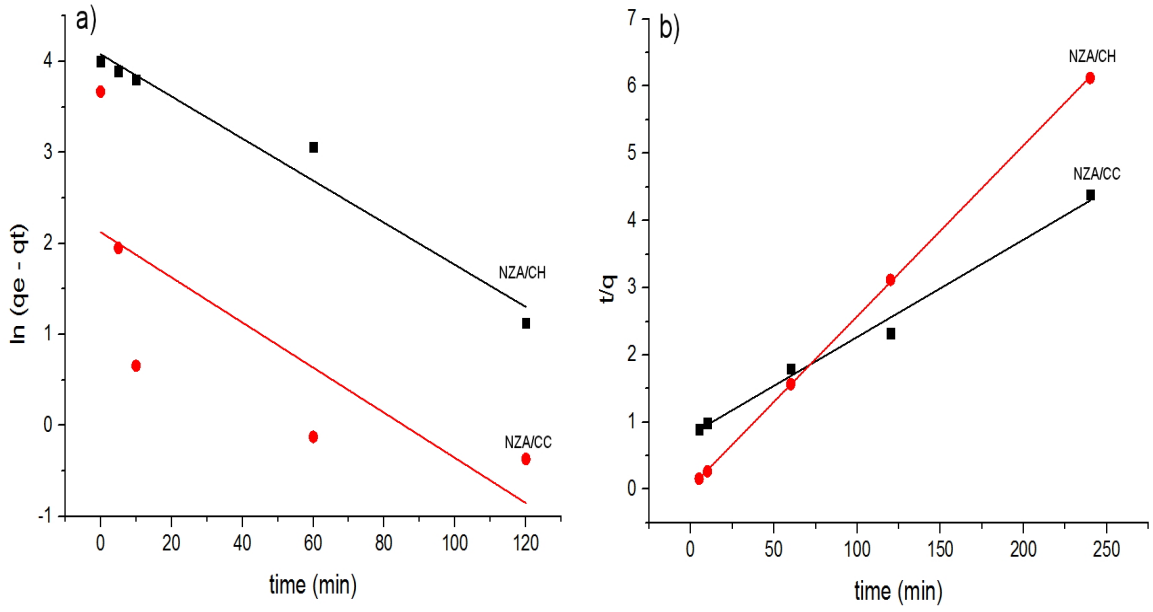

Figure 8.26: First and Second Order Equations for NZA/CC and NZA/CH

NZA/CC showed a marked multi-linear behaviour before and after 20 min when PFO was fitted. In difference to NZA/CH, that shows a linear correlation with the data agreeing with PFO model as Figure 8.26 a) shows. Overall sorption rates of NZA composites k_1 showed very similar values, as is shown in Table 8.2. However NZA/CC showed an increased rate over NZA and NZA/CH materials. This also can be related to the presence of a different sorption resistances in the materials. Interestingly, both

composites showed a good agreement with PSO model as Figure 8.26 b) shows.

8.3.5.1.2 Weber-Morris Model Weber-Morris intraparticle model results for NZA composites are presented in Figure 8.27. These results match with pure NZA behaviour where film diffusion was not observed. Both materials exhibit a different trend; NZA/CH shows a more defined linear behaviour suggesting that process is mainly controlled by intraparticle diffusion as line intercept close to the origin. Both interception values are close to zero confirming intraparticle diffusion as the main resistance before equilibrium. Accordingly, k_2 value is higher for NZA/CC, 12.2 g mg^{-1} min^{-1}, when compared to pure NZA material. Table 8.2 summarises Weber-Morris model coefficients.

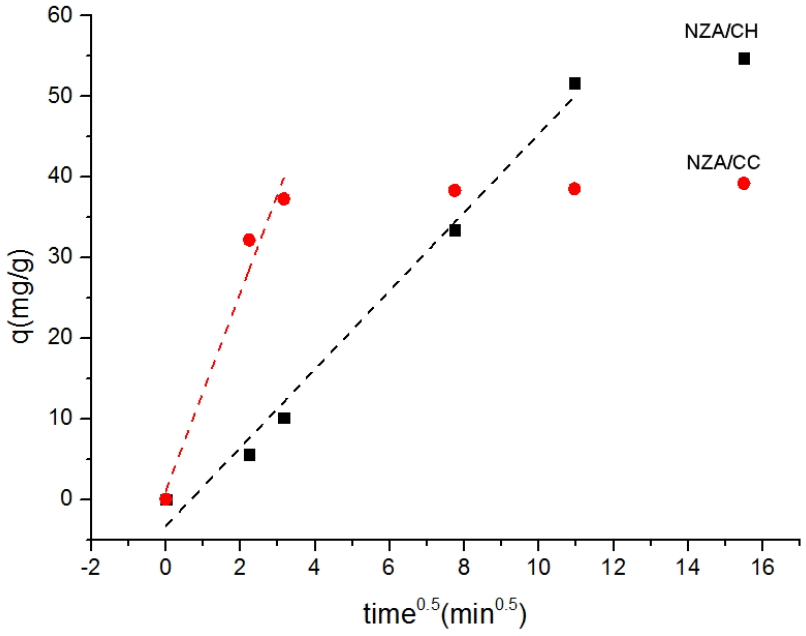

Figure 8.27: Weber-Morris plots for NZA composites. Dotted line represents the intraparticle diffusion stage

Noticeably, NZA supported on CC (NZA/CC) showed improved kinetics characteristics associated to the reduction of diffusive resistances. The equilibrium stage was also earlier achieved. Although NZA supported over CH exhibits higher sorption capacity due to the amount of zeolite present in the composite. The main thought is CC as support with this type of zeolite, regardless the particle size of NZA and LTA,

can be more effective in terms of diffusion than using corn husk (CH) as support. However, NZA zeolite has the shortest intraprticle diffusion stages meaning that this material has shorter diffusion paths. These results agreed with zeolite particle size being approximately ten times smaller than LTA, FAU and HEU.

Table 8.2: Kinetic parameters of zeolite/carbon composites in the sorption of cobalt ions

	LTA/CH	LTA/CC	FAU/CH	FAU/CC	HEU/CH	HEU/CC	NZA/CH	NZA/CC
Zeolite %wt.	83.5	70.0	35.0	37.5	49.0	53.9	15.6	11.5
$q_{e,exp}$ (mg g^{-1})	52.86	47.14	25.29	24.80	17.31	18.36	54.71	39.19
Pseudo First Order								
$q_{e,calc}$ / (mg g^{-1})	38.21	14.85	28.40	25.62	13.20	13.90	59.00	8.36
k_1/(min^{-1})	0.0283	0.0284	0.0418	0.0275	0.0271	0.0278	0.0231	0.0248
R^2	0.9605	0.6630	0.8786	0.8743	0.8244	0.8839	0.9585	0.4394
Pseudo Second Order								
$q_{e,calc}$ (mg g^{-1})	55.56	47.62	27.23	27.52	18.60	19.44	68.92	39.29
k_2 / (g mg^{-1} min^{-1})	0.0017	0.0090	0.0021	0.0013	0.0034	0.0040	0.0003	0.0203
R^2	0.9997	0.9999	0.9961	0.9898	0.9916	0.9902	0.9953	0.9997
Weber-Morris								
k_{id} (mg g^{-1} $min^{-0.5}$)	0.3148	0.1422	1.849	1.925	2.103	2.198	4.861	12.262
C	47.98	44.92	4.3762	1.5783	-1.553	-1.069	-3.286	1.073
R^2	1.0000	0.9942	0.9758	0.8444	0.9074	0.9995	0.9841	0.9478

8.3.6 Adsoprtion Equilibrium

In order to obtain thermodynamic parameters, Langmuir and Freundlich models have been utilised. Since the application of linear methods has risen some controversy, in this thesis both models were approached following a non-linear methodology. The sum of squares of the error was the function to minimse by the use of Solver function in Microsoft Excel. The solver uses a "Generalised Reduced Gradient (GRG2) Algorithm for optimising nonlinear problems"[1].

In Figure 8.28 adsorption isotherms for LTA and LTA composites are shown. The experimental values for three materials are presented in 8.28 a) (dotted lines are only a visual guide). In Figures 8.28 b), c) and d) experimental values are being compared to Langmuir and Freundlich models as graphs indicate. For the three systems, the Freundlich model seems to represent better the experimental data, as this can be confirmed by the correlation coefficients presented in Table 8.3. This result suggests the formation of multilayer of adsorbed ions and the heterogeneity of sorptive sites of these materials. b_F values are considered to be the degree of non-linearity between the solution and adsorbent [275]. b_F values closer to unit means that surface is more heterogeneous [275], as expected, both composites have higher values than pure LTA.

For Langmuir model, the phyisical meaning of b constant in Langmuir model is related to adsorption energy,: the higher b value, the higher affinity of the adsorbent of the adsorbate [276]. As expected, pure zeolite LTA shows better affinity for cobalt ions than both LTA composites, relating this result to the amount of zeolite present in composite. Also, LTA shows to have higher Q_m value than other two materials.

[1]Microsoft Office Support Site `http://support.microsoft.com/kb/82890`

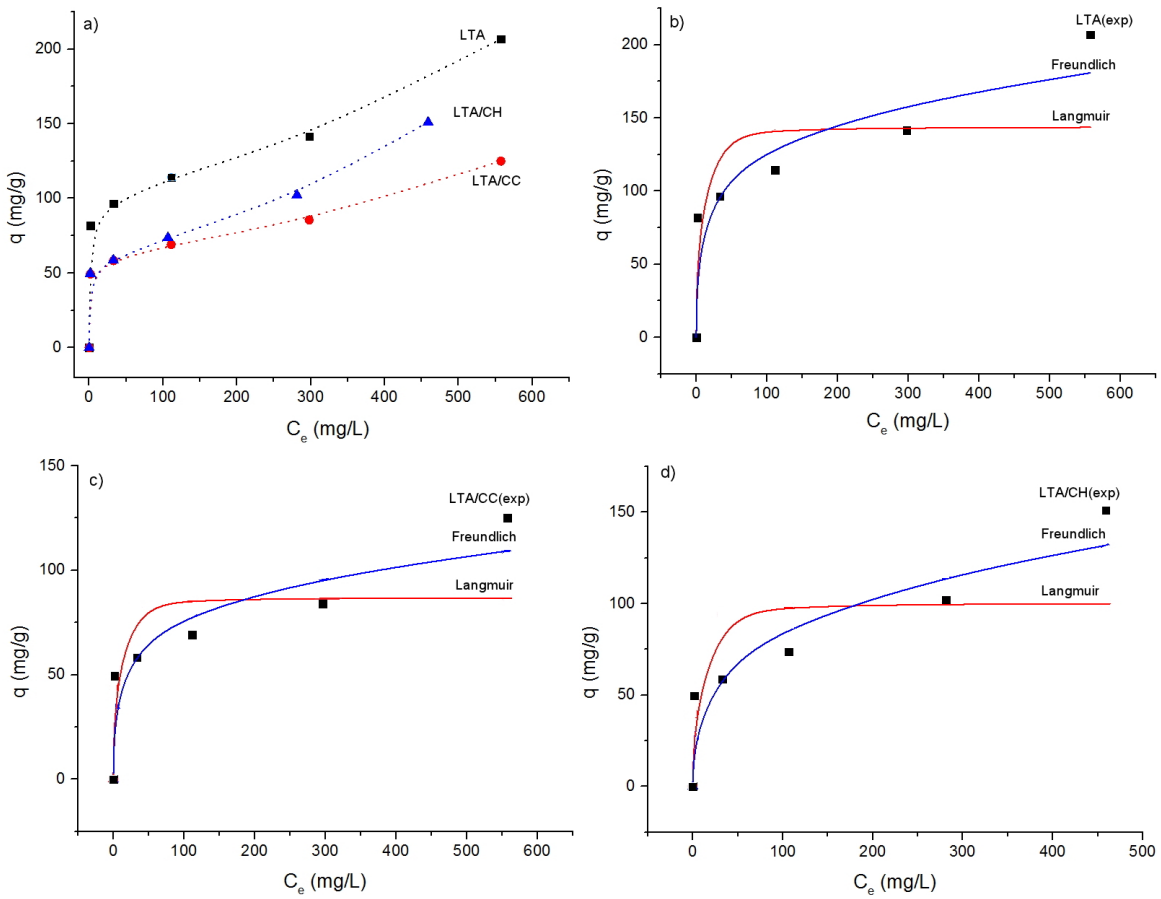

Figure 8.28: Adsorption Isotherms of LTA, LTA/CC, LTA/CH and their corresponding fittings to Langmuir and Freundlich models

Table 8.3: Calculated parameters for Langmuir and Freundlich isotherms

Material	Langmuir			Freundlich		
	Q_m mg g^{-1}	b L mg^{-1}	R^2	K_f $(mg\ g^{-1})(mg\ L^{-1})^n$	b_F	R^2
LTA	143.97	0.590	0.7234	52.39	0.166	0.9089
LTA / CH	87.03	0.473	0.6843	31.67	0.197	0.9163
LTA / CC	100.48	0.441	0.6503	24.52	0.274	0.9048

8.4 Conclusions

In this chapter, the synthesis of hierarchical composites using zeolite A (micro and nanosized), zeolite Y and synthetic clinoptilolite supported on carbonaceous materials prepared from two agroindustrial residues such as corn husk and corn cob, was achieved by two different methods. The first method was based on the use of seeded carbons, that allowed the growth of zeolite crystals on carbons surface. Ball milling has been demonstrated to be a suitable methodology for the size-reduction of zeolites being a straightforward and cheap method. However, in the composites preparation, it is not always possible to have a homogeneous concentration of dispersed seeds and this can have an influence on the final crystallised zeolite particles over the different carbons as results showed.

HEU composite materials have shown to have a three-dimensional morphology. Thick layers of crystals are coating the carbons, which are providing supporting structure to zeolite particles. SEM images showed that the original voids in the carbon are present in the final composites. For LTA and FAU composites, carbon supports were also successfully covered with the corresponding zeolite crystals. The use of corn husk and cob as carbon sources led to lower yields, after pyrolysis, compared to fruit stones or nutshells. The use rigid and more compact materials, having more yields after thermal process, is analysed in further chapters.

The second method involved the immersion of carbons inside the zeolite precursors solution to allow the nucleation and growth of nano LTA (NZA) on the carbon surface. Organic templates for the formation of nanozeolite A, were not removed by calcination, since this would cause the gasification of carbon supports. Nevertheless, sorption results using these materials do not follow the same trend of other prepared composites, possibly due to the interaction of TMA-OH molecules in the zeolite pores with cobalt ions. In general, the use of nanozeolites should be after calcination in order to remove all organic template inside the pores and attached to carbon surface and thus to take advantage of the all surface area as can be seen in further chapters.

The evidence found in this section suggested that the characteristics of ball-milled seeds create heterogeneous materials. Also, it is suggested that seeds possibly do not have a significant effect on carbon surface since the conditioning of the supports is carried out in ultrasonic bath, the impacts of these particles against the support surface (carbon walls in this case) are believed to create cracks on the support surface which would allow the precursor gel to penetrate and generate a strong bond at the interface when zeolite crystals grow.

This chapter also described the sorption kinetic characteristics of cobalt ions by the zeolites and prepared composites. Results showed that NZA has the highest uptake capacity, followed by LTA, FAU, HEU(s) and HEU(n). Also, the sorption of cobalt fitted more accurately the Pseudo Second Order model, suggesting chemical interactions between ions and active solid sites, this shows that the ion exchange is the main sorption mechanism as expected. LTA was shown to have the highest kinetic rate under the described conditions. Intraparticle diffusion has different levels of influence in the sorption using different zeolites; for both HEU materials, boundary (film) diffusion takes place at the beginning of the process; meanwhile for LTA, FAU and NZA a combination of film and intraparticle resistances take place as Weber-Morris model showed. According to presented results, NZA over CC (NZA/CC) showed to be the best material when compared to others in this chapter since it removed more cobalt ions and more efficiently.

In general, kinetic results using composites showed all materials have a good agreement with the PSO model, agreeing with previous zeolite results and confirming chemical interactions as ion exchange theory states. In general, the use of composites modify the diffusive characteristics, reducing in some extent the mass transfer resistances and contributing to an enhanced overall performance. All zeolites forming part of the composites, showed an increased adsorption capacity when compared to the corresponding zeolite. This can be a consequence of the reorganised geometry of zeolite particles for the batch adsorption.

Adsorption equilibrium results showed that systems presented in this chapter are

better represented by the Freundlich model, attributing this to the heterogeneity of sites in composites.

Chapter 9

The Synthesis and Characterisation of Hierarchical Zeolite Composites by the Chemical Modification of Supports and their Copper (Cu^{2+}) Adsorption

9.1 Introduction

In this chapter three different zeolitic materials such as ball-milled zeolite A (BMZA), natural clinoptilolite (HEU) and synthetic nano-sized LTA (NZA) were deposited onto different carbonaceous supports made of agroindustrial wastes from cherry stones (CS) and hazelnut shells (HN) taking advantage of their three-dimensional architecture.

Zeolites studied in this chapter were chosen in order to analyse the feasibility to attach materials with different particle sizes and also to compare between natural and synthetic types. Carbon precursors were selected based on their higher yields after carbonisation process, compared to other sources, and also they presented a more homogeneous morphology as previous chapter shows. The method for the attachment

of zeolites particles is based on the chemical modification of carbonaceous supports. All carbons were preconditioned by using polyelectric cations to modify their surface chemistry and at same time to promote a homogeneous zeolite coating. This is based on electrostatic interactions between the crystallites and the modified carbon surface [277, 278]. Also, the copper ions adsorption was investigated using prepared materials. Copper ions are commonly found in industrial effluents similarly to cobalt ions described in the last chapter and both metals represent an elevated toxicity risk. In order to have a better understanding about the adsorption limiting-steps, Pseudo First Order (PFO) and Pseudo Second Order (PSO) equations were used. Finally, Weber-Morris intraparticle model was used to investigate the diffusive resistances present in the sorption process. These materials have been prepared to allow adsorbed metals encapsulation by vitrification reducing the volume of final disposal.

9.2 Methodology

9.2.1 Carbon Conditioning

Hazelnut shell (HN) and cherry stone (CS) were used as raw materials. The carbonisation process was carried out following methodology presented in Section 7.2.5.1 (p. 120). After carbonisation, the carbons were conditioned using Polydiallyldimethylammonium chloride (PDDA, 20,000 MW, Sigma) solution (1 % and 2 % wt. in 0.1 M NaCl, pH 9.5) under ultrasonic mixing for 1 h (1 g of carbon in 20 ml solution). Finally, PDDA excess was removed with deionised water and the treated carbons were dried overnight at 70°C.

9.2.2 Preparation of Hierarchical Structures

Zeolites were dispersed in 0.1 M NaCl solution to promote particle mobility and solid retention. PDDA treated carbons were then submerged in a zeolite suspension (1 % and 2 % wt. in 0.1 M NaCl) and sonicated for 1 h (1 g of carbon in 20 ml of suspension).

Also a control sample was prepared using untreated carbons. A range of pH (2-10) at constant ionic strength (0.1 M) was studied. Materials were recovered by filtration and then washed with deionised water, to remove zeolite that was not attached to the carbon, and finally dried at 70°C overnight.

9.2.3 Characterisation of Prepared Materials

As in previous chapters, material characteristics such as particle size distribution, zeta potential, crystallographic phases, morphology, and zeolite/carbon ratio were determined by Malvern Zetasizer 1000HS, X-ray diffraction (Rigaku powder diffractometer), Scanning Electron Microscopy (FEI Quanta 200) and Thermogravimetric instrument (TA QA5000) respectively.

9.2.4 Adsorption of Copper by Prepared Hierarchical Zeolite Structures

Kinetic experiments to determine the contact time after which equilibrium is reached were carried out. A liquid/solid ratio of 200 ml/g was used. Cu^{2+} initial concentration was 400 mg l^{-1} (from $Cu(NO_3)_2$ $3H_2O$, Sigma-Aldrich) and initial was pH 4, adjusted with HNO_3. Adsorbate and adsorbent were mixed in a 150 ml beaker using a magnetic stirrer and aliquots were taken after the determined time (0-180 min) at room temperature (25 °C). Samples were filtered and Cu^{2+} concentration was assessed using Inductively Coupled Plasma - Optical Emission Spectroscopy (ICP-OES)(Varian MX). The total number of aliquots did not exceed 2 % of total volume. Cu^{2+} uptake was calculated using Equation 8.1 (p. 145). The total uptake can be considered as a contribution of zeolite and carbon phases, thus, Equation 8.2 (p. 145) was used for the analysis of zeolite uptake when present in composite.

9.3 Results and Discussion

9.3.1 Characterisation of Composites

9.3.1.1 Ball-Milled Zeolite A (BMZA) Composites

XRD patterns for BMZA/HN and BMZA/CS presented in Figure 9.1 show the presence of LTA framework in both composites. Also, patterns for both materials revealed the characteristic zeolite diffraction for the carbonaceous samples.

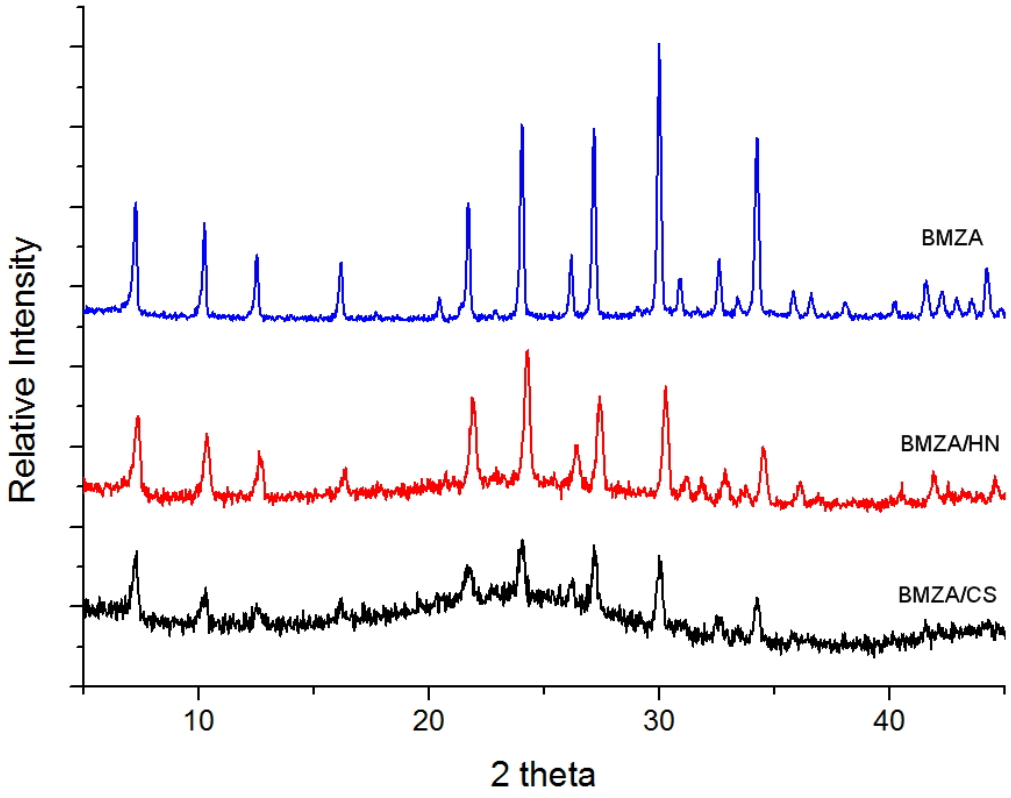

Figure 9.1: X-ray patterns of BMZA and BMZA/carbon composites

Figure 9.2 shows the images of prepared zeolite/carbon composite without PDDA preconditioning. SEM images showed that some zeolite particles are attached to the carbons surface. However they are not forming a very homogeneous zeolite layer. Figures 9.2 a) and b) show composite using hazelnut shell carbon (HN) and Figures 9.2 c) and d) are images for cherry stone carbon (CS) material at different magnifications.

In contrast, Figure 9.3 shows BMZA/HN composites that used PDDA-treated car-

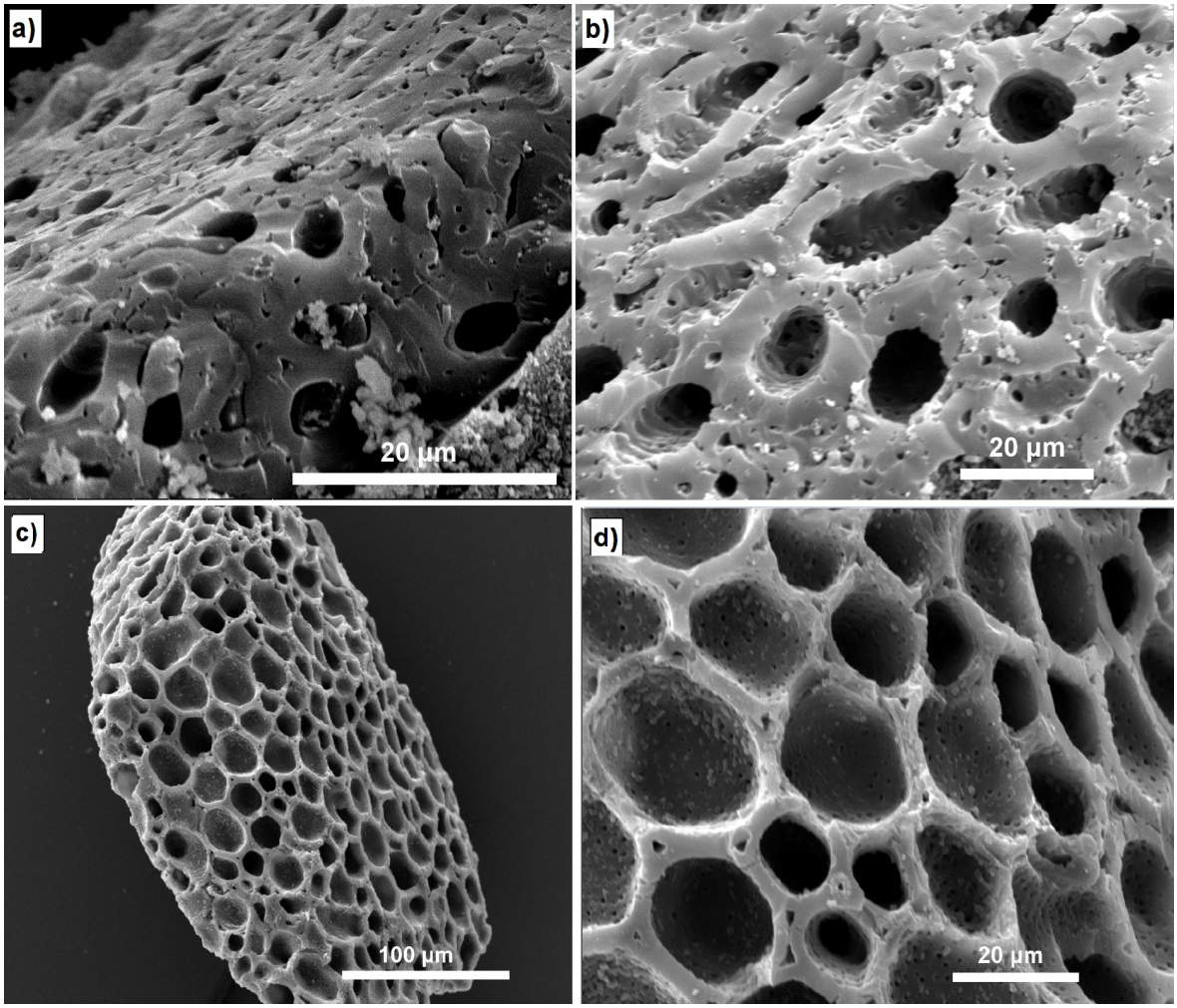

Figure 9.2: SEM images for a) and b) BMZA/HN and c) and d) BMZA/CS composites. Carbon surface was not pretreated with any substance

bons. These images show that particles of ground zeolite A (BMZA) are attached to carbon surface forming an well-defined zeolite layer. These results also confirm that zeolite crystals are present on the surface of the honeycomb-like carbon macroporous structure. Figure 9.3 a) and b) shows materials with 1% PDDA and c) and d) correspond to carbons treated with 2 % PDDA solution. According to these results, there is no a clear evidence that PDDA concentration affects the amount of attached zeolite onto the carbons.

In Figure 9.4 BMZA composites using cherry stone (BMZA/CS) using 1 % PDDA are shown. These results also agreed with previous materials observing a well-spread layer of ball-milled zeolite A (BMZA) on cherry stone carbon (CS) as images show.

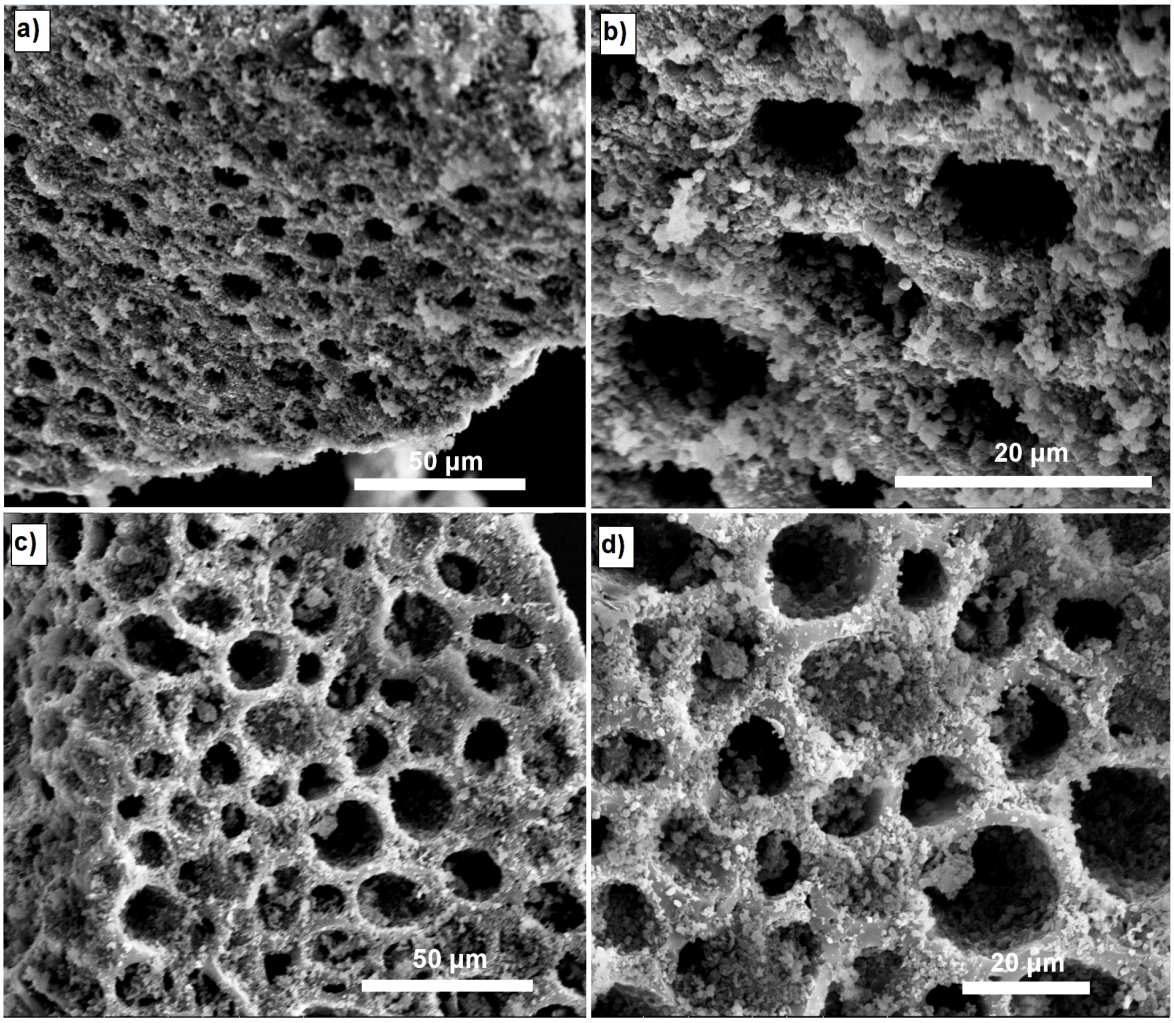

Figure 9.3: SEM for BMZA/HN composites. Figures a) and b) represent carbons with 1% PDDA and c) and d) carbons treated with 2% PDDA

In order to determine zeolite/carbon ratio, the composites' final weight after thermogravimetric analysis is assumed to correspond only to zeolitic phase. After SEM results, where only a small amount of zeolite was attached without surface conditioner, composites using pretreated carbons where analysed by thermogravimetric technique since these were also used in sorption experiments as is further described in this chapter. Figure 9.5 shows that BMZA zeolite composition correspond to 23.74 % for BMZA/CS and 26.78 % BMZA/HN.

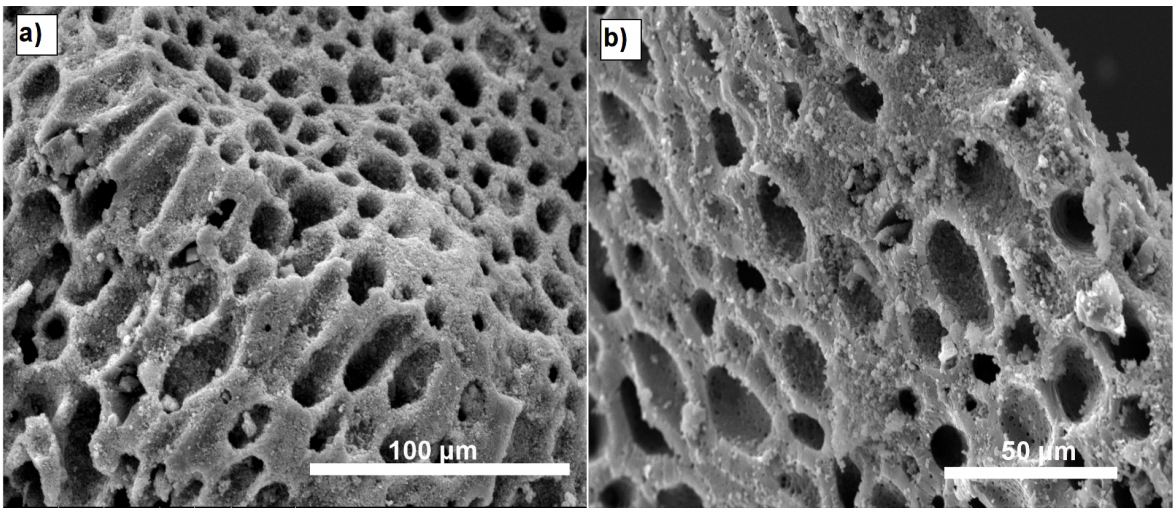

Figure 9.4: SEM of BMZA/CS composites using pretreated carbons with 1% PDDA

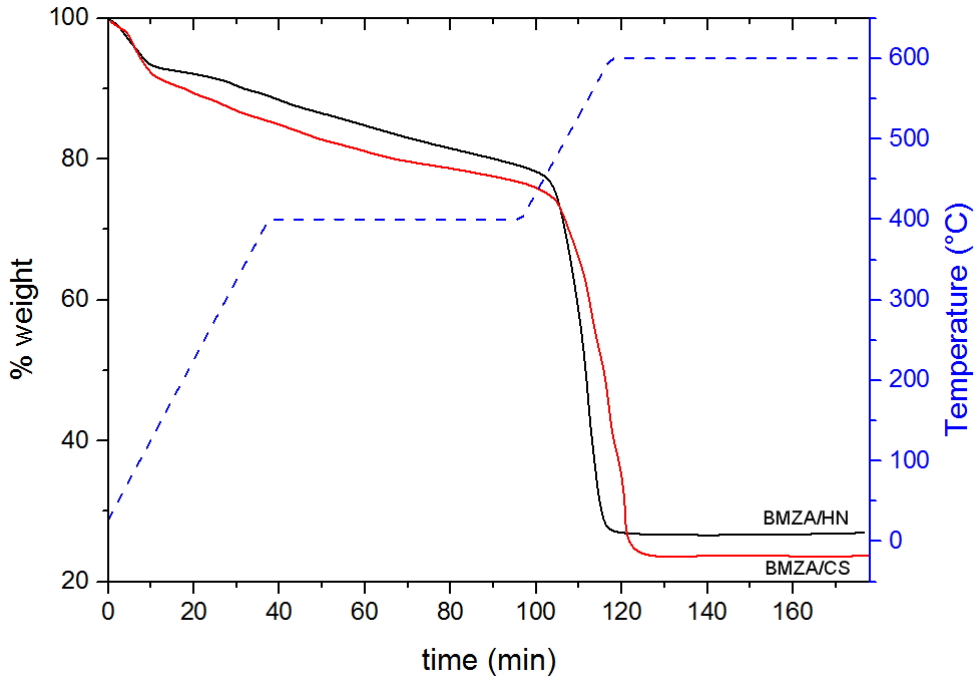

Figure 9.5: TGA for BMZA/HN and BMZA/CS using 1% PDDA

9.3.1.2 Nanozeolite A (NZA) Composites

In Figure 9.6, the prepared NZA composites revealed a similar diffraction pattern, in which the LTA zeolite phase is confirmed. Also, in all composites patterns the characteristic curvature for amorphous carbon phase was observed and a peak reduction related possibly to the amount of zeolite in the composite.

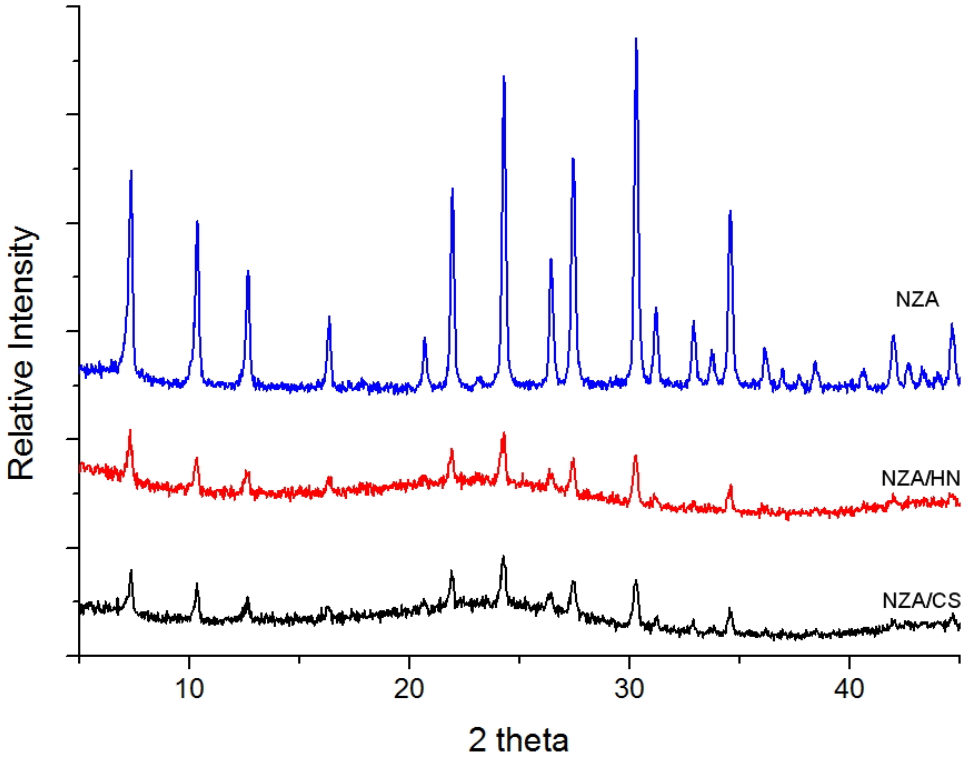

Figure 9.6: X-ray patterns of NZA/carbon composites

From Figure 9.7, where carbons were not conditioned with PDDA, it is possible to observe that a reduced amount of zeolite particles were attached to the carbon surface compared to preconditioned carbons. Figure 9.7 a) shows CS materials as support and b) HN composites accordingly. These results agreed with previous ones where carbons were not conditioned. It is apparent from these graphs that very few zeolitic particles were retained on the carbonaceous structure. In contrast, there was a significant difference when carbons were previously conditioned with PDDA solution.

Nanozeolite A (NZA) particles are also completely coating hazelnut shell (HN) using different PDDA concentration as observed in Figures 9.8. 1 % for Figures 9.8

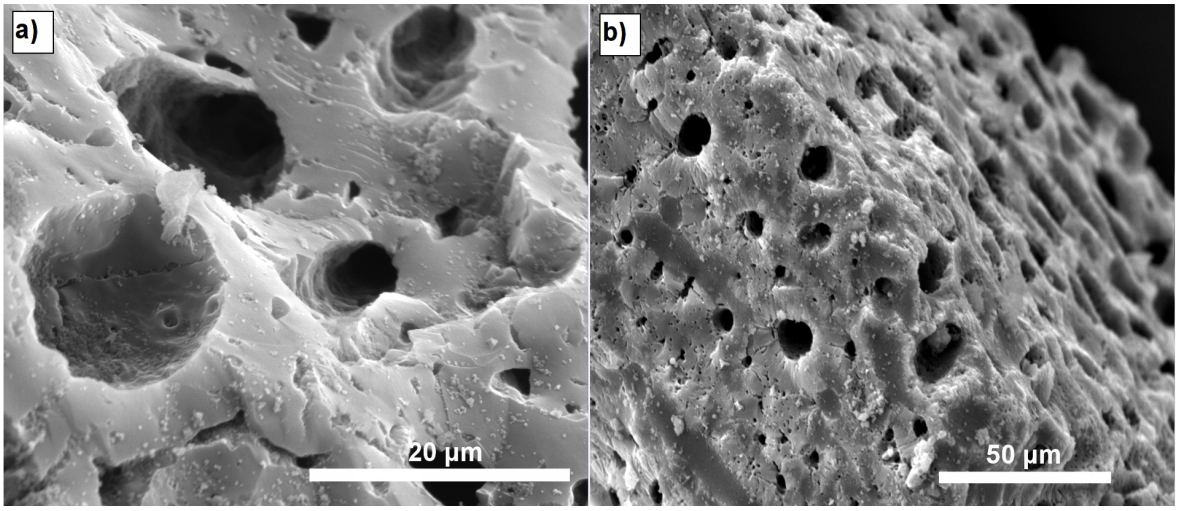

Figure 9.7: SEM images for a) NZA/HN materials and b) NZA/CS composites. Carbon surface was no pretreated

a) and b) and 2 % for c) and d) without showing any clear difference of the amount of the zeolite coating. Additionally, a considerable amount was attached to carbon surfaces preserving its original three-dimensional honeycomb architecture as can be clearly observed.

Also, in Figure 9.9 NZA/CS composite is shown. Again, nanozeolite A is uniformly coating the carbon surface after using only 1 % PDDA. These results have also suggested that PDDA concentration (1 % and 2 %) does not have an effect on the process confirming the hypothesis that the modification of zeta potential on surface favours the zeolite fixation.

Results from thermogravimetric analysis for NZA-composites are presented in Figure 9.10 b). Zeolite load ranges from 12 % to 47 %. These differences can be associated to differences on carbons surface functional groups but also to morphology, surface area or particle size. All due to the different carbons nature and how they can interact with zeolites suspensions.

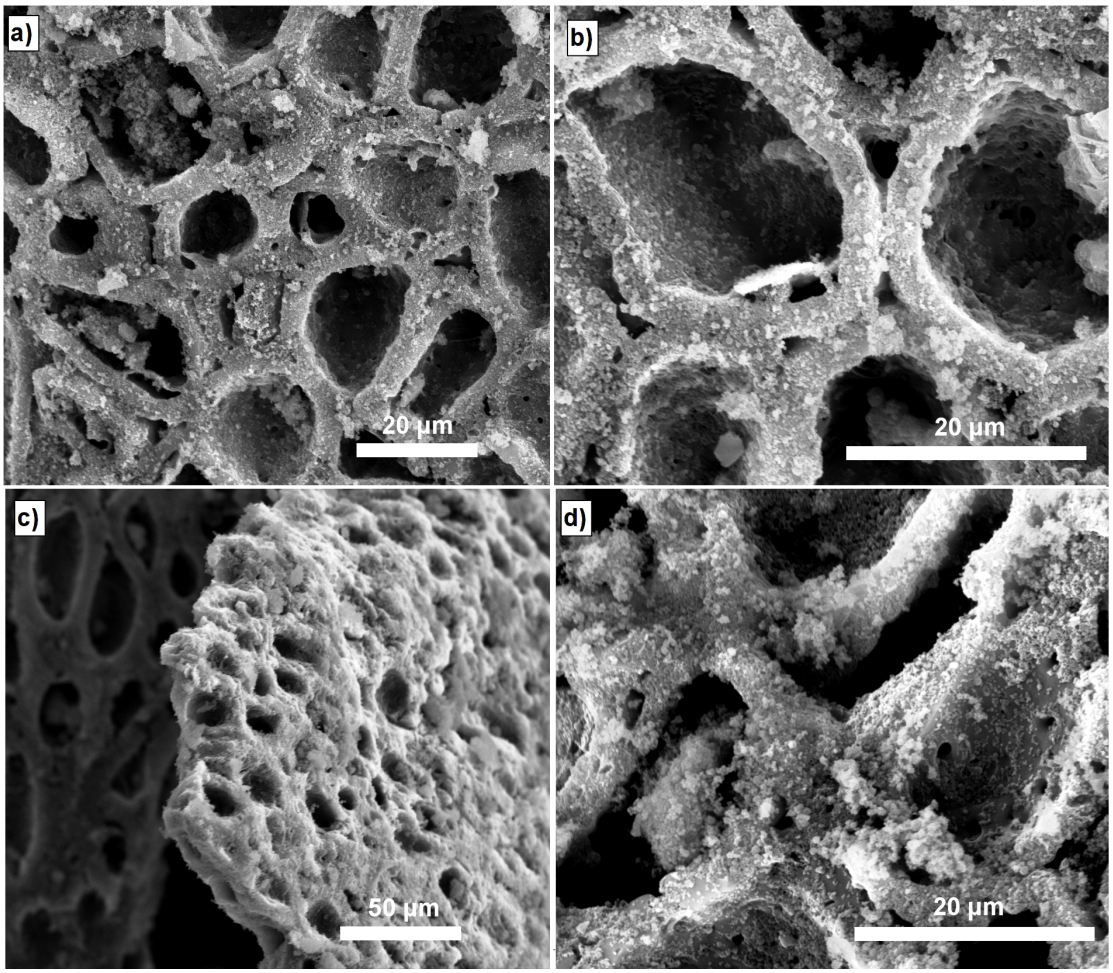

Figure 9.8: Scanning Electron Micrographies of NZA/HN a) and b) 1 % PDDA; c) and d) 2 % PDDA

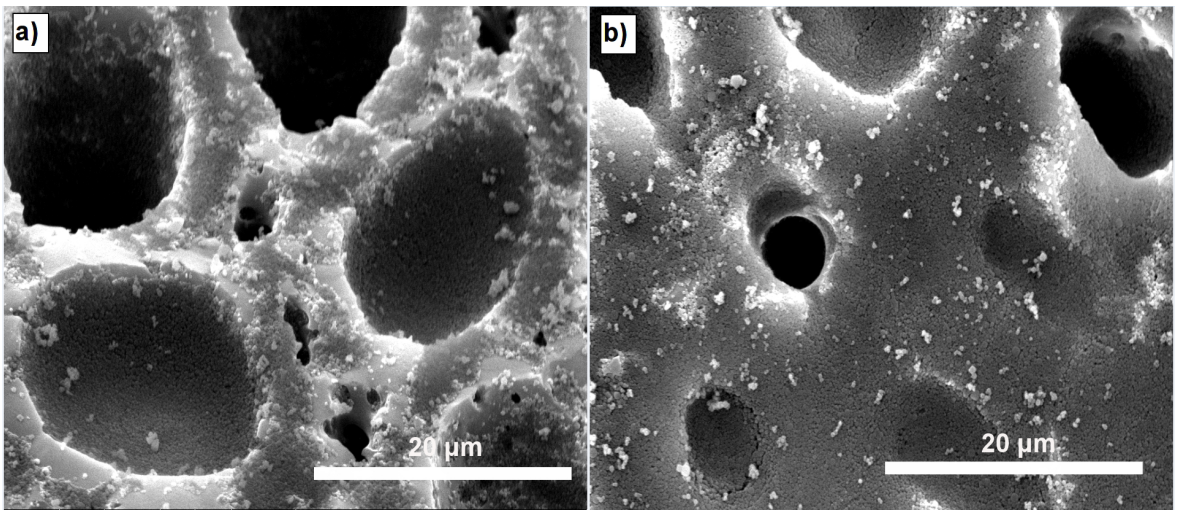

Figure 9.9: Scanning Electron Micrographies of NZA/CS composites with 1% PDDA at different magnifications

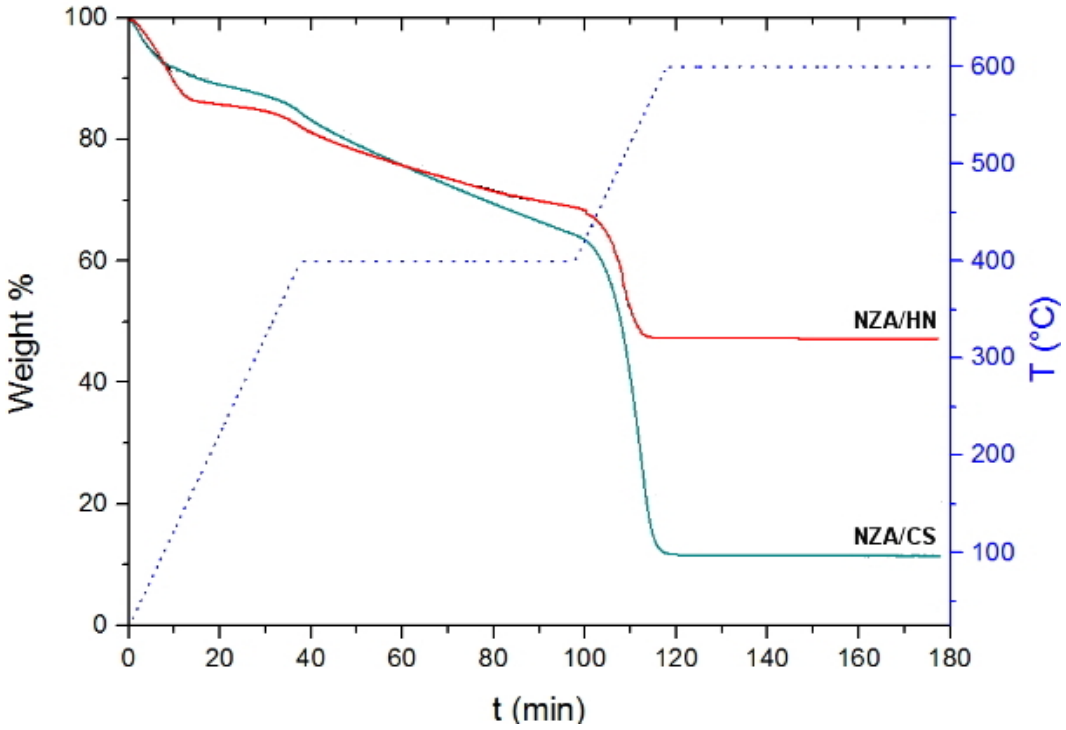

Figure 9.10: Thermogravimetric Analyses of NZA/HN and NZA/CS composites using 1% PDDA, dotted line represents different temperature levels of the program

9.3.1.3 HEU Composites

Figure 9.11 presents the XRD patterns for HEU/CS and HEU/HN. Diffraction peaks corresponding to 2-theta angles of the reference material showing the presence of HEU phases in both materials.

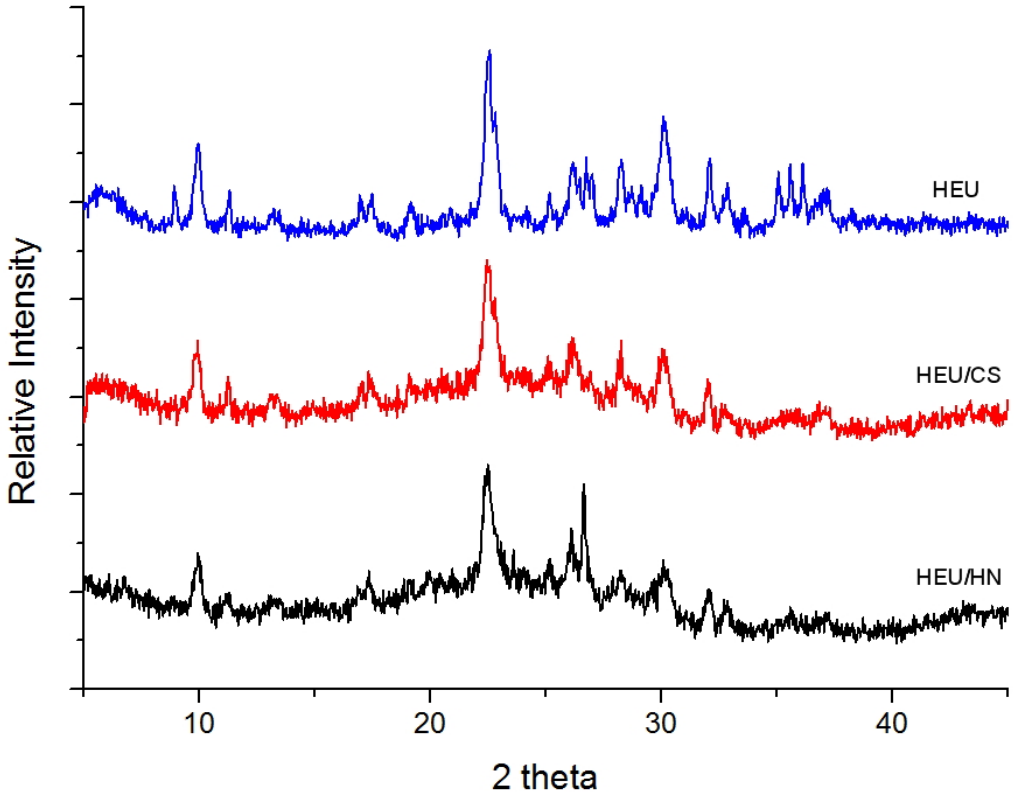

Figure 9.11: X-ray patterns of HEU/carbon composites

The PDDA concentration effect was also analysed for HEU composites. In Figure 9.12 HN and CS composites are shown after the attempt to fix zeolite particles on surfaces without any previous treatment. Results showed that it was not possible to achieve a zeolite coating.

The success of the pre-treatment using PDDA in previous materials is confirmed and extrapolated to natural clinoptilolite as can be seen in Figure 9.13. Figures a) and b) show only HN support conditioned with 1 % and, c) and d) with 2 % PDDA solution. From images, it was not possible to distinguish significant differences about the morphology of the analysed materials using different concentrations.

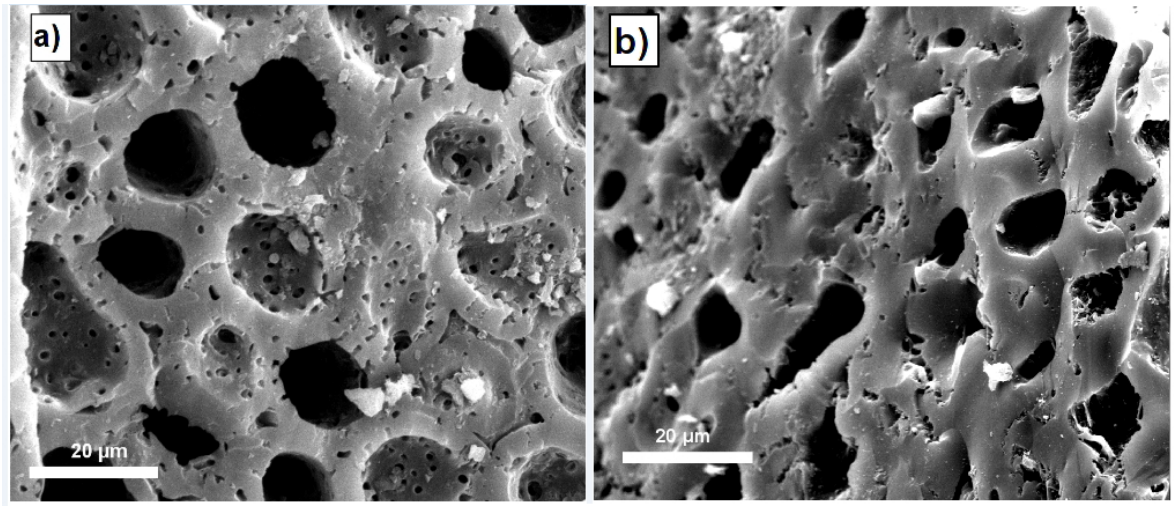

Figure 9.12: Scanning Electron Micrographieand HEU over carbonaceous hazelnut shell and CS b). without PDDA pretreatment respectively

Finally, pretreated carbonaceous cherry stones (CS) also show an excellent coverage of HEU particles as Figure 9.14 shows. This composite was prepared using 1 % PDDA solution observing good coating characteristics attaching the zeolite particles to the carbon scaffold geometry.

Thermogravimetric results obtained for HEU-over-carbons composites are shown in Figure 9.15, final HEU amounts in composites, varied from 15 % to 18 %. The graph shows a decreasing weight as temperature increases, at 200 °C moisture is evaporated and from 400 °C carbon begins to react with oxygen and it is transformed to CO_2. All solid carbon was displaced when temperature level reached 600 °C.

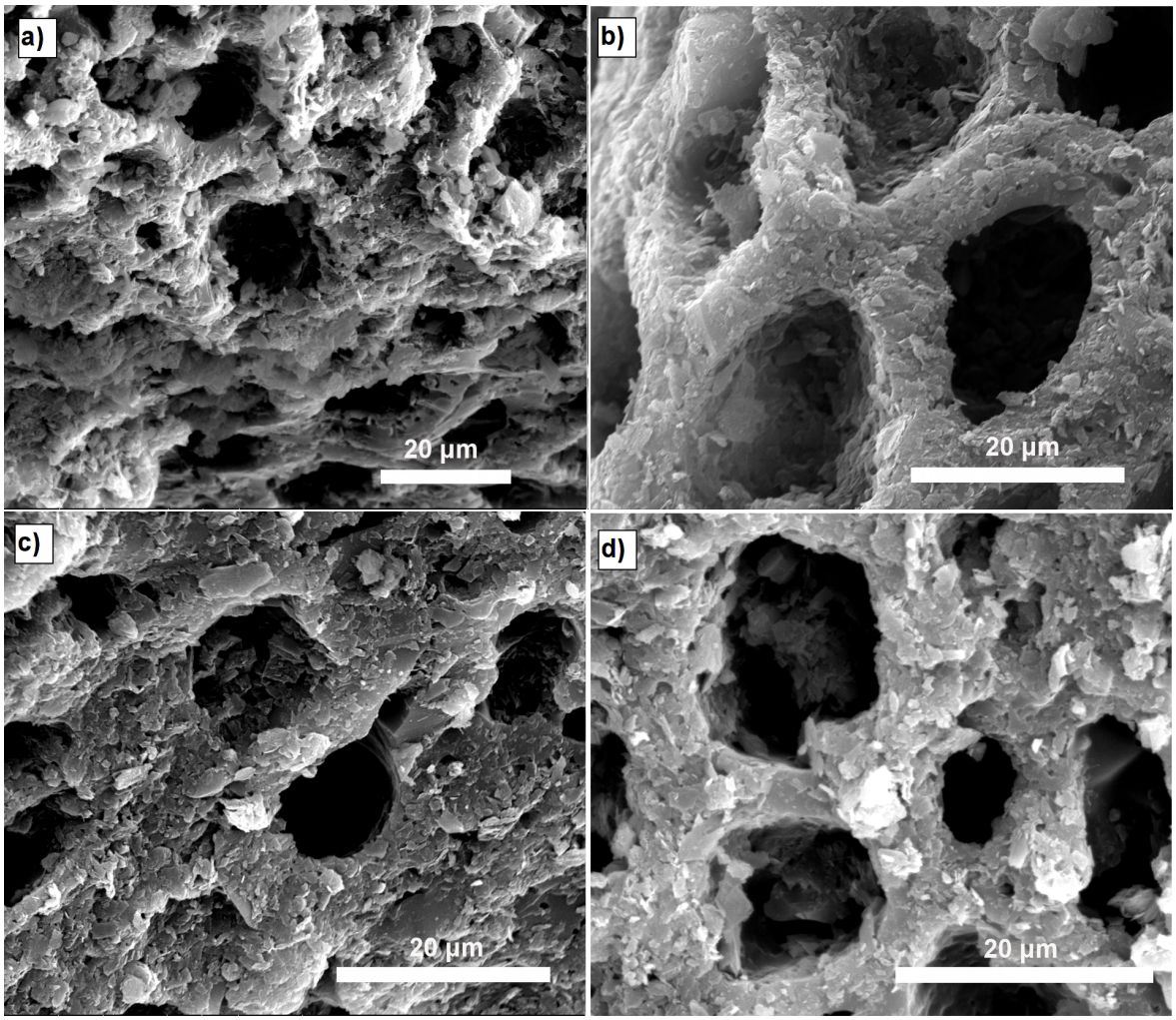

Figure 9.13: Scanning Electron images for HEU/HN using 1% PDDA, a) and b); and 2% PDDA c) and d)

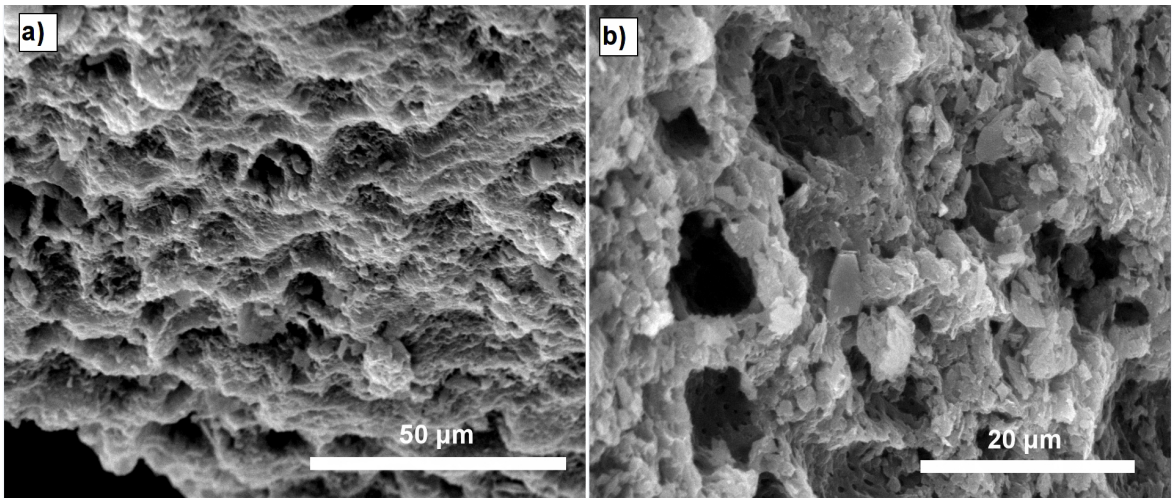

Figure 9.14: Scanning Electron Micrographies of HEU over carbonaceous cherry stone (HEU/CS); a) and c) correspond to 1 % PDDA composites using pretreated carbons as supports

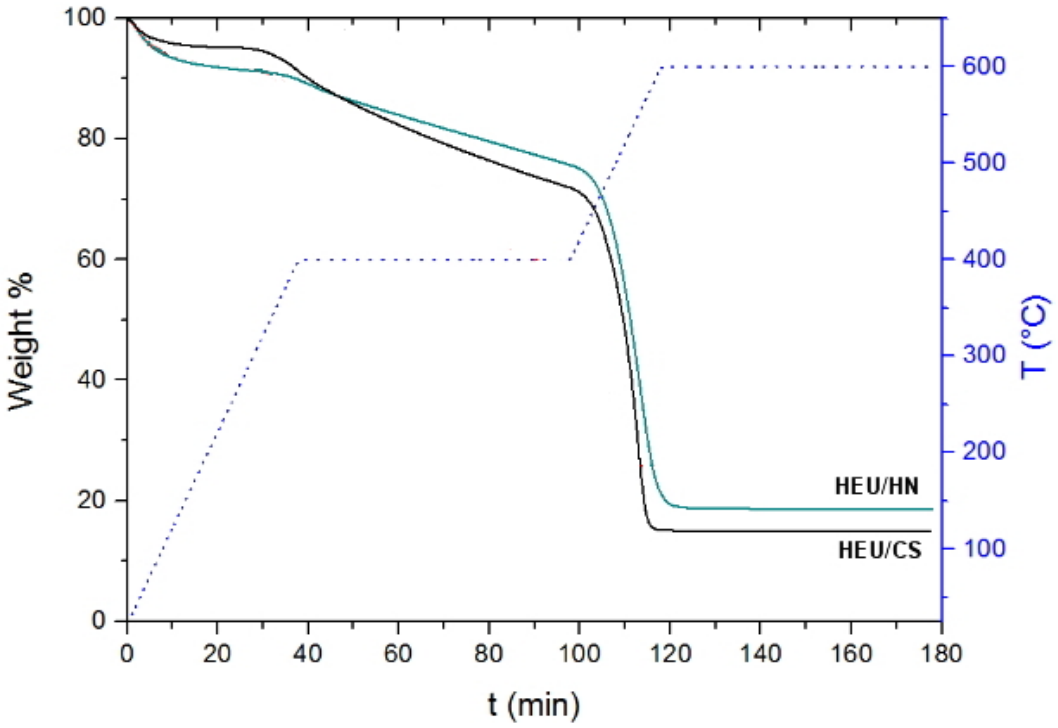

Figure 9.15: Thermogravimetric Analyses of HEU/Carbon composites using 1% PDDA, dotted line represents different temperature levels of the program

9.3.1.3.1 Effect of PDDA Concentration Thermogravimetric analyses were carried out as a method to confirm the hypothesis that PDDA concentration does not have a effect on the amount of zeolite attached on carbon. According to these results, it was possible to observe that different PDDA concentrations, 1 % and 2 %, did not have an influence on final zeolite deposition as can be seen in Figure 9.16. In Figure 9.16 a) the weight percentage for HN composites is presented and the weight difference between two pretreatments was only about 1.5 %, and for CS composites. Both lines in Figure 9.16 b) are overlapped concluding that two PDDA used concentrations had same behaviour under this analysis. Thus, further experiments were conducted using only 1 % PDDA since there is no need to employ higher concentrations when preparing these composite materials. Also two different temperature programs were applied as blue-dotted line is indicating in Figures 9.16 a) and b).

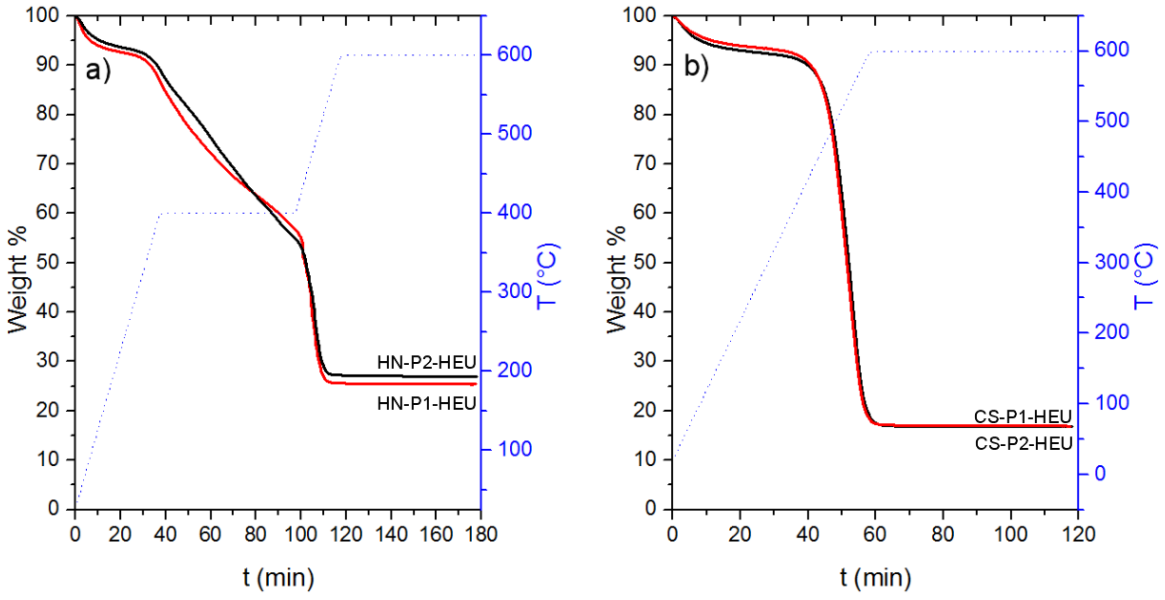

Figure 9.16: TGA to study the effect of PDDA concentration on final zeolite amount in composite. a) HEU on hazelnut carbon pretreated with 1 % and 2 % and b) HEU on hazelnut carbon pretreated with 1 % and 2 %

9.3.2 Adsorption Results

9.3.2.1 Cu^{2+} Removal with Pure Zeolites

Figure 9.17 shows the kinetic behaviour of the removal of copper ions using ground-zeolite LTA (BMZA), nanozeolite A (NZA) and natural clinoptilolite (HEU). Noticeably, NZA has the highest sorption capacity, 74.4 mg g^{-1}, meanwhile BMZA and HEU have 33.5 and 22.5 mg g^{-1} respectively. According to these results, equilibrium under described conditions was achieved after approx 20 min for all zeolites. In a previous report, Wang *et al.* [279] reviewed the use of natural zeolites, mainly clinoptilolite, to remove copper ions where typical values ranged from 5.9 mg g^{-1} to 12.8 mg g^{-1}.

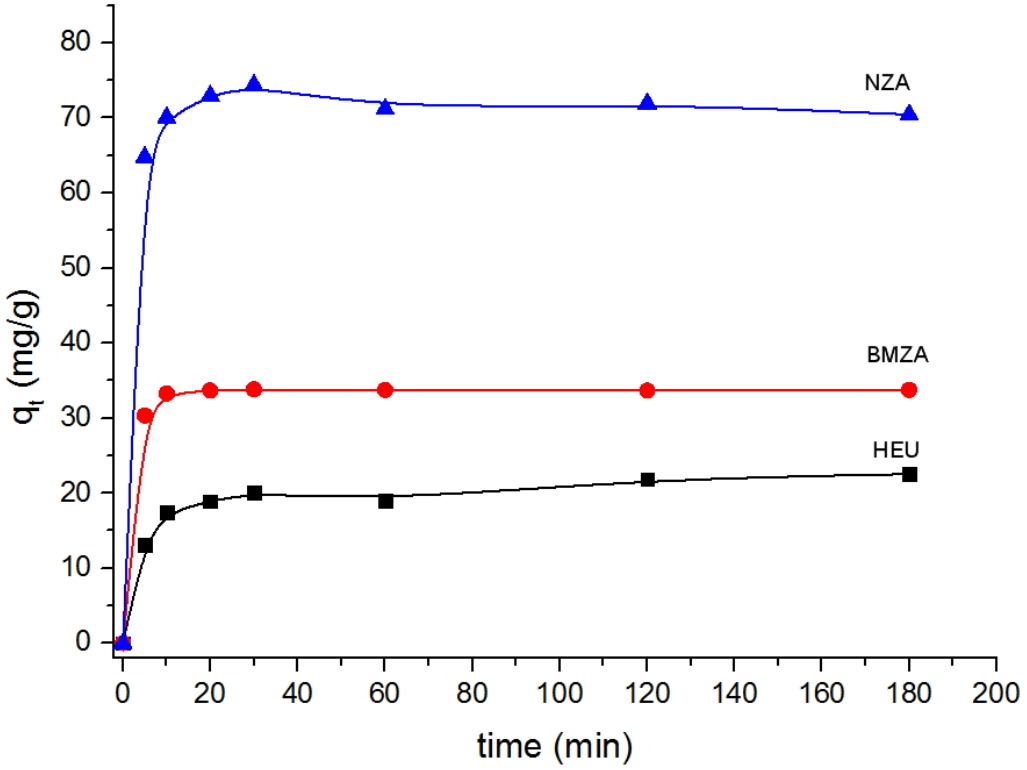

Figure 9.17: Sorption of copper ions using pure zeolites NZA, BMZA and HEU; 400 mg l^{-1}, initial pH 4 and 0.1 g of sorbent

9.3.2.1.1 Pseudo First and Second Order Models Kinetic models for pure zeolites showed a better agreement with Second Order model (PSO) than for First Order model (PFO) as Figure 9.18 shows. Also, a pronounced two-line behaviour

before and after 20 minutes was observed.

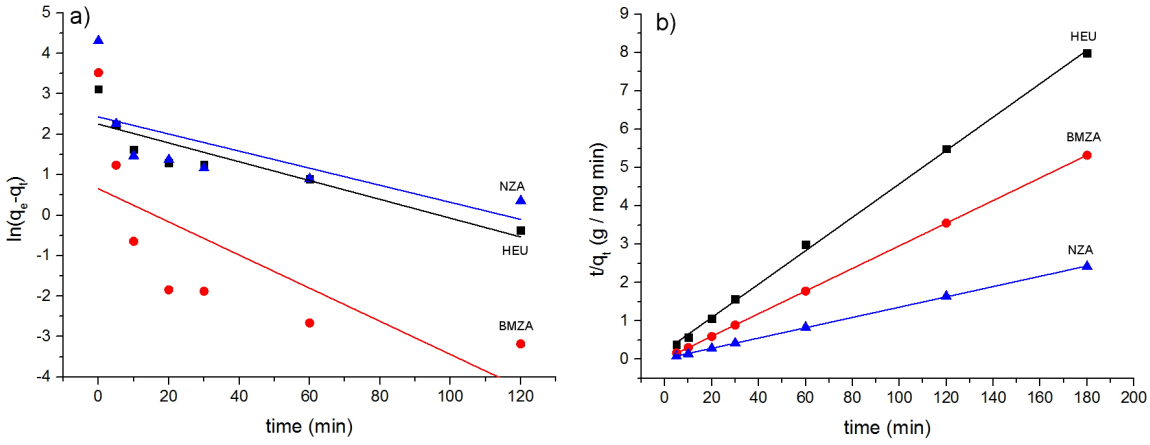

Figure 9.18: First and Second Order models for pure zeolites in the Sorption of copper ions using pure zeolites NZA, BMZA and HEU

The PSO model showed good fit, $R^2 > 0.999$, for all the range under which the experiment was carried out as Figure 9.18 b) shows. The slope of the trend lines for different materials are related to different sorption capacities. These results are in agreement with those presented in previous chapter removing cobalt ions, in which the kinetic process using pure zeolites is well-represented by PSO model. Previous research [233] has indicated that adsorptive processes following Pseudo First Order equation, their adsorption rate is directly related to the concentration of ions in solution, and if the model fits the Pseudo Second Order equation then the rate is directly proportional to solid capacity involving interactions between sorbate and sorbent valence forces. Kinetic parameters are presented in Table 9.2. According to rate constant values, BMZA performs slightly "faster", 0.1101 min^{-1}, than NZA, 0.108 min^{-1}, but the latter has the highest capacity under the described conditions.

9.3.2.1.2 Weber-Morris Model According to Weber-Morris results presented in Figure 9.19 a combination of film and intraparticle diffusion resistances are taking place at similar times. For HEU, results suggest that only intraparticle diffusion occurs without film diffusion being observed.

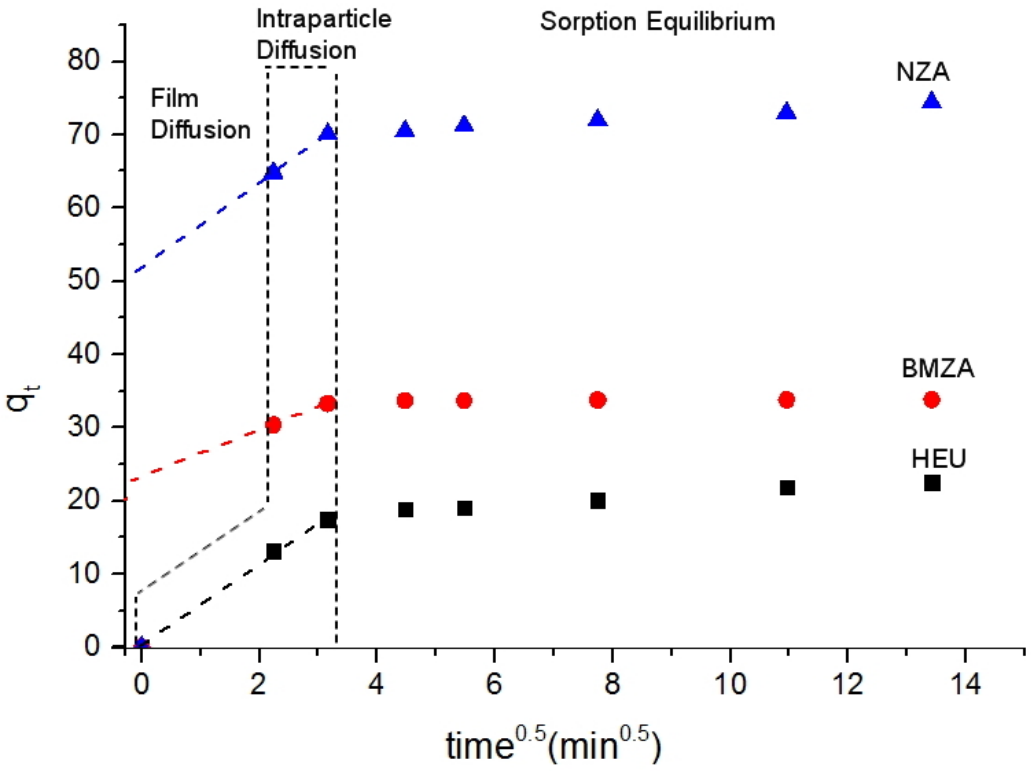

Figure 9.19: Weber-Morris Model for pure zeolites in the sorption of copper ions using pure zeolites NZA, BMZA and HEU.

It is possible to observe multi-linear segments for all zeolites indicating a contribution of different diffusive resistances. Intraparticle diffusion for all materials can be observed inside the dotted area. The linear plots interception is related to the diffusion layer thickness [60]. Thus, since the line for HEU crosses near the origin, it can be said that only intraparticle diffusion is the only resistance before the equilibrium stage [60]. In contrast, in BMZA and NZA the process seems to be jointly controlled by intraparticle and film diffusion. The corresponding coefficients indicate that intraparticle diffusion is more relevant in NZA, 5.691 mg g^{-1} min$^{-0.5}$, than in BMZA 3.158 mg g^{-1} min$^{-0.5}$.

9.3.2.2 Removal of Cu^{2+} ions with BMZA composites

It was believed that pure carbons, conditioned with PDDA, will have a very low capacity to adsorb copper cations. The sorption results in Figure 9.20 confirm this being able to uptake up to 4 mg g^{-}1. In Figure 9.20 the performance of BMZA hierarchi-

cal composites is compared. An enhanced copper sorption can be observed after the balance given by Equation 8.2, that quantifies the contribution in the adsorption by carbon and zeolite in the composite. The supported zeolite supported on CS and HN, i.e. BMZA*/CS, 69.3 mg g^{-1} and BMZA* / HN, 57.85 mg g^{-1} if compared with 33.53 mg g^{-1} as pure BMZA showed.

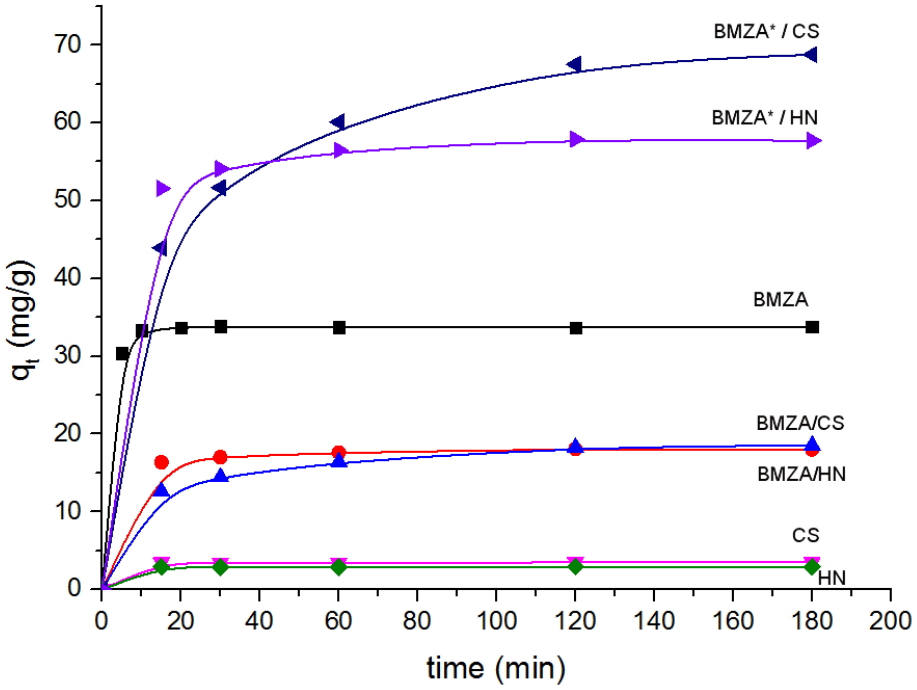

Figure 9.20: Sorption of BMZA composites and theoretical sorption uptake of BMZA on composites

9.3.2.2.1 Pseudo First and Second Order Models Results in Figure 9.21 shows that BMZA composites removing copper ions follow more accurately PSO than PFO.

These results are in agreement with pure zeolite A (BMZA) where trend lines are similar. The fitting to the model can be associated again, to the influence of the ion exchange interactions at the active zeolite sites. All R^2 coefficients are > 0.999 for PSO model as can be seen in Table 9.2.

9.3.2.2.2 Weber-Morris Model Film diffusion is taking place at the initial stage for both BMZA composites, and after 15 min, intraparticle diffusion is controlling the

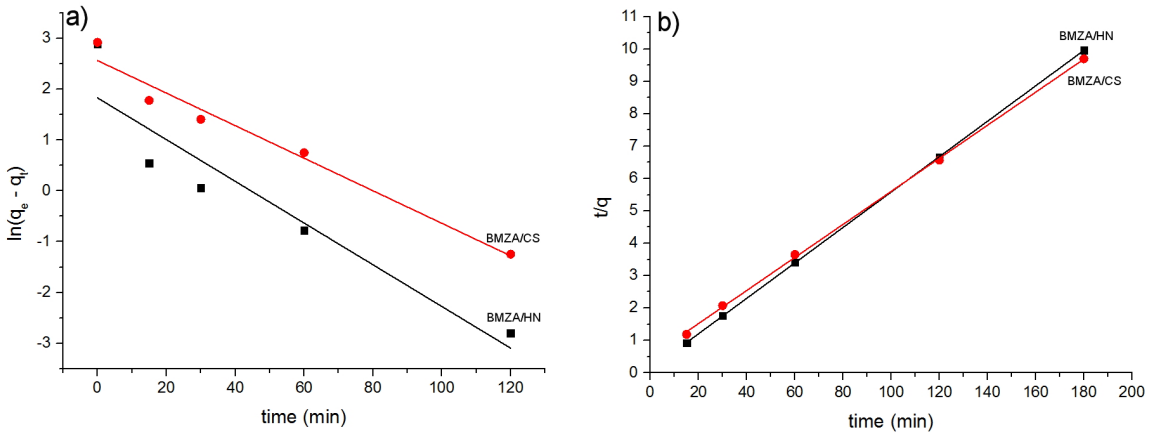

Figure 9.21: Kinetic models for BMZA composites a) PFO model and b) PSO model

process as Figure 9.22 shows.

From the Weber-Morris model results for BMZA composites three diffusive mechanisms (film, intraparticle diffusion and soprtion equilibrium) are clearly observed. These consecutive stages simultaneously occurred in both composites. The first stage, film diffusion, occurred during the first 15 minutes. After this interval, intraparticle diffusion occurred up to 120 minutes, being the slower process and controlling the overall process. After this time equilibrium plateau was reached. Since the two slopes are different it is inferred that film diffusion thickness is larger in BMZA/HN than BMZA/CS. This can be related to the different morphology of the support as the amount of zeolite in both composites is similar. The coefficients can be seen in Table 9.2. For both materials, the amount of zeoilte is very similar, thus, the diffusive characteristics are being influenced by the support. HN shows a reduced intraparticle diffusion if compared to CS, in which intraprticle diffusion contibutes most. When both materials were used equilibrium was achieved at similar time periods.

9.3.2.3 Removal of Cu^{2+} ions with NZA Composites

Figure 9.23 shows the obtained results for the uptake of copper ions by NZA composites. Adsorption results balancing the contributions of zeolite and carbons present in composite showed that NZA* supported over CS had the highest copper removal ca-

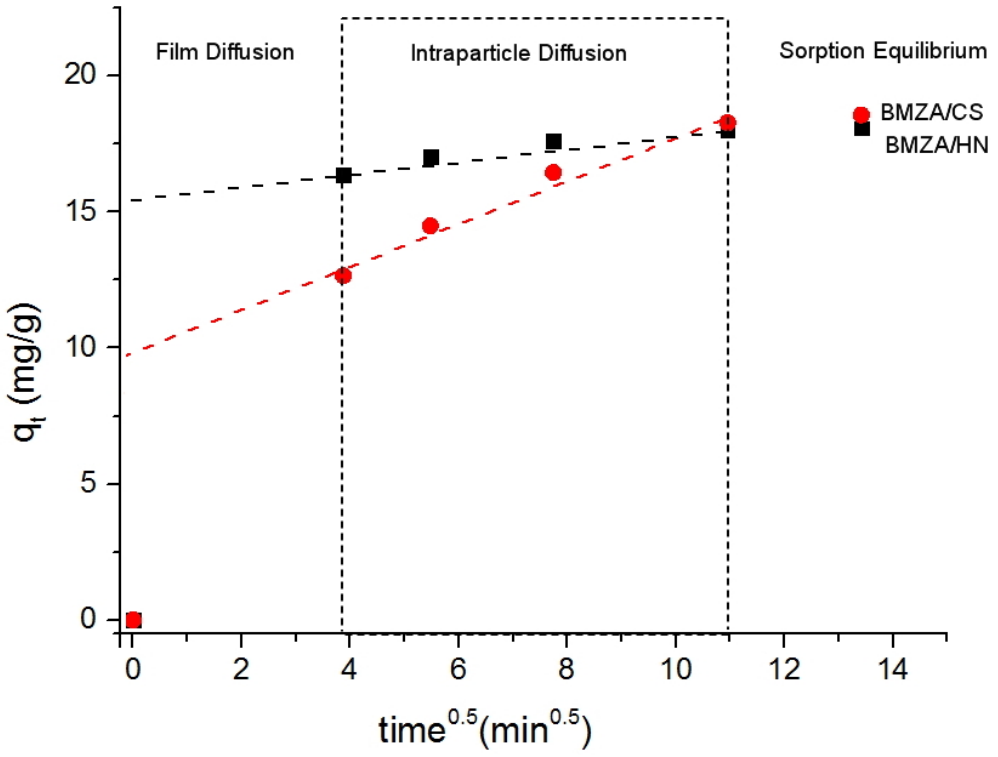

Figure 9.22: Weber Morris model for BMZA composites

pacity, 182.4 mg g^{-1}, and NZA* over HN showed 123.2 mg g^{-1}. Nevertheless, NZA/CS seems to be faster than in NZA/HN. This result has a direct relation with k_2 values. These results show a direct relationship between amount of zeolite in composite and experimental q_e values. For NZA a faster process is observed, after 30 minutes uptake does not change significantly achieving 74.4 mg g^{-1}. One of the most significant aspects is that the volume of vitrified waste can be reduced by approx 50 % based on the amount of zeolite present in composite.

9.3.2.3.1 Pseudo First and Second Order Models The results based on kinetic models indicated that both NZA composites fit better the Pseudo Second Order (PSO) equation than First Order (PFO) because R^2 coefficients are closer to 1. The graphical analysis is presented in Figure 9.24.

All q_e calculated values using PSO equation have much better agreement with experimental data suggesting that rate-limiting step could be chemisorption including exchange of charged particles between adsorbate and adsorbent as high linearity is

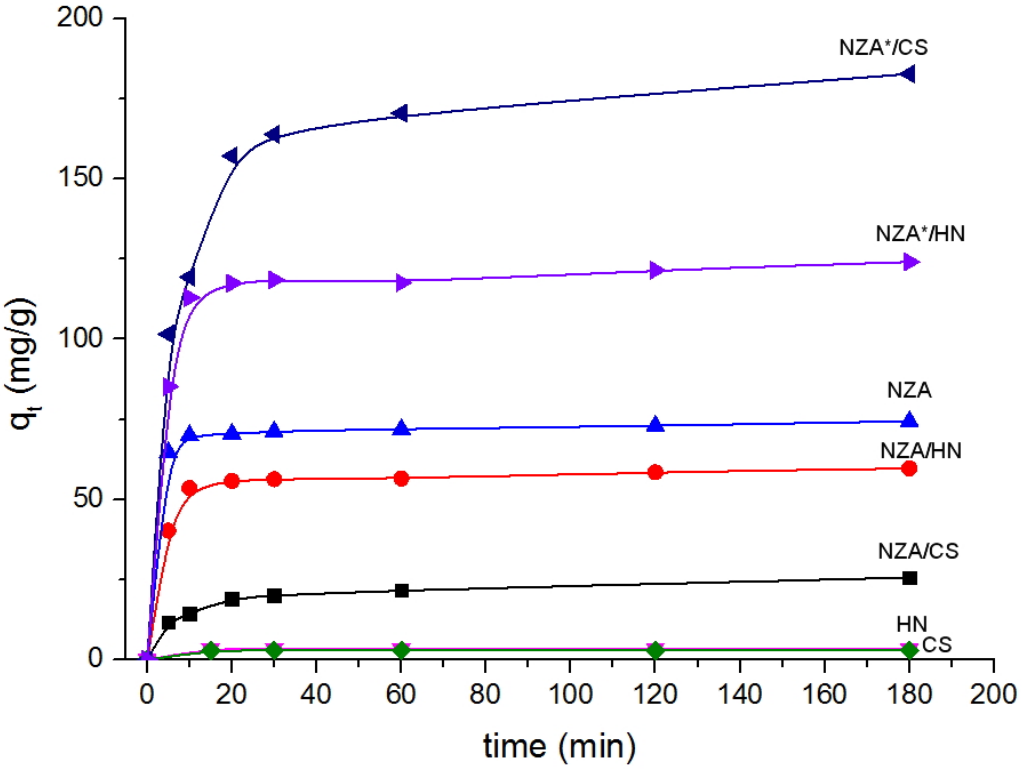

Figure 9.23: Sorption of Cu^{2+} using NZA composites and theoretical sorption uptake of NZA* on composites

presented in Figure 9.24 b). These findings are consistent with those of Ho *et al.* [232] who found that heavy metals usually have stronger correlation with the second order than with the first order equation. Rate k values, experimental and predicted uptake values are presented on Table 9.2. The main assumption for Pseudo Second Order suggests that chemical adsorption is the rate-limiting step and, adsorption is dependant on adsorptive solid capacity in the form of the available fraction of active sites [232].

9.3.2.3.2 Weber-Morris Model Figure 9.25 presents the Weber-Morris model to identify intraparticle diffusion characteristics of NZA composites. Three linear segments can be clearly observed, corresponding to film diffusion, intraparticle diffusion and sorption equilibrium respectively.

From these results it can be inferred that NZA/CS has a larger film diffusion influence than NZA/HN where this occurs faster. Also, NZA /CS has a larger intraparticle diffusion contribution that lasts longer. According to these results, the greater amount

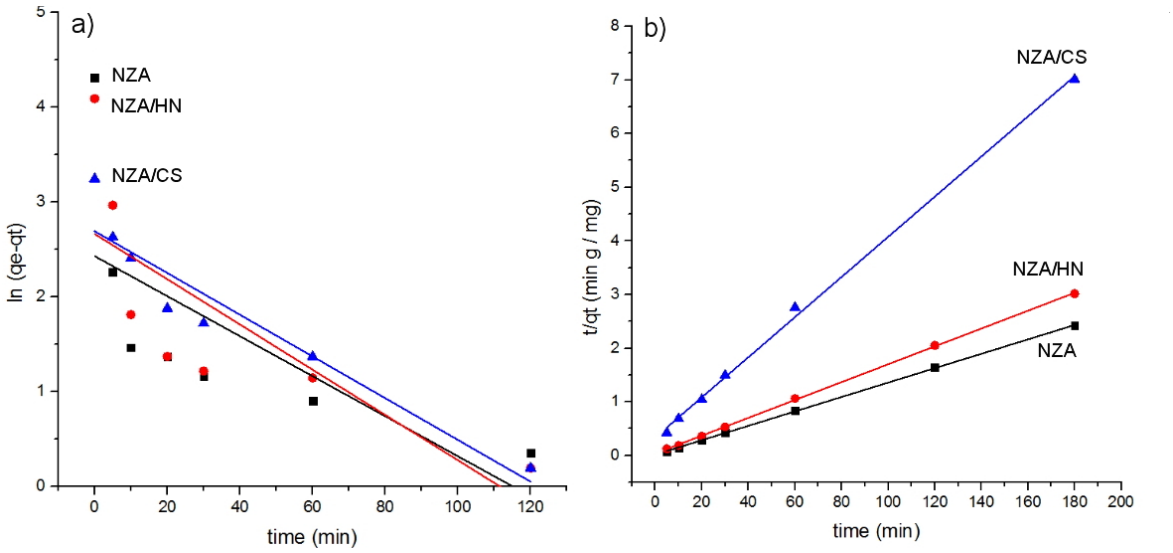

Figure 9.24: a) Pseudo First Order Model and b) Pseudo Second Order Model for NZA composites

of NZA in the material is related to the smaller diffusive resistance and also, the state of equilibrium can be early achieved. k_{id} coefficients and C intercepts values can be observed in Table 9.2. Considering that adsorption capacity is directly related to the amount of zeolite, the diffusive behaviour is being influenced by these two and also, the kind of support. When HN is used, intraprticle diffusion is faster and equilibrium state was early achieved than when CS was used as support.

9.3.2.4 Removal of Cu^{2+} ions with HEU Composites

Sorption carried out by HEU composites, it takes up 1 h to reach the equilibrium plateau removing up to 22.5 mg g^{-1} as Figure 9.26 shows. Consequently each set of composites exhibit similar behaviour with lower uptakes due to different zeolite loadings. Compared to BMZA and NZA, possibly the smaller particle size and thus external surface area of both zeolites have an effect on final copper uptake. Also the presence of different ions can affect final equilibrium. The theoretical adsorption, after taking in account carbon uptake, is described. For HEU-composites, in Figure 9.26 a), final uptake values seem to favour HEU*/CS, 60 mg g^{-1}, but a sharp increase when in the plot makes HEU*/DS a better adsorbent in terms of adsorption rate, this result

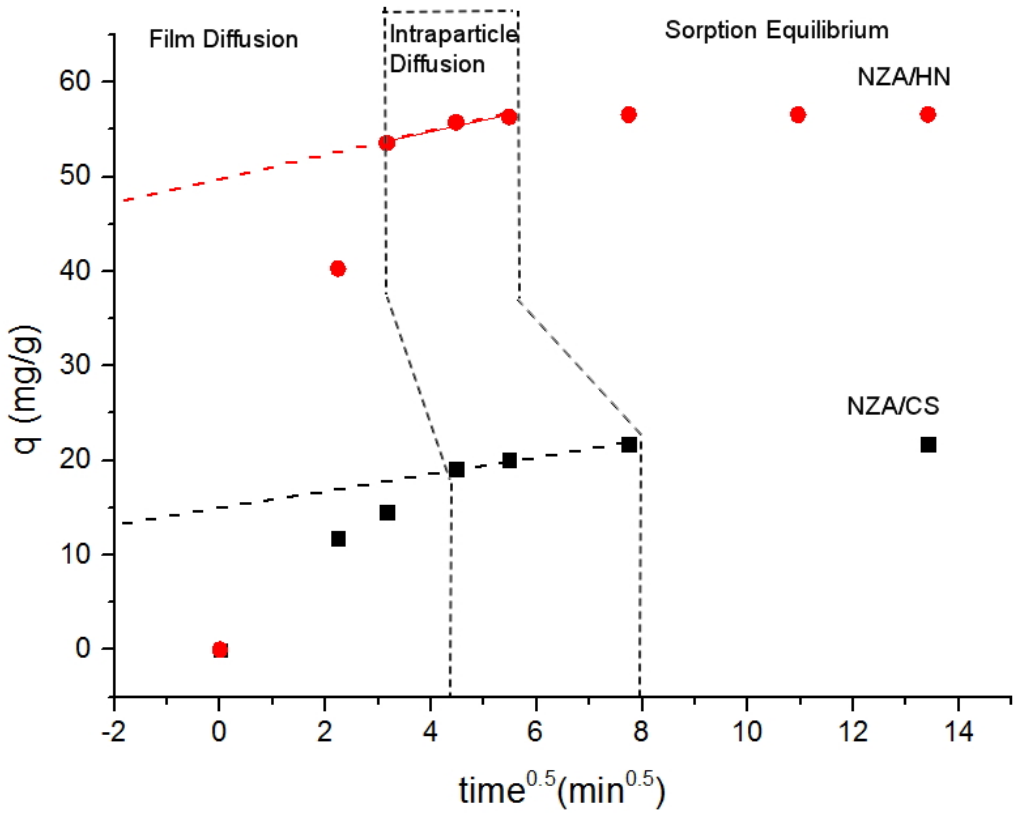

Figure 9.25: Weber-Morris model for NZA composites. Area inside dotted lines represent intraprticle diffusion

agrees with k_2 rate in which DS has higher value than CS.

9.3.2.4.1 Pseudo First and Second Order Models Pseudo First Order and Pseudo Second Order kinetics models are presented in Figure 9.27. Correlation coefficients revealed a better agreement to PSO model ($R^2 > 0.999$) as trend lines show.

Noticeably, HEU/HN has the highest k_2 coefficient, 0.0133 g mg^{-1} min^{-1}, even higher than using pure HEU, 0.0087 g mg^{-1} min^{-1}, possibly attributed to an improved access to zeolite particles for copper ions.

9.3.2.4.2 Weber-Morris Model Intraparticle diffusion model results for HEU composites are shown in Figure 9.28. Film diffusion occurred faster for HEU/HN than HEU/CS. Similarly to previous results, film and intraparticle diffusion resistances are jointly controlling the sorptive process using both materials.

In this case intraparticle diffusion takes place at longer intervals when compared to

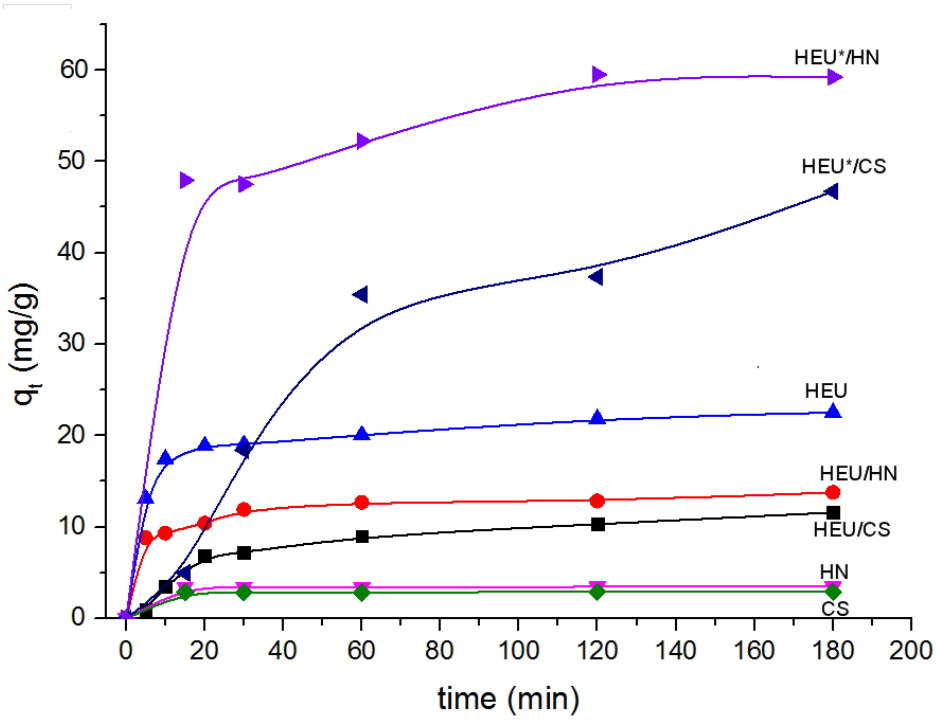

Figure 9.26: Sorption of HEU composites and theoretical sorption uptake of HEU on composites

other NZA and BMZA composites agreeing with pure HEU results where film diffusion was not observed. Consistent with previous results which indicated that HN support provides enhanced diffusive features (since intraparticle diffusion is reduced and equilibrium can be rapidly achieved) HEU supported on HN shows a reduced intraparticle diffusion contribution to the adsorptive process. Interestingly, in the three different types of composites presented in this chapter, NZA composites had a shorter intraparticle diffusion resistance when compared to BMZA and HEU composites, as can be seen in corresponding graphs. These reduced resistances using NZA can be directly related to the smaller particle size of NZA and consequently to a higher active surface area value. Also, NZA has a larger capacity and also is able to remove larger amounts of copper.

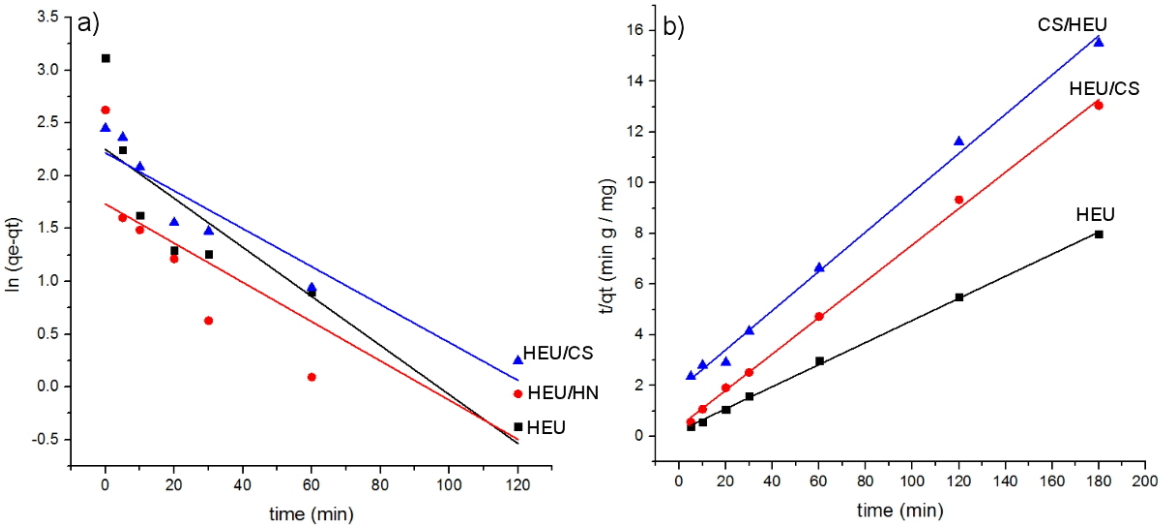

Figure 9.27: Kinetic models for HEU composites

Table 9.1: Kinetic parameters of zeolite/carbon composites in the sorption of copper ions

	HEU	HEU/HN	HEU/CS	NZA	NZA/HN	NZA/CS	BMZA	BMZA/HN	BMZA/CS
Zeolite %wt.	100	18.4	15.0	100	47.2	11.6	100	26.78	23. 74
$q_{e,exp}$ (mg g^{-1})	22.5	13.8	11.6	74.4	59.7	25.6	33.53	17.86	18.43
Pseudo First Order									
$q_{e,calc}$ / (mg g^{-1})	9.5	5.6	9.1	11.3	14.3	16.2	1.92	6.21	12.96
k_1/(min^{-1})	0.0232	0.0186	0.018	0.0211	0.0239	0.0279	0.041	0.041	0.032
R^2	0.8216	0.7032	0.9167	0.4821	0.6102	0.8035	0.5321	0.8452	0.9616
Pseudo Second Order									
$q_{e,calc}$ (mg g^{-1})	22.9	13.9	12.8	74.6	60.2	28.8	33.89	18.27	19.58
k_2 / (g mg^{-1} min^{-1})	0.0087	0.0133	0.0032	0.0108	0.0075	0.0035	0.1101	0.026	0.0052
R^2	0.9991	0.9984	0.9956	0.9998	0.9998	0.9984	0.9999	0.9999	0.9994
Weber-Morris									
k_{id} (mg g^{-1} $min^{-0.5}$)	5.586	0.5559	0.7494	5.691	0.942	1.209	3.158	0.2277	0.7825
C	0.1376	7.7187	4.3803	52.08	14.902	49.92	23.31	15.69	9.9696
R^2	1	0.9645	0.9343	1	1	0.9765	1	0.9014	0.9665

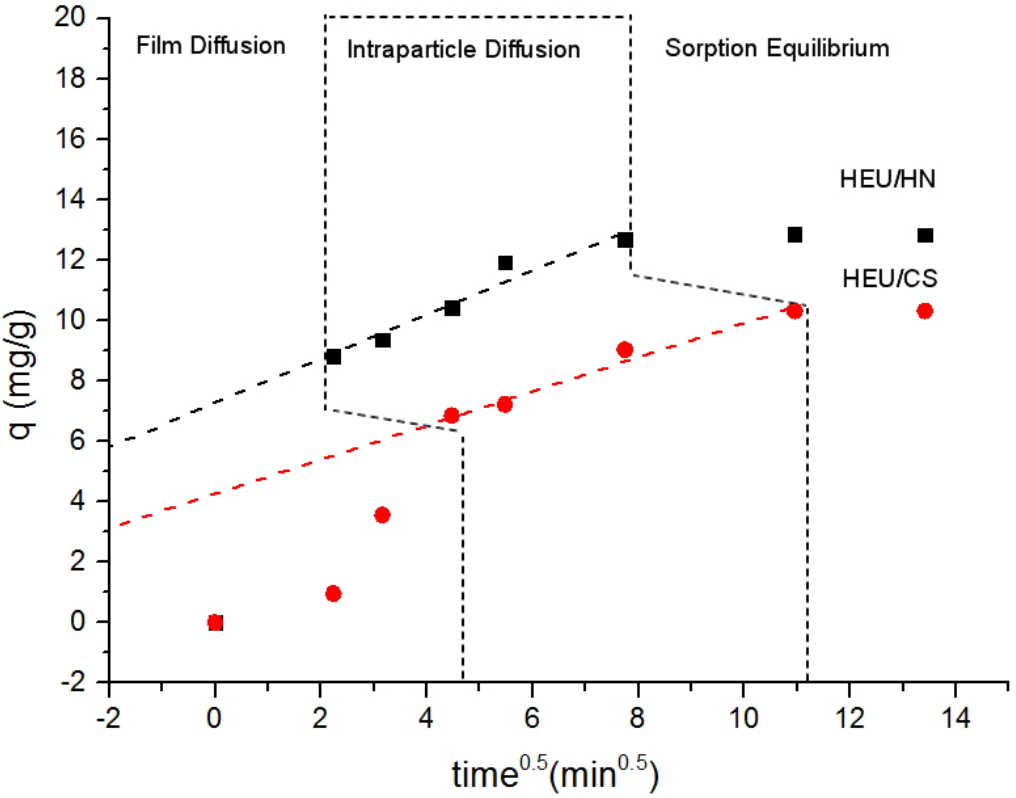

Figure 9.28: Weber-Morris model for HEU composites. Area inside dotted line represent intraparticle diffusion segment

Table 9.2: Calculated parameters for Langmuir and Freundlich isotherms

Material	Langmuir			Freundlich		
	Q_m mg g^{-1}	b L mg^{-1}	R^2	K_f (mg g^{-1})(mg L^{-1})^n	b_F	R^2
HEU	61.08	0.0091	0.9901	1.00008	0.68	0.9611
HEU/HN	21.57	0.0092	0.9627	1.1765	0.45	0.9861
HEU/CS	22.68	0.0300	0.7910	1.4001	0.2	0.8765
NZA	139.56	0.0051	0.9846	3.904	0.5385	0.9963
NZA/ HN	27.57	0.1036	0.9814	9.002	0.1965	0.7820
NZA/CS	37.87	0.0366	0.9352	6.751	0.2940	0.7937

9.3.3 Adsorption Equilibrium

The adsorption isotherms for the copper ions adsorption at specified conditions using HEU and HEU composites are presented in Figure 9.29. Similarly, in Figure 9.30 isotherms and both models for NZA and NZA composites are presented. Langmuir and Freundlich models can represent the process for HEU composites, and Langmuir model adjust better for NZA composites relating this to the formation of a monolayer of adsorbed cations. According to Langmuir model, the maximum capacity is 61.06 mg g^{-1} and 139.56 mg g^{-1} for HEU and NZA respectively. This result is in agreement with previous kinetic results where particle size and zeolite type suggested to be responsible for these differences. For each set of analysed materials, the constant b is higher for systems involving composites, relating this with a higher affinity of cations for supported zeolitic materials. The b_F parameters obtained from Freundlich model suggest that pure zeolites HEU and NZA have more heterogeneous adsorptive sites than composites due to its higher b_F values. The thermodynamic parameters and correlation coefficients are summarised in Table 9.2.

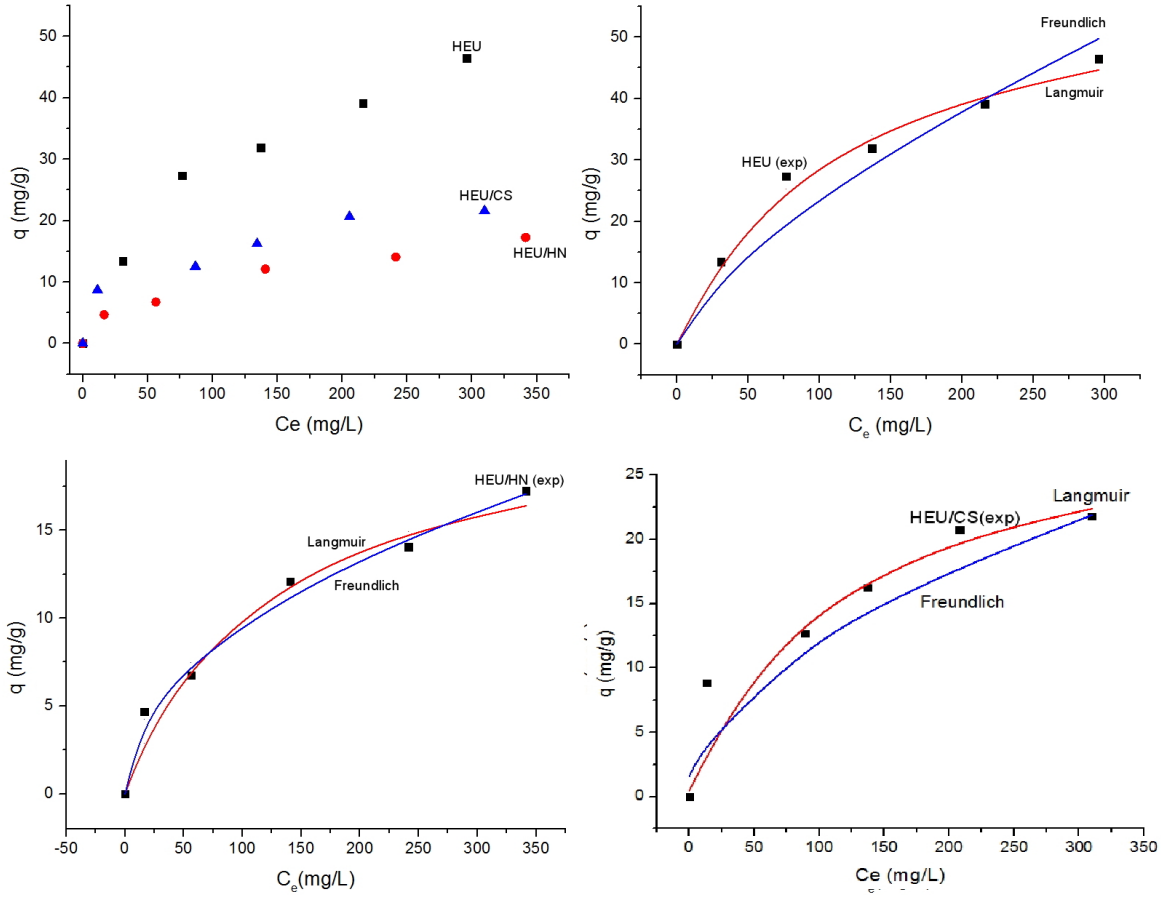

Figure 9.29: Isotherms for HEU and HEU composites with the corresponding Langmuir and Freundlich fitting

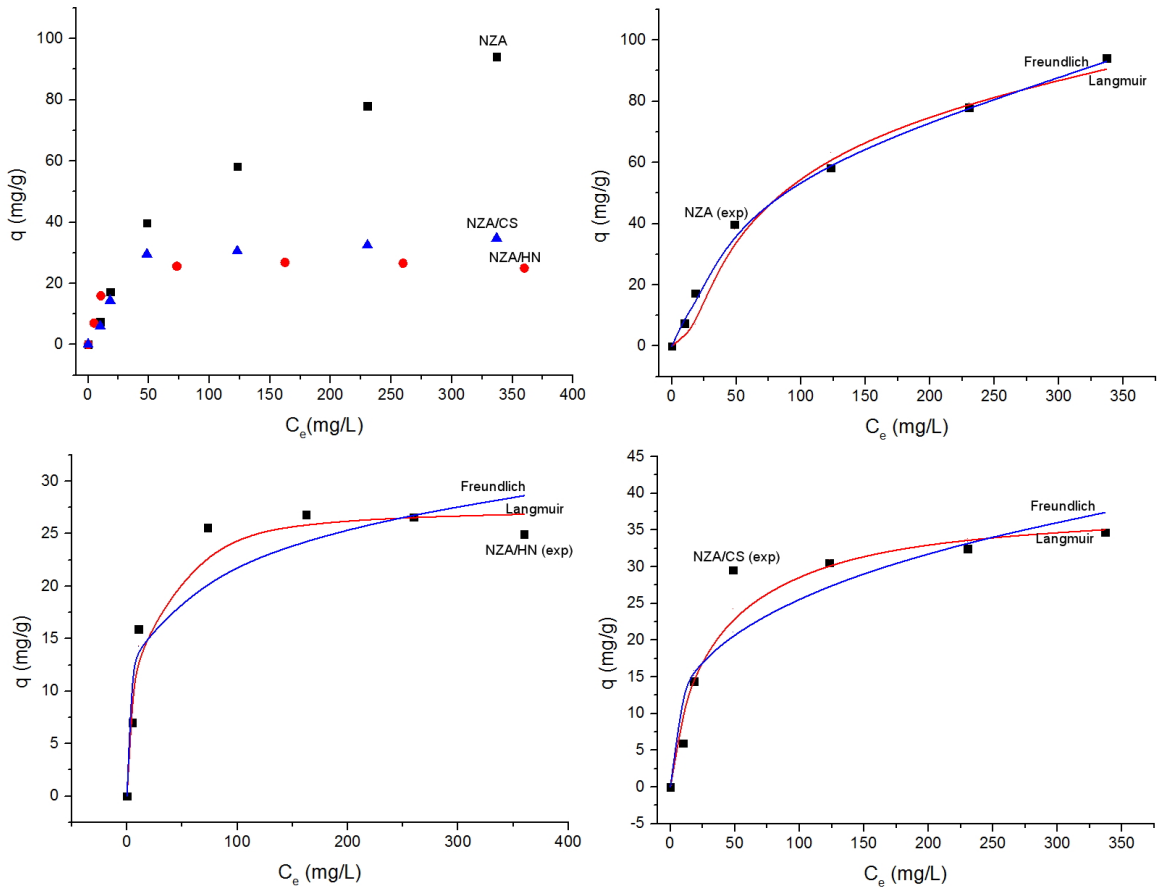

Figure 9.30: Isotherms for NZA and NZA composites with the corresponding Langmuir and Freundlich fitting

9.4 Conclusions

In this chapter was showed the feasibility to convert two different agroindustrial wastes, such hazelnut shell and cherry stone, into adequate and effective scaffolding systems useful in the preparation of zeolitic hierarchical composites. This was achieved using synthetic zeolites BMZA and NZA along with natural clinoptilolite. The ball milling method for the BMZA composites preparation showed an easy and effective way to produce hierarchical materials. Also, natural zeolite represents an effective and cheaper option although has less capacity than synthetic materials for copper removal as results showed.

According to the results presented here, carbon pretreatment using PDDA is the main factor responsible for zeolite coating; further, PDDA concentration has not a significant effect on zeolite load in final materials, SEM results proved the successful extrapolation of the method for two synthetic and one natural zeolites over different carbons from agroindustrial wastes. The amount of zeolite present in composite is not dependant on PDDA concentration as results suggest. This result can be connected more to other carbon characteristics such as surface area, or different functional groups on surface.

Kinetic experiments showed that equilibrium was reached at different time intervals under described conditions. All tested materials are better represented by the Pseudo Second Order model. Previous research has indicated that for adsorptive processes following Pseudo First Order equation, the adsorption rate is directly related to the concentration of ions in solution, and if the model fits the Pseudo Second Order equation then the rate is directly proportional to solid capacity involving interactions between sorbate and sorbent valence forces. The uptake was more favourable using pure zeolites (74.4 mg g^{-1} for NZA, 33.5 mg g^{-1} for BMZA and 22.5 mg g^{-1} for HEU) than composites, however, the best performance under these conditions is attributed to the zeolites present in composite as shown (60 mg g^{-1} for HEU*, 69.3 mg g^{-1} for BMZA*and a remarkable 182.4 mg g^{-1} for *NZA).

Weber Morris results showed that in the removal of copper ions from water, film and intraparticle diffusion are taking place as contribution of combined resistances when NZA and BMZA composites were used, meanwhile only intraparticle diffusion is the rate-controlling step in the sorptive process using HEU composites according to the presented results. The analysed phenomena showed that from two carbonaceous supports used in this part, CS and HN, the latter showed better properties reducing the restrictive diffusion before equilibrium state is achieved in all zeolite composites under described conditions. Finally, it was shown that the nanosized material presented a reduced intraparticle resistance in the process. From all materials studied in this chapter, NZA composites, besides having more capacity, reached before the equilibrium state than BMZA and HEU composites. This can be directly associated to the particle size and reduced diffusion path of NZA compared to other zeolites. The combination of NZA supported on HN presented the best results in terms of capacity and also diffusive characteristics.

For these materials, both models can correlate the experimental data in difference with previous chapter where Freundlich model adjusted better than Langmuir. These diferences can be related to the type of interactions between sorbate and sorbent (since it is a different dissolved metal), the zeolite type and different carbonaceous support.

Chapter 10

Removal of Caesium Ions using Supported Clinoptilolite over Date Stone Carbons. The Effect of Solution pH and Sorbent Dosage

10.1 Introduction

This last chapter describes how natural clinoptilolite particles (HEU) were supported on carbonaceous supports made of date stone (DS). The materials preparation is based upon the chemical modification of the scaffolds surface by the use of polycations providing positive electrical potential suitable for zeolite fixation as previously described. These supports will provide micro-architecture and auxiliary porosity adequate for zeolite deposition. The evaluation of the prepared materials in the sorption of non-radioactive Cs^+ ions from aqueous solutions was carried out: the effect of pH was investigated. Finally, kinetic soprtion data was analysed using kinetic models as in previous chapters and the intraparticle diffusion mechanism was investigated by using the Weber-Morris.

10.2 Methodology

10.2.1 Preparation of Hierarchical Zeolite Composites

Natural clinoptilolite (HEU) used here was previously described in Section 7.2.4.1 (p. 119). Carbonaceous supports were produced using date stone (DS). Carbon precursors were cut, washed with deionised water and dried at 70°C for 12 h and then, stones were heated in tubular furnace under a nitrogen atmosphere and subject to a thermal treatment (200°C, 600°C and 900 °C) for 2 h in each step at a ramp rate of 5 °C min^{-1} as described in Section 7.2.5.1 (p. 120).

After the thermal treatment carbon was crushed, sieved and preconditioned as described in Section 7.2.5.2 (p. 121). Finally, the material (HEU/DS) was recovered by filtration and washed with deionised water to remove zeolite that was not attached to the carbon and dried at 70°C overnight.

10.2.2 Characterisation of Prepared Materials

The materials characterisation was carried out using previously described techniques in Section 7.2.6 (p. 122).

10.2.3 Batch Sorption Studies

Caesium removal experiments were carried out dissolving CsCl (Sigma-Aldrich) in water in order to form the different concentration solutions. The initial pH was adjusted using 0.1 M HCl and NaOH. The experiments were carried out at ambient temperature. In a typical run, 100 ml of Cs^+ solution (400 mg l^{-1}, pH 5) were added to 0.5 g of material and stirred in an rocker for different time intervals (5, 10, 20, 30, 60, 120 and 180 min) and then the suspension was separated by filtration. The quantitative analysis to determine caesium concentration was made by ICP-OES (Varian MX). The effect of solution's initial pH (2-10) was conducted in order to find the best conditions. All samples were duplicated and averages are reported. The Cs^+ uptake was quanti-

fied using Equation 8.1 (p. 145). In order to quantify the sorption performance of the zeolite present in the composite, Equation 8.2 (p. 145) was used.

10.3 Results and Discussion

10.3.1 Materials Characterisation

Figure 10.1 shows the XRD patterns corresponding to the natural zeolite phase (HEU) and the composite (HEU/DS).

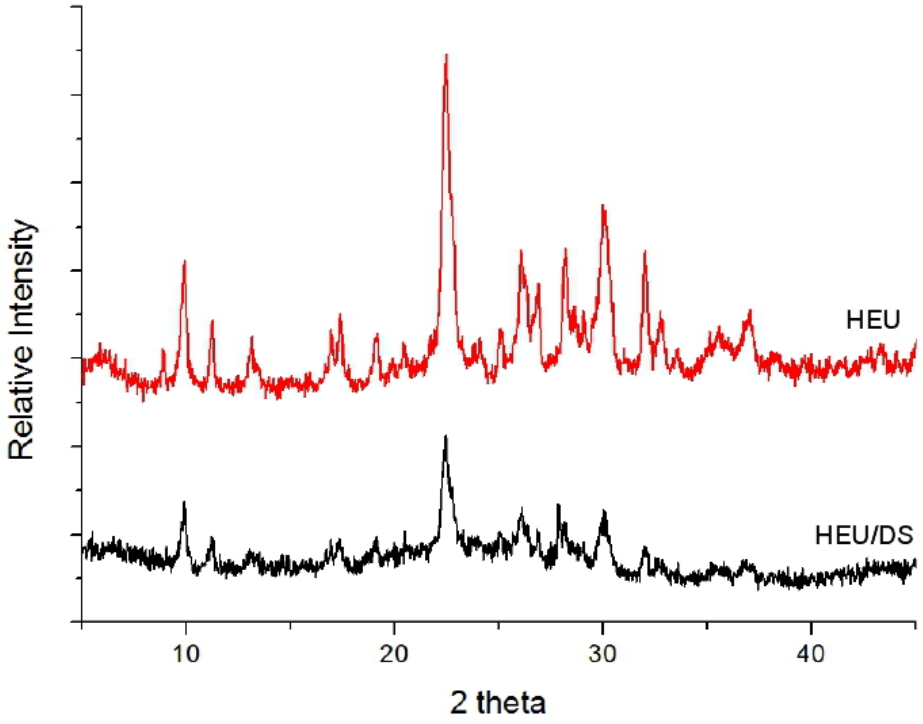

Figure 10.1: XRD patterns of HEU and HEU/DS

Both diffractograms show the characteristic peaks for heulandite framework at 9.86°, 11.17° and 22.34° [274]. For the DS/HEU it confirms the presence of clinoptilolite in the material. For the composite, the reduction of the intensity of the peaks can be explained in terms of the amount of supported zeolite present in material. The characteristic amorphous hump of the carbon can be also observed.

Figure 10.2 shows the SEM images that compare the morphological characteristics of HEU, DS, HEU/DS without any carbon preconditioning and HEU/DS using PDDA

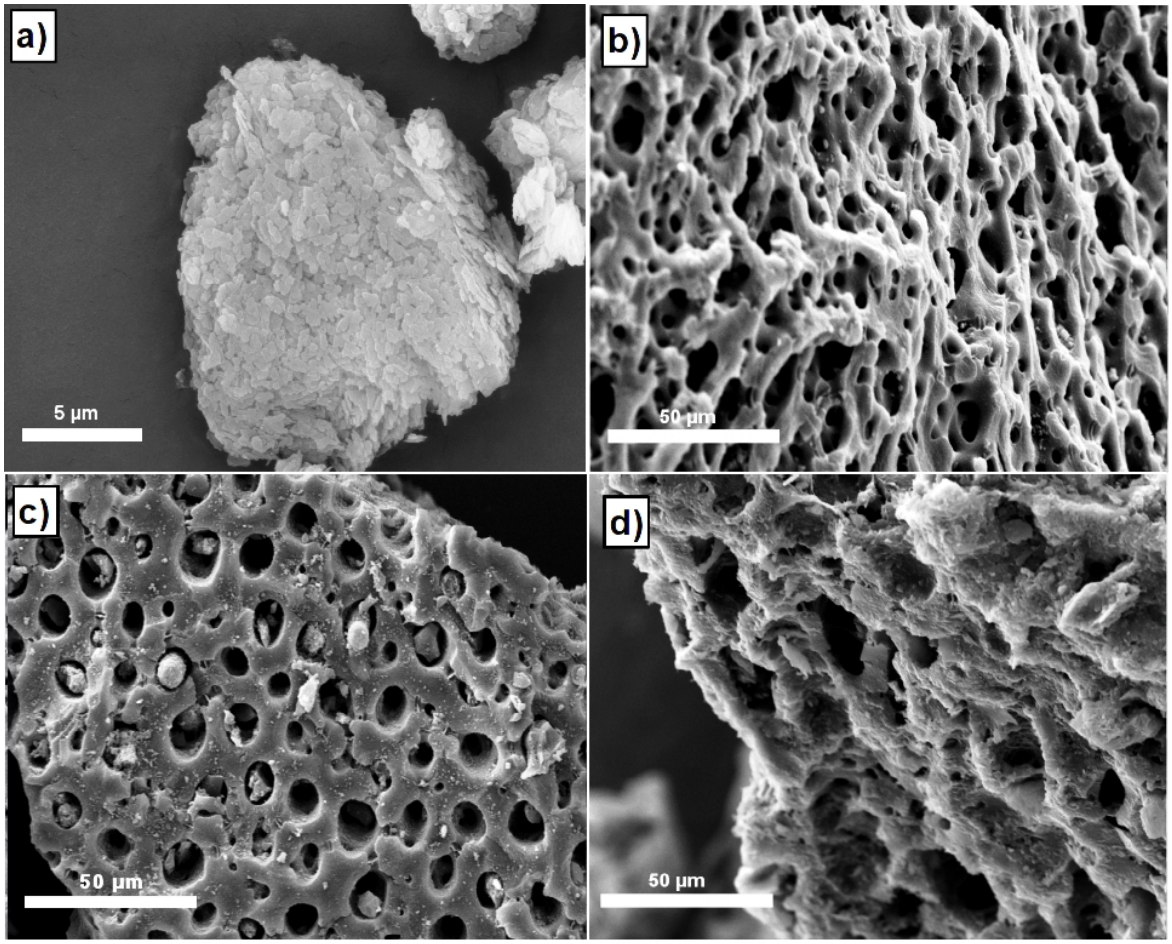

Figure 10.2: SEM images of a) HEU, b) DS carbon after PDDA treatment and c) HEU/DS composite

respectively. Figure 3 a) shows agglomerated pure HEU particles having sizes less than 1 μm with a flake shape. Figure 10.2 b) shows the date stone carbon after the surface treatment with PDDA, exhibiting a rigid honeycomb-like structure with a wide range of opening sizes. Figure 10.2 c) shows few zeolite particles on the carbon surface. However it was not possible to achieve zeolite coating. In Figure 10.2 d) it is possible to observe a complete and even zeolite coating onto the carbon surface with a noticeable spreading over the carbon scaffolding system.

Thermogravimetric analysis was conducted to obtain the zeolite-carbon composition in the final material. Figure 10.3 shows the result illustrating the initial sample losing weight by the action of temperature under the oxidising atmosphere (O_2 atmosphere). The program runs for 160 min the temperature was held at 400°C for 2 h then ramped

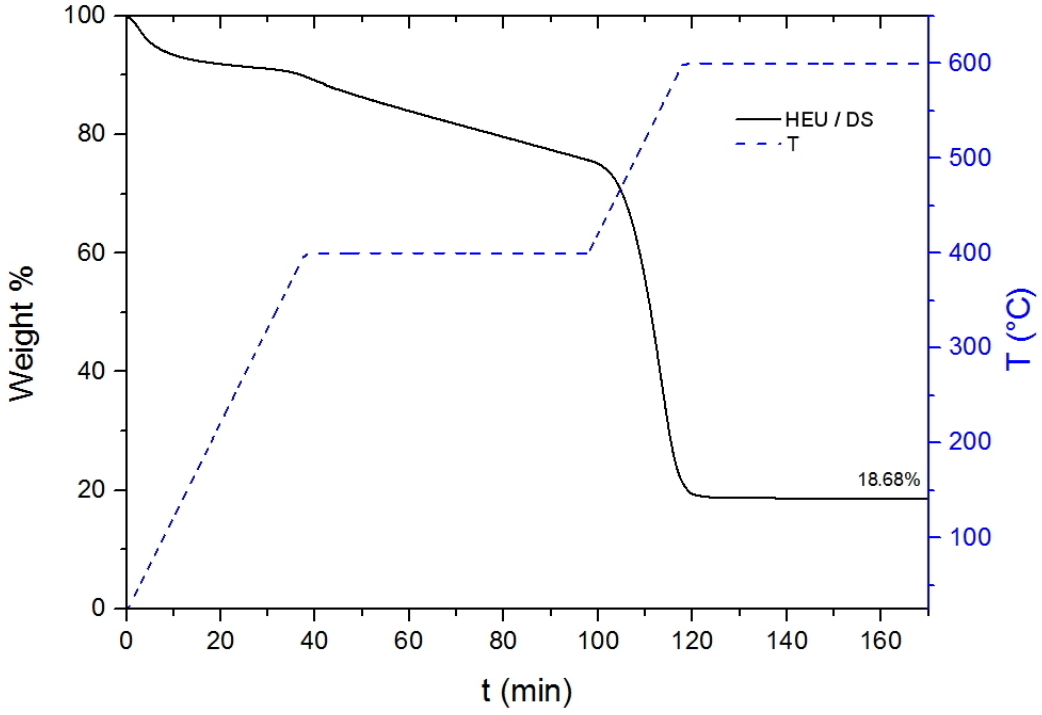

Figure 10.3: Thermogravimetric plot of HEU/DS composite

to 600°C. At ∼ 200°C all moisture is evaporated and over the 400°C the beginning of carbon gasification occurs as all the solid carbon is transformed into gases. At 600°C (up to 2 h) all carbon has been removed and mass of sample remained constant the final weight percentage (the zeolite component) was 18.6%.

10.3.2 Sorption Experiments

10.3.2.1 Effect of pH

The sorption capacity of the materials as a function of pH was investigated. HEU and HEU/DS materials exhibit the same behaviour: an increase of the final equilibrium sorption capacity when pH level increases, as is shown in Figure 10.4. This is due to lower pH levels, having a competition for the sorptive sites involving Cs^+ ions and protons H^+ present in the media [280]. However, previous studies have reported that precipitation of caesium hydroxide can occur at values higher than pH 8 [281]. The change in uptake after pH 8 can be attributed in part to a saturation of zeolite and possibly some precipitation of caesium species.

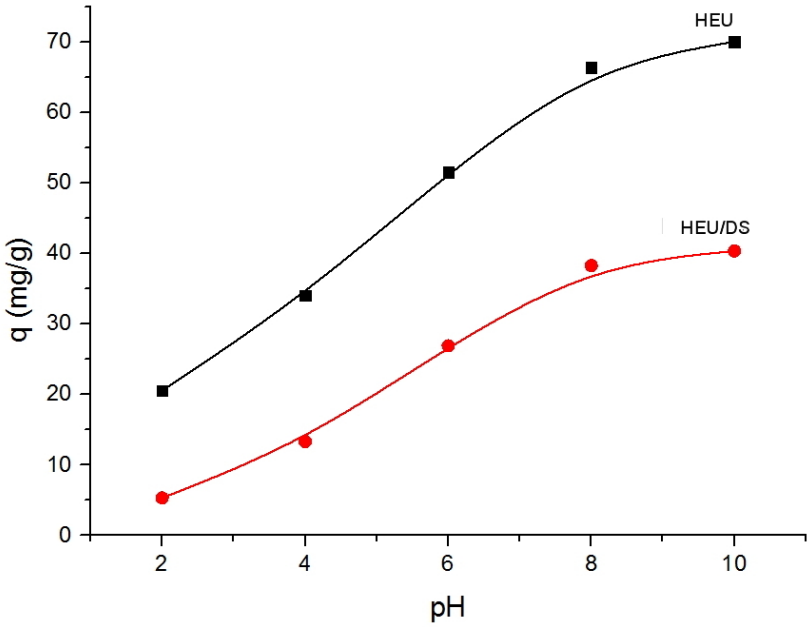

Figure 10.4: Effect of the pH on the sorption capacity of HEU and HEU/DS at room temperature and 400 mg l^{-1}, 0.5 g and 24 h

10.3.2.2 Kinetics

Figure 10.5 presents the kinetic behaviour of the prepared materials on the Cs^+ (400 mg l^{-1}) sorption at room temperature. PDDA-pretreated carbon with no zeolite shows a poor Cs^+ uptake, the graph shows a low Cs^+ uptake of 5.3 mg g^{-1}. HEU reaches equilibrium after 30 min contact with a capacity of 50.6 mg g^{-1}. Meanwhile for HEU/DS, equilibrium was reached after 2 h achieving 27.7 mg g^{-1}. This uptake difference is about 54 %, the amount of zeolitic phase in the composite material is close to 18 %. After the mass balance based on TGA results, the uptake capacity by HEU* (performance of zeolite in composite only) was 120 mg g^{-1}. This result is shown to be a direct consequence of the new arrangement of zeolite particles having more accessible sites for Cs ions to be sorbed. Interestingly, the sorption capacity of HEU* is similar to HEU during the first hour, but then, the uptake of HEU* increased.

A SEM image of the material after the sorption process is shown in Figure 10.6, this image shows that zeolite particles remained attached to carbon surface after sorption caesium ions for 24 h.

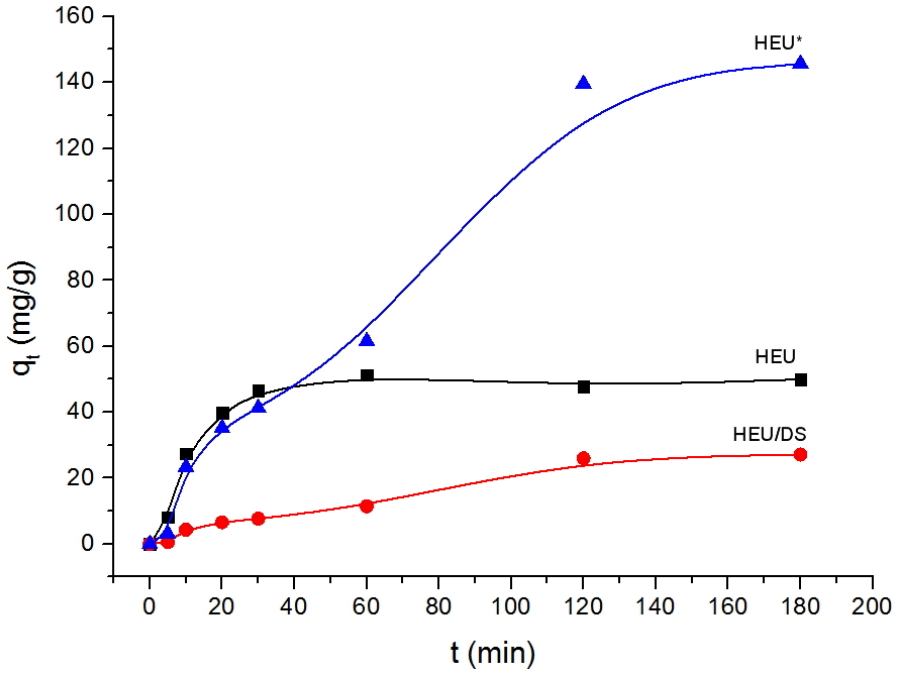

Figure 10.5: Comparison of kinetic behaviour of HEU and HEU/DS

10.3.2.3 Pseudo First Order and Pseudo Second Order Equations

Two different methods, Pseudo First Order (PFO) and Pseudo Second Order (PSO) and equations, were used to study the sorption kinetic features. These models were previously described in Section 10.1 (p. 217).

The Pseudo First Order model did not fit adequately the whole data range for pure HEU ($R^2 = 0.769$), but it did for HEU/DS ($R^2 = 0.9605$) as shown in Figure 10.7 a). However, the adjustment of HEU to PFO by dividing into two linear sections, with a reduction in the sorption rate suggests the possibility of two different uptake resistances, i.e. external mass transfer and internal diffusion. Each linear section for HEU shows a strong correlation with PFO model, $R^2 = 0.991$ and 0.998 respectively. Interestingly, HEU/DS shows an enhanced rate compared to the overall process when using HEU, $0.0252\ min^{-1} > 0.0189\ min^{-1}$, even when the amount of zeolite in composite is less than 20 % wt. This result implies the more efficient use of the active surface area for the removal of caesium. Also, the agreement to PFO model suggests that the equilibrium is dependent upon the initial concentrations [232] at least for HEU/DS. The PFO model predicts closely the q_e experimental value for HEU/DS but it differs

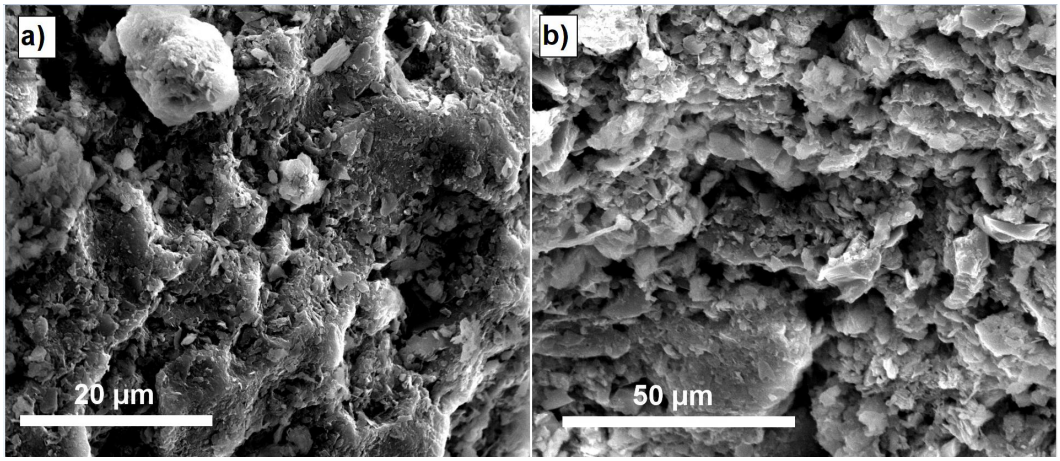

Figure 10.6: HEU/DS composites after ion exchange process at different magnifications.

from value for HEU.

In Figure 10.7 b) the HEU and HEU/DS fit with PSO model are compared. In these plots, the adjustment of the experimental results compared to the model is shown. For HEU, the correlation coefficient was higher than 0.98 and the calculated q_e values closely matched with experimental ones suggesting that chemical interactions are involved in the mechanism when using HEU. Moreover, the sorption performance depends more on the solid capacity in the form of available sites than on the initial concentration as the first order equation proposes [232]. HEU/DS did not show a good agreement with PSO model, confirming that the kinetics are more dependent on solution concentration. Differences in k_2 values can be a consequence of this, where the number of available sites is related to the amount of zeolite present in the material, thus the value of k_2 is smaller in the composite. In Table 10.1 the values for kinetic parameters and experimental uptake q_e values are summarised.

10.3.2.3.1 Weber-Morris Model Kinetic data were also analysed using Weber-Morris model [282]. If the the plot q_t v $t^{1/2}$ is linear and passes through the origin. It is assumed that intraparticle diffusion is the rate controlling-step in the process. Also, the slope of this line corresponds to rate of intraparticle diffusion k_{id} [238]. Figure 10.8 shows the plots correspondent to intraparticle Weber-Morris model.

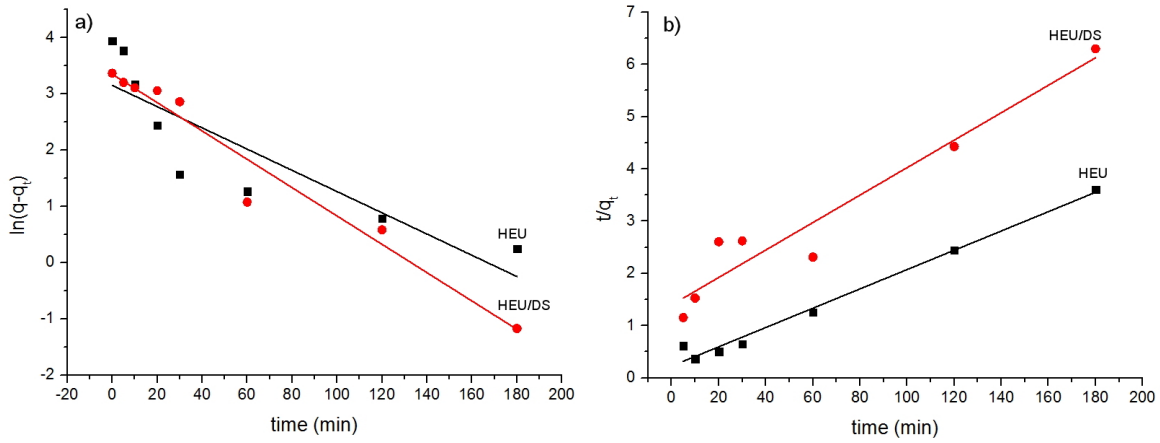

Figure 10.7: a) Pseudo First Order and b) Pseudo Second Order models for HEU and HEU/DS. Dotted line represents the model.

For HEU, two sections are observed in which the plot is divided after 30 min. Some authors have found similar multilinear behaviour [283, 284] suggesting the influence of other mechanisms in addition to intraparticle diffusion, i.e. film diffusion. The first linear segment is related to boundary diffusion and the latter is the segment related to the intraparticle diffusion [238]. In contrast, HEU/DS shows a good fit, therefore, it can be assumed that the rate-controlling step is intraparticle diffusion. However the fact the line is not crossing through origin suggests a small contribution from external mass diffusion. The k_{id} values have been obtained from the slope of the curve and for HEU from the last linear segment, values are for HEU 0.4385 mg g^{-1} $min^{-0.5}$ and HEU/DS 2.215 mg g^{-1} $min^{-0.5}$ observing an enhanced overall intraparticle diffusion coefficient possibly due to the new configuration of the zeolite in the composite.

Table 10.1: Kinetic parameters of zeolite/carbon composites in the sorption of caesium ions

Material	Zeolite %wt.	q_{exp}	Pseudo First Order			Pseudo Second Order		
			$q_{e,calc}$	k_1	R^2	$q_{e,calc}$	k_2	R^2
		mg g^{-1}	mg g^{-1}	min^{-1}		mg g^{-1}	g mg^{-1} min^{-1}	
HEU	100	51.23	23.29	0.0189	0.7692	54.05	0.0015	0.9862
HEU/DS	18.6	28.57	28.39	0.0252	0.9605	38.022	0.00049	0.9326

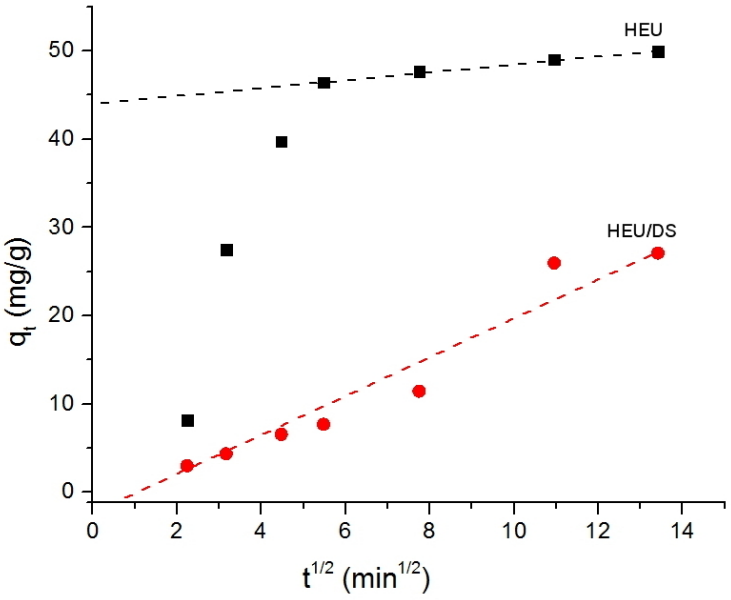

Figure 10.8: Weber-Morris intraparticle diffusion model for HEU and HEU/DS

10.4 Conclusions

The purpose of the current chapter was to determine the sorptive kinetic and diffusive characteristics of caesium ions using carbon-supported clinoptilolite composites. In this chapter has been show the feasibility to produce a hierarchical zeolitic material using an agroindustrial residue such as date stones, and natural clinoptilolite. According to the results presented here, carbon pre-treatment with PDDA is the factor responsible for zeolite coating as shown in previous chapters. SEM results confirmed a uniform and complete zeolite coating of the carbon support. Also it can be observed that zeolite particles remained after ion exchange process.

The effect initial pH was investigated showing an uptake increase at higher levels, pH 8. This study has shown that clinoptilolite can remove 50.6 mg g^{-1} after 30 min in contact with solution and theoretical value of zeolite present in composite reached 120.9 mg g^{-1}, related to an improved distribution of the particles clinoptilolite on composite.

The Pseudo First Order (PFO) equation fitted better for HEU/DS than HEU at all time intervals, but two straight lines suggest two mechanisms. However, the PFO model showed a better adjustment for the composite suggesting that sorption kinetics is more influenced by initial concentrations than by the solid sorptive capacity. Also, the

uptake q_e calculated values were better predicted for HEU/DS than for HEU. A larger first order rate k_1 value for HEU/DS implies an enhanced rate. On the other hand, the Pseudo Second Order (PSO) equation shows a better adjustment with HEU, and is closer to the predicted uptake q_e value suggesting a process influenced by chemical reactions and exchangeable sites on the solid.

According to diffusion results, different mechanisms can occur when using either HEU or HEU/DS, confirming kinetic results. For HEU it seems that film diffusion along with intraparticle diffusion play an important role in the sorption when the Weber-Morris model was applied. Meanwhile for HEU/DS only intraparticle diffusion seems to be rate-controlling step. Also, the diffusion coefficient was higher for HEU/DS.

Finally, it was shown the feasibility to prepare a composite that can potentially reduce the volume of final adsorbent along with adsorbed toxic materials. The most common practice to dispose radioactive materials is in underground repositories after vitrification, thus the volume reduction of radioactive wastes is crucial. The composites described here are all designed to allow vitrification and the enhanced uptake of the zeolite on the carbon support means that the volume of the vitrified zeolite will be approximately 40 % of the original composite volume, or more than twice the amount of caesium can be encapsulated (120 mg g^{-1} against 50 mg g^{-1}) in the same mass of zeolite and hence the same volume of final vitrified material. Finally, it was found that the approximate cost of one gram of composite is £0.025 based on PDDA and commercial natural clinoptilolite costs (£0.021 per gram of pure clinoptilolite) which is industrially important when the cost of the adsorbents plays a crucial role in the design of processes.

Part III

General Conclusions and Further Work

Chapter 11

General Conclusions

The production of hierarchical composites by the chemical modification of the carbon surface using PDDA, allowed to successfully fix different types of zeolites (LTA, FAU and HEU) in the range to nano to micrometer sizes. This method been has shown to produce a more homogeneous material being straightforward, easy to implement and allowed the extrapolation to different types of zeolites and carbons. Also, it was showed that there is no a direct relation on PDDA concentration and the amount of attached zeolite particles. This method allowed to produce natural clinoptilolite composites, which it has never been produced following this method.

Also, previously reported methodologies based on the production of seeds were adapted and compared. Zeolites were prepared and produced in their hierarchical forms using cheap and easy ball milling as the technique to produce nanosized dispersions to be used as seeds. Hierarchical structures were successfully prepared using zeolitic seeds.

The zeolite family offers a wide range of materials with different properties thus different sorption capacities and performances. In this work different types of zeolite were compared. Zeolites with low framework density and low Si/Al ratio as FAU and LTA were prepared. The latter being synthesised in nano and micrometer range. Nanosized zeolite preparation led the project towards the study of colloids and the clear solutions methodologies. Nanoparticles showed to have the highest sorption capabilities in the

copper and cobalt ions removal. However, its preparation is time consuming and final yields are reduced. Nevertheless, if this material is used as supported in these composites, the amount of zeolite can be reduced without loosing effectiveness making this material also attractive for more demanding applications. Two forms of HEU members were used and compared too: synthetic (HEUs) and natural clinoptilolite (HEUn). The synthetic material was prepared in an attempt to produce it in its hierarchical form, two protocols were used and both succeed although the presence of some impurities was inevitable. The incorporation of natural clinoptilolite represents one of the main achievements in this investigation since it was the cheapest prepared material as is clinoptilolite is natural resource that can be used without major conditioning.

Carbons produced by thermal treatments using agroindustrial wastes, showed to be a range of suitable materials to be used as zeolite supports. Under mild hydrothermal conditions, i.e. when preparing zeolites A and Y (100 °C) corn residues represent a good alternative to be used as scaffolds. However, materials with wood-like characteristics such as hazelnut shell, date and cherry stones represent a better alternative since results suggested that less-dense materials collapsed under more harsh conditions (180 °C). Also, these characteristics allowed us to achieve higher yields at the moment of carbonisation when compared to lighter materials such as corn residues.

As a general trend, most of the materials were shown to follow Pseudo Second Order model in the sorption of copper, cobalt and caesium cations. According to the model's theoretical background, the driving force in the adsorptive process has a closer relation to the chemical interaction between sorptive and the active sites in solid. Something that could be easily confirmed since ion exchange is the main sorptive mechanism in zeolites. Also, the new arrangements of zeolite particles allowed to improve the kinetic rates and reduce the diffusive restrictions in the sorption of ions from aqueous solutions. In the study of the diffusive characteristics of prepared materials, it was shown to have a overall better performance due to the modification of the diffusive mechanisms contributions when pure zeolites are used. All materials were shown to be governed by a combination of different diffusive resistance such as film and intraparticle

diffusion with the exception of pure clinoptilolite and composites. These did not show any evidence of intraparticle diffusion and the limiting-step was film diffusion. When composites were used, these contributions were reduced.

Langmuir and Freundlich models were used as the thermodynamic models to correlate the experimental results varying the initial concentrations. For the adsorption of cobalt, Langmuir model represented better the studied systems and both Langmuir and Freundlich represented accurately the data for the adsorption of copper.

This work also presented a range of materials designed for a further pollutant encapsulation after the adsorption by vitrification method. This method has been shown to be an effective way to confine hazardous wastes. The materials use will have a beneficial and direct impact in the final volume, since zeolite can retain a large amount of contaminant but in a reduced volume after the removal of carbon support. This means that the volume of the vitrified zeolite will be reduced, since it is a fraction of whole composite composition when sometimes is not even the 20 % of the original composite volume, but having in this reduced volume an increased capacity, as results showed.

Chapter 12

Further Work

The final materials vitrification is the main recommendation, in the form of a methodology to encapsulate the adsorbed ions by the zeolite particles vitrification allowing to reduce the volume before final disposal. Also, an investigation about the regeneration of the adsorbents in order to be reused, would be advisable.

Nanozeolites showed to be the most effective materials but also their preparation involves longer synthesis time periods and energy consuming. Thus, the incorporation of microwaves in the synthesis protocols can help to overcome this restriction. It would be advisable to investigate the use of other substances different to PDDA in order to modify the surface chemistry of supports. Also, to investigate an optimal and ecological way to remove the carbonaceous supports and the preparation pure-zeolite monoliths with hierarchical characteristics capable of being used in the heavy metals adsorption.

A surface properties extended characterisation by gas adsorption/desorption is recommended. A relation between the porous characteristics (surface area, pore size distribution and micropore volume) and the sorptive performance of the prepared materials can be established. These connections will provide information about how pure zeolites and prepared composites have influenced the sorptive process in terms of available surface area. Also, a further chemical analysis of adsorbed species in order to confirm the sorptive mechanism.

In this work natural clinoptilolite was evaluated, but the use of different types of

natural zeolites can be a good alternative in order to investigate and compare capacity and selectivity. Moreover, the investigation of alternative cheaper sources to produce zeolite such as natural clays or other residues such as rice or corn husk (with high silica content).

Finally, the evaluation in packed columns of prepared materials in order to investigate the diffusion and back pressure characteristics.

Chapter 13

Bibliography

[1] G. Limousin, J.-P. Gaudet, L. Charlet, S. Szenknect, V. Barths, and M. Krimissa, "Sorption isotherms: A review on physical bases, modeling and measurement," *Applied Geochemistry*, vol. 22, no. 2, pp. 249 – 275, 2007.

[2] US Environmental Protection Agency (USEPA), "Identification and listing of hazardous waste," January 2012.

[3] Y. Onishi, "Fukushima and Chernobyl nuclear accidents environmental assessments and U.S. hanford site's waste management," *Procedia* {*IUTAM*}, vol. 10, no. 0, pp. 372 – 381, 2014. Mechanics for the World: Proceedings of the 23rd International Congress of Theoretical and Applied Mechanics.

[4] R. Arutyunyan, L. Bolshov, D. Pripachkin, V. Semyonov, O. Sorokovikova, A. Fokin, K. Rubinstein, R. Ignatov, and M. Smirnova, "Estimation of radionuclide emission during the March 15, 2011 accident at the Fukushima-1 npp (Japan)," *Atomic Energy*, vol. 112, no. 3, pp. 188–193, 2012.

[5] V. Inglezakis and S. Poulopoulos, *Adsorption, Ion Exchange and Catalysis: Design of Operations and Environmental Applications*. No. v. 3, Elsevier Science, 2006.

[6] D. Bruce, D. O'Hare, and R. Walton, *Porous Materials*. Inorganic Materials Series, Wiley, 2011.

[7] J. F. Haw, "Zeolite acid strength and reaction mechanisms in catalysis," *Phys. Chem. Chem. Phys.*, vol. 4, pp. 5431–5441, 2002.

[8] Z. L. Hua, J. Zhou, and J. L. Shi, "Recent advances in hierarchically structured zeolites: synthesis and material performances," *Chem. Commun.*, vol. 47, pp. 10536–10547, 2011.

[9] A. R. Loiola, L. R. D. da Silva, P. Cubillas, and M. W. Anderson, "Synthesis and characterization of hierarchical porous materials incorporating a cubic mesoporous phase," *J. Mater. Chem.*, vol. 18, pp. 4985–4993, 2008.

[10] M. E. Davis, "Ordered porous materials for emerging applications," *Nature.*, vol. 417, pp. 813–821, 2002.

[11] D. Zhao, C. Nie, Y. Zhou, S. Xia, L. Huang, and Q. Li, "Comparison of disordered mesoporous aluminosilicates with highly ordered Al-MCM-41 on stability, acidity and catalytic activity," *Catalysis Today*, vol. 68, no. 13, pp. 11 – 20, 2001. Nanomaterials in Catalysis.

[12] S. Lopez-Orozco, A. Inayat, A. Schwab, T. Selvam, and W. Schwieger, "Zeolitic materials with hierarchical porous structures," *Advanced Materials*, vol. 23, no. 22-23, pp. 2602–2615.

[13] D. Verboekend, T. C. Keller, S. Mitchell, and J. Perez-Ramirez, "Hierarchical FAU- and LTA-Type zeolites by post-synthetic design: A new generation of highly efficient base catalysts," *Advanced Functional Materials*, pp. n/a–n/a, 2012.

[14] S. P. Poonsu Prastertsan and A. H-Kittikun, "Recycling of agro-industrial wastes through cleaner technology," *Biotechnology*, vol. 10, no. 0, p. NA, 2008.

[15] N. Srivastava and C. Majumder, "Novel biofiltration methods for the treatment of heavy metals from industrial wastewater," *Journal of Hazardous Materials*, vol. 151, no. 1, pp. 1 – 8, 2008.

[16] *Minerals Yearbook 2006*. U S Geological Survey & Orienteering S, U.S. Government Printing Office, 2010.

[17] P. H. J.H. Kim, H.J. Gibb and M. Sheffe, *Cobalt and Inorganic Cobalt Compounds*. Concise International Chemical Assessment Document Series, World Health Organization, 2006.

[18] T. A. Kurniawan, G. Y. Chan, W.-H. Lo, and S. Babel, "Physicochemical treatment techniques for wastewater laden with heavy metals," *Chemical Engineering Journal*, vol. 118, no. 12, pp. 83 – 98, 2006.

[19] M. T. Alvarez, C. Crespo, and B. Mattiasson, "Precipitation of Zn(II), Cu(II) and Pb(II) at bench-scale using biogenic hydrogen sulfide from the utilization of volatile fatty acids," *Chemosphere*, vol. 66, no. 9, pp. 1677 – 1683, 2007.

[20] S. Mirbagheri and S. Hosseini, "Pilot plant investigation on petrochemical wastewater treatmentfor the removal of copper and chromium with the objective of reuse," *Desalination*, vol. 171, no. 1, pp. 85 – 93, 2005.

[21] Q. Chen, Z. Luo, C. Hills, G. Xue, and M. Tyrer, "Precipitation of heavy metals from wastewater using simulated flue gas: Sequent additions of fly ash, lime and carbon dioxide," *Water Research*, vol. 43, no. 10, pp. 2605 – 2614, 2009.

[22] M. Barakat, "New trends in removing heavy metals from industrial wastewater," *Arabian Journal of Chemistry*, vol. 4, no. 4, pp. 361 – 377, 2011.

[23] J. Watson, *Separation Methods for Waste and Environmental Applications*. Environmental Science & Pollution, Taylor & Francis, 1999.

[24] E. Assaad, A. Azzouz, D. Nistor, A. Ursu, T. Sajin, D. Miron, F. Monette, P. Niquette, and R. Hausler, "Metal removal through synergic coagulation–flocculation using an optimized chitosanmontmorillonite system," *Applied Clay Science*, vol. 37, no. 34, pp. 258 – 274, 2007.

[25] F. Fu and Q. Wang, "Removal of heavy metal ions from wastewaters: A review," *Journal of Environmental Management*, vol. 92, no. 3, pp. 407 – 418, 2011.

[26] R. Molinari, T. Poerio, and P. Argurio, "Selective separation of copper(II) and nickel(II) from aqueous media using the complexationultrafiltration process," *Chemosphere*, vol. 70, no. 3, pp. 341 – 348, 2008.

[27] R. Camarillo, J. Llanos, L. Garcia-Fernandez, A. Perez, and P. Canizares, "Treatment of copper(II)-loaded aqueous nitrate solutions by polymer enhanced ultrafiltration and electrodeposition," *Separation and Purification Technology*, vol. 70, no. 3, pp. 320 – 328, 2010.

[28] G. Steenkamp, K. Keizer, H. Neomagus, and H. Krieg, "Copper(II) removal from polluted water with alumina/chitosan composite membranes," *Journal of Membrane Science*, vol. 197, no. 12, pp. 147 – 156, 2002.

[29] S. Akita, L. P. Castillo, S. Nii, K. Takahashi, and H. Takeuchi, "Separation of Co(II)/Ni(II) via micellar-enhanced ultrafiltration using organophosphorus acid extractant solubilized by nonionic surfactant," *Journal of Membrane Science*, vol. 162, no. 12, pp. 111 – 117, 1999.

[30] A. Kryvoruchko, L. Yurlova, and B. Kornilovich, "Purification of water containing heavy metals by chelating-enhanced ultrafiltration," *Desalination*, vol. 144, no. 13, pp. 243 – 248, 2002.

[31] Z. Murthy and L. B. Chaudhari, "Application of nanofiltration for the rejection of nickel ions from aqueous solutions and estimation of membrane transport parameters," *Journal of Hazardous Materials*, vol. 160, no. 1, pp. 70 – 77, 2008.

[32] K.-H. Choo, D.-J. Kwon, K.-W. Lee, and S.-J. Choi, "Selective removal of cobalt species using nanofiltration membranes," *Environmental Science and Technology*, vol. 36, no. 6, pp. 1330–1336, 2002. cited By (since 1996)27.

[33] K.-H. Choo, D.-J. Kwon, K.-W. Lee, and S.-J. Choi, "Selective removal of cobalt species using nanofiltration membranes," *Environmental Science and Technology*, vol. 36, no. 6, pp. 1330–1336, 2002.

[34] H. A. Qdais and H. Moussa, "Removal of heavy metals from wastewater by membrane processes: a comparative study," *Desalination*, vol. 164, no. 2, pp. 105 – 110, 2004.

[35] K. Scott and R. Hughes, *Industrial Membrane Separation Technology*. Springer Netherlands, 1996.

[36] J. Chen, *Decontamination of Heavy Metals: Processes, Mechanisms, and Applications*. Advances in Industrial and Hazardous Wastes Treatment, Taylor & Francis, 2012.

[37] B. V. der Bruggen and C. Vandecasteele, "Distillation vs. membrane filtration: overview of process evolutions in seawater desalination," *Desalination*, vol. 143, no. 3, pp. 207 – 218, 2002.

[38] T. Sadyrbaeva, "Recovery of cobalt(II) by the hybrid liquid membrane electrodyalisis electrolysis process," *Electrochimica Acta*, vol. 133, no. 0, pp. 161 – 168, 2014.

[39] R. Noble and S. Stern, *Membrane Separations Technology: Principles and Applications*. Membrane Science and Technology, Elsevier Science, 1995.

[40] A. Chaudhary, J. Donaldson, S. Grimes, and N. Yasri, "Separation of nickel from cobalt using electrodialysis in the presence of EDTA," *Journal of Applied Electrochemistry*, vol. 30, no. 4, pp. 439–445, 2000.

[41] F. Rouquerol, J. Rouquerol, and K. Sing, "Chapter 9 - adsorption by active carbons," in *Adsorption by Powders and Porous Solids* (F. Rouquerol, J. Rouquerol, and K. Sing, eds.), pp. 237 – 285, London: Academic Press, 1999.

[42] S. Pollard, G. Fowler, C. Sollars, and R. Perry, "Low-cost adsorbents for waste and wastewater treatment: a review," *Science of The Total Environment*, vol. 116, no. 12, pp. 31 – 52, 1992.

[43] K. Kadirvelu, K. Thamaraiselvi, and C. Namasivayam, "Removal of heavy metals from industrial wastewaters by adsorption onto activated carbon prepared from an agricultural solid waste," *Bioresource Technology*, vol. 76, no. 1, pp. 63–65, 2000.

[44] M. Kobya, E. Demirbas, E. Senturk, and M. Ince, "Adsorption of heavy metal ions from aqueous solutions by activated carbon prepared from apricot stone," *Bioresource Technology*, vol. 96, no. 13, pp. 1518 – 1521, 2005.

[45] E. Demirba, "Adsorption of cobalt(II) ions from aqueous solution onto activated carbon prepared from hazelnut shells," *Adsorption Science and Technology*, vol. 21, no. 10, pp. 951–963, 2003. cited By (since 1996)42.

[46] J. Rivera-Utrilla and M. Ferro-Garcia, "Study of cobalt adsorption from aqueous solution on activated carbons from almond shells," *Carbon*, vol. 25, no. 5, pp. 645 – 652, 1987.

[47] A. Ahmadpour, M. Tahmasbi, T. R. Bastami, and J. A. Besharati, "Rapid removal of cobalt ion from aqueous solutions by almond green hull," *Journal of Hazardous Materials*, vol. 166, no. 23, pp. 925 – 930, 2009.

[48] K. Krishnan and T. Anirudhan, "Kinetic and equilibrium modelling of cobalt(II) adsorption onto bagasse pith based sulphurised activated carbon," *Chemical Engineering Journal*, vol. 137, no. 2, pp. 257–264, 2008. cited By (since 1996)29.

[49] M. Ferro-Garca, J. Rivera-Utrilla, J. Rodrguez-Gordillo, and I. Bautista-Toledo, "Adsorption of zinc, cadmium, and copper on activated carbons obtained from agricultural by-products," *Carbon*, vol. 26, no. 3, pp. 363 – 373, 1988.

[50] A. Kongsuwan, P. Patnukao, and P. Pavasant, "Binary component sorption of Cu(II) and Pb(II) with activated carbon from Eucalyptus camaldulensis Dehn bark," *Journal of Industrial and Engineering Chemistry*, vol. 15, no. 4, pp. 465 – 470, 2009.

[51] C. Colella, "Chapter 27 Natural zeolites and environment," in *Introduction to Zeolite Science and Practice* (A. C. Jiri Cejka, Herman van Bekkum and F. Schth, eds.), vol. 168 of *Studies in Surface Science and Catalysis*, pp. 999 – 1035, Elsevier, 2007.

[52] S. Babel and T. A. Kurniawan, "Low-cost adsorbents for heavy metals uptake from contaminated water: a review," *Journal of Hazardous Materials*, vol. 97, no. 13, pp. 219 – 243, 2003.

[53] D. Breck, *Zeolite Molecular Sieves: Structure, Chemistry, and Use*. R.E. Krieger, 1984.

[54] P. Misaelides, "Application of natural zeolites in environmental remediation: A short review," *Microporous and Mesoporous Materials*, vol. 144, no. 13, pp. 15 – 18, 2011.

[55] P. Jacobs, E. Flanigen, J. Jansen, and H. van Bekkum, *Introduction to Zeolite Science and Practice*. Studies in Surface Science and Catalysis, Elsevier Science, 2001.

[56] J. Peri, M. Trgo, and N. V. Medvidovi, "Removal of zinc, copper and lead by natural zeolitea comparison of adsorption isotherms," *Water Research*, vol. 38, no. 7, pp. 1893 – 1899, 2004.

[57] O. Yavuz, Y. Altunkaynak, and F. Gzel, "Removal of copper, nickel, cobalt and manganese from aqueous solution by kaolinite," *Water Research*, vol. 37, no. 4, pp. 948 – 952, 2003.

[58] W. W. Ngah and M. Hanafiah, "Removal of heavy metal ions from wastewater by chemically modified plant wastes as adsorbents: A review," *Bioresource Technology*, vol. 99, no. 10, pp. 3935 – 3948, 2008.

[59] K. Thirugnanasambandham, V. Sivakumar, and J. P. Maran, "Application of chitosan as an adsorbent to treat rice mill wastewater–mechanism, modelling and optimization," *Carbohydrate Polymers*, vol. 97, no. 2, pp. 451 – 457, 2013.

[60] A. Bhatnagar, A. Minocha, and M. Sillanp, "Adsorptive removal of cobalt from aqueous solution by utilizing lemon peel as biosorbent," *Biochemical Engineering Journal*, vol. 48, no. 2, pp. 181 – 186, 2010.

[61] H. Parab, S. Joshi, N. Shenoy, A. Lali, U. Sarma, and M. Sudersanan, "Determination of kinetic and equilibrium parameters of the batch adsorption of Co(II), Cr(III) and Ni(II) onto coir pith," *Process Biochemistry*, vol. 41, no. 3, pp. 609 – 615, 2006.

[62] W. Marshall, L. Wartelle, D. Boler, M. Johns, and C. Toles, "Enhanced metal adsorption by soybean hulls modified with citric acid," *Bioresource Technology*, vol. 69, no. 3, pp. 263 – 268, 1999.

[63] T. Vengris, R. Binkien, and A. Sveikauskait, "Nickel, copper and zinc removal from waste water by a modified clay sorbent," *Applied Clay Science*, vol. 18, no. 34, pp. 183 – 190, 2001.

[64] G. Annadurai, R. Juang, and D. Lee, "Adsorption of heavy metals from water using banana and orange peels," *Water Science and Technology*, vol. 47, no. 1, pp. 185–190, 2003. cited By (since 1996)133.

[65] K. Periasamy and C. Namasivayam, "Removal of copper(ii) by adsorption onto peanut hull carbon from water and copper plating industry wastewater," *Chemosphere*, vol. 32, no. 4, pp. 769 – 789, 1996.

[66] F. Rouquerol, J. Rouquerol, and K. Sing, *Adsorption by Powders and Porous Solids: Principles, Methodology and Applications*. Academic Press, 1999.

[67] B. Zdravkov, J. J. Cermak, M. Sefara, and J. Janku, "Pore classification in the characterization of porous materials: A perspective," *Central European Journal of Chemistry*, vol. 5, no. 2, pp. 385–395, 2007.

[68] K. Kaneko, "Determination of pore size and pore size distribution: 1. adsorbents and catalysts," *Journal of Membrane Science*, vol. 96, no. 12, pp. 59 – 89, 1994.

[69] J. Rouquerol, D. Avnir, D. Everett, C. Fairbridge, M. Haynes, N. Pernicone, J. Ramsay, K. Sing, and K. Unger, "Guidelines for the characterization of porous solids," *Studies in Surface Science and Catalysis*, vol. 87, no. C, pp. 1–9, 1994.

[70] R. Xu, W. Pang, J. Yu, Q. Huo, and J. Chen, *Chemistry of Zeolites and Related Porous Materials: Synthesis and Structure*. Wiley, 2009.

[71] M. L. Occelli and H. E. Robson, *Zeolite Synthesis*. Washington, DC: American Chemical Society, 1989.

[72] C. Colella and A. F. Gualtieri, "Cronstedts zeolite," *Microporous and Mesoporous Materials*, vol. 105, no. 3, pp. 213 – 221, 2007. Zeolite 06 (Proceedings of the 7th International Conference on the Occurrence, Properties and Utilization of Natural Zeolites).

[73] A. F. Masters and T. Maschmeyer, "Zeolites from curiosity to cornerstone," *Microporous and Mesoporous Materials*, vol. 142, no. 23, pp. 423 – 438, 2011.

[74] K. Dorfner, *Ion Exchangers*. De Gruyter, 1991.

[75] J. ejka and H. van Bekkum, "Preface," in *Zeolites and Ordered Mesoporous Materials: Progress and Prospects* (J. Cejka and H. van Bekkum, eds.), vol. 157 of *Studies in Surface Science and Catalysis*, pp. v –, Elsevier, 2005.

[76] J. McBain, *The Sorption of Gases and Vapours by Solids*. Twentieth-century chemistry, G. Routledge & sons, Limited, 1932.

[77] E. M. Flanigen, R. W. Broach, and S. T. Wilson, *Chapter 1 Introduction*, pp. 1–26. Wiley-VCH Verlag GmbH and Co. KGaA, 2010.

[78] *Zeolite Synthesis, Copyright, ACS Symposium Series, Foreword*, ch. 0, pp. i–iv.

[79] R. M. Barrerr, "The sorption of polar and non-polar gases by zeolites," *Proceedings of The Royal Society*, vol. 33, pp. 127– 132, 1938.

[80] R. M. Barrer, "Synthesis of a zeolitic mineral with chabazite-like sorptive properties," *J. Chem. Soc.*, pp. 127–132, 1948.

[81] R. M. Milton, *Molecular Sieve Science and Technology*, ch. 2, pp. 1–10.

[82] W. H. Baur and R. X. Fischer, "A historical note on the sodalite framework: The contribution of frans maurits jaeger," *Microporous and Mesoporous Materials*, vol. 116, no. 13, pp. 1 – 3, 2008.

[83] E. M. Flanigen, R. W. Broach, and S. T. Wilson, *Introduction*, pp. 1–26. Wiley-VCH Verlag GmbH & Co. KGaA, 2010.

[84] R. Szostak, *Handbook Of Molecular Sieves: Structures*. Springer, 1992.

[85] C. Baerlocher, L. McCusker, and D. Olson, *Atlas of Zeolite Framework Types*. Elsevier Science, 2007.

[86] S. T. Wilson, B. M. Lok, C. A. Messina, T. R. Cannan, and E. M. Flanigen, "Aluminophosphate molecular sieves: a new class of microporous crystalline inorganic solids," *Journal of the American Chemical Society*, vol. 104, no. 4, pp. 1146–1147, 1982.

[87] B. M. Lok, C. A. Messina, R. L. Patton, R. T. Gajek, T. R. Cannan, and E. M. Flanigen, "Silicoaluminophosphate molecular sieves: another new class of microporous crystalline inorganic solids," *Journal of the American Chemical Society*, vol. 106, no. 20, pp. 6092–6093, 1984.

[88] S. Hedge, P. Ratnasamy, L. Kustov, and V. Kazansky, "Acidity and catalytic activity of SAPO-5 and AlPO-5 molecular sieves," *Zeolites*, vol. 8, no. 2, pp. 137 – 141, 1988.

[89] C. Kresge, M. Leonowicz, W. Roth, J. C. Vartuli, and J. S. Beck, "Ordered mesoporous molecular sieves synthesized by a liquid-crystal template mechanism," *Nature*, vol. 359, pp. 710–712, 1992.

[90] T. Wong, *Handbook of zeolites: structure, properties and applications*. Materials science and technologies series, Nova Science Publishers, 2009.

[91] J. Gilson, *Zeolites for Cleaner Technologies*. Catalytic science series, Imperial College Press, 2002.

[92] R. Stepto and R. Szostak, *Molecular Sieves: Principles of Synthesis and Identification*. Van Nostrand Reinhold Electrical/Computer Science and Engineering Series, Springer, 1998.

[93] R. Xu, W. Pang, and Q. Huo, *Modern Inorganic Synthetic Chemistry*. Elsevier, 2011.

[94] A. Dyer, *An Introduction to Zeolite Molecular Sieves*. John Wiley & Sons Australia, Limited, 1988.

[95] S. Auerbach, K. Carrado, and P. Dutta, *Handbook of Zeolite Science and Technology*. Taylor & Francis, 2003.

[96] J. Cejka, A. Corma, and S. Zones, *Zeolites and Catalysis: Synthesis, Reactions and Applications*. Wiley, 2010.

[97] W. M. Meier, *Symmetry Aspects of Zeolite Frameworks*, ch. 4, pp. 39–51.

[98] L. B. McCusker and C. Baerlocher, "Chapter 3 Zeolite Structures," in *Introduction to Zeolite Science and Practice*, vol. 137 of *Studies in Surface Science and Catalysis*, pp. 37 – 67, Elsevier, 2001.

[99] I. Z. A. S. Commission, "New framework type codes," July 2014.

[100] O. Ursini, E. Lilla, and R. Montanari, "The investigation on cationic exchange capacity of zeolites: The use as selective ion trappers in the electrokinetic soil technique," *Journal of Hazardous Materials*, vol. 137, no. 2, pp. 1079 – 1088, 2006.

[101] R. P. Townsend and E. N. Coker, "Chapter 11 ion exchange in zeolites," in *Introduction to Zeolite Science and Practice* (P. J. H. van Bekkum, E.M. Flanigen and J. Jansen, eds.), vol. 137 of *Studies in Surface Science and Catalysis*, pp. 467 – 524, Elsevier, 2001.

[102] G. Maurin, P. Llewellyn, T. Poyet, and B. Kuchta, "Influence of extra-framework cations on the adsorption properties of X-faujasite systems: microcalorimetry and molecular simulations," *The Journal of Physical Chemistry B*, vol. 109, no. 1, pp. 125–129, 2005. PMID: 16850994.

[103] G. D. Pirngruber, P. Raybaud, Y. Belmabkhout, J. Cejka, and A. Zukal, "The role of the extra-framework cations in the adsorption of CO2 on faujasite Y," *Phys. Chem. Chem. Phys.*, vol. 12, pp. 13534–13546, 2010.

[104] H. Soscun, O. Castellano, J. Hernandez, and A. Hinchliffe, "Acidity of the Bronsted acid sites of zeolites," *International Journal of Quantum Chemistry*, vol. 82, no. 3, pp. 143–150, 2001.

[105] H. Pfeifer, "Bronsted and Lewis acidity of zeolites and related catalysts studied by nuclear magnetic resonance spectroscopy," *Colloids and Surfaces*, vol. 36, no. 2, pp. 169 – 177, 1989. International Conference at Bristol University.

[106] L. Smart and E. Moore, *Solid State Chemistry: An Introduction, 2nd Edition.* Taylor & Francis, 1995.

[107] L. Damjanovi and A. Auroux, "Determination of acid/base properties by temperature programmed desorption (tpd) and adsorption calorimetry," in *Zeolite Characterization and Catalysis* (A. Chester and E. Derouane, eds.), pp. 107–167, Springer Netherlands, 2009.

[108] M. A. Camblor, "The synthetic zeolites as geoinspired materials," vol. 6, pp. 19–22, Sociedad Espaola de Mineraloga, 2006.

[109] J. Yu, "Chapter 3 Synthesis of Zeolites," in *Introduction to Zeolite Science and Practice* (A. C. J. Cejka, Herman van Bekkum and F. Schuth, eds.), vol. 168 of *Studies in Surface Science and Catalysis*, pp. 39 – 103, Elsevier, 2007.

[110] M. Yoshimura and K. Byrappa, "Hydrothermal processing of materials: past, present and future," *Journal of Materials Science*, vol. 43, no. 7, pp. 2085–2103, 2008.

[111] R. M. Barrer, "Zeolites and their synthesis," *Zeolites*, vol. 1, no. 3, pp. 130 – 140, 1981.

[112] C. S. Cundy and P. A. Cox, "The hydrothermal synthesis of zeolites: Precursors, intermediates and reaction mechanism," *Microporous and Mesoporous Materials*, vol. 82, no. 12, pp. 1 – 78, 2005.

[113] B. Schoeman, *Synthesis and properties of colloidal zeolite.* Doktorsavhandlingar vid Chalmers Tekniska Högskola, Chalmers tekniska högsk., 1994.

[114] M. Rahman, A. Mokhlesur, N. Hasnida, N. Wan, and W. M. Norsani, "Preparation of zeolite Y using local raw material rice husk as a silica source," *Journal of Scientific Research*, vol. 1, no. 2, pp. 285–291, 2009.

[115] M. E. Davis and R. F. Lobo, "Zeolite and molecular sieve synthesis," *Chemistry of Materials*, vol. 4, no. 4, pp. 756–768, 1992.

[116] P. Slangen, J. Jansen, and H. van Bekkum, "The effect of ageing on the microwave synthesis of zeolite NaA," *Microporous Materials*, vol. 9, no. 56, pp. 259 – 265, 1997.

[117] C. Cundy, "Synthesis of Zeolites and Zeotypes ," in *Zeolites and Ordered Mesoporous Materials: Progress and Prospects* (J. Cejka and H. van Bekkum, eds.), vol. 157 of *Studies in Surface Science and Catalysis*, pp. 65 – 90, Elsevier, 2005.

[118] R. Thompson, "Recent advances in the understanding of zeolite synthesis," in *Synthesis*, vol. 1 of *Molecular Sieves*, pp. 1–33, Springer Berlin Heidelberg, 1998.

[119] P. Cubillas and M. W. Anderson, *Synthesis Mechanism: Crystal Growth and Nucleation*, pp. 1–55. Wiley-VCH Verlag GmbH & Co KGaA, 2010.

[120] R. M. Barrer and G. S. Perry, "Sorption of mixtures, and selectivity in alkylammonium montmorillonites. Part I. Monomethylammonium bentonite," *J. Chem. Soc.*, pp. 842–849, 1961.

[121] Y. Kamimura, K. Itabashi, and T. Okubo, "Seed-assisted, OSDA-free synthesis of MTW-type zeolite and Green MTW from sodium aluminosilicate gel systems ," *Microporous and Mesoporous Materials*, vol. 147, no. 1, pp. 149 – 156, 2012.

[122] R. Siegel and W. T. E. Center, *Nanostructure Science and Technology: R & D Status and Trends in Nanoparticles, Nanostructured Materials and Nanodevices.* Springer, 1999.

[123] L. Tosheva and V. P. Valtchev, "Nanozeolites: synthesis, crystallization mechanism, and applications," *Chemistry of Materials*, vol. 17, no. 10, pp. 2494–2513, 2005.

[124] S. Mintova, B. Fieres, and T. Bein, "Crystal growth of nanosized lta zeolite from precursor colloids," in *Impact of Zeolites and other Porous Materials on the new Technologies at the Beginning of the New Millennium Proceedings of the 2nd International FEZA (Federation of the European Zeolite Associations)*

Conference (G. G. R. Aiello and F. Testa, eds.), vol. 142 of *Studies in Surface Science and Catalysis*, pp. 223 – 229, Elsevier, 2002.

[125] O. Larlus, S. Mintova, and T. Bein, "Environmental syntheses of nanosized zeolites with high yield and monomodal particle size distribution," *Microporous and Mesoporous Materials*, vol. 96, no. 1-3, pp. 405–412, 2006. cited By (since 1996)48.

[126] S. Valente, N. Burriesci, S. Cavallaro, S. Galvagno, and C. Zipelli, "Utilization of zeolites as soil conditioner in tomato-growing," *Zeolites*, vol. 2, no. 4, pp. 271 – 274, 1982.

[127] G. Blanchard, M. Maunaye, and G. Martin, "Removal of heavy metals from waters by means of natural zeolites," *Water Research*, vol. 18, no. 12, pp. 1501 – 1507, 1984.

[128] T. Armbruster, "Natural zeolites: Cation exchange, cation arrangement and dehydration behavior," in *Minerals as Advanced Materials I* (S. Krivovichev, ed.), pp. 1–6, Springer Berlin Heidelberg, 2008.

[129] P. Van Straaten, *Agrogeololgy: The Use of Rocks for Crops*. Enviroquest Limited & Peter van Straaten, 2007.

[130] D. Zhao, R. Szostak, and L. Kevan, "Role of alkali-metal cations and seeds in the synthesis of silica-rich heulandite-type zeolites," *J. Mater. Chem.*, vol. 8, pp. 233–239, 1998.

[131] B.-L. Su, C. Sanchez, and X.-Y. Yang, *Insights into Hierarchically Structured Porous Materials: From Nanoscience to Catalysis, Separation, Optics, Energy, and Life Science*, pp. 1–27. Wiley-VCH Verlag GmbH & Co. KGaA, 2011.

[132] J. Liu, Z. Guo, F. Meng, Y. Jia, T. Luo, M. Li, and J. Liu, "Novel single-crystalline hierarchical structured ZnO nanorods fabricated via a wet-chemical

route: Combined high gas sensing performance with enhanced optical properties," *Crystal Growth and Design*, vol. 9, no. 4, pp. 1716–1722, 2009.

[133] J. R. Jones, P. D. Lee, and L. L. Hench, "Hierarchical porous materials for tissue engineering," *Philosophical Transactions of the Royal Society A: Mathematical, Physical and Engineering Sciences*, vol. 364, no. 1838, pp. 263–281, 2006.

[134] D. Verboekend and J. Perez-Ramirez, "Design of hierarchical zeolite catalysts by desilication," *Catal. Sci. Technol.*, vol. 1, pp. 879–890, 2011.

[135] J.-S. Hu, L.-S. Zhong, W.-G. Song, and L.-J. Wan, "Synthesis of hierarchically structured metal oxides and their application in heavy metal ion removal," *Advanced Materials*, vol. 20, no. 15, pp. 2977–2982, 2008.

[136] K. Egeblad, C. H. Christensen, M. Kustova, and C. H. Christensen, "Templating mesoporous zeolites," *Chemistry of Materials*, vol. 20, no. 3, pp. 946–960, 2008.

[137] X. Meng, F. Nawaz, and F.-S. Xiao, "Templating route for synthesizing mesoporous zeolites with improved catalytic properties," *Nano Today*, vol. 4, no. 4, pp. 292 – 301, 2009.

[138] K. Moller and T. Bein, "Mesoporosity - a new dimension for zeolites," *Chem. Soc. Rev.*, vol. 42, pp. 3689–3707, 2013.

[139] L.-H. Chen, X.-Y. Li, G. Tian, Y. Li, H.-Y. Tan, G. VanTendeloo, G.-S. Zhu, S.-L. Qiu, X.-Y. Yang, and B.-L. Su, "Multimodal zeolite-beta-based catalysts with a hierarchical, three-level pore structure," *ChemSusChem*, vol. 4, no. 10, pp. 1452–1456, 2011.

[140] F.-S. Xiao and X. Meng, *Zeolites with Hierarchically Porous Structure: Mesoporous Zeolites*, pp. 435–455. Wiley-VCH Verlag GmbH & Co. KGaA, 2011.

[141] D. Verboekend, G. Vile, and J. Perez-Ramirez, "Mesopore formation in usy and beta zeolites by base leaching: Selection criteria and optimization of pore-directing agents," *Crystal Growth & Design*, vol. 12, no. 6, pp. 3123–3132, 2012.

[142] A. Dean, "Hydrocarbon conversion process and catalyst comprising a crystalline alumino-silicate leached with sodium hydroxide," June 20 1967. US Patent 3,326,797.

[143] K. Li, J. Valla, and J. Garcia-Martinez, "Realizing the commercial potential of hierarchical zeolites: New opportunities in catalytic cracking," *ChemCatChem*, vol. 6, no. 1, pp. 46–66, 2014.

[144] R. Chal, C. Gerardin, M. Bulut, and S. vanDonk, "Overview and industrial assessment of synthesis strategies towards zeolites with mesopores," *ChemCatChem*, vol. 3, no. 1, pp. 67–81, 2011.

[145] H. Karge, J. Weitkamp, and P. Anderson, *Post-Synthesis Modification I.* No. v. 1,p. 1 in Molecular Sieves, Springer, 2002.

[146] O. Sel and B. M. Smarsly, *Hierarchically Structured Porous Materials by Dually Micellar Templating Approach*, pp. 41–53. Wiley-VCH Verlag GmbH & Co. KGaA, 2011.

[147] L. Jian, D.-W. W. Tianyu, Y., L. G. Qing, Z. Dongyuan, and Q. S. Zhang, "A facile soft-template synthesis of mesoporous polymeric and carbonaceous nanospheres," *Nat Commun*, vol. 4, 2013.

[148] Z. Wang, F. Li, and A. Stein, "Direct synthesis of shaped carbon nanoparticles with ordered cubic mesostructure," *Nano Letters*, vol. 7, no. 10, pp. 3223–3226, 2007.

[149] J. Perez-Ramirez, C. Christensen, K. Egeblad, C. Christensen, and J. Groen, "Hierarchical zeolites: Enhanced utilisation of microporous crystals in catalysis by advances in materials design," *Chemical Society Reviews*, vol. 37, no. 11, pp. 2530–2542, 2008. cited By (since 1996)396.

[150] F.-S. Xiao, L. Wang, C. Yin, K. Lin, Y. Di, J. Li, R. Xu, D. S. Su, R. Schlgl, T. Yokoi, and T. Tatsumi, "Catalytic properties of hierarchical mesoporous zeo-

lites templated with a mixture of small organic ammonium salts and mesoscale cationic polymers," *Angewandte Chemie International Edition*, vol. 45, no. 19, pp. 3090–3093, 2006.

[151] Y. Tao, H. Kanoh, and K. Kaneko, "Uniform mesopore-donated zeolite Y using carbon aerogel templating," *The Journal of Physical Chemistry B*, vol. 107, no. 40, pp. 10974–10976, 2003.

[152] I. Schmidt, C. Madsen, and C. J. H. Jacobsen, "Confined space synthesis. a novel route to nanosized zeolites," *Inorganic Chemistry*, vol. 39, no. 11, pp. 2279–2283, 2000.

[153] L.-H. Chen, X.-Y. Li, J. C. Rooke, Y.-H. Zhang, X.-Y. Yang, Y. Tang, F.-S. Xiao, and B.-L. Su, "Hierarchically structured zeolites: synthesis, mass transport properties and applications," *J. Mater. Chem.*, vol. 22, pp. 17381–17403, 2012.

[154] I. Schmidt, A. Boisen, E. Gustavsson, K. Stahl, S. Pehrson, S. Dahl, A. Carlsson, and C. Jacobsen, "Carbon nanotube templated growth of mesoporous zeolite single crystals," *Chemistry of Materials*, vol. 13, no. 12, p. 4416, 2001.

[155] V. Valtchev, B. J. Schoeman, J. Hedlund, S. Mintova, and J. Sterte, "Preparation and characterization of hollow fibers of Silicalite-1," *Zeolites*, vol. 17, no. 56, pp. 408 – 415, 1996.

[156] K. Zhu, K. Egeblad, and C. H. Christensen, "Mesoporous carbon prepared from carbohydrate as hard template for hierarchical zeolites," *European Journal of Inorganic Chemistry*, vol. 2007, no. 25, pp. 3955–3960, 2007.

[157] D. P. Serrano, J. M. Escola, and P. Pizarro, "Synthesis strategies in the search for hierarchical zeolites," *Chem. Soc. Rev.*, vol. 42, pp. 4004–4035, 2013.

[158] Y. Yan, M. Davis, and G. Gavalas, "Preparation of zeolite ZSM-5 membranes by in-situ crystallization on porous a-Al2O3," *Industrial and Engineering Chemistry Research*, vol. 34, no. 5, pp. 1652–1661, 1995. cited By (since 1996)278.

[159] E. Geus, M. Den Exter, and H. Van Bekkum, "Synthesis and characterization of zeolite (MFI) membranes on porous ceramic supports," *Journal of the Chemical Society, Faraday Transactions*, vol. 88, no. 20, pp. 3101–3109, 1992.

[160] V. Valtchev, J. Hedlund, B. Schoeman, J. Sterte, and S. Mintova, "Deposition of continuous silicalite-1 films on inorganic fibers," *Microporous Materials*, vol. 8, no. 1-2, pp. 93–101, 1997.

[161] R. Van Der Vaart, H. Bosch, K. Keizer, and T. Reith, "Preparation of an MFI zeolite coating on activated carbon," *Microporous Materials*, vol. 9, no. 3-4, pp. 203–207, 1997. cited By (since 1996)12.

[162] J. Garcia-Martnez, D. Cazorla-Amoros, A. Linares-Solano, and Y. Lin, "Synthesis and characterisation of MFI-type zeolites supported on carbon materials," *Microporous and Mesoporous Materials*, vol. 42, no. 23, pp. 255 – 268, 2001.

[163] O. Hernandez-Ramirez, S. K. Al-Nasri, and S. M. Holmes, "Hierarchical structures based on natural carbons and zeolites," *J. Mater. Chem.*, vol. 21, pp. 16529–16534, 2011.

[164] N. van der Puil, F. Dautzenberg, H. van Bekkum, and J. Jansen, "Preparation and catalytic testing of zeolite coatings on preshaped alumina supports," *Microporous and Mesoporous Materials*, vol. 27, no. 1, pp. 95 – 106, 1999.

[165] F. Akhtar, A. Ojuva, S. K. Wirawan, J. Hedlund, and L. Bergstrom, "Hierarchically porous binder-free silicalite-1 discs: a novel support for all-zeolite membranes," *J. Mater. Chem.*, vol. 21, pp. 8822–8828, 2011.

[166] M. Anderson, S. Holmes, N. Hanif, and C. Cundy, "Hierarchical pore structures through diatom zeolitization," *Angewandte Chemie*, vol. 112, no. 15, pp. 2819–2822, 2000.

[167] W. Xu, J. Dong, J. Li, J. Li, and F. Wu, "A novel method for the preparation of zeolite ZSM-5," *J. Chem. Soc., Chem. Commun.*, pp. 755–756, 1990.

[168] J. Sudhakar Reddy and A. Sayari, "Nanoporous zirconium oxide prepared using the supramolecular templating approach," *Catalysis Letters*, vol. 38, no. 3-4, pp. 219–223, 1996.

[169] Y. Wang, Y. Tang, A. Dong, X. Wang, N. Ren, and Z. Gao, "Zeolitization of diatomite to prepare hierarchical porous zeolite materials through a vapor-phase transport process," *J. Mater. Chem.*, vol. 12, pp. 1812–1818, 2002.

[170] X. Wang, W. Cai, Y. Lin, G. Wang, and C. Liang, "Mass production of micro/nanostructured porous ZnO plates and their strong structurally enhanced and selective adsorption performance for environmental remediation," *Journal of Materials Chemistry*, vol. 20, no. 39, pp. 8582–8590, 2010. cited By (since 1996)48.

[171] H. Hu, J. Xu, C. Deng, and X. Ge, "Hierarchical mesoporous MoO2 hollow microspheres: Synthesis, mechanism and application in removing Cr (VI) from wastewater," *Materials Research Bulletin*, vol. 51, pp. 402–410, 2014. cited By (since 1996)0.

[172] Z. Zhang, K. Wang, J. D. Atkinson, X. Yan, X. Li, M. J. Rood, and Z. Yan, "Sustainable and hierarchical porous enteromorpha prolifera based carbon for CO2 capture," *Journal of Hazardous Materials*, vol. 229230, no. 0, pp. 183 – 191, 2012.

[173] X. Ma, L. Li, L. Yang, C. Su, K. Wang, S. Yuan, and J. Zhou, "Adsorption of heavy metal ions using hierarchical caco3maltose meso/macroporous hybrid materials: Adsorption isotherms and kinetic studies," *Journal of Hazardous Materials*, vol. 209210, no. 0, pp. 467 – 477, 2012.

[174] D. Xu, G. R. Swindlehurst, H. Wu, D. H. Olson, X. Zhang, and M. Tsapatsis, "On the synthesis and adsorption properties of single-unit-cell hierarchical zeolites made by rotational intergrowths," *Advanced Functional Materials*, vol. 24, no. 2, pp. 201–208, 2014.

[175] J. Yang, J. Y. Yang, Y. Zhou, F. Wei, W. G. Lin, and J. H. Zhu, "Hierarchical functionalized MCM-22 zeolite for trapping tobacco specific nitrosamines (tsnas) in solution," *Journal of Hazardous Materials*, vol. 179, no. 13, pp. 1031 – 1036, 2010.

[176] T.-Y. Ma, X.-J. Zhang, and Z.-Y. Yuan, "Hierarchical meso-/macroporous aluminum phosphonate hybrid materials as multifunctional adsorbents," *The Journal of Physical Chemistry C*, vol. 113, no. 29, pp. 12854–12862, 2009.

[177] I. Langmuir, "The adsorption of gases on plane surfaces of glass, mica and platinum.," *Journal of the American Chemical Society*, vol. 40, no. 9, pp. 1361–1403, 1918.

[178] S. Brunauer, P. H. Emmett, and E. Teller, "Adsorption of gases in multimolecular layers," *Journal of the American Chemical Society*, vol. 60, no. 2, pp. 309–319, 1938.

[179] P. H. Emmett and S. Brunauer, "The use of low temperature van der waals adsorption isotherms in determining the surface area of iron synthetic ammonia catalysts," *Journal of the American Chemical Society*, vol. 59, no. 8, pp. 1553–1564, 1937.

[180] J. Rouquerol, F. Rouquerol, P. Llewellyn, G. Maurin, and K. Sing, *Adsorption by Powders and Porous Solids: Principles, Methodology and Applications*. Elsevier Science, 2013.

[181] K. S. W. Sing, D. H. Everett, R. A. W. Haul, L. Moscou, R. A. Pierotti, J. Rouquerol, and T. Siemieniewska, *Reporting Physisorption Data for Gas/Solid Systems*. Wiley-VCH Verlag GmbH and Co. KGaA, 2008.

[182] M. M. Dubinin, "The potential theory of adsorption of gases and vapors for adsorbents with energetically nonuniform surfaces.," *Chemical Reviews*, vol. 60, no. 2, pp. 235–241, 1960.

[183] H. Kayser, "Ueber die verdichtung von gasen an oberflchen in ihrer abhngigkeit von druck und temperatur," *Annalen der Physik*, vol. 248, no. 4, pp. 526–537, 1881.

[184] Aristotle, *Works*, vol. 7.

[185] C. A. Lucy, "Evolution of ion-exchange: from Moses to the Manhattan Project to modern times," *Journal of Chromatography A*, vol. 1000, no. 12, pp. 711 – 724, 2003. A Century of Chromatography 1903-2003.

[186] A. Bahrdt, "Eine volumetrische bestimmungsmethode von schwefelsure (sulfat-ion) im trink- und gebrauchswasser," *Zeitschrift fr Analytische Chemie*, vol. 70, no. 3-4, pp. 109–119, 1927. cited By (since 1996)1.

[187] C. Colella, "Ion exchange equilibria in zeolite minerals," *Mineralium Deposita*, vol. 31, no. 6, pp. 554–562, 1996.

[188] C. E. Harland, *Ion Exchange: Theory and Practice*. RSC Paperbacks Series, Royal Society of Chemistry, 1994.

[189] E. Hgfeldt, "Comparison of some isotherms for representing ion-exchange equilibria," *Reactive Polymers*, vol. 23, no. 1, pp. 19 – 22, 1994.

[190] E. Demirbas, N. Dizge, M. Sulak, and M. Kobya, "Adsorption kinetics and equilibrium of copper from aqueous solutions using hazelnut shell activated carbon," *Chemical Engineering Journal*, vol. 148, no. 23, pp. 480 – 487, 2009.

[191] G. Donmez and Z. Aksu, "Removal of chromium(VI) from saline wastewaters by Dunaliella species," *Process Biochemistry*, vol. 38, no. 5, pp. 751 – 762, 2002.

[192] A. Ozcan, A. S. Ozcan, S. Tunali, T. Akar, and I. Kiran, "Determination of the equilibrium, kinetic and thermodynamic parameters of adsorption of copper(II) ions onto seeds of Capsicum annuum," *Journal of Hazardous Materials*, vol. 124, no. 13, pp. 200 – 208, 2005.

[193] Q. Li, H. Liu, T. Liu, M. Guo, B. Qing, X. Ye, and Z. Wu, "Strontium and calcium ion adsorption by molecularly imprinted hybrid gel," *Chemical Engineering Journal*, vol. 157, no. 23, pp. 401 – 407, 2010.

[194] P. Atkins, V. Walters, and J. De Paula, *Physical Chemistry*. Macmillan Higher Education, 2006.

[195] H. Wang and F. Shadman, "Effect of particle size on the adsorption and desorption properties of oxide nanoparticles," *AIChE Journal*, vol. 59, no. 5, pp. 1502–1510, 2013.

[196] W. Xu, L. Y. Li, and J. R. Grace, "Zinc removal from acid rock drainage by clinoptilolite in a slurry bubble column," *Applied Clay Science*, vol. 50, no. 1, pp. 158 – 163, 2010.

[197] F. Kanwal, R. Rehman, T. Mahmud, A. Jamil, and R. Ilyas, "Isothermal and thermodynamic modeling of Cr(III) adsorption by composites of polyaniline with rice husk and saw dust," *Journal of the Chilean Chemical Society*, vol. 57, pp. 1058 – 1063, 03 2012.

[198] M. Borkovec and G. Papastavrou, "Interactions between solid surfaces with adsorbed polyelectrolytes of opposite charge," *Current Opinion in Colloid & Interface Science*, vol. 13, no. 6, pp. 429 – 437, 2008.

[199] R. V. Jasra, N. V. Choudary, and S. G. T. Bhat, "Separation of gases by pressure swing adsortpion," *Separation Science and Technology*, vol. 26, no. 7, pp. 885–930, 1991.

[200] M. W. Ackley, S. U. Rege, and H. Saxena, "Application of natural zeolites in the purification and separation of gases," *Microporous and Mesoporous Materials*, vol. 61, no. 13, pp. 25 – 42, 2003.

[201] S. Wang, H. Li, and L. Xu, "Application of zeolite MCM-22 for basic dye removal from wastewater," *Journal of Colloid and Interface Science*, vol. 295, no. 1, pp. 71 – 78, 2006.

[202] C.-K. Lee, S.-S. Liu, L.-C. Juang, C.-C. Wang, K.-S. Lin, and M.-D. Lyu, "Application of MCM-41 for dyes removal from wastewater," *Journal of Hazardous Materials*, vol. 147, no. 3, pp. 997 – 1005, 2007.

[203] A. Dyer, "Separation of closely related systems by molecular sieve zeolites," *Separation Science and Technology*, vol. 13, no. 6, pp. 501–516, 1978.

[204] A. Gnay, E. Arslankaya, and smail Tosun, "Lead removal from aqueous solution by natural and pretreated clinoptilolite: Adsorption equilibrium and kinetics," *Journal of Hazardous Materials*, vol. 146, no. 12, pp. 362 – 371, 2007.

[205] T. Motsi, N. Rowson, and M. Simmons, "Adsorption of heavy metals from acid mine drainage by natural zeolite," *International Journal of Mineral Processing*, vol. 92, no. 12, pp. 42 – 48, 2009.

[206] L. Curkovic, S. Cerjan-Stefanovic, and T. Filipan, "Metal ion exchange by natural and modified zeolites," *Water Research*, vol. 31, no. 6, pp. 1379 – 1382, 1997.

[207] U. Wingenfelder, C. Hansen, G. Furrer, and R. Schulin, "Removal of heavy metals from mine waters by natural zeolites," *Environmental Science and Technology*, vol. 39, no. 12, pp. 4606–4613, 2005.

[208] Y. Zhao, B. Zhang, X. Zhang, J. Wang, J. Liu, and R. Chen, "Preparation of highly ordered cubic NaA zeolite from halloysite mineral for adsorption of ammonium ions," *Journal of Hazardous Materials*, vol. 178, no. 13, pp. 658 – 664, 2010.

[209] X. Querol, N. Moreno, J. Umana, A. Alastuey, E. Hernandez, A. Lopez-Soler, and F. Plana, "Synthesis of zeolites from coal fly ash: an overview," *International Journal of Coal Geology*, vol. 50, no. 14, pp. 413 – 423, 2002. Volume 50.

[210] A. El-Kamash, M. El-Naggar, and M. El-Dessouky, "Immobilization of cesium and strontium radionuclides in zeolite-cement blends," *Journal of Hazardous Materials*, vol. 136, no. 2, pp. 310 – 316, 2006.

[211] I. C. Ostroski, M. A. Barros, E. A. Silva, J. H. Dantas, P. A. Arroyo, and O. C. Lima, "A comparative study for the ion exchange of Fe(III) and Zn(II) on zeolite NaY," *Journal of Hazardous Materials*, vol. 161, no. 23, pp. 1404 – 1412, 2009.

[212] C. J. Adams, A. Araya, S. W. Carr, A. P. Chapple, P. Graham, A. R. Minihan, and T. J. Osinga, "Zeolite map: A new detergent builder," in *Zeolite Science 1994: Recent Progress and Discussions Supplementary Materials to the 10th International Zeolite Conference, Garmish-Partenkirchen, Germany, July 17-22, 1994* (H. Karge and J. Weitkamp, eds.), vol. 98 of *Studies in Surface Science and Catalysis*, pp. 206 – 207, Elsevier, 1995.

[213] F. Helfferich, *Ion Exchange*. Dover science books, Dover, 1962.

[214] J. Kammerer, R. Carle, and D. R. Kammerer, "Adsorption and ion exchange: Basic principles and their application in food processing," *Journal of Agricultural and Food Chemistry*, vol. 59, no. 1, pp. 22–42, 2011.

[215] J. Martens and P. Jacobs, "Chapter 14 Introduction to acid catalysis with zeolites in hydrocarbon reactions," in *Introduction to Zeolite Science and Practice* (P. J. H. van Bekkum, E.M. Flanigen and J. Jansen, eds.), vol. 137 of *Studies in Surface Science and Catalysis*, pp. 633 – 671, Elsevier, 2001.

[216] R. Roque-Malherbe, *The Physical Chemistry of Materials: Energy and Environmental Applications*. Taylor & Francis, 2010.

[217] J. A. Rabo and M. W. Schoonover, "Early discoveries in zeolite chemistry and catalysis at Union Carbide, and follow-up in industrial catalysis," *Applied Catalysis A: General*, vol. 222, no. 12, pp. 261 – 275, 2001. Celebration Issue.

[218] W. Vermeiren and J.-P. Gilson, "Impact of zeolites on the petroleum and petrochemical industry," *Topics in Catalysis*, vol. 52, no. 9, pp. 1131–1161, 2009.

[219] H. Dogan and N. D. Hilmioglu, "Zeolite-filled regenerated cellulose membranes for pervaporative dehydration of glycerol," *Vacuum*, vol. 84, no. 9, pp. 1123 – 1132, 2010.

[220] A. Corma, V. Fornes, J. L. Jorda, F. Rey, R. Fernandez-Lafuente, J. M. Guisan, and C. Mateo, "Electrostatic and covalent immobilisation of enzymes on ITQ-6 delaminated zeolitic materials," *Chem. Commun.*, pp. 419–420, 2001.

[221] H. Chiku, M. Matsui, S. Murakami, Y. Kiyozumi, F. Mizukami, and K. Sakaguchi, "Zeolites as new chromatographic carriers for proteins–easy recovery of proteins adsorbed on zeolites by polyethylene glycol," *Analytical Biochemistry*, vol. 318, no. 1, pp. 80 – 85, 2003.

[222] K. Pavelic, M. Hadzija, L. Bedrica, J. Pavelic, I. Dikic, M. Katic, M. Kralj, M. H. Bosnar, S. Kapitanovic, M. Poljak-Blazi, S. Krizanac, R. Stojkovic, M. Jurin, B. Subotic, and M. Colic, "Natural zeolite clinoptilolite: new adjuvant in anticancer therapy," *Journal of Molecular Medicine*, vol. 78, no. 12, pp. 708–720, 2001.

[223] D. L. Bailey, G. Snowdon, R. G. Cooper, and P. J. Roach, "The use of molecular sieves to produce point sources of radioactivity," *Physics in Medicine and Biology*, vol. 49, no. 3, p. N21, 2004.

[224] N. Alam and R. Mokaya, "Characterisation and hydrogen storage of Pt-doped carbons templated by Pt-exchanged zeolite Y ," *Microporous and Mesoporous Materials*, vol. 142, no. 23, pp. 716 – 724, 2011.

[225] L. Jian-Ming, Z. Ri-Guang, Z. Qiang, D. Jin-Xiang, W. Bao-Jun, and L. Jin-Ping, "Hydrogen adsorption on zeolite Na-MAZ and Li-MAZ clusters," *Acta Physico-Chimica Sinica*, vol. 27, no. 07, p. 1647, 2011.

[226] Y. Li and R. T. Yang, "Hydrogen storage in low silica type X zeolites," *The Journal of Physical Chemistry B*, vol. 110, no. 34, pp. 17175–17181, 2006.

[227] S. Azizian, "Kinetic models of sorption: a theoretical analysis," *Journal of Colloid and Interface Science*, vol. 276, no. 1, pp. 47 – 52, 2004.

[228] S. Lagergren, B. Svenska, and R. Swed *Acad. Sci. Doc., Band*, vol. 24, pp. 1–13, 1898.

[229] H. Yuh-Shan, "Citation review of lagergren kinetic rate equation on adsorption reactions," *Scientometrics*, vol. 59, no. 1, pp. 171–177, 2004.

[230] Y. Miyake, H. Ishida, S. Tanaka, and S. D. Kolev, "Theoretical analysis of the pseudo-second order kinetic model of adsorption. application to the adsorption of Ag(I) to mesoporous silica microspheres functionalized with thiol groups," *Chemical Engineering Journal*, vol. 218, pp. 350 – 357, 2013.

[231] Y. Ho and G. McKay, "A comparison of chemisorption kinetic models applied to pollutant removal on various sorbents," *Process Safety and Environmental Protection*, vol. 76, no. 4, pp. 332 – 340, 1998.

[232] Y. Ho and G. McKay, "Pseudo-second order model for sorption processes," *Process Biochemistry*, vol. 34, no. 5, pp. 451 – 465, 1999.

[233] Y.-S. Ho, "Review of second-order models for adsorption systems," *Journal of Hazardous Materials*, vol. 136, no. 3, pp. 681 – 689, 2006.

[234] J.-Z. Zhang, "Avoiding spurious correlation in analysis of chemical kinetic data," *Chem. Commun.*, vol. 47, pp. 6861–6863, 2011.

[235] G. E. Boyd, A. W. Adamson, and L. S. Myers, "The exchange adsorption of ions from aqueous solutions by organic zeolites," *Journal of the American Chemical Society*, vol. 69, no. 11, pp. 2836–2848, 1947.

[236] M. I. El-Khaiary, "Kinetics and mechanism of adsorption of methylene blue from aqueous solution by nitric-acid treated water-hyacinth," *Journal of Hazardous Materials*, vol. 147, no. 12, pp. 28 – 36, 2007.

[237] Y. Onal, C. Akmil-Basar, and C. Sarc-Ozdemir, "Investigation kinetics mechanisms of adsorption malachite green onto activated carbon," *Journal of Hazardous Materials*, vol. 146, no. 12, pp. 194 – 203, 2007.

[238] S. Basha, Z. V. P. Murthy, and B. Jha, "Removal of Cu(II) and Ni(II) from industrial effluents by brown seaweed, Cystoseira indica," *Industrial & Engineering Chemistry Research*, vol. 48, no. 2, pp. 961–975, 2009.

[239] K. V. Kumar and S. Sivanesan, "Sorption isotherm for safranin onto rice husk: Comparison of linear and non-linear methods," *Dyes and Pigments*, vol. 72, no. 1, pp. 130 – 133, 2007.

[240] K. Foo and B. Hameed, "Insights into the modeling of adsorption isotherm systems," *Chemical Engineering Journal*, vol. 156, no. 1, pp. 2 – 10, 2010.

[241] C. H. Giles, D. Smith, and A. Huitson, "A general treatment and classification of the solute adsorption isotherm. i. theoretical," *Journal of Colloid and Interface Science*, vol. 47, no. 3, pp. 755 – 765, 1974.

[242] K. V. Kumar, K. Porkodi, and F. Rocha, "Isotherms and thermodynamics by linear and non-linear regression analysis for the sorption of methylene blue onto activated carbon: Comparison of various error functions," *Journal of Hazardous Materials*, vol. 151, no. 23, pp. 794 – 804, 2008.

[243] Y.-S. Ho, "Selection of optimum sorption isotherm," *Carbon*, vol. 42, no. 10, pp. 2115 – 2116, 2004.

[244] Y.-S. Ho, "Isotherms for the sorption of lead onto peat: Comparison of linear and non-linear methods," *Polish Journal of Environmental Studies*, vol. 15, no. 1, pp. 81–86, 2006. cited By (since 1996)112.

[245] J. Konya and N. M. Nagy, "Misleading information on homogeneity and heterogeneity obtained from sorption isotherms," *Adsorption*, vol. 19, no. 2-4, pp. 701–707, 2013.

[246] N. Z. Misak, "Langmuir isotherm and its application in ion-exchange reactions," *Reactive Polymers*, vol. 21, no. 12, pp. 53 – 64, 1993.

[247] Y. Waseda, E. Matsubara, and K. Shinoda, *X-Ray Diffraction Crystallography: Introduction, Examples and Solved Problems*. Springer, 2011.

[248] L. B. McCusker and C. Baerlocher, "Chapter 2 zeolite structures," in *Introduction to Zeolite Science and Practice* (A. C. Ji ejka, Herman van Bekkum and F. Schth, eds.), vol. 168 of *Studies in Surface Science and Catalysis*, pp. 13 – 37, Elsevier, 2007.

[249] W. Callister and D. Rethwisch, *Fundamentals of Materials Science and Engineering: An Integrated Approach*. Wiley, 2012.

[250] A. Putnis, *An Introduction to Mineral Sciences*. Cambridge University Press, 1992.

[251] B. Post, "X-ray diffraction procedures for polycrystalline and amorphous materials. harold p. klug and leroy e. alexander, john wiley & sons, new york, 1974, pp. 960. $37.50," *X-Ray Spectrometry*, vol. 4, no. 4, pp. A18–A18, 1975.

[252] W. Zhou and Z. Wang, *Scanning Microscopy for Nanotechnology: Techniques and Applications*. Chemistry and Materials Science 2005-2008, Springer, 2007.

[253] J. M. Thomas and P. L. Gai, "Electron microscopy and the materials chemistry of solid catalysts," vol. 48 of *Advances in Catalysis*, pp. 171 – 227, Academic Press, 2004.

[254] J. Menter, "The electron microscopy of crystal lattices," *Advances in Physics*, vol. 7, no. 27, pp. 299–348, 1958.

[255] R. Frety, D. Ballivet, D. Barthomeuf, and Y. Trambouze, *Electron Microscopy Examination of the Porous Structure of an L-type Zeolite*. 1972.

[256] I. Diaz and A. Mayoral, "TEM studies of zeolites and ordered mesoporous materials," *Micron*, vol. 42, no. 5, pp. 512 – 527, 2011.

[257] D. Williams and C. Carter, "The transmission electron microscope," in *Transmission Electron Microscopy*, pp. 3–17, Springer US, 1996.

[258] K. Hodgkinson, O. U. Images, and I. C. Team, *Images and information*. Images and information, Open University, 1996.

[259] V. Ramachandran and J. Beaudoin, *Handbook of Analytical Techniques in Concrete Science and Technology: Principles, Techniques and Applications*. Materials Science and Process Technology, Elsevier Science, 2000.

[260] H. Merkus, *Particle Size Measurements: Fundamentals, Practice, Quality*. Particle Technology Series, Springer, 2009.

[261] D. Hendricks, *Water Treatment Unit Processes: Physical and Chemical*. Civil and Environmental Engineering, Taylor & Francis, 2006.

[262] M. Kaszuba, J. Corbett, F. M. Watson, and A. Jones, "High-concentration zeta potential measurements using light-scattering techniques," *Philosophical Transactions of the Royal Society A: Mathematical, Physical and Engineering Sciences*, vol. 368, no. 1927, pp. 4439–4451, 2010.

[263] A. Jentys and J. Lercher, "Chapter 8 Techniques of zeolite characterization," in *Introduction to Zeolite Science and Practice* (P. J. H. van Bekkum, E.M. Flanigen and J. Jansen, eds.), vol. 137 of *Studies in Surface Science and Catalysis*, pp. 345 – 386, Elsevier, 2001.

[264] S. Lowell and J. Shields, *Powder Surface Area and Porosity*. Chapman & Hall Series in Accounting and Finance, Springer, 1991.

[265] Department of Chemistry - University of Oxford, "Basic operating principles of the sorptomatic," July 2014.

[266] F. Ribeiro, *Zeolites: Science and Technology: Science and Technology*. E: Nato advanced science institutes series, M. Nijhoff, 1984.

[267] E. Brown, *Introduction to Thermal Analysis: Techniques and Applications*. Hot Topics in Thermal Analysis and Calorimetry, Springer, 2001.

[268] J. Menczel and R. Prime, *Thermal Analysis of Polymers, Fundamentals and Applications*. Wiley, 2009.

[269] J. Cazes, *Analytical Instrumentation Handbook, Third Edition*. Taylor & Francis, 2004.

[270] C. Brundle, C. Evans, and S. Wilson, *Encyclopedia of Materials Characterization: Surfaces, Interfaces, Thin Films*. Characterization Series, Butterworth-Heinemann, 1992.

[271] "Chapter 46 - {FAU} Linde Type Y Si(71), Al(29)," in *Verified Syntheses of Zeolitic Materials* (H. Robson and K. P. Lillerud, eds.), pp. 156 – 158, Amsterdam: Elsevier Science, 2001.

[272] O. Guvenir, H. Kalpclar, and A. Culfaz, "Crystallization field study for the formation of single phase sodium clinoptilolite: Batch composition, seed and temperature effects," *Crystal Research and Technology*, vol. 44, no. 3, pp. 293–299, 2009.

[273] D. Zhao, K. Cleare, C. Oliver, C. Ingram, D. Cook, R. Szostak, and L. Kevan, "Characteristics of the synthetic heulandite-clinoptilolite family of zeolites," *Microporous and Mesoporous Materials*, vol. 21, no. 4 - 6, pp. 371 – 379, 1998.

[274] M. M. Treacy and J. B. Higgins, *Collection of Simulated XRD Powder Patterns for Zeolites Fifth (5th) Revised Edition*. Elsevier, 2007.

[275] F. Gimbert, N. Morin-Crini, F. Renault, P.-M. Badot, and G. Crini, "Adsorption isotherm models for dye removal by cationized starch-based material in a single component system: Error analysis," *Journal of Hazardous Materials*, vol. 157, no. 1, pp. 34 – 46, 2008.

[276] B. Volesky, *Biosorption of Heavy Metals*. Taylor & Francis, 1990.

[277] S. Aguado, J. Gascon, D. Farrusseng, J. C. Jansen, and F. Kapteijn, "Simple modification of macroporous alumina supports for the fabrication of dense naa zeolite coatings: Interplay of electrostatic and chemical interactions," *Microporous and Mesoporous Materials*, vol. 146, no. 13, pp. 69 – 75, 2011. Special Issue - Corma60.

[278] X. D. Wang, W. L. Yang, Y. Tang, Y. J. Wang, S. K. Fu, and Z. Gao, "Fabrication of hollow zeolite spheres," *Chem. Commun.*, pp. 2161–2162, 2000.

[279] S. Wang and Y. Peng, "Natural zeolites as effective adsorbents in water and wastewater treatment," *Chemical Engineering Journal*, vol. 156, no. 1, pp. 11 – 24, 2010.

[280] C. O. Ijagbemi, M.-H. Baek, and D.-S. Kim, "Montmorillonite surface properties and sorption characteristics for heavy metal removal from aqueous solutions," *Journal of Hazardous Materials*, vol. 166, no. 1, pp. 538 – 546, 2009.

[281] J.-O. Kim, S.-M. Lee, and C. Jeon, "Adsorption characteristics of sericite for cesium ions from an aqueous solution," *Chemical Engineering Research and Design*, vol. 92, no. 2, pp. 368 – 374, 2014.

[282] F. Pagnanelli, "Equilibrium, kinetic and dynamic modelling of biosorption processes," in *Microbial Biosorption of Metals* (P. Kotrba, M. Mackova, and T. Macek, eds.), pp. 59–120, Springer Netherlands, 2011.

[283] P. Xiangliang, W. Jianlong, and Z. Daoyong, "Biosorption of Pb(II) by pleurotus ostreatus immobilized in calcium alginate gel," *Process Biochemistry*, vol. 40, no. 8, pp. 2799 – 2803, 2005.

[284] L. Caceres-Jensen, J. Rodrguez-Becerra, J. Parra-Rivero, M. Escudey, L. Barrientos, and V. Castro-Castillo, "Sorption kinetics of diuron on volcanic ash derived soils," *Journal of Hazardous Materials*, vol. 261, no. 0, pp. 602 – 613, 2013.